AD NUMBER
AD922632
LIMITATION CHANGES

TO:

Approved for public release; distribution is unlimited.

FROM:

Distribution authorized to U.S. Gov't. agencies only; Test and Evaluation; 03 JUN 1974. Other requests shall be referred to Air Force Flight Dynamics Laboratory, ATTN: FYS, Wright-Patterson AFB, OH 45433.

AUTHORITY

AFFDL ltr dtd 28 Nov 1979

AFFDL-TR-74-67

PRELIMINARY DESIGN OF ACTIVE/WING STORE FLUTTER SUPPRESSION SYSTEMS FOR MILITARY AIRCRAFT

WILLIAM E. TRIPLETT
ROBERT J. LANDY
DONALD W. IRWIN

MCDONNELL AIRCRAFT COMPANY
MCDONNELL DOUGLAS CORPORATION
SAINT LOUIS, MISSOURI

TECHNICAL REPORT AFFDL—TR—74—67

FINAL REPORT FOR PERIOD 26 FEBRUARY 1973 — 28 JUNE 1974

AUGUST 1974

NOTICE

When Government drawings, specifications, or other data are used for any purpose other than in connection with a definitely related Government procurement operation, the United States Government thereby incurs no responsibility nor any obligation whatsoever; and the fact that the government may have formulated, furnished, or in any way supplied the said drawings, specifications, or other data, is not to be regarded by implication or otherwise as in any manner licensing the holder or any other person or corporation, or conveying any rights or permission to manufacture, use, or sell any patented invention that may in any way be related thereto.

This technical report has been reviewed and is approved for publication.

WALTER J. MYKYTOW
Asst. for Research and Technology
Vehicle Dynamics Division
AF Flight Dynamics Laboratory

Copies of this report should not be returned unless return is required by security considerations, contractual obligations, or notice on a specific document.

REPORT DOCUMENTATION PAGE		READ INSTRUCTIONS BEFORE COMPLETING FORM
1. REPORT NUMBER AFFDL-TR-74-67	2. GOVT ACCESSION NO. NA	3. RECIPIENT'S CATALOG NUMBER NA
4. TITLE *(and Subtitle)* PRELIMINARY DESIGN OF ACTIVE WING/STORE FLUTTER SUPPRESSION SYSTEMS FOR MILITARY AIRCRAFT		5. TYPE OF REPORT & PERIOD COVERED FINAL – Feb 1973 – Jun 1974
		6. PERFORMING ORG. REPORT NUMBER NA
7. AUTHOR(s) William E. Triplett Robert J. Landy Donald W. Irwin		8. CONTRACT OR GRANT NUMBER(s) F33615-73-C-3063
9. PERFORMING ORGANIZATION NAME AND ADDRESS McDonnell Aircraft Company McDonnell Douglas Corporation P. O. Box 516 St. Louis, Missouri 63166		10. PROGRAM ELEMENT, PROJECT, TASK AREA & WORK UNIT NUMBERS Project 1370 Task 137001
11. CONTROLLING OFFICE NAME AND ADDRESS Air Force Flight Dynamics Laboratory Attn: AFFDL/FYS Wright Patterson Air Force Base, Ohio 45433		12. REPORT DATE August 1974
		13. NUMBER OF PAGES 176
14. MONITORING AGENCY NAME & ADDRESS(if different from Controlling Office) Same		15. SECURITY CLASS. (of this report) Unclassified
		15a. DECLASSIFICATION/DOWNGRADING SCHEDULE NA

16. DISTRIBUTION STATEMENT *(of this Report)*

Distribution limited to U.S. Government agencies only; test and evaluation; statement applied 3 June 1974. Other requests for this document must be referred to AF Flight Dynamics Laboratory, (FYS), Wright Patterson AFB, Ohio 45433.

17. DISTRIBUTION STATEMENT *(of the abstract entered in Block 20, if different from Report)*

Same

18. SUPPLEMENTARY NOTES

None

19. KEY WORDS *(Continue on reverse side if necessary and identify by block number)*

Active Control	Flutter
Active Suppression	Flutter Control System
Aeroelastic Instabilities	Flutter Suppression System
Control System Analysis	Redundant Systems
Flight Control Systems	Wing/Store Flutter

20. ABSTRACT *(Continue on reverse side if necessary and identify by block number)*

This report presents the results of an analytical study directed toward the preliminary design of an adaptive flutter control system for fighter type aircraft carrying external wing mounted stores. The report develops and supports the following conclusions:

1. Active flutter control with acceptable stability margins is predicted for flight throughout the entire velocity-altitude envelope for store loadings both with and without symmetry.

2. An adaptive flutter control system, based on a digital evaluation of interrogated aircraft response data, appears to be feasible for use in gusty environments with small input test signal levels and after smoothing of the measured response data.

3. Hardware requirements and aircraft modifications are practical for fighter aircraft wing/store flutter control for frequencies up to approximately 20 Hz.

4. The weight attributable to an operational flutter control system is estimated to be 131 lbs.

In addition plans are presented for semispan and full-span low speed and semispan transonic wind tunnel tests, "Iron Bird" simulation tests, ground vibration and installed system tests, and flight test demonstrations with three store configurations having widely differing dynamic characteristics.

FOREWORD

TABLE OF CONTENTS

TABLE OF CONTENTS (Cont'd)

LIST OF ILLUSTRATIONS

LIST OF ILLUSTRATIONS (Continued)

LIST OF ILLUSTRATIONS (Concluded)

1. INTRODUCTION

1.1 Background

High performance aircraft are required to carry many combinations of
external wing mounted stores. Some of these stores are critical from the
design standpoint of preventing dangerous aeroelastic instabilities within
the required operational flight envelope. Historically, during the preli-
minary design stage of an aircraft, only a few external stores are considered
for employment, and flutter prevention is not too troublesome. Flutter can
be prevented by either relocating the store spanwise and/or chordwise, or by
tuning the pylon stiffness characteristics. Once the aircraft has been
developed and made operational, using command missions require additional
external stores that have not been evaluated or certified during the original
aircraft design and flight test. This results in extensive and costly store
clearance programs, aircraft modifications and, quite frequently, flight
envelope degradation through speed limitations for various reasons including
flutter prevention.

The dynamic characteristics of the store-vehicle system are considerably
altered as stores with different mass and inertia characteristics are added,
causing wide variations in frequency and opening the possibility for flutter
problems. The flutter speed for each wing/store configuration is established
using various schemes combining analyses, wind tunnel tests, ground vibration
tests, and flight flutter tests. If the flutter speed is within the aircraft
flight boundary, the configuration is placarded and thus the full use of the
potential capability of the weapon system is not possible.

The F-4 Phantom aircraft has experienced the above design evolution pro-
cess and is discussed by Barkey in Reference 1. The aircraft was originally
designed for air defense and, therefore, required the external carriage of
only centerline fuel tanks and missiles semi-submerged within the bottom of
the fuselage. Figure 1 illustrates the growth in number of external stores
certified for carriage on the F-4 versus years of service. After sixteen
years of service the number of different stores carried is more than 100.
The greater the number of external stores the aircraft is required to carry,
the more likelihood that difficulties including flutter will occur within
the flight envelope. The F-4 has a flutter placard for the carriage of some

---

1. Barkey, H. D., "Evolution of the F-4 Phantom," MCAIR 71-017, Presented
   at the Technical Program Management Seminar of the American Institute
   of Industrial Engineers, 19-21 April 1971.

1
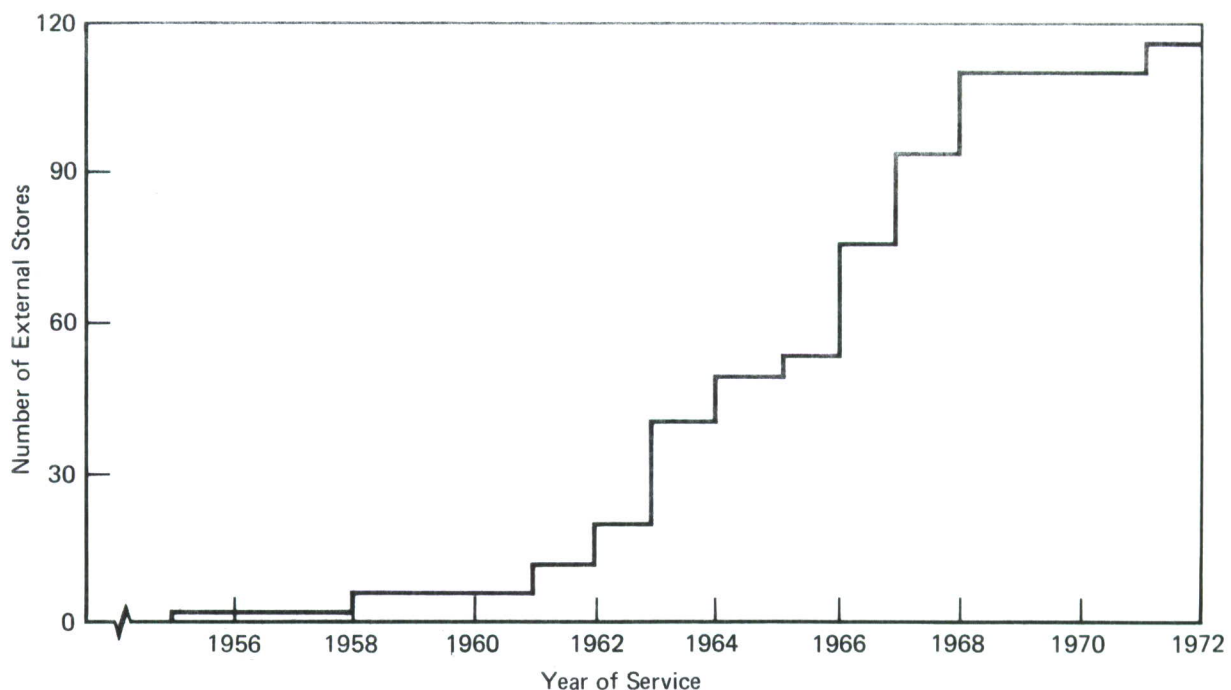
FIGURE 1
EXTERNAL WING STORES GROWTH ON FIGHTER ATTACK AIRCRAFT

stores or weapons. This is only one example; similar restrictions can be found on other fighter attack aircraft in the USAF inventory.

The Air Force Flight Dynamics Laboratory sponsored a feasibility study in 1971 to investigate the potential of applying active control technology to the high frequency, unstable structural modes associated with fighter aircraft (References 2 through 4). The objective of this study was to conduct detailed analyses of fighter aircraft lifting surface components to determine where the use of active flutter control systems would be more efficient than the use of conventional structural and mass balance flutter prevention techniques.

2. Triplett, William E., "A Feasibility Study of Active Wing/Store Flutter Control," Journal of Aircraft, Vol. 9, No. 6, June 1972.
3. Triplett, William E., Kappus, Hans-Peter F., and Landy, Robert J., "Active Flutter Control - An Adaptable Application to Wing/Store Flutter," Journal of Aircraft, Vol. 10, No. 11, November 1973.
4. Triplett, William E., Kappus, Hans-Peter F., and Landy, Robert J., "Active Flutter Suppression Systems for Military Aircraft, A Feasibility Study," AFFDL-TR-72-116, February 1973

Active control systems for wing/external store flutter was determined to be the most promising application compared with the more conventional passive flutter prevention techniques. The stores studied included a fuel tank, a 2000 lb bomb, and 500 lb bombs. The frequency of the flutter modes varied from approximately 7.67 Hz up to 10.71 Hz. All of these store configurations were restricted to the 550 KEAS (Knots Equivalent Air Speed) flutter placard. For these cases an adaptable flutter control system, modifying a wing mounted sensor signal, can remove wing/store flutter placards and thus permit significantly increased aircraft performance. The performance gain possible for the aircraft is approximately 33 percent (550 to 730 KEAS) in terms of maximum permissible speed. The studies indicate that, for the present state-of-the-art, active flutter control systems for mild or moderately severe wing/store flutter modes are feasible and have very high payoff in increasing performance.

1.2 Study Objectives

The Air Force Flight Dynamics Laboratory, therefore, sponsored this follow-on effort in 1973 (Reference 5) to extend these results in a preliminary system design to determine realistic system integration features, and to provide a feasibility evaluation of a completely automatic (pilot-out-of-the-loop) adaptive active flutter control system which automatically adjusts system gain and compensation for different stores on the aircraft. Information to be obtained included a definition of details involving hydraulic and structural modifications, various self-adaptive control concepts including hardware and software components, flight safety features, expected performance benefits and limitations, and program plans for a wind tunnel verification effort and subsequent flight test demonstrations. Requirements for the suppression of symmetric, anti-symmetric and asymmetric (non-symmetric store loading conditions) flutter modes were to be defined. Actuators and other control system components which may require improvement beyond the current state-of-the-art to suppress flutter in the 10-20 Hertz frequency range were to be identified. This report presents the results of that investigation.

---

5. Air Force Contract F33615-73-C-3063, "Statement of Work," dated 26 February 1973.

2. PROGRAM DEFINITION

This section of the report defines the ground rules followed in these studies. The following items are defined:

o Study configurations

o Analytical approaches

o Flutter control scheme

o Flight conditions

o Design criteria

2.1 Study Configurations

The work performed by MCAIR under AFFDL Contract F33615-71-C-1481 and reported in Reference 4 demonstrated the feasibility of active wing/store flutter control using an F-4 Phantom aircraft for several diverse store configurations. Both linear and nonlinear stability analyses were used in these studies to establish preliminary hardware requirements for a reliable, general application, active flutter control system.

In order to make maximum use of these previously generated data an identical structural model of the F-4 was used in most of these new studies. This wing/store dynamic idealization is presented in detail in Appendix I of Reference 4. The three specific store configurations described in Paragraph 2.1 of Reference 4 were considered with this model:

o 370 gallon fuel tank - 90% full

o MK-84EO guided bomb - max weight, min inertia, forward CG

o MK-82 bombs on MER rack inboard shoulder locations 3 and 4.

The slatted F-4E wing model, described in detail in Reference 6, was also evaluated for the two weapon configurations listed above. A third configuration considered was the current production version of the 370 gallon tank, the Sargent Fletcher tank, 85% full.

2.2 Analytical Approaches

2.2.1 Control System Stability and Design Analyses - The Active Control of Flutter (ACF) computer programs described in Reference 7 were used in this effort. The subsonic Doublet Lattice (Reference 8) and the supersonic Mach

---

6. Burkhart, T. H., Gongloff, H. R., Volker, R. E., "Model F-4E (Slat) Aircraft Wing Flutter and Divergence Analysis," McDonnell Aircraft Co. Report MDC A1639, May 1972.
7. Triplett, William E., "Computer Programs for the Frequency Response Stability Evaluations of Servoaeroelastic Systems," McDonnell Aircraft Co. Report MDC A2888, May 1974.
8. Giesing, J. P., Kalman, T. P., Rodden, W. P., "Subsonic Unsteady Aerodynamics for General Configurations, Volumes I and II," AFFDL-TR-71-5, November 1971.

Box (Reference 9) lifting surface aerodynamic theories were used with the version of the computer program based on classical V-g (k type) formulations. Mikhailov and Nyquist stability criteria described in Reference 7 were used to generate analytical transfer function expressions for the flutter control loop compensation electronics. Control loop elements for these studies differ from those listed in Paragraph 4.1.2 of Reference 4 as a result of refinements in the transfer function representations for the aerodynamic, flight control system, and hydraulic components.

2.2.2 <u>Dynamic Response Analyses</u> - The time based computer program (FLTR) described in Reference 10 was used in this effort. The aeroelastic data was identical to that which was used in the Reference 4 studies since constant coefficient aerodynamic data is not currently available using the theories of References 8 and 9.

2.2.3 <u>Flutter Control System Interaction Studies</u> - A root locus computer program (MATLOC), described in Appendix IV of Reference 4, was used in these studies. Fuselage data for the F-4 anti-symmetric modes included in the analysis, as well as a description of the F-4 Stability Augmentation System, were obtained from the Survivable Flight Control System (SFCS) aircraft data given in Reference 11.

2.2.4 <u>Adaptive Flutter Control System Investigation</u> - Extensive investigations of adaptive control systems were conducted. The FLTR program, in combination with the IBM Fast Fourier Transform (FFT) Subroutine HARM was used to generate frequency response functions for the flutter control system. Constant coefficient aerodynamic data from Reference 4 was used in these studies.

2.3 <u>Flutter Control Scheme</u>

2.3.1 <u>Flutter Control Aerodynamic Force Producers</u> - Means to provide the required aerodynamic forces for use in an active flutter control system were investigated. The use of the ailerons for this purpose, as illustrated

---

9. Donato, Vincent W., and Huhn, Charles, R., "Supersonic Unsteady Aerodynamics for Wings with Trailing Edge Control Surfaces and Folded Tips," AFFDL-TR-68-30, January 1968.

10. Landy, Robert J., "Computer Program for Time Response, Fast Fourier Transform, and Adaptive Flutter Control Algorithm Calculations for Servo-aeroelastic Systems," McDonnell Aircraft Co. Report MDC A2889, May 1974.

11. Kisslinger, R. L., Vetsch, G. J., "Survivable Flight Control System Interim Report No. 1 - Studies, Analyses and Approach," AFFDL-TR-71-20, Supplement 2, May 1971.

in Figure 2, appears to be the most practical approach. The F-4 ailerons can produce the required aerodynamic forces for both flutter control and roll control while the flutter control system is in operation.

2.3.2 _Sensor Types and Locations_ - It was determined in the previous feasibility studies that several types of sensor signals were suitable for the flutter control system. Both rate gyro and accelerometer sensors were considered in these studies. Single and double integration was used to obtain the wing twist angle. The sensor locations considered were restricted to the wing and pylon areas.

2.3.3 _Electronic Compensation Technique_ - The compensation technique used is shown in Figure 3. The concept is built on the use of a gain and a pure phase lag network to give the required feedback signal for flutter control of variable store loadings. This requires that the other elements in the control loop be specific and unchanging. This requirement for commonality of components allows for the implementation of the adaptive control system concept which is based on changing a single gain and phase setting.

2.4 _Flight Conditions_

Flight conditions were defined for the study in terms of flight envelope and point design mission.

2.4.1 _Flight Envelope_ - The flight envelopes considered for the F-4 aircraft are shown for the 370 gallon tank and MK-84 cases in Section 4.3. The placards currently in effect for the study configurations are:

	Knots Equivalent Airspeed (KEAS)	Mach Number
370 gallon tank	550	1.6
MK-84 guided bomb	550	.95
MK-82 bombs	550	1.1

(The Mach number placard for a general purpose MK-84 bomb is 1.1.)

2.4.2 _Point Design Mission_ - The mission defined for the study, using the F-4 as a data base, is low or mid altitude interdiction. A duty cycle considering a dash for up to 5 minutes was used in the fatigue, flight safety and operational analysis investigations. Several additional point design missions were considered in the operational analysis investigations.

2.5 _Design Criteria_

Design constraints considered as guidelines for these studies are presented in the following paragraphs. These guidelines are in general agreement with the proposed requirements for Class IV aircraft in the new Military Specification, "Flight Control Systems - Design, Installation and Test of Piloted
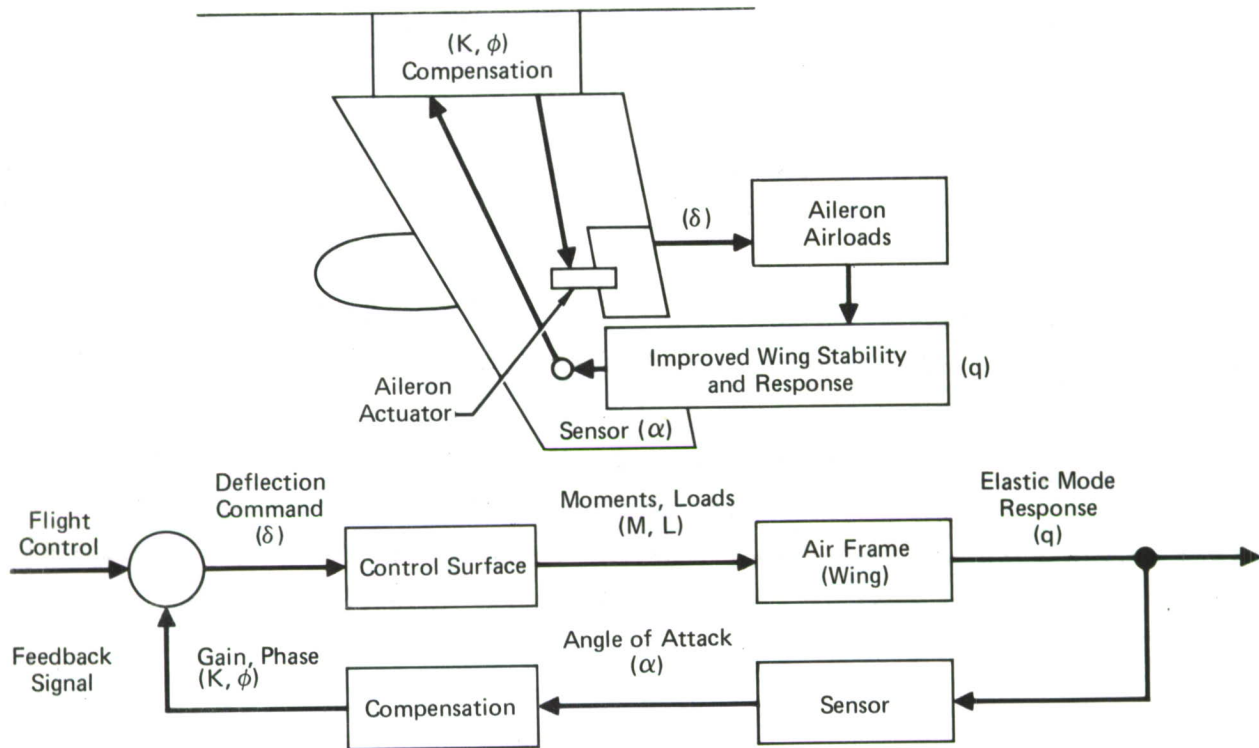
FIGURE 2
ACTIVE FLUTTER CONTROL SCHEME
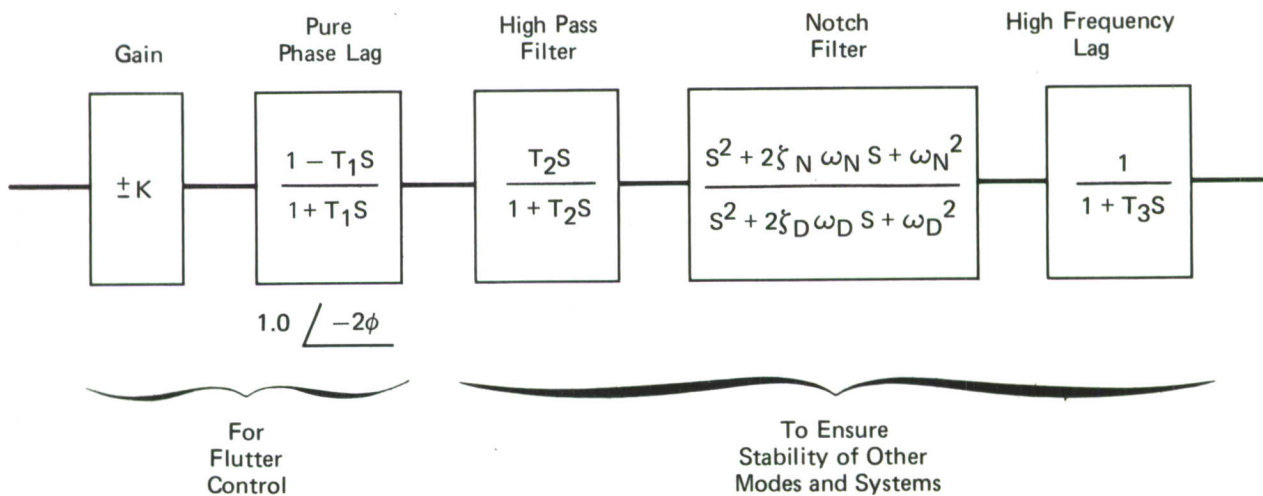
FIGURE 3
GENERAL COMPENSATION NETWORK DESIGN SUITABLE FOR ALL
WING/STORE STUDY CONFIGURATIONS

Aircraft, General Specification for," MIL-F-9490D (Draft), dated March 1974, paragraph 3.1.3.2, 3.1.3.6, 3.1.3.7 and 3.1.7.

2.5.1 Stability Margins - For speeds up to the aircraft limit speed the goals for relative stability were:

	Linear Studies	Nonlinear Studies
Gain Margins	±6.0 dB	±4.5 dB
Phase Margins	±60 deg	±45 deg

2.5.2 Damping Levels - The flutter control system was required to demonstrate positive damping in dynamic response studies when subjected to realistic turbulence levels.

2.5.3 Flight Safety Requirements - The design objective was to use a minimum number of control system components necessary to ensure system reliability with a failure rate of less than one Category IV catastrophic failure (loss of aircraft) per million flight hours. A one-fail-operate criterion was also used.

3. STUDIES AND ANALYSES

3.1 Stability Analyses and Flutter Control System Designs

Results are presented in this section which are based on models for both unslatted and slatted versions of the F-4 wing. The slatted version was used in the later studies, as suggested by the AFFDL, since current plans call for all of the USAF F-4 aircraft to be retrofitted with leading edge slats.

3.1.1 Studies with Unslatted F-4 Wing Model - Flutter onset velocity determinations were made for the unslatted F-4 wing used in the Reference 4 feasibility studies with the three principal store configurations:

o 370 gallon tank - 90% full

o MK-84EO guided bomb

o MK-82 bombs on rack locations 3 and 4

The studies were made using the following three-dimensional aerodynamic representations:

o Doublet Lattice

o Supersonic Mach Box

o Kernel Function

The first two methods were developed under AFFDL sponsorship (References 8 and 9). The third method was previously developed by the contractor.

3.1.1.1 Flutter Velocities Using Three-Dimensional Aerodynamic Theories - The flutter velocity results are plotted in Figures 4 - 6 as a function of Mach number. The new flutter data points are shown along with the experimental coefficient strip theory results reported in Reference 4.

The various three-dimensional aerodynamic representations result in remarkably similar flutter speeds and frequencies. They also show excellent agreement with the experimental coefficient strip theory results. Figure 7 shows the V-g plots of the critical mode (3rd still-air mode) at M = 0.9 and 1.2 for both strip theory and three-dimensional aerodynamics for the 370 gallon tank - 90% full configuration. The flutter mechanism for this configuration involves coupling between the first wing bending mode and a new wing torsion mode created by the large pitch inertia of the store. The new mode has a frequency (8.78 Hz) just above the wing bending frequency (7.18 Hz) at zero airspeed. The slope ($\Delta g/\Delta V$) at the crossing for the coalesced flutter mode is a measure of the energy content, or "explosiveness," of the flutter mechanism. It was shown in Reference 4 that this slope at flutter onset is also a primary measure of the "controllability" of flutter; that is the less steep
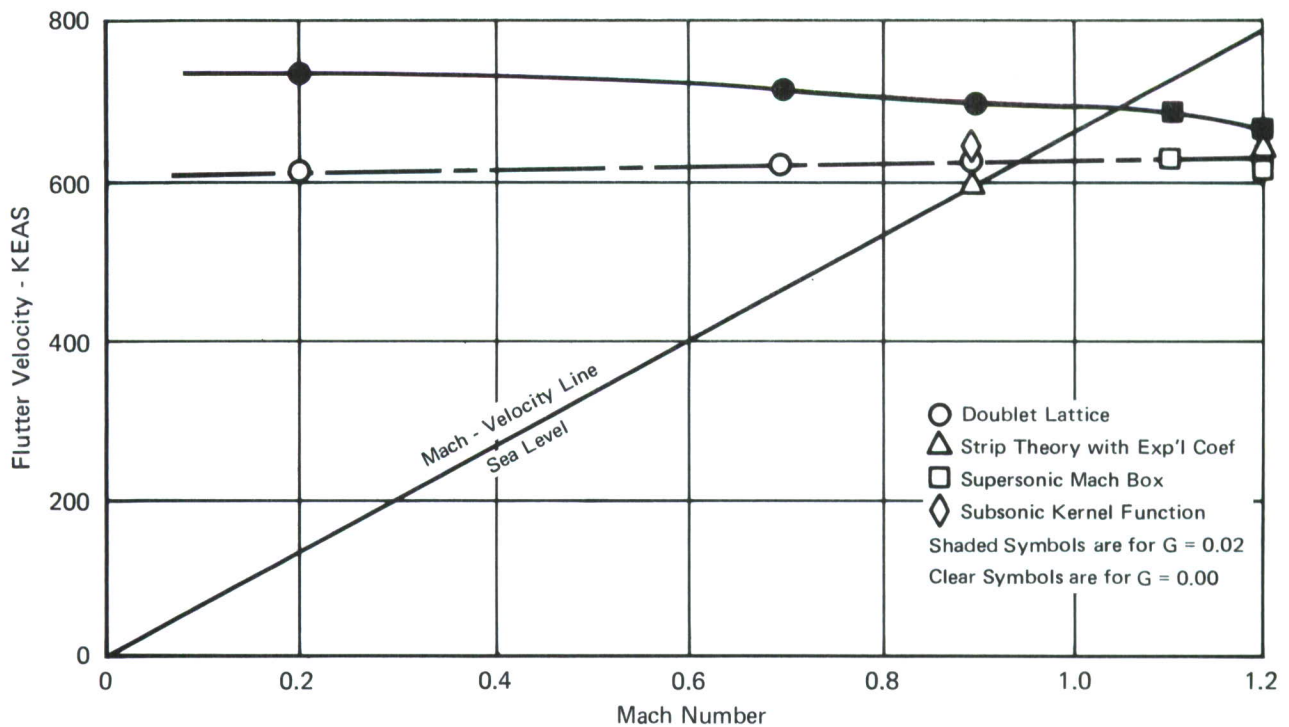
FIGURE 4
**SUMMARY OF FLUTTER ONSET VELOCITIES FOR THE F-4 WING/370 GALLON TANK -
90% FULL CONFIGURATION WITH VARIOUS AERODYNAMIC THEORIES**

FIGURE 5
**SUMMARY OF FLUTTER ONSET VELOCITIES FOR THE F-4 WING/MK-84EO
CONFIGURATION WITH VARIOUS AERODYNAMIC THEORIES**

10

FIGURE 6
**SUMMARY OF FLUTTER ONSET VELOCITIES FOR THE F-4 WING/MK-82(3,4)
CONFIGURATION WITH VARIOUS AERODYNAMIC THEORIES**

FIGURE 7
**FLUTTER CROSSINGS AT M = 0.9 AND 1.2 FOR THE 370 GALLON TANK - 90%
FULL CONFIGURATION WITH VARIOUS AERODYNAMIC THEORIES**

the flutter crossings the larger the flutter control system stability margins. The crossings with three-dimensional aerodynamics were always less steep than with the strip theory aerodynamics.

Table 1 summarizes the Mach-airspeed match-point flutter velocities at sea level for the three study configurations based on the three-dimensional aerodynamic theories. The F-4 with stores has a maximum velocity capability of approximately 725 knots at sea level with full afterburner when carrying stores. Only one of the configurations, the 370 gallon tank - 90% full, flutters at less than 725 knots when structural damping of g = 0.02 is included in the analysis.

3.1.1.2 Flutter Control System Compensation Designs - Figure 8 is a Nyquist plot for the uncompensated 370 gallon tank - 90% full configuration at 750 KEAS with Mach box aerodynamics and g = 0.02 structural damping. Since 750 KEAS is above the passive flutter speed a counter-clockwise (CCW) encirclement of the origin is required for stability. A wing tip twist sensor (two linear accelerometers integrated twice) is used as the feedback signal. The transfer functions for the power actuator, secondary actuator, accelerometers, and high pass filter are identical to those used in Reference 4. The unstable loop with compensation will yield stability margins of about ±6.6 dB and ±47 deg. The margins for the same case with strip theory aerodynamics were ±6 dB and ±35 deg. The figure shows that about 46 deg of phase lead are required to stabilize the system. With strip

TABLE 1
SUMMARY OF F-4 FLUTTER VELOCITY MATCH POINTS WITH
THREE-DIMENSIONAL AERODYNAMICS

Configuration	G = 0.00			G = 0.02		
	Flutter Velocity (knots)	Mach	Frequency (Hz)	Flutter Velocity (knots)	Mach	Frequency (Hz)
370 Gal. Tank - 90% Full	629	0.95	8.5	695	1.05	8.42
MK-84EO	800	1.20	10.64	>925	>1.40	
MK-82(3,4)	370	0.55	7.54	770	1.17	7.74
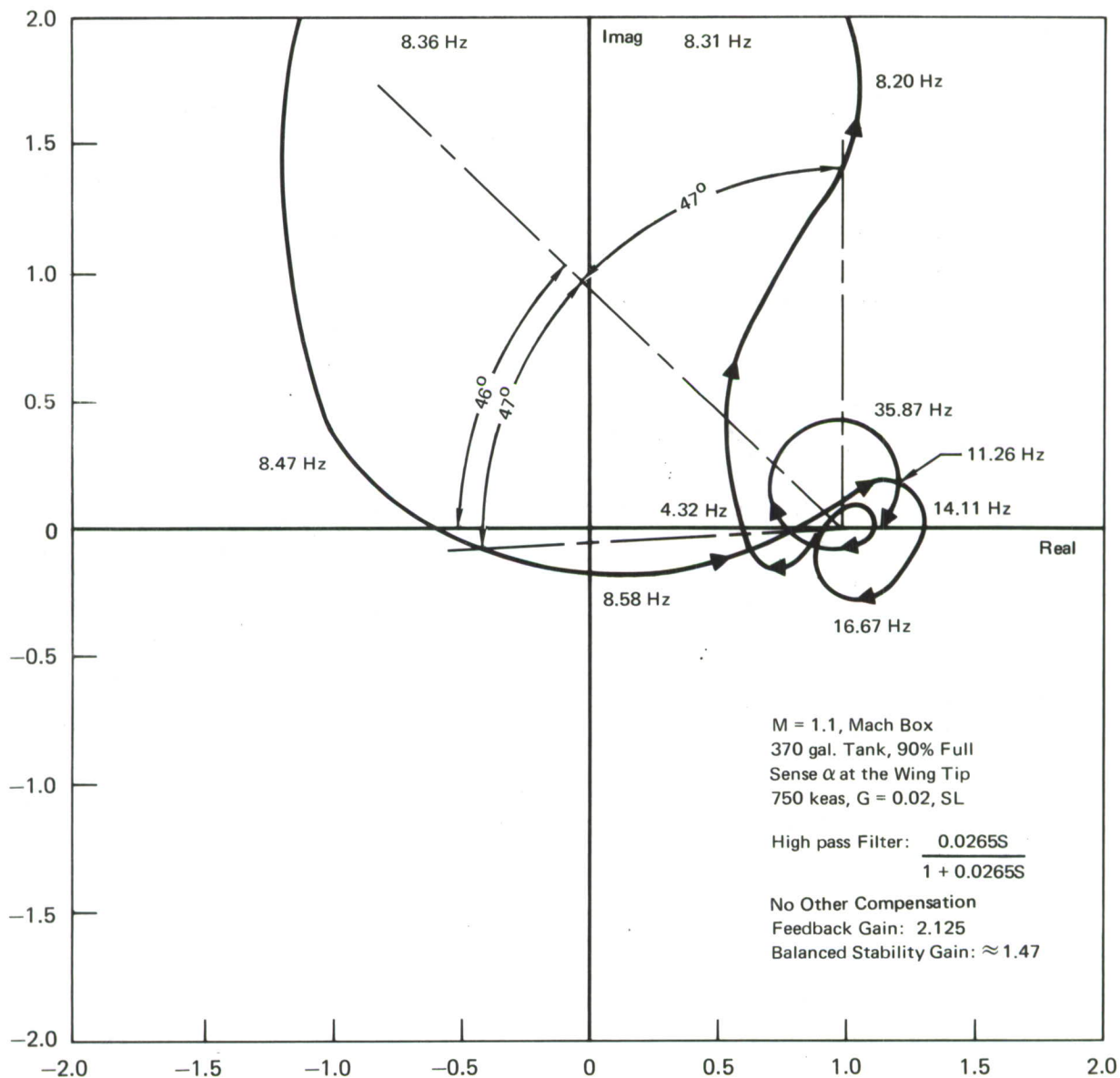
FIGURE 8

NYQUIST PLOT FOR THE UNCOMPENSATED 370 GALLON TANK - 90% FULL CONFIGURATION WITH MACH BOX AERODYNAMICS

theory aerodynamics about 16 deg was necessary. The feedback gain for the compensated system would be approximately 1.5. This compares with 5.34 for the strip theory aerodynamics. The demands on the hydraulic system are thus reduced. These results indicate that the use of three-dimensional aerodynamics, although altering the system compensation requirements, improve the stability margin data over the strip theory results presented in Reference 4.
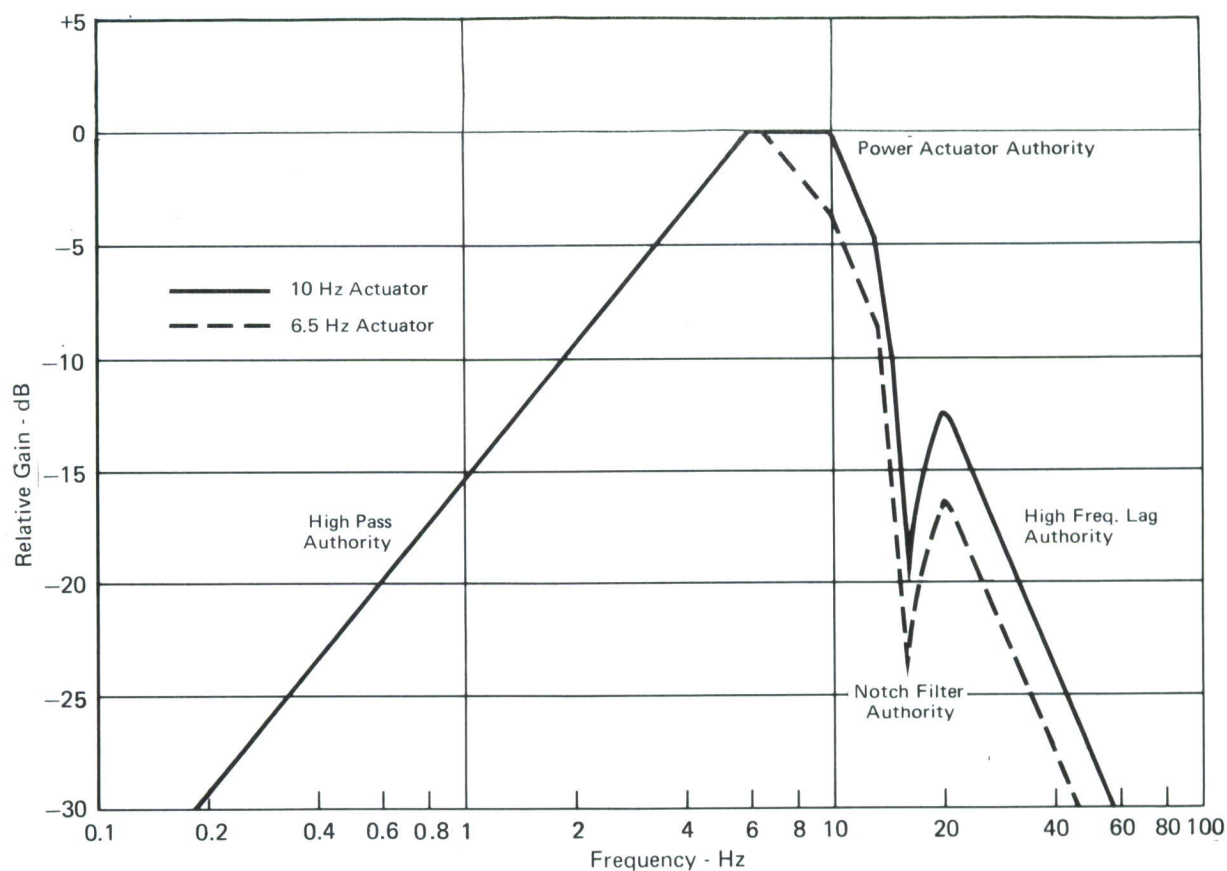
FIGURE 9
BODE GAIN PLOT FOR 6.5 Hz AND 10 Hz ACTUATOR BANDWIDTHS

Control system design studies were performed with the three wing/store study configurations. The transfer functions used for the secondary actuator, accelerometer, and high pass filter were identical to those listed in Reference 4. A more realistic surface power actuator transfer function with a break frequency at 6.5 Hz, rather than the previously used 10 Hz break frequency, was incorporated in the control loop model. The reasons for this break frequency shift are discussed in Section 3.5.4 of this report. A Bode gain plot illustrating the effect of using a 6.5 Hz rather than a 10 Hz bandwidth is shown in Figure 9. The new break frequency when compared with the old break will require that the feedback compensation be designed with

about 30% more gain and 10 deg less phase lag to stabilize a 10 Hz flutter instability.

The high pass filter, notch filter and high frequency lag elements in the feedback loop were not changed with the study configurations. Transfer functions for these fixed elements were selected to permit stabilization of each of the study configurations by altering only the feedback gain and the pure phase lag term to facilitate the implementation of an adaptable flutter control system. A complete summary of transfer functions for the active flutter control system, including compensation, is given in Table 2. The compensations are designed to give balanced stability margins for g = 0.02 Mach 1.1, sea level conditions. The phase and gain compensations for the two sub-flutter configurations, MK-84EO and MK-82(3,4) center the flutter mode loop of the Nyquist plot about the positive real axis while maintaining at least a 6 dB gain margin against control system instability. This compensation will allow the flutter control system to reduce the flutter mode response to gust turbulence below flutter onset and, if flutter were to occur at the max "q" condition, it would be stabilized.

Figure 10 shows the stability margins for the 370 gallon tank - 90% full configuration. All of the solid line data was derived from Mach-velocity matched point aerodynamic data based on the supersonic Mach box and doublet lattice theories. Also shown in the plot are strip theory results, reported in Reference 4, using M = 0.9 aerodynamics. At high post-flutter onset velocities, outside the flight envelope of the aircraft, the range of stable feedback gains diminishes and the balanced gain margin feedback gain increases sharply. This is due to the collapse of the flutter mode loop in the Nyquist plot with increasing airpseed. At the design condition, in the region of 725 knots with g = 0.02, the 370 gallon tank - 90% full configuration has gain and phase margins of about ±6.4 dB and ±50 deg.

3.1.1.3 <u>Stability Margins with Altitude Variation</u> - Stability margin surveys with altitude variations conducted for the 370 gallon tank - 90% full configuration showed that phase and gain margins are generally independent of altitude at the same equivalent airspeed when using three-dimensional aerodynamic theories. Figure 11 is the "high q" portion of the F-4 flight envelope showing the 370 gallon tank flutter onset boundary and several g = 0.02 gain margin data points. In light of the Figure 10 results, gain

TABLE 2
SUMMARY OF F-4 FLUTTER CONTROL SYSTEM
TRANSFER FUNCTIONS

Common Control Loop Elements

Power Actuator	$\dfrac{1}{1 + 0.0244S}$	6.5 Hz Break
Secondary Actuator	$\dfrac{226^2}{226^2 + 2\,(0.86)\,(226)S + S^2}$	36 Hz Resonance
Accelerometer	$\dfrac{502^2}{502^2 + 2\,(0.6)\,(502)S + S^2}$	80 Hz Resonance
High Pass Filter	$\dfrac{0.0265S}{1 + 0.0265S}$	6 Hz Break
Notch Filter	$\dfrac{100^2 + 2\,(0.1)\,(100)S + S^2}{100^2 + 2\,(0.7)\,(100)S + S^2}$	16 Hz Resonance
High Frequency Lag	$\dfrac{1}{1 + 0.0158S}$	10 Hz Break

Specialized Compensation

Configuration	Gain	Pure Phase Lag
370 Gal. - 90% Full	−2.21	$\dfrac{1 - 0.00607S}{1 + 0.00607S}$
MK-84 EO	2.00	None Required
MK-82 (3,4)	−1.50	$\dfrac{1 - 0.00920S}{1 + 0.00920S}$
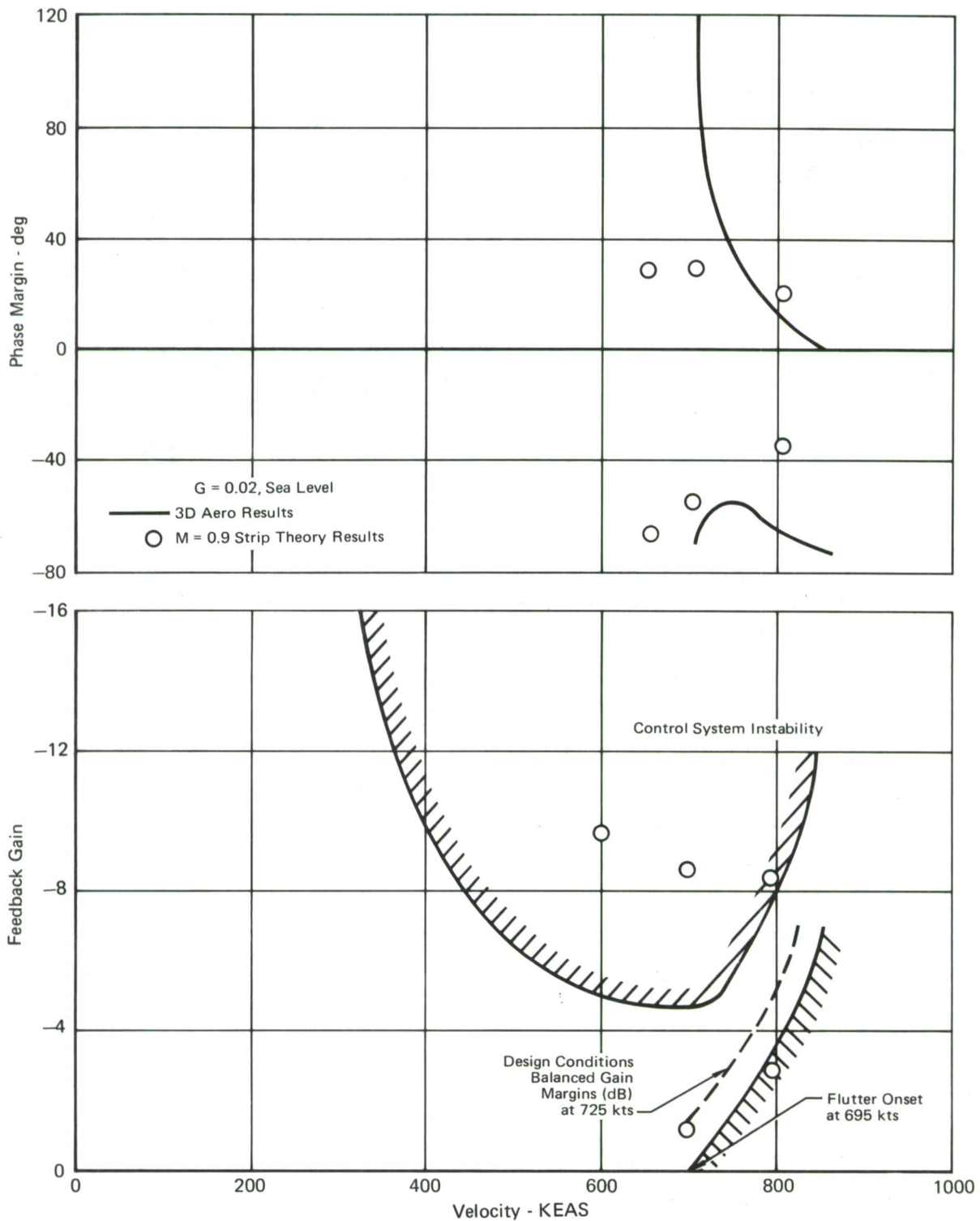
FIGURE 10
SUMMARY OF STABLE GAIN AND PHASE MARGIN RESULTS FOR THE
370 GALLON TANK - 90% FULL CONFIGURATION WITH VARIOUS
AERODYNAMIC THEORIES
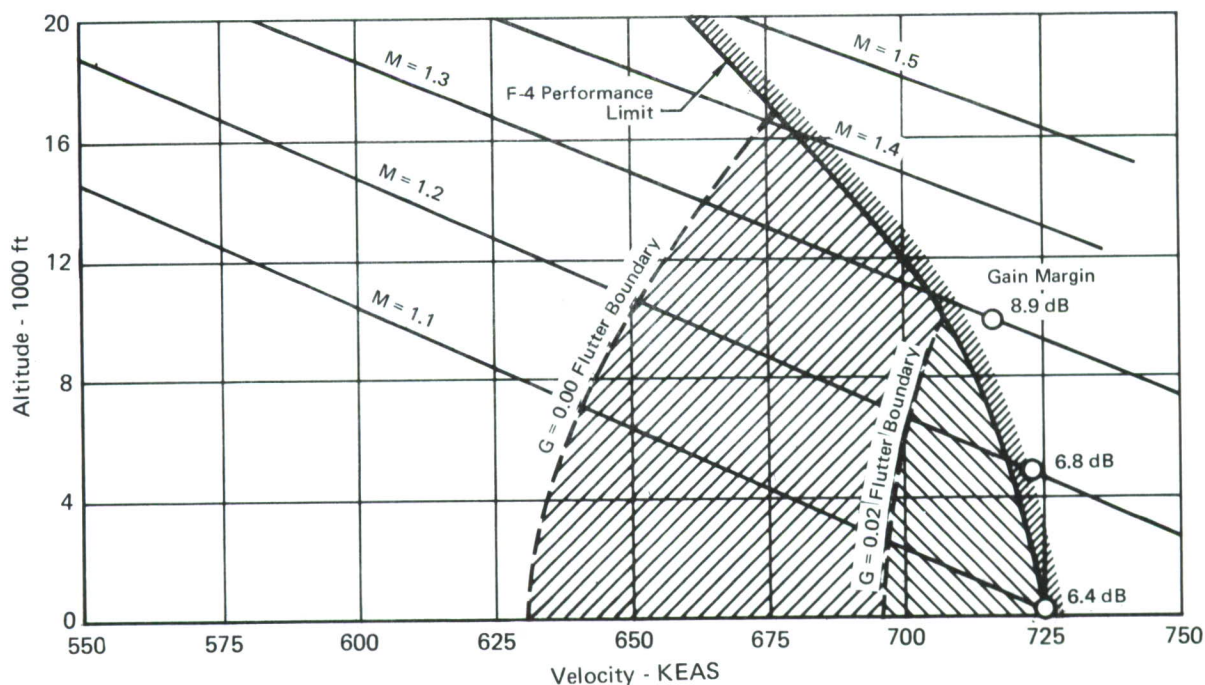
FIGURE 11
HIGH "q" CORNER OF THE F-4 FLIGHT ENVELOPE SHOWING MACH BOX
FLUTTER ONSET VELOCITIES AND ACTIVE CONTROL GAIN MARGINS
FOR THE 370 GALLON TANK - 90% FULL CONFIGURATION

margins at lower velocities would be expected to exceed those near the F-4 performance limit. The lowest margin is ±6.4 dB at M = 1.1, sea level conditions. Phase margins are shown in Figure 12 as a function of airspeed and altitude. Unlike the studies performed with M = .9 strip theory reported in Reference 4, the supersonic Mach box stability studies show relatively little phase margin degradation with altitude increase. Both Figures 11 and 12 assume that the flutter control system feedback gain and phase compensation are adjusted slightly with altitude for maximum stability margins. The necessary compensation adjustments are given in Figures 13 and 14 for the 370 gallon tank - 90% full configuration. For g = 0.02, for example, the plots show that between sea level and 10 thousand feet the gain should range between -2.21 and -4.5 with an accompanying phase lag range of 126 deg to 156 deg. For this particular case the best <u>fixed</u> compensation is a gain of -2.8 and a phase lag of 137 deg resulting in gain margins and phase margins of at least ±4.4 dB and ±30 deg, respectively, throughout the F-4 flight envelope. Figure 13 shows that a feedback gain of -3.15 at sea level is necessary to give balanced stability margins for g = 0.00. With strip theory aerodynamics the necessary gain at M = 1.1, g = 0.00 sea level conditions was -5.34. Thus, even with the adverse gain effect of the new

18
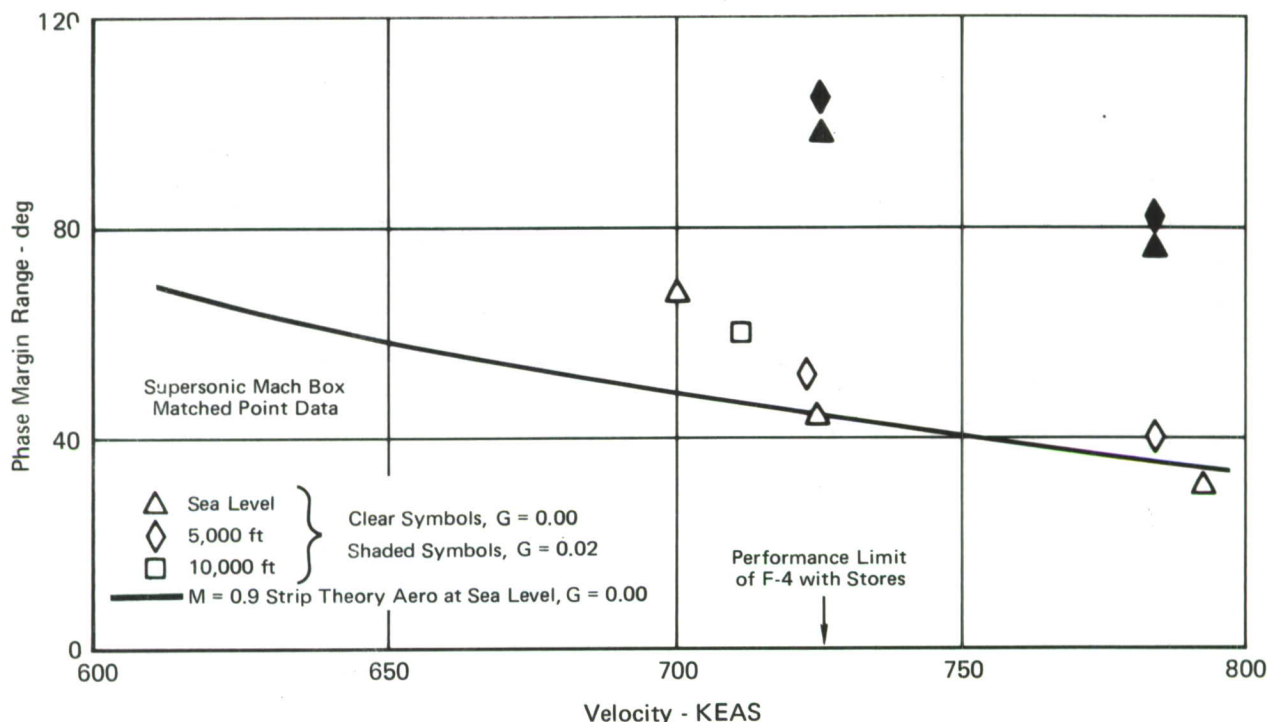
FIGURE 12

**VARIATION OF PHASE MARGIN RANGE WITH ALTITUDE AND VELOCITY
FOR THE 370 GALLON TANK - 90% FULL CONFIGURATION**

power actuator included, the use of three-dimensional "matched-point" aero-dynamics has resulted in about a 40% decrease in required feedback gain and, thus,a reduction in the performance demands on the hydraulic system.

    3.1.2 <u>Studies with Slatted F-4 Wing Model</u> - Several slatted F-4 wing/ store configurations were evaluated for active flutter control. The slatted F-4 wing model (described in detail in Reference 6) is a lumped-mass, finite element structural representation. The wing is represented by 57 influence coefficient points and associated mass points. The wing is divided into 8 aerodynamic sections identical to those used in the unslatted F-4 wing model.

    3.1.2.1 <u>Effects of Symmetric and Anti-Symmetric Modes</u> - Flutter onset speeds resulting with various aerodynamic theories are compared in Figures 15 through 17 for both symmetric and anti-symmetric modes for three wing/ store configurations. The current production version of the 370 gallon tank, the Sargent Fletcher tank, was used as the tank store in these studies rather than the older McDonnell designed tank. The minimum flutter speed for the Sargent Fletcher tank with the slatted wing occurs at the 85% full

19
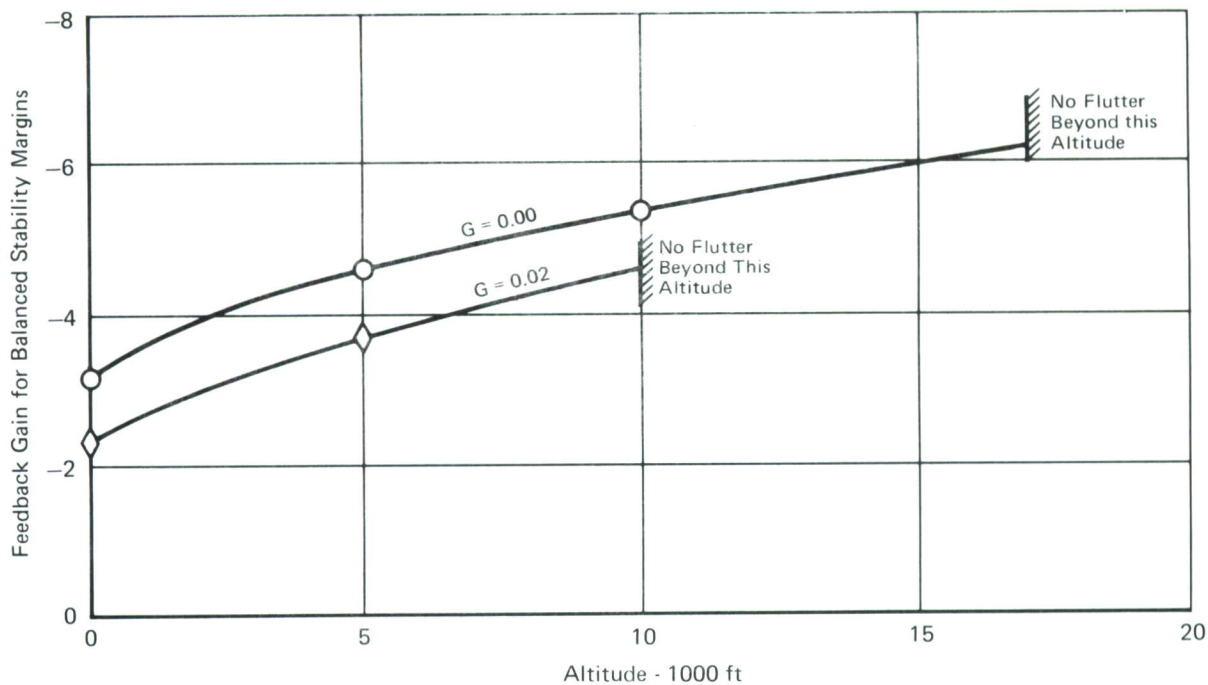
FIGURE 13
VARIATION OF BALANCED STABILITY MARGIN FEEDBACK GAIN FOR THE 370 GALLON TANK - 90% FULL CONFIGURATION FLYING AT MAXIMUM q
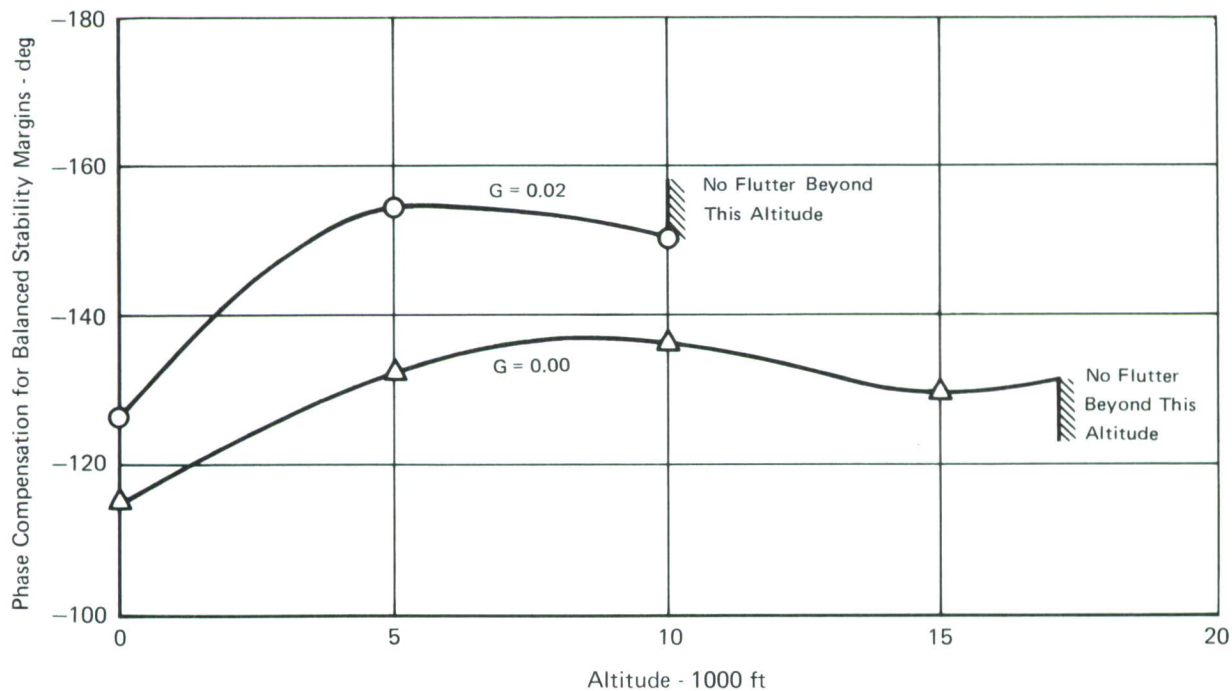
FIGURE 14
VARIATION OF BALANCED STABILITY MARGIN PHASE COMPENSATION FOR THE 370 GALLON TANK - 90% FULL CONFIGURATION FLYING AT MAXIMUM q

Mach 0.9

Strip Theory — 8.26 Hz
Doublet Lattice — 8.25 Hz
} Symmetric Modes

Strip Theory — 8.73 Hz
Doublet Lattice — 8.55 Hz
} Anti-Symmetric Modes

Flutter Velocity - KEAS

Mach 1.2

Strip Theory — 8.18 Hz
Mach Box — 8.25 Hz
} Symmetric Modes

Strip Theory — 8.90 Hz
Mach Box — 9.10 Hz
} Anti-Symmetric Modes

Flutter Velocity - KEAS

Flutter speed increase resulting from addition of G = 0.02 structural damping
All studies used sea level air density
Frequencies are for G = 0.02 structural damping

FIGURE 15
SUMMARY OF FLUTTER ONSET VELOCITIES FOR THE SLATTED F-4 WING/
370 GALLON - 85% FULL SGT. FLETCHER TANK CONFIGURATION
WITH VARIOUS AERODYNAMIC THEORIES
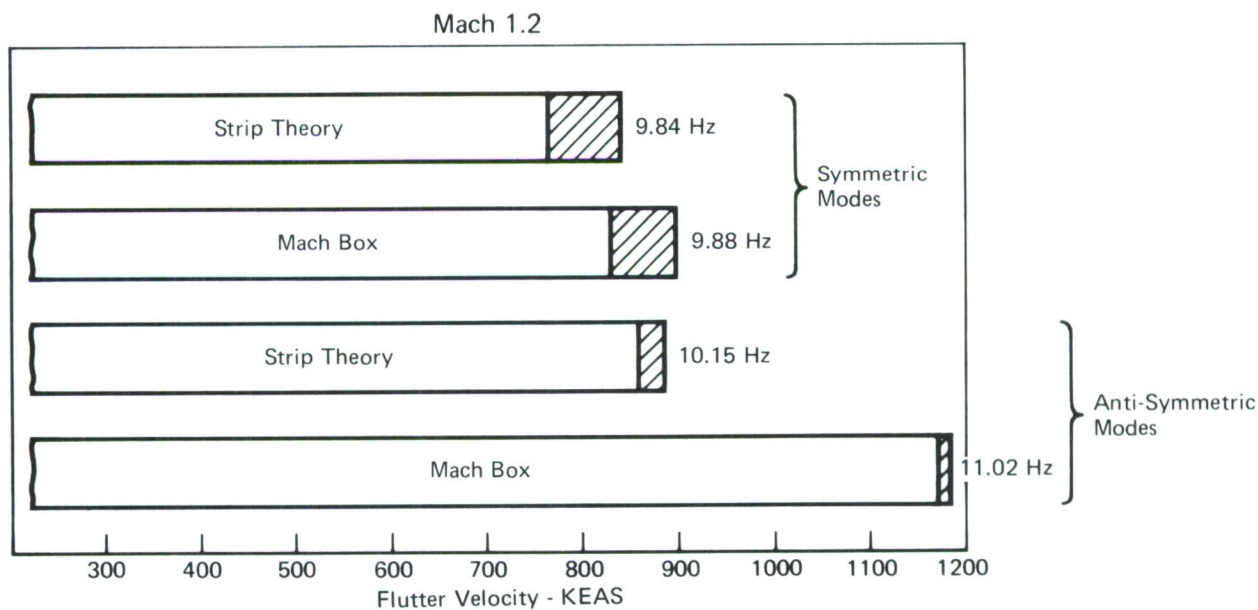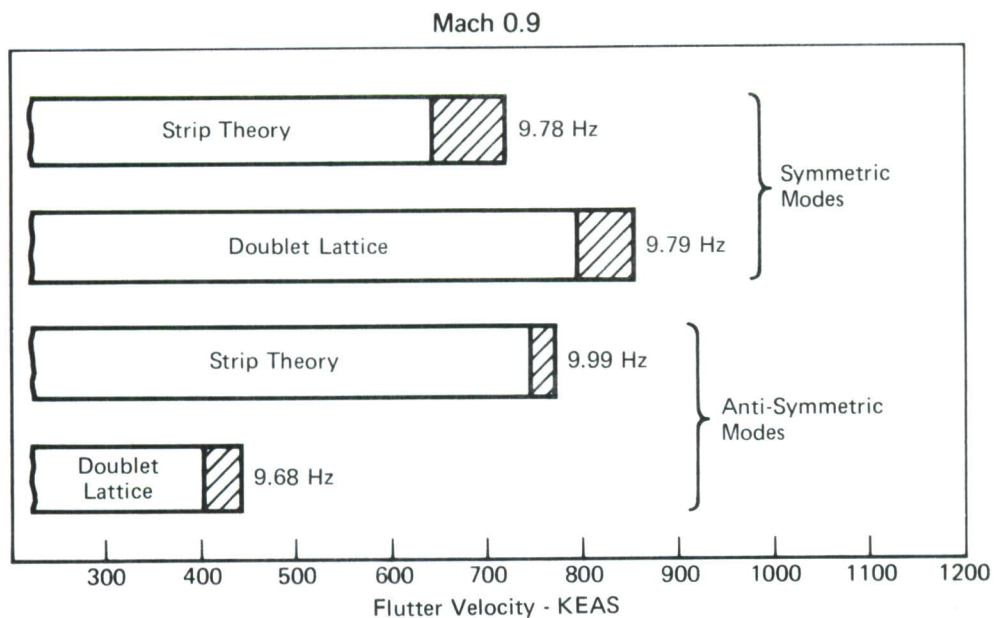
Mach 0.9

Strip Theory	9.78 Hz	Symmetric Modes
Doublet Lattice	9.79 Hz	
Strip Theory	9.99 Hz	Anti-Symmetric Modes
Doublet Lattice	9.68 Hz	

Flutter Velocity - KEAS

Mach 1.2

Strip Theory	9.84 Hz	Symmetric Modes
Mach Box	9.88 Hz	
Strip Theory	10.15 Hz	Anti-Symmetric Modes
Mach Box	11.02 Hz	

Flutter Velocity - KEAS

Flutter speed increase resulting from addition of G = 0.02 structural damping

All studies used sea level air density

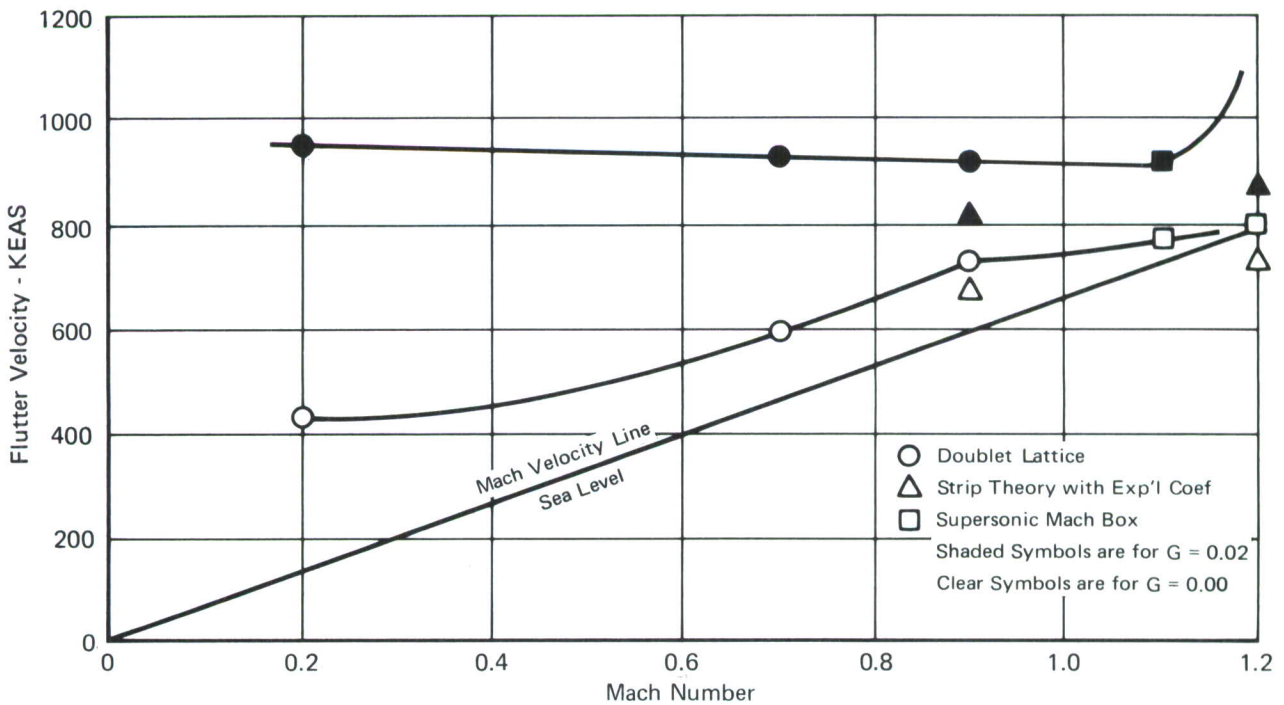Frequencies are for G = 0.02 structural damping

FIGURE 16

SUMMARY OF FLUTTER ONSET VELOCITIES FOR THE SLATTED F-4 WING/
MK-84EO CONFIGURATION WITH VARIOUS AERODYNAMIC THEORIES
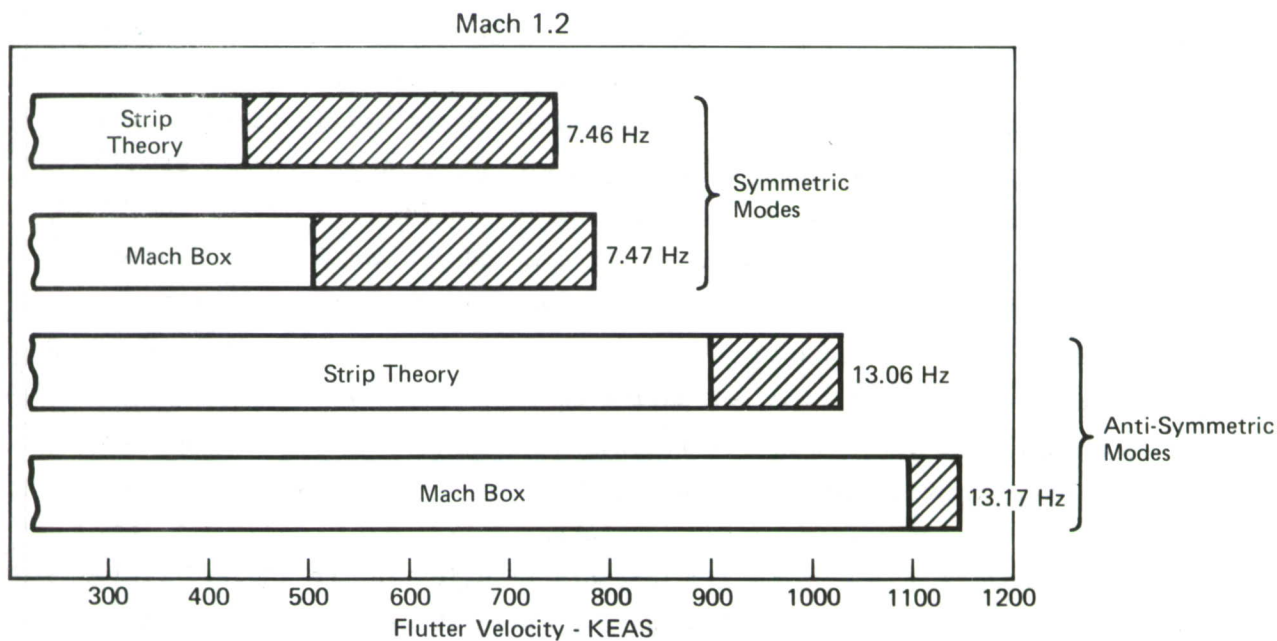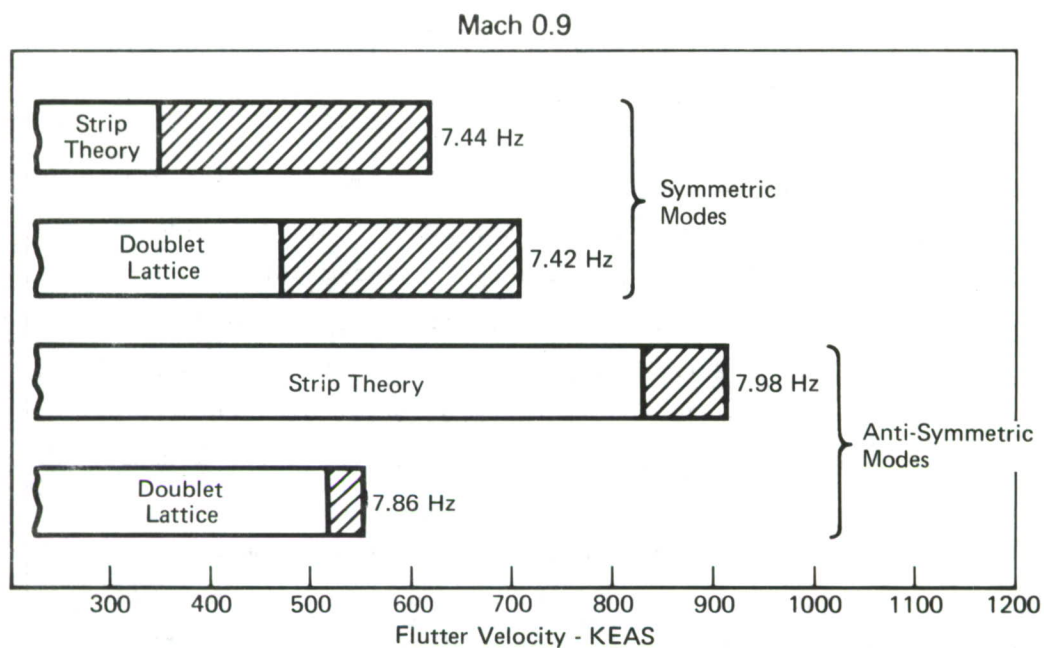
FIGURE 17

**SUMMARY OF FLUTTER ONSET VELOCITIES FOR THE SLATTED F-4 WING/
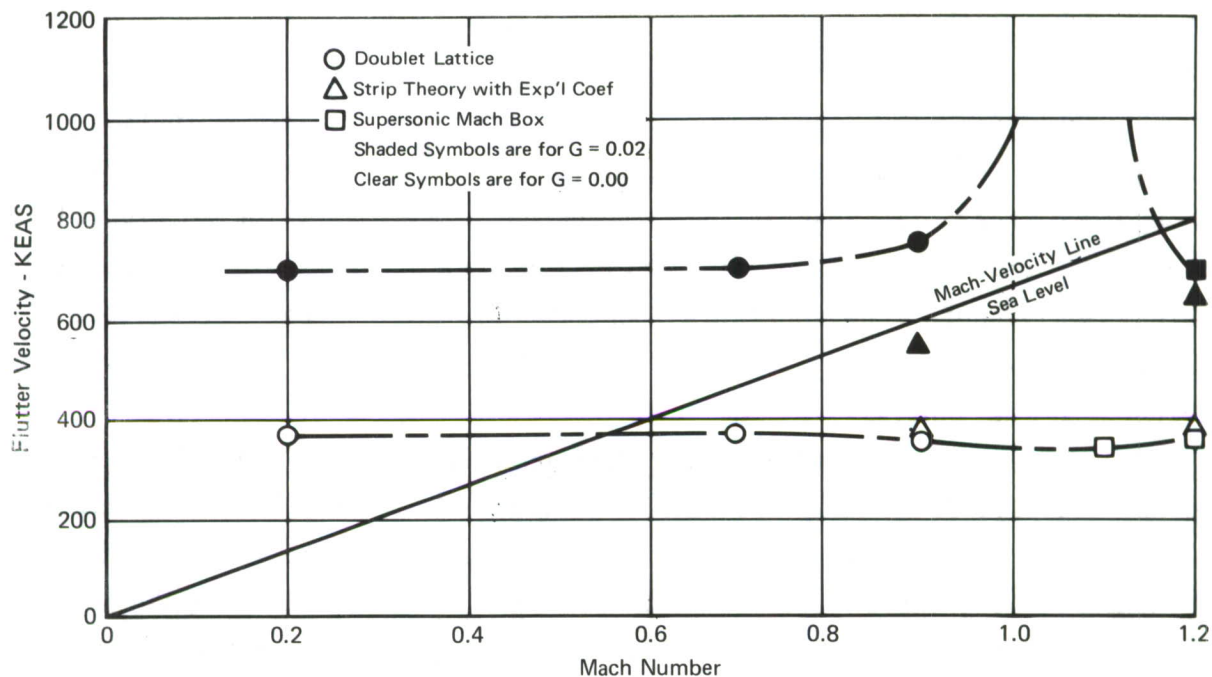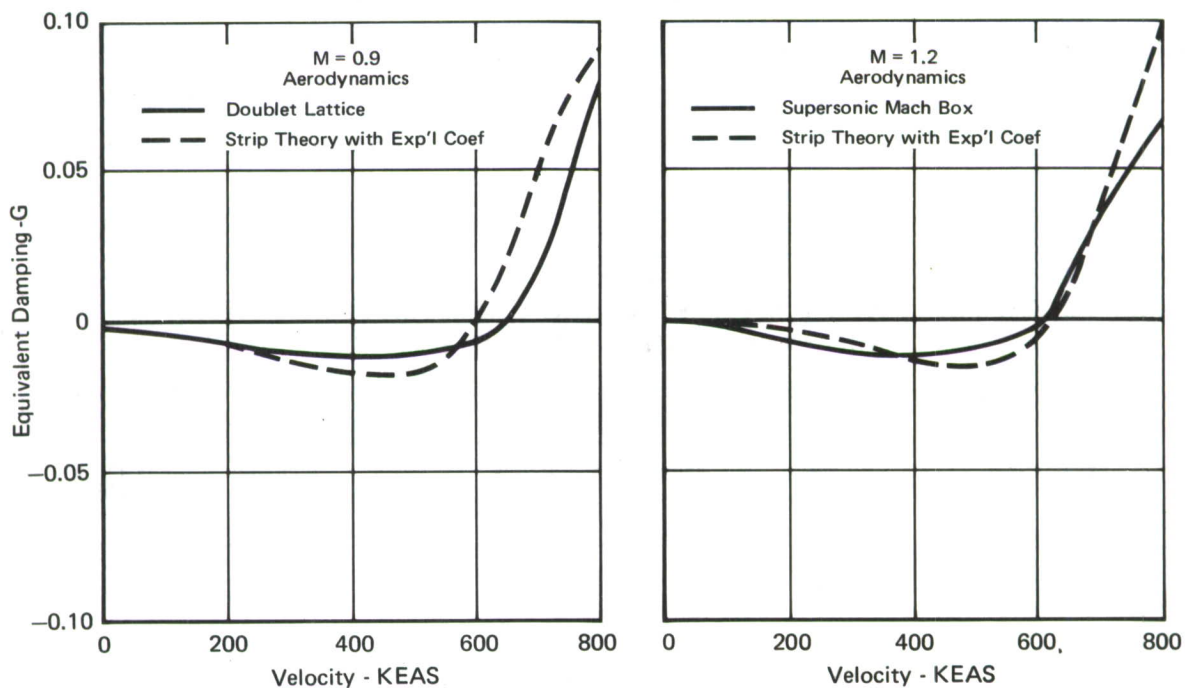MK-82(3,4) CONFIGURATION WITH VARIOUS AERODYNAMIC THEORIES**

condition and this configuration was thus chosen for analysis. The MK 84EO and MK-82(3,4) configurations are identical to those used with the original unslatted F-4 wing model.

The most noticeable aspect of the data shown in Figures 15 through 17 is that the anti-symmetric doublet lattice flutter results are quite low. The flutter speed for the MK-84EO (with forward cg) anti-symmetric case, for example, decreases from 780 KEAS with strip theory to 450 KEAS with doublet lattice aerodynamics. The reduction in flutter speed runs contrary to the trend, noted in the previously reported symmetric studies and the current Mach box supersonic anti-symmetric studies, that the three-dimensional theories generally give higher speeds than strip theory.

The flutter onset data when using doublet lattice anti-symmetric aerodynamics also conflict with observed flight test data and are obviously in error. The large store cases were investigated further in an effort to determine a reason for the low predicted flutter speeds. Studies were made using identical anti-symmetric vibration modes but with doublet lattice aerodynamic influence coefficients assuming symmetric rather than anti-symmetric flow conditions. The flutter speeds from these studies were more than double those determined with "pure" anti-symmetric doublet lattice studies (i.e., anti-symmetric aerodynamics and anti-symmetric modes) and substantially higher than the "pure" symmetric studies. A full summary of the MK-84 EO flutter results is given in Table 3. The mixed doublet lattice studies fall in line with the flutter speed improvement noted for both the strip theory and Mach box aerodynamics with anti-symmetric modes. Strip theory and Mach box make no provision for anti-symmetric aerodynamics.

The anti-symmetric and symmetric air load distributions used with doublet lattice differ principally in the inboard region of the wing. It was conjectured that the large differences in flutter speed could conceivably be attributed to the difference in air load distribution in the inboard region of the wing. To test out this hypothesis a strip theory anti-symmetric analysis was conducted with no aerodynamics acting on the inboard two sections of the wing planform, representing 27% of the exposed wing semi-span. The configuration employed was the F-4 with MK-84EO at Mach 0.9, sea level. The resulting flutter speed and flutter frequency agreed within a fraction of a percent with the prior studies where strip theory aerodynamics were included over the whole wing, leading to the conclusion that the inboard aerodynamic variations have only a very slight effect on the flutter mechanism.

TABLE 3
SUMMARY OF MK-84EO/SLATTED F-4 MACH 0.9 FLUTTER STUDIES
G = 0.00, SL

Idealization	1st Crossing			2nd Crossing		
	Velocity (kts)	Frequency (Hz)	Modal Inter-action	Velocity (kts)	Frequency (Hz)	Modal Inter-action
Doublet Lattice Symmetric Aero Symmetric Modes	804.5	9.83	2, 3			
Doublet Lattice Anti-Symmetric Aero Anti-Symmetric Modes	409.1	9.81	2, 4	495.7	11.36	3, 4
Doublet Lattice Symmetric Aero Anti-Symmetric Modes	957.8	10.43	2, 4	1083.9	11.18	3, 4
Strip Theory Symmetric Modes	646.6	9.88	2, 3			
Strip Theory Anti-Symmetric Modes	756.3	9.99	2, 4	838.0	11.29	3, 4

The obviously erroneous results using doublet lattice anti-symmetric aero-dynamics has not been resolved to date.

The phase lag compensation required for flutter control for each of these slatted F-4 configurations is shown in Table 4. As would be expected from the flutter onset data shown in Figures 15 through 17 significantly different compensations are required as a function of both Mach number and the modal idealizations.

3.1.2.2 <u>Effects of Normal Store Manufacturing Tolerances</u> - Four slatted F-4/MK-84 configurations with different mass characteristics were selected to show the effect of the normal variation in the mass characteristics of production stores on the feedback compensation required for flutter control. The four configurations, selected to give a maximum variation in flutter frequency and velocity, are:

    I.   Nominal MK-84 without the 320 lb nose-mount laser guidance unit

    II.   Nominal MK-84 with the laser guidance unit (MK-84EO)

    III. MK-84EO with max weight, min pitch inertia, most forward CG

    IV.   MK-84EO with max weight, max pitch inertia, most aft CG

Case III is the previously analyzed MK-84 configuration.

Mach 0.9 experimental aerodynamic coefficient data, C_{L_α} = 4.6/radian and CP = 25% (strip theory aerodynamics), was used in the analysis. Table 5 summarizes the MK-84 store mass characteristics and stability results for a symmetric airplane analysis. Configuration III, as with the unslatted F-4, remains the critical flutter case at 647 knots (g = 0.00) and 9.88 Hz. This compares with the unslatted wing values of 683 knots and 10.71 Hz. The phase lags required by the various store configurations to obtain balanced phase margins are listed at the bottom of Table 5. If the feedback compensation is adjusted prior to flight for a nominal MK-84EO configuration (Case II) then the phase compensation required at the flight velocity of 800 KEAS would be 4 deg less for Case III but 40 deg more for Case IV. Even for configurations with very large phase margins, such as all of these MK-84 cases, this 44 deg phase variation with manufacturing tolerances reemphasizes the inherent difficulties with the use of fixed compensation networks.

These data, in addition to the rather unsatisfactory comparisons of Section 3.1.2.1, firmly establish the desirability of an adaptive control system in an operational application. The phase variation described above would result in unacceptable phase margins with a fixed feedback compensation design. The

TABLE 4
SUMMARY OF PHASE LAG REQUIRED FOR FLUTTER CONTROL WITH THREE-DIMENSIONAL AERODYNAMICS FOR SYMMETRIC AND ANTI-SYMMETRIC MODES - SLATTED F-4

G = 0.02 Structural Damping
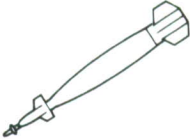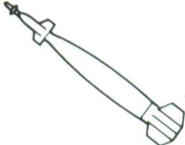
Mach = 0.9 (Doublet Lattice - Sea Level)

Configuration		Phase Lag (deg)
370 Gal. - 85% Full	Symmetric	30
	Anti-Symmetric	62
MK-84 EO	Symmetric	137
	Anti-Symmetric	63
MK-82 (3,4)	Symmetric	82
	Anti-Symmetric	92

Mach = 1.2 (Mach Box - Sea Level)

Configuration		Phase Lag (deg)
370 Gal. - 85% Full	Symmetric	76
	Anti-Symmetric	143
MK-84 EO	Symmetric	124
	Anti-Symmetric	140
MK-82 (3,4)	Symmetric	153
	Anti-Symmetric	159

TABLE 5
RESULTS OF MK-84/SLATTED F-4 STABILITY STUDIES

Mass Characteristics	I	II	III	IV
	MK-84 Nominal	MK-84EO Nominal	MK-84EO Fore CG	MK-84EO Aft CG
Weight (lb)	1954.0	2276.5	2351.5	2351.5
I_{pitch} and I_{yaw} (slug-ft^2)	375.0	490.2	470.2	530.2
I_{roll} (slug-ft^2)	17.6	24.3	24.3	24.3
CG inches Aft of Forward Lug	14.9	15.0	12.0	18.0

M = 0.9 Strip Theory

Flutter Characteristics	I		II		III		IV	
	G = 0.00	G = 0.02	G = 0.00	G = 0.02	G = 0.00	G = 0.02	G = 0.00	G = 0.02
Velocity (KEAS)	812	832	719	763	647	725	768	795
Frequency (Hz)	10.86	10.79	9.97	9.86	9.88	9.78	9.62	9.57

Phase Lag Required to Suppress Flutter Mechanism (G = 0.02) at 800 Knots

I	II	III	IV
152°	97°	93°	137°

compensation should be responsive not only to variations in mass characteristics of the same store but also to changes in store type.

While continuing these MK-84 mass variation studies, it was found that an increase in the airstream velocity resulted in an almost linear decrease in the desired phase lag compensation. Figure 18 shows the optimum feedback compensation phase lag as a function of velocity for the four versions of the MK-84 under study. The critical configuration, MK-84EO with forward CG (Case III), has a compensation phase lag decrease of approximately 40 deg when going from 750 to 800 knots. The phase margins at these velocities range from nearly ± 180 deg to ± 60 deg. It is apparent that for this particular store a feedback compensation which is adjusted not only as a function of the mass characteristics but also as a function of the velocity would ensure the best possible balanced phase margins.

3.1.3 <u>Discussion of Asymmetric Effects</u> - The general problem of flutter for aircraft carrying external stores is extremely complex. The complexity is amplified because of the great number of possible configurations. The F-4, for example, has a number of possible combinations in excess of 2,000,000 if mixed asymmetric store loadings are considered with the current spectrum of stores. If weight and center of gravity variations caused by manufacturing tolerances are included the number of possible combinations increases astronomically.

There are, however, just three basic types of wing/external store flutter. These are,

Type 1)   store flutter on a flexible pylon

Type 2)   existing wing flutter mode modified by the stores (primarily light stores - frequency near wing flutter frequency)

Type 3)   new wing flutter mode created by the stores (primarily heavy stores - frequency much lower than wing flutter frequency).

Type one flutter, in which the store itself is unstable, is possible for a store with large aerodynamic surfaces mounted on a flexible pylon. This type of instability is easily recognized in the early stages of an aircraft design. It is usually easy to fix by pylon stiffening, and thus in "real world" aircraft, such as the F-4, type one flutter is not a problem area. The second and third types represent most of the external store flutter problems in operational aircraft. Type 2 flutter does not occur within the F-4 envelope. Flutter type 3 is the flutter mechanism considered in these
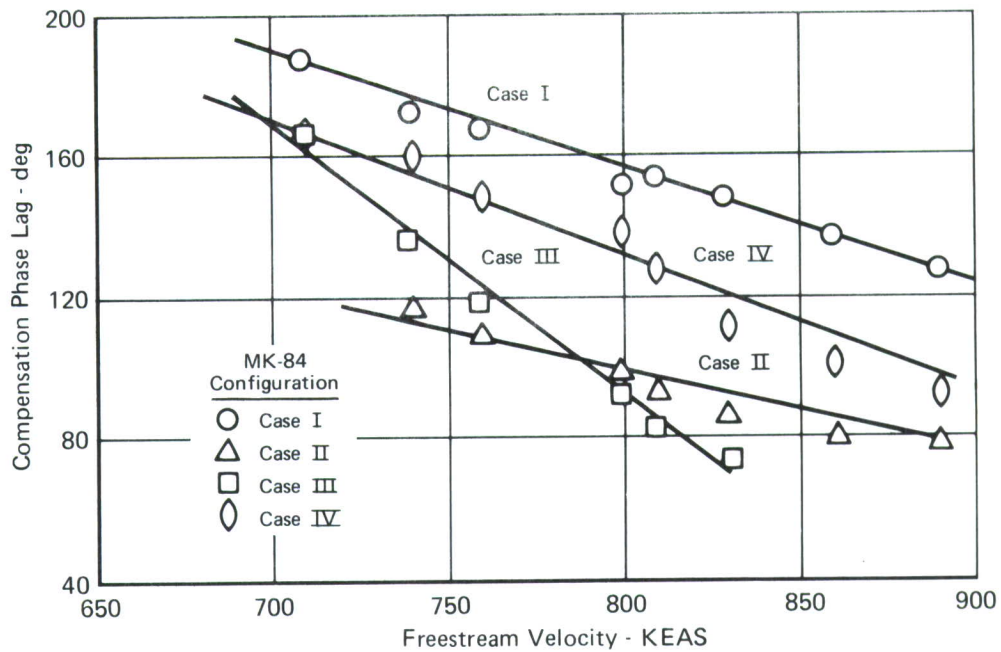
FIGURE 18
PHASE LAG COMPENSATION FOR BALANCED PHASE MARGINS FOR
VARIOUS SLATTED F-4 WING/MK-84 CONFIGURATIONS

F-4 wing/store flutter control studies and the feasibility of active control has been established, as least as far as both symmetric and anti-symmetric modes are concerned. This section of the report discusses asymmetric flutter effects. The major portion of the information is derived from Reference 12.

3.1.3.1 Effects of Asymmetric Loading - One is at times confronted with external store configurations which are carried asymmetrically; that is, the store loading on the left wing differs from that on the right wing. If configuration "X" carried on one side and configuration "Y" on the other side, it is generally assumed that the flutter speed of the combination will in no case be lower than the lowest of either configuration if it were to be carried symmetrically. Figure 19 presents data to evaluate this approach. These results were obtained for the F-4 on a passive analog computer. This figure presents flutter boundaries for both a nominal mass and an increased mass store carried symmetrically. A third boundary is shown for an asymmetric loading with the normal mass on the right wing and the increased mass on the left wing. In no case does the asymmetric configuration flutter at a speed lower than the lower one of the two symmetric configurations. The most interesting aspect of Figure 19, however, is that for a large range of pylon pitch stiffness the asymmetric configuration has a flutter velocity which is lower than one or the other of the symmetric configurations.

3.1.3.2 Effects of Asymmetric Pylon Pitch Stiffness - The fact that for some particular loadings there is an improvement in flutter velocity leads to the question of whether it is feasible to "build in" asymmetry by, for example, making the left pylon of different stiffness than the right pylon. Because of the importance of the pitch mode to flutter of both types 2 and 3 the pitch stiffness was investigated.

Figure 20 shows flutter boundaries for a combination of pylon pitch frequencies on both the left-hand wing and the right-hand wing. The diagonal line corresponds to the case of symmetric (that is, equal) pylon pitch stiffness.

Consider first the case represented by Point D in Figure 20. This flutter mode is one involving the basic wing flutter (type 2) which is

_____

12. Katz, Henry, "Flutter of Aircraft with External Stores," Presented at the Aircraft/Stores Compatibility Symposium, November 1969.

31
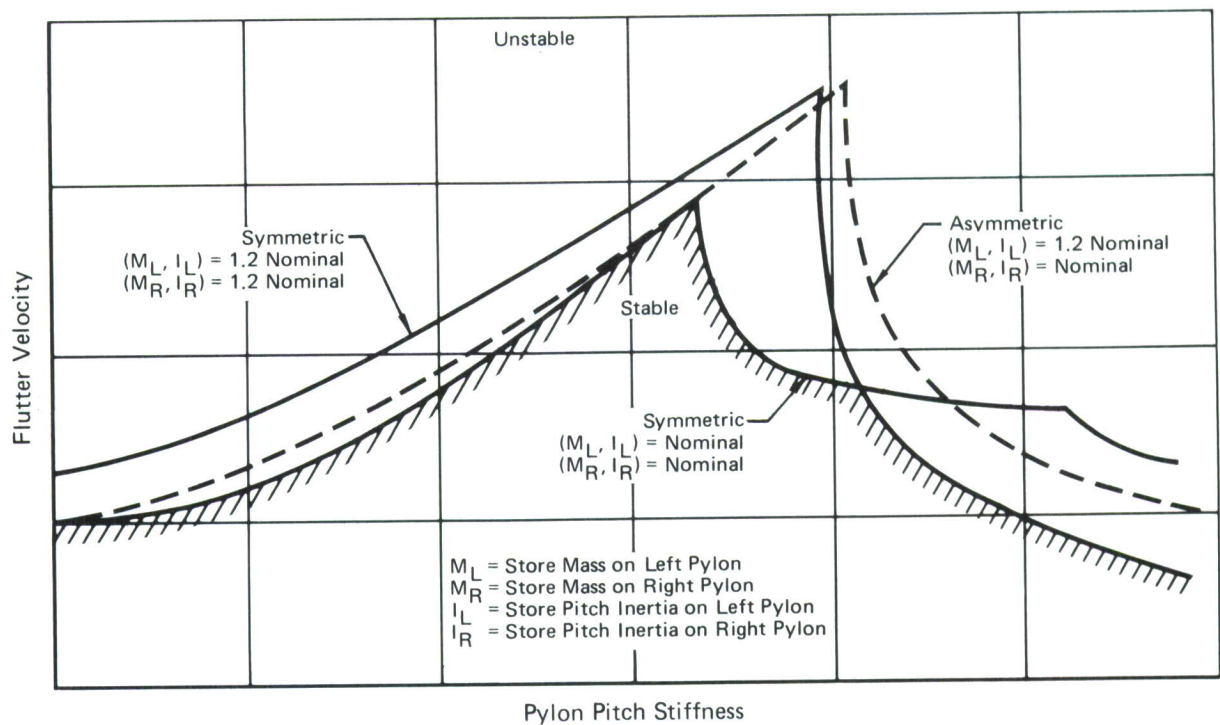
FIGURE 19
EFFECT OF ASYMMETRIC STORE MASS CHARACTERISTICS
ON FLUTTER BOUNDARY

Within Figure 19:

Unstable

Symmetric
(M_L, I_L) = 1.2 Nominal
(M_R, I_R) = 1.2 Nominal

Stable

Asymmetric
(M_L, I_L) = 1.2 Nominal
(M_R, I_R) = Nominal

Symmetric
(M_L, I_L) = Nominal
(M_R, I_R) = Nominal

M_L = Store Mass on Left Pylon
M_R = Store Mass on Right Pylon
I_L = Store Pitch Inertia on Left Pylon
I_R = Store Pitch Inertia on Right Pylon

Flutter Velocity

Pylon Pitch Stiffness
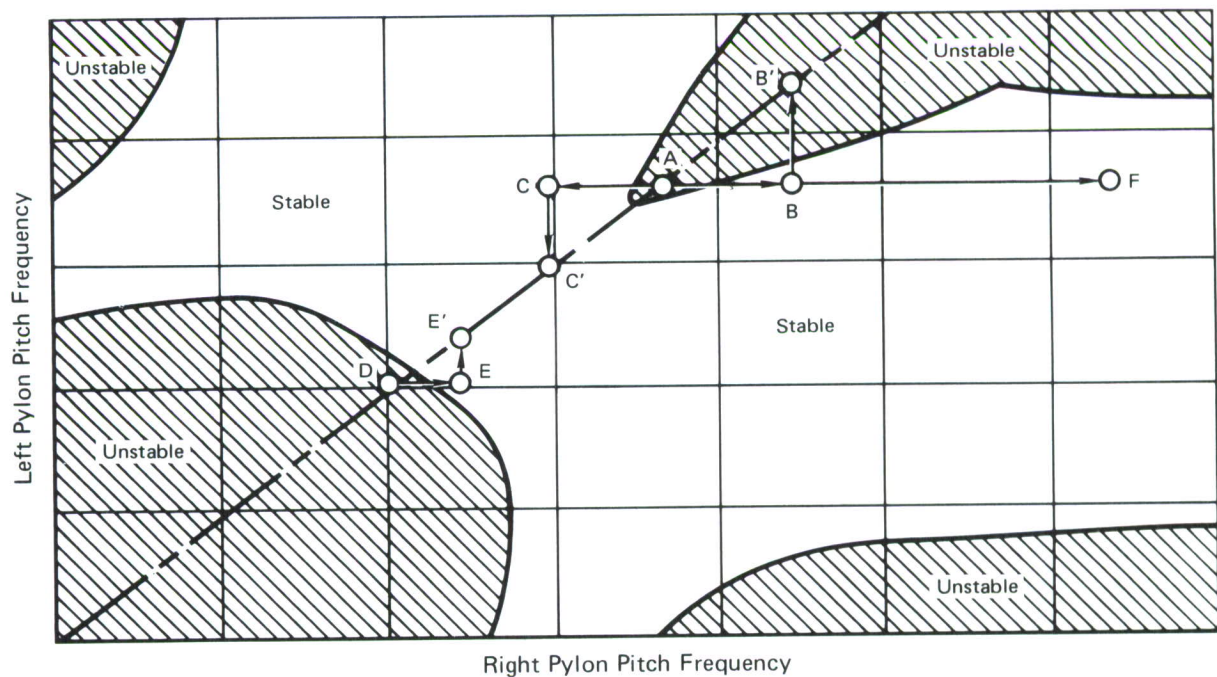
FIGURE 20
EFFECT OF ASYMMETRIC PYLON PITCH STIFFNESS ON FLUTTER BOUNDARY -
NOMINAL VELOCITY REQUIREMENT

Within Figure 20:

Unstable

Stable

Left Pylon Pitch Frequency

Unstable

Stable

Unstable

Right Pylon Pitch Frequency

being made more stable by increasing the pylon stiffness. The improvement occurs primarily because of the change in the generalized masses in the flutter mode, specifically in a more stabilizing coupling factor. This configuration can be made stable by increasing the pitch stiffness of both pylons (e.g. along the diagonal to point E') or by just increasing the pitch stiffness of one pylon (e.g. to point E). Providing stability through a symmetric increase of pylon stiffness will help this configuration, but it will only do so at the expense of some other configuration. It should be remembered that the mode considered (type 2) is one involving only a modification of basic wing flutter caused by pylon/store contributions. Very little benefit can be expected for such a mode from asymmetric pylons.

If the instability is in the second flutter mode, represented by Point A, the story changes considerably. This second mode is type 3 flutter in which a new mode is created by the store. For example, the carriage of a heavy store (say a 370 gallon tank or an MK-84) on a stiff pylon at about midspan on the wing introduces a large effective angle-of-twist outboard of the store. This large twist angle causes outer wing bending-torsion flutter. This flutter is usually at a relatively low frequency compared with the basic wing flutter mode.

From Point A stability is achieved by either decreasing the stiffness of both pylons (Point C') or by increasing or decreasing the stiffness of one of the pylons (Points B and C). This case can be explained as follows: if an essential aspect of the aircraft/store/suspension characteristics changes on only one side the character of the overall system can be affected so that each side of the aircraft responds with significantly different mode shapes. Thus, when the pylon stiffness is increased on only one side (Point B) the modal deflections on both sides are sufficiently different from each other that there is an energy transfer between the two sides which results in a stable overall configuration.

It can be seen from Figure 20 that, the deeper one proceeds into the flutter mode (along the diagonal - up from Point A), the more of a difference in pitch-stiffness is needed between the two sides to provide stability. This is because of the increased amount of energy which has to be dissipated. With a combination of widely different modes, such as would be represented by Point F in Figure 20, the overall configuration is still stable. The

prerequisite is always that there be a good path of energy flow between the separate wing modes.

The configuration cannot be made stable by pitch stiffness variations if both sides are unstable in the third flutter mode represented by the upper right-hand corner in Figure 20. The reason is that, once the pitch stiffness is sufficiently high to produce this unstable mode, it is rather insensitive to further variations in this stiffness. This third mode is a high frequency mode coupling second wing bending and second wing torsion.

Figure 21 presents the results of an analysis equivalent to that presented in Figure 20, except that the speed requirement has been increased. While no symmetric pylon configuration is stable, there is a relatively wide range of asymmetric configurations which provide stability.

Clearly, each wing of a fighter aircraft with external stores should be treated independently. This view has been consistently maintained throughout all of these investigations. The expectation has been that "real-world" configurations will always be asymmetric to some degree, if for no other reason than the combination of manufacturing tolerances and "Murphy's Law." It is our opinion that active flutter control is feasible for asymmetric loading with independent flutter control loops. This feasibility will be tested in the Series II wind tunnel tests described in Section 5.1.5.2.

3.2 Dynamic Response Analyses

This section consists of two parts. The first is a summary of the studies of the wind gust effects on flutter control system operation. The second section considers the probability of certain gust levels occurring.

3.2.1 Summary of Wind Gust Studies - The following is a summary of the three types of gust analyses which have been used to analyze wind gust effects on the operation of the adaptable flutter control system. These three types are discrete cosine gust, transient analog, and Monte Carlo. The F-4 with a 370 gallon tank - 90% full was used in all analyses (Reference 4, page 88). The Monte Carlo is both the most correct and most conservative of the approaches.

3.2.1.1 Discrete Gust Approach - This is the type of gust analysis which was described and used in Reference 4, page 120. It is assumed that the gust is of the form of a cosine wave acting for 1 period at the flutter frequency.

$$\text{Gust} = \text{Amplitude} (1 - \cos \omega_f t)$$
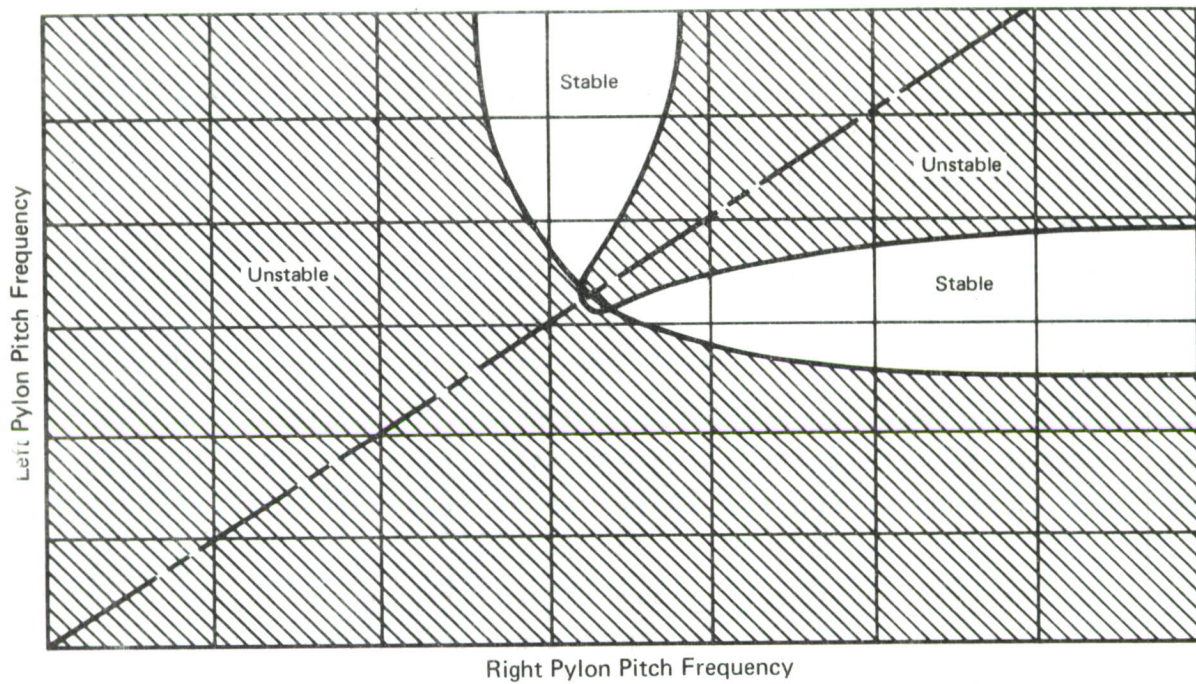
FIGURE 21
EFFECT OF ASYMMETRIC PYLON PITCH STIFFNESS ON FLUTTER BOUNDARY -
INCREASED VELOCITY REQUIREMENT

Actuator rate limits were included in the discrete gust analyses. This analysis is somewhat conservative in that the gust is assumed to hit the aircraft at the flutter frequency (for maximum response) but is unconservative in that the gust only acts for 1 period (0.12 sec).

The active flutter control system designed in Reference 4, page 88, for the F-4 with a 370 gallon tank - 90% full was used in an investigation to determine the maximum level of discrete cosine wind gust under which this system could still stabilize the flutter mode. The 700 KEAS, g = 0.02, sea level conditions were specified. The aileron actuator bandwidth and rate limits were 10 Hz and 100 deg/sec respectively. The conclusions reached in this study was that it would take a discrete gust of approximately 30 fps root mean square (RMS) to render the system unable to stabilize the flutter mode.

3.2.1.2 <u>Transient Analog Approach</u> - This approach assumes a wind gust of the Dryden form (Reference 13). The technique then finds the ensemble variances of all state variables of interest (aeroelastic mode and aileron deflection and rate) due to a continuously acting random Dryden gust of a specified RMS value.

The Dryden atmospheric turbulence model from MIL SPEC 8785B was used to simulate a vertical wind gust. The power spectral density (PSD) is

$$\phi(\omega) = \frac{L}{V} (W_G)^2 \left[\frac{1 + \frac{3L^2}{V^2} \omega^2}{(1 + \frac{L^2}{V^2} \omega^2)^2} \right]$$

where ϕ = vertical wind gust PSD - $(ft/sec)^2/(rad/sec)$

V = aircraft velocity - ft/sec

W_G = standard deviation of wind gust velocity - ft/sec

L = turbulence scale factor - ft

The recommended values for L are,

$$L = \begin{cases} altitude & for & alt < 1750 \ ft \\ 1750 & for & alt > 1750 \ ft \end{cases}$$

13. Chalk, C.R., et al, "Background Information and User Guide for MIL-F-8785B (ASG) Military Specification - Flying Qualities of Piloted Airplanes," AFFDL-TR-69-72, August 1969.

In this case the parameters were chosen as:

V = 1180 ft/sec (700 KEAS)

W_G = 13.38 ft/sec corresponding to a typical thunderstorm

L = 200, 1000 ft (2 cases)

The approach is described in Reference (14). The method involves factoring the power spectral density:

$$\phi(S) = \left| U(S)\ U(-S)\ \Big|_{S=i\omega} \right|$$

where S is the Laplace transform variable. In this case,

$$U(S) = \frac{W_G\sqrt{\dfrac{L}{V}}\ \left(1 + \sqrt{3}\ \dfrac{L}{V}\ S\right)}{\left(1 + \dfrac{L}{V}\ S\right)^2}$$

The inverse Laplace transform of this is:

$$u(t) = W_G e^{-\frac{V}{L}t}\left[\frac{V}{L}\left(\sqrt{\frac{V}{L}} - \sqrt{\frac{3V}{L}}\right)t + \sqrt{\frac{3V}{L}}\right]$$

This input is used as a forcing function to the aeroelastic equations of motion. The variance is obtained by integrating the square of any system variable of interest.

In this case the aeroelastic equations of motion are:

$$\left(M + \frac{Q}{V^2}\ I\right)\ddot{q} + \left(C + \frac{Q}{V}\ B\right)\dot{q} + (K + QA)\ q$$

$$+\ QA_c\left[q_o\ \phi(s) + \int_o^s\ \frac{dq}{d\sigma}\ \phi(s-\sigma)\ d\sigma\right]$$

$$+\ \frac{Q}{V}\ B_c\left[\dot{q}_o\ \phi(s) + \int_o^s\ \frac{d^2q}{d\sigma^2}\ \phi(s-\sigma)\ d\sigma\right]$$

$$=\ F \cdot u(t)$$

14. Magdaleno, Raymond and Wolkovitch, Julian, "Performance Criteria for Linear Constant-Coefficient Systems with Random Inputs," Systems Technology, Inc., ASD-TDR-62-470, January 1963.

The symbols used above are defined in the List of Abbreviations and Symbols. The equations are described in detail in Reference 4.

F is the generalized force per unit gust velocity and is derived from the following considerations:

o Generalized gust force

$$F \cdot u = \frac{\partial w}{\partial q}$$

o Virtual work due to gust

$$\partial w = \partial q \int \phi \, d\ell$$

where ϕ is the bending component of the modal deflections and $d\ell$ is the gust induced lift on a strip of width dy.

o Gust induced lift

$$d\ell = \frac{1}{2} \rho V^2 c \, C_{\ell_\alpha} \, \alpha_g \, dy$$

$$= \frac{1}{2} \rho V u S \, C_{L_\alpha} \, \frac{c \, C_{\ell_\alpha}}{\bar{c} \, C_{L_\alpha}} \, d\eta$$

where η normalized spanwise coordinate = y/y_T

  ρ air density

  V freestream velocity

  u gust velocity

  α_g gust induced angle of attack = u/V

  S wing area (semispan)

  c wing chord

  $\bar{c}$ average wing chord

  C_{ℓ_α} section lift curve slope

  C_{L_α} average wing lift curve slope

From these considerations, the generalized gust force becomes

$$F \cdot u = \int \phi \, d\ell = \left[\frac{1}{2} \rho V S \, C_{L_\alpha} \int_o^1 \phi \, \frac{c \, C_{\ell_\alpha}}{\bar{c} \, C_{L_\alpha}} \, d\eta \right] \cdot u$$

which yields as the generalized gust force per unit gust velocity, the expression

$$F = \frac{1}{2} \rho \ V \ S \ C_{L_\alpha} \int_o^1 \phi \ \frac{c \ C_{\ell_\alpha}}{\bar{c} \ C_{L_\alpha}} \ d\eta$$

The normalized wing air load distribution is assumed to be

$$\frac{c \ C_{\ell_\alpha}}{\bar{c} \ C_{L_\alpha}} = \frac{6}{5} \left(1 - \frac{2}{3} \ \eta^3\right)$$

and the approximated elastic mode shape is given by

$$\phi = \eta^2$$

which results in

$$F = \rho \ V \ S \ C_{L_\alpha} \cdot \frac{1}{2} \int_o^1 \frac{6}{5} \ \eta^2 \left(1 - \frac{2}{3} \ \eta^3\right) \ d\eta$$

$$= (.002377)(1180)(265)(3.44)(.1335)$$

$$= 341 \ \text{lb sec/ft}$$

The time domain program FLTR was run using F and u(t) as the transient analog excitation. Standard deviations of the aeroelastic generalized coordinates were calculated and are given in Table 6.

Two dimensional aerodynamics were used in this preliminary study. This is conservative due to recently reported studies which show increased aerodynamic damping with three-dimensional aerodynamics. However, since this is a linear statistical technique, no rate limits were considered. For the flutter stabilized case chosen (370 gallon tank - 90% full at 700 KEAS with the flutter control system operating) the response will be stable for any and all values of RMS gust chosen but will require larger deflection and rates to control flutter for the larger RMS gusts. In practice rate limits will likely be exceeded so that this analysis is no longer valid. Hence Monte Carlo runs were made as described below.

3.2.1.3 _Monte Carlo Approach_ - The Monte Carlo approach involves using the flutter time domain program (FLTR) where the excitation for the aeroelastic equations of motion is obtained by sampling from a Gaussian

TABLE 6
STANDARD DEVIATIONS FOR TRANSIENT ANALOG ANALYSES
370 Gallon Tank 90% Full - No Rate Limits
13.38 FPS RMS   700 KEAS

Mode	L = 200 ft	L = 1000 ft
q_1 Pylon Roll - in.	1.15	0.80
q_2 Wing First Bending - in.	1.97	1.31
q_3 Tank Pitch/ Wing Torsion - in.	1.32	0.61
q_4 Aileron Rotation - deg	1.90	0.80

random number generator and then shaping this signal using appropriate filters to give the wind gust signal the Dryden power spectral density shape. The force acting on the wing modes due to the gust and the shaping filters are obtained in the same manner as described in the Section 3.2.1.2 for the transient analog method. The gust is assumed to act continuously. The idea is to make many computer runs with different noise sequences, then calculate ensemble statistics based on these runs. The Monte Carlo approach is valid for the statistical analysis of nonlinear systems such as a flutter control system with rate limits.

With Monte Carlo techniques it is necessary to determine how many runs to make to ensure that the ensemble variances have converged to the true variances. To study this problem, 9 seven second Monte Carlo runs were made for a 13.38 fps RMS wind gust for the F-4 with 370 gallon tank - 90% full at 700 KEAS velocity at an altitude of 200 ft with no rate limits (linear) to check how the ensemble variance compares to the reference variance obtained from transient analog method in Section 3.2.1.2. The resulting deviations are shown in Table 7.

TABLE 7
COMPARISON OF STANDARD DEVIATIONS FROM MONTE CARLO AND TRANSIENT ANALOG ANALYSES
370 Gallon Tank 90% Full - No Rate Limits
13.38 FPS RMS   L = 200 Ft   700 KEAS

Method	Mode				Mode Rate			
	q_1 (in.)	q_2 (in.)	q_3 (in.)	q_4 (deg)	$\dot{q}_1$ (in./sec)	$\dot{q}_2$ (in./sec)	$\dot{q}_3$ (in./sec)	$\dot{q}_4$ (deg/sec)
Monte Carlo	1.21	2.16	1.30	2.15	41.9	87.0	67.5	99.0
Transient Analog	1.15	1.97	1.32	1.90	39.8	82.0	69.5	82.0

These runs lead to the conclusion that one can expect standard deviation errors of approximately 10% for the linear system, when making 9 seven second Monte Carlo runs. (Seven second runs were chosen to ensure that the run had passed through the transient stage and was exhibiting steady state effects.

It was decided to make 15 seven second Monte Carlo runs for the same case as above with rate limits of 100 degrees/second included. To use the Dryden gust it is necessary to pick the scale factor L. The military specifications (Reference 13) say that L should equal the altitude up to 1750 feet, and L = 1750 ft at altitudes above 1750 feet. In the flutter case, as described for the transient analog results, the smaller the L the more adverse the effect of the gust on flutter control. The reason for this is shown in Figure 22 which shows plots of power spectral density versus frequency for various values of L for the same RMS gust. The important frequency is the flutter frequency (approximately 55 rad/sec). It can be seen that with a lower L, the gust has more power in the neighborhood of the flutter frequency, even though the RMS values (which is proportional to the area under the curve) is the same in all cases.

Therefore, two runs were made, one at L = 200 ft which is very conservative, and the other at L = 500 ft which is near the recommended
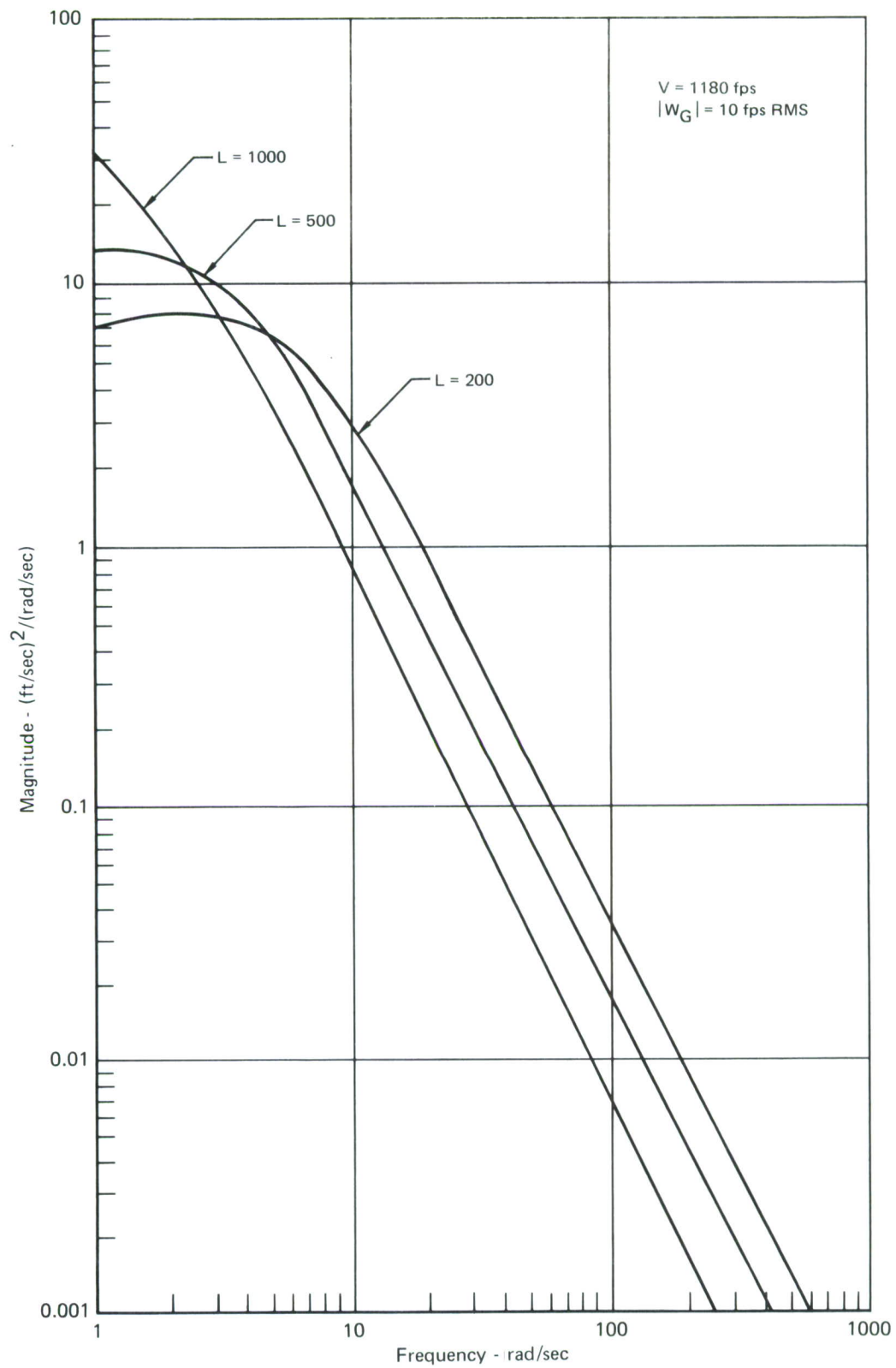
FIGURE 22
**EFFECT OF SCALE FACTOR L ON POWER SPECTRAL
DENSITY OF DRYDEN WIND GUST**

value in Reference 15, page 367. The gust magnitude was 13.38 fps RMS. In three of the fifteen cases at L = 200 ft flutter was not controlled. The results for the L = 500 ft case showed none of the fifteen cases went unstable even though the aileron rate limit was hit in most of the cases. The standard deviations for the variables of interest are shown in Table 8.

The substance of these studies suggests that rate limiting of 100 degrees per second will not interfere with flutter control in a 13.38 fps RMS gust environment at altitudes of 500 feet or more, for which L is greater than 500. At an altitude of 200 feet, L = 200, there is a possibility of losing flutter control in the 13.38 fps gust environment. However, the probability of encountering such a gust is only about one in ten thousand, as will be seen in Section 3.2.2, and it is quite unlikely that flight at 200 feet altitude would even be attempted at 700 KEAS in such a gust environment.

3.2.2 <u>Probability of Wind Gust Occurrence</u> - Measurements indicate that gustiness affecting aircraft is most frequent and severe near the ground during the daytime. It drops to a relative minimum at about 15,000 to 20,000 feet, increases to a secondary maximum in the vicinity of the jet stream between 25,000 and 45,000 feet, then decreases slowly above the jet stream. In addition, there is a pronounced shift of the frequency spectrum toward lower frequencies with increasing altitude.

The AFFDL has sponsored extensive recent investigations of atmospheric turbulence over a wide range of altitudes in the overall program known as ALLCAT. The effort of primary interest to these active flutter suppression studies is the LO-LOCAT (Low-Low Altitude Critical Atmospheric Turbulence) research reported in Reference 15. This program was concerned with the altitudes of 250 to 1000 feet where the most frequent high magnitude turbulence occurs and where active flutter control shows the most promise. Figure 23 (reproduced from Reference 15) shows the cumulative probability of occurrence of vertical gust velocity RMS values obtained from the LO-LOCAT program. Data from several other recent efforts (References 16-19) are shown

15. Jones, J.W., et al, "Low Altitude Atmospheric Turbulence - Lo-Locat Phase III," Volume I, Part 1 Data Analysis, AFFDL-TR-70-10, November 1970.
16. Pritchard, Francis, E., "The Turbulence and Terrain Environments Affecting Low-Altitude, High-Speed Flight," FDM No. 393, Cornell Aeronautical Laboratory, Inc., Buffalo, New York, July 1966.
17. Dempster, J.B. and Bell, C.A., "Summary of Flight Load Environmental Data Taken on B-52 Fleet Aircraft," Journal of Aircraft, Vol. 2, No. 5, September-October 1965.

TABLE 8
STANDARD DEVIATIONS FOR NONLINEAR MONTE CARLO ANALYSIS
370 Gallon Tank 90% Full - Rate Limited (100 Deg/Sec)
13.38 FPS RMS Gust   L = 500 Ft   V = 700 KEAS

Method	Mode				Mode Rate			
	q_1 (in.)	q_2 (in.)	q_3 (in.)	q_4 (deg)	$\dot{q}_1$ (in./sec)	$\dot{q}_2$ (in./sec)	$\dot{q}_3$ (in./sec)	$\dot{q}_4$ (deg/sec)
Monte Carlo	0.923	1.55	1.24	1.15	25.6	52	57.3	54.2
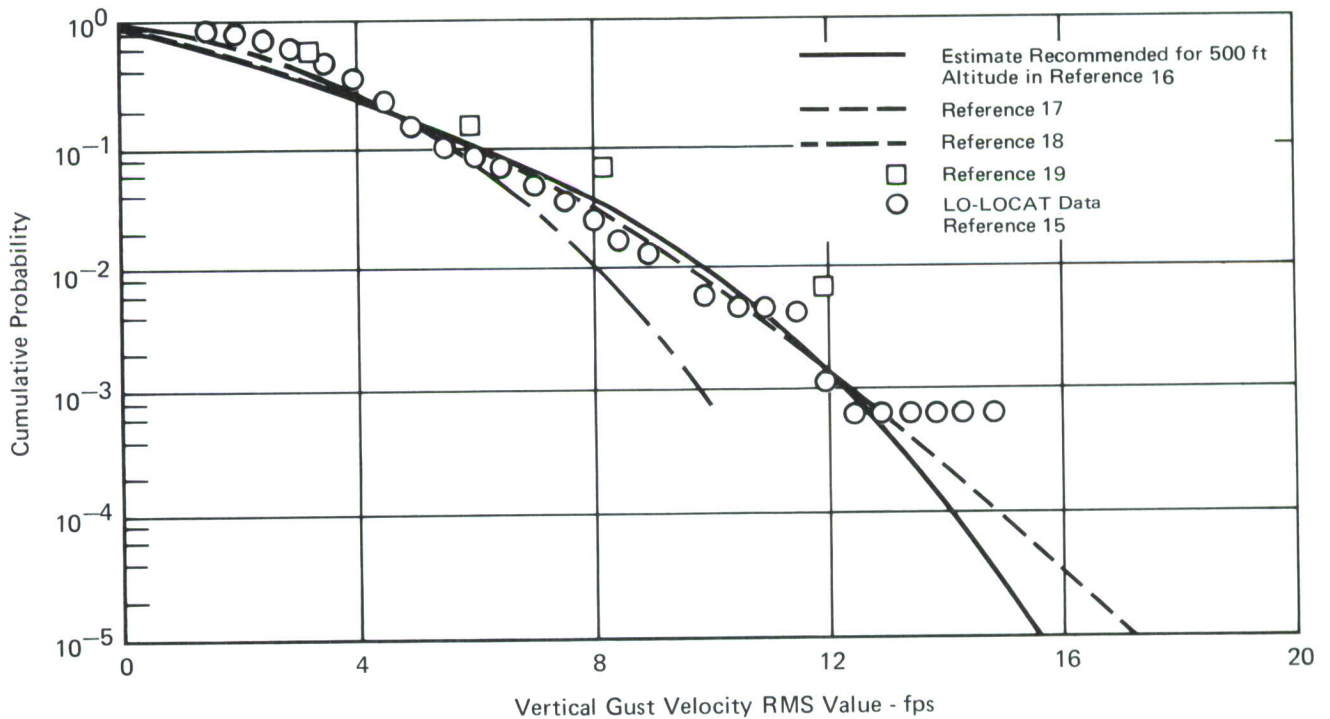
FIGURE 23
COMPARISON OF VERTICAL GUST VELOCITY RMS VALUES FROM
VARIOUS RESEARCH PROGRAMS

44

in the figure for comparison. The most impressive aspect of these data is
the remarkable agreement among the references.

The LO-LOCAT data shown in Figure 23 was obtained primarily from flights
near Peterson Field, Colorado. The most severe turbulence occurred in high
mountains west of Trinidad, Colorado. The greatest variations in expected
turbulence levels are attributable to the terrain type, as shown in Figure 24.
Other geophysical conditions have significantly less effect on gust levels.
There is, however, a tendency for relatively higher levels to occur during
the winter and spring seasons. In general, also, the probability of a given
RMS gust is greater at mid-afternoon than at mid-morning or dawn, greater
at 250 ft than at 750 ft altitude, and greater for an unstable ($\Delta T > 6°F/1000$ ft)
than for a stable atmosphere. The overall wind direction is another factor,
with the higher gust levels generally on the leeward side of a major terrain
feature.

3.3 Flutter Control System Interaction Studies

The F-4 wing/store flutter control system (Reference 4) was designed
without including the low frequency airframe and primary flight control
system dynamics. It was assumed that a high pass filter would be used in
the flutter control loop to separate the high frequency elastic dynamics
from the low frequency airframe, flight control dynamics. Previous experi-
ence has indicated that this is a valid approach. In the course of this
contract a root locus study was performed to confirm the validity of this
assumption by including the basic airframe equations and the stability
augmentation system equations in the analyses. In addition, certain
significant fuselage elastic modes were included in the study to determine
their effect on the operation of the flutter control system.

18. Notess, C.B., "The Effects of Atmospheric Turbulence Upon Flight at
    Low Altitude and High Speed," FDM No. 325, Cornell Aeronautical Lab-
    oratory, Buffalo, New York, October 1961.
19. Zbrozek, J.K., "The Relationship Between the Discrete Gust and Power
    Spectra Representations of Atmospheric Turbulence, with a Suggested Model
    of Low-Altitude Turbulence," Aeronautical Research Council (England),
    R and M No. 3216, 1961.
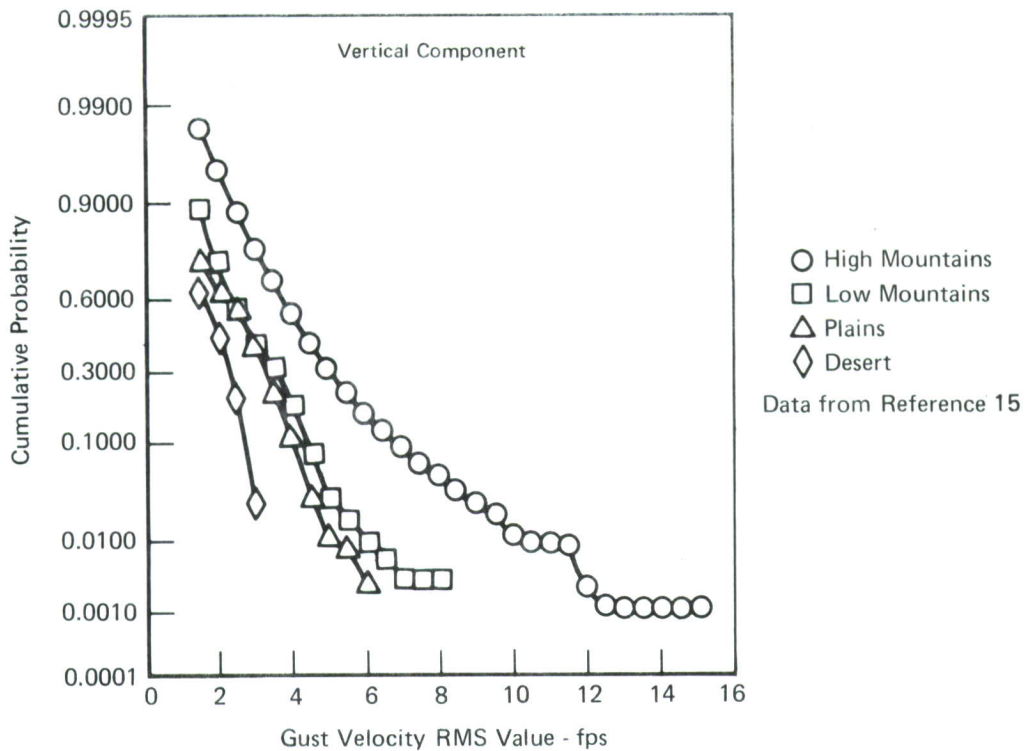
FIGURE 24

GUST VELOCITY RMS CUMULATIVE PROBABILITY ASSOCIATED WITH TYPE OF TERRAIN

The specific case considered in these studies was the F-4 at a flight condition of 0.84 Mach at sea level carrying a 370 gallon tank - 90% full. Root loci runs were made for the F-4 with the lateral/directional stability augmentation system both on and off (basic airframe). Root loci were also made both with and without the anti-symmetric fuselage elastic modes. These cases will be discussed in detail with representative block diagrams and root loci in the following paragraphs.

3.3.1 F-4 Basic Airframe with Flutter Control - A block diagram of the basic F-4 lateral channel with the flutter control system, for one wing only, as an inner loop is shown in Figure 25. The degrees of freedom are rigid aircraft roll, rigid aircraft yaw, the three lowest elastic wing modes, aileron and rudder actuator deflections, and the aileron elastic rotation mode.

The corresponding root locus is shown in Figure 26. The locus parameter in this case is the gain (KF) in the flutter control loop. The locus shows that all closed loop roots are stable for the design gain of -5.34. The second wing mode can be driven unstable if the flutter feedback loop gain (KF) is increased from -5.34 to -7.8. The third wing mode locus shows the increased damping in the potentially unstable flutter mode.

46
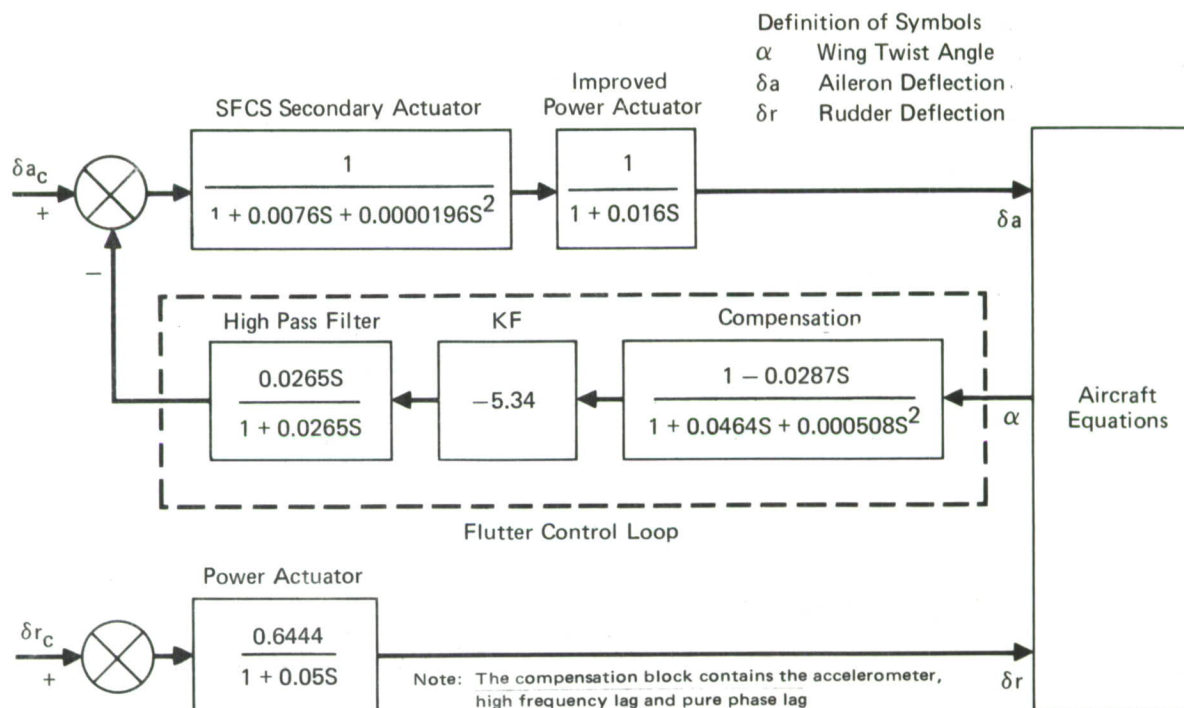
FIGURE 25
BLOCK DIAGRAM OF F-4 LATERAL DIRECTIONAL CHANNEL

3.3.2 <u>F-4 Stability Augmentation System with Flutter Control</u> –
The block diagram of the F-4 with both the lateral/directional stability
augmentation system (SAS) and the flutter control system is shown in Figure 27.
The degrees of freedom are the same as in Section 3.3.1. The lateral channel
of the SAS uses signals from a roll rate gyro to add damping to the basic
aircraft in roll. The channel is interrupted whenever the pilot maneuvers
in roll so as not to obtain roll inhibiting action from the SAS. The gain
of the roll rate loop is fixed. The directional channel uses signals from
a yaw rate gyro to add damping to the aircraft dutch roll mode. Signals from
a lateral accelerometer are used to provide coordinated turns. The gains
of the yaw rate and lateral acceleration loops are fixed.

The root locus plot for this case is shown in Figure 28. The roll rate
gain KP is the locus parameter. For the nominal gain KP = 0.265 all closed
loop roots are stable. However, the second wing mode can again be driven
unstable but at a much larger value of KP = .83. The third wing mode can
be driven unstable with KP = 4.5.

3.3.3 <u>F-4 Basic Airframe with Flutter Control Including Anti-Symmetric
Fuselage Elastic Modes</u> – The effect of anti-symmetric elastic modes on the
operation of the flutter control system was also studied using root locus. The
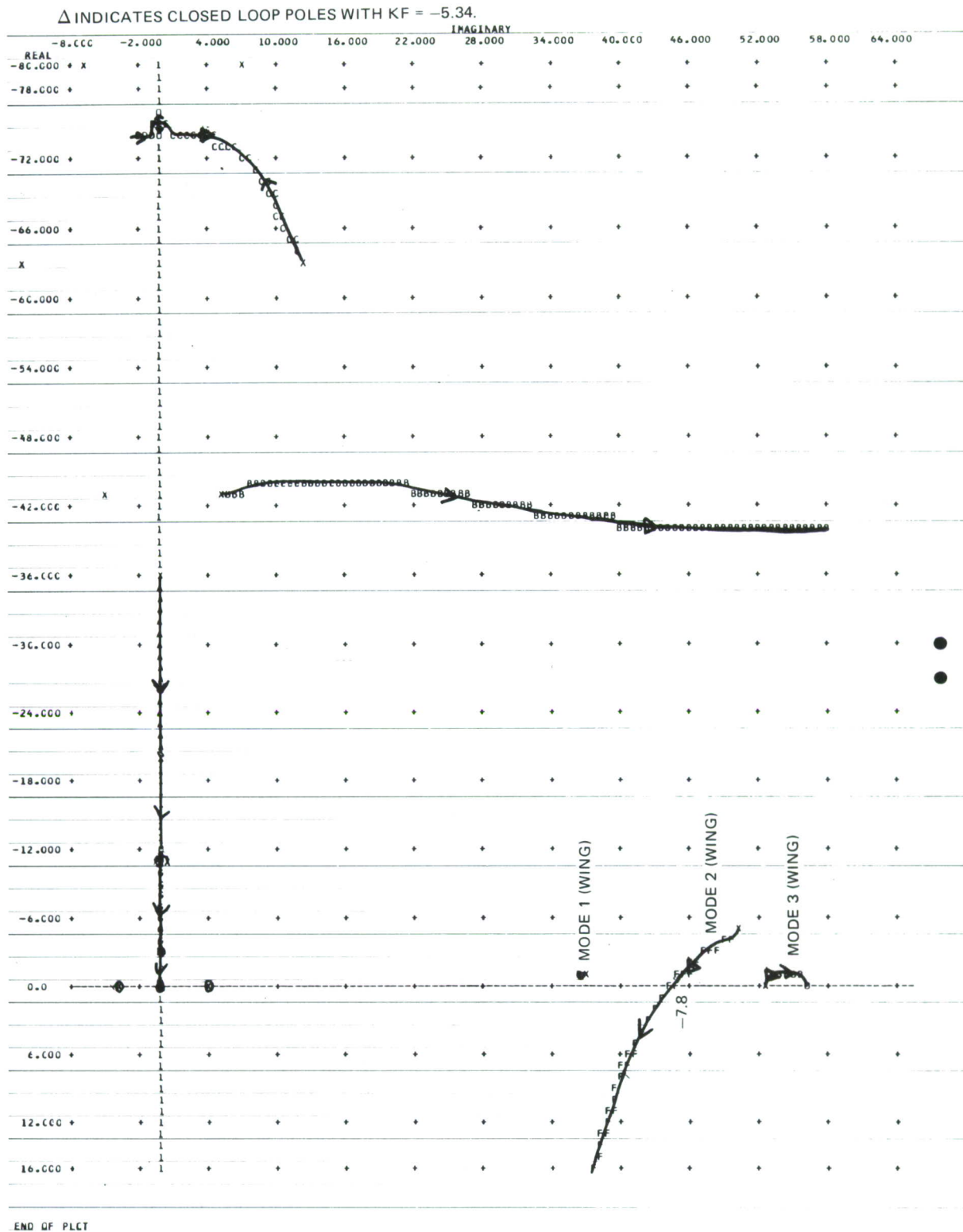
FIGURE 26
F-4 BASIC AIRFRAME WITH FLUTTER CONTROL
KF (Flutter Loop Gain) is Locus Parameter

48

Definition of Symbols

a   Aircraft Yaw Acceleration
p   Aircraft Roll Rate
r   Aircraft Yaw Rate
α Wing Twist Angle
δa Aileron Deflection
δr Rudder Deflection

δa_c

SFCS Secondary Actuator
$$\frac{1}{1 + 0.0076S + 0.0000196S^2}$$

Improved Power Actuator
$$\frac{1}{1 + 0.016S}$$

δa

High Pass Filter
$$\frac{0.0265S}{1 + 0.0265S}$$

KF
-5.34

Compensation
$$\frac{1 - 0.0287S}{1 + 0.0464S + 0.000508S^2}$$

α

FLUTTER CONTROL LOOP

KP
0.265

Rate Gyro
$$\frac{1}{1 + 0.0067S + 0.00004S^2}$$

p

δr_c

Power Actuator
$$\frac{0.6444}{1 + 0.05S}$$

δr

Series Servo
$$\frac{1}{1 + 0.01S + 0.0001S^2}$$

0.0168

Accelerometer
$$\frac{1}{1 + 0.02S + 0.0004S^2}$$

a

Series Servo
$$\frac{1}{1 + 0.01S + 0.0001S^2}$$

Canceller
$$\frac{S}{1 + S}$$

3.0

Rate Gyro
$$\frac{1}{1 + 0.0067S + 0.00004S^2}$$

r

Aircraft Equations

Note: The compensation block contains the accelerometer, high frequency lag and pure phase lag

FIGURE 27
BLOCK DIAGRAM OF F-4 LATERAL/DIRECTIONAL
STABILITY AUGMENTATION SYSTEM

△ INDICATES CLOSED LOOP POLES WITH KP = 0.265
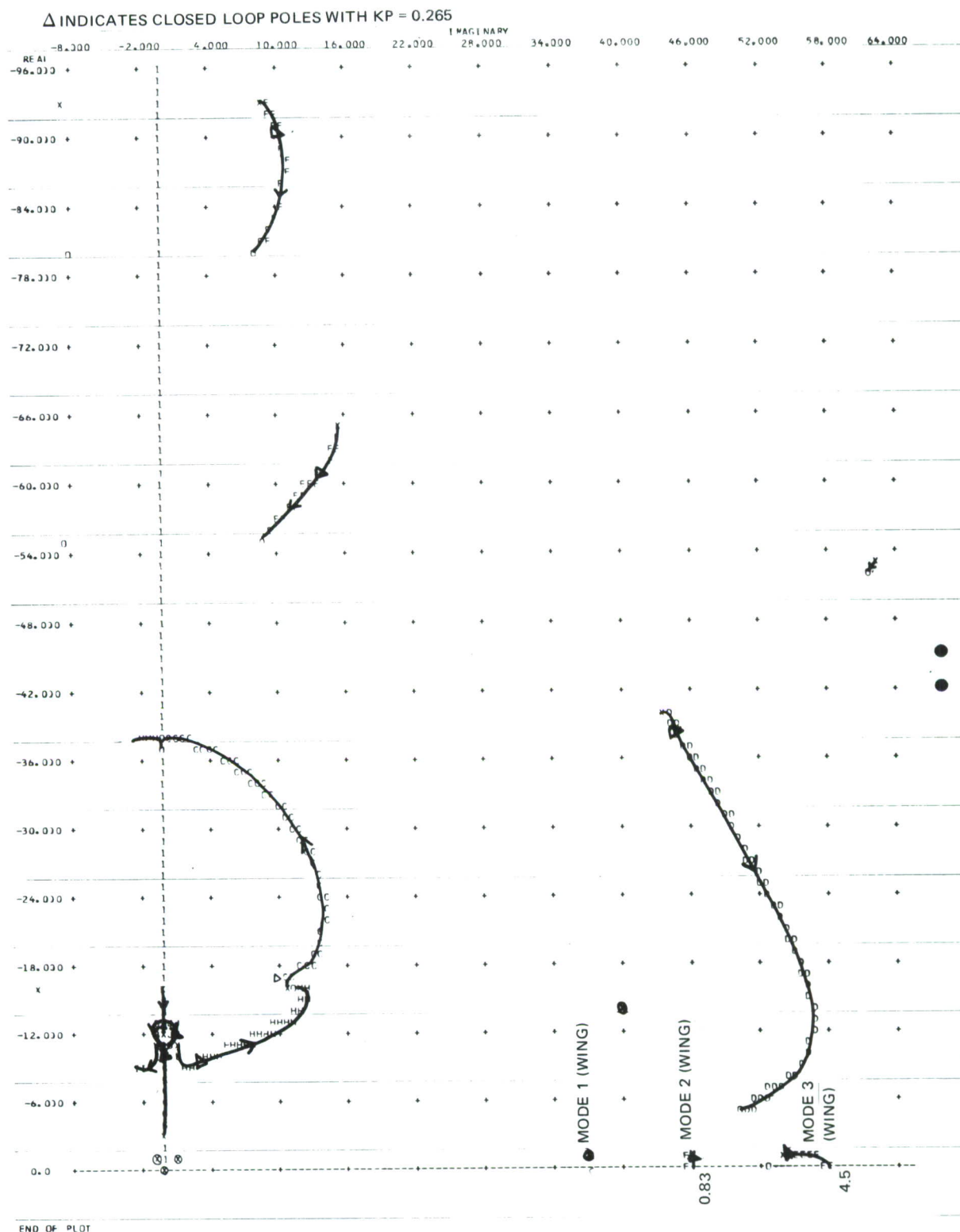
FIGURE 28
F-4 SAS WITH FLUTTER CONTROL
KP (Roll Rate Gain) is Locus Parameter

50

three additional modes considered were the fuselage first torsion, the wing anti-symmetric bending, and the fuselage first lateral bending. The definitions and data for these modes were obtained from Reference 11 pages 283-295.

The root locus for the F-4 basic airframe with active flutter control and including the anti-symmetric elastic modes is shown in Figure 29. The root locus parameter is the flutter control loop gain KF. For the nominal gain KF = -5.34 the system is stable. However, the second wing mode may be driven unstable by increasing KF to about -7.6. When compared to the root loci of Figure 26 it is seen that the effect of the fuselage modes is minimal.

3.3.4 <u>F-4 Stability Augmentation System with Flutter Control Including Anti-Symmetric Fuselage Elastic Modes</u> - The effect of the anti-symmetric elastic modes on the F-4 with the stability augmentation system and active flutter control system is shown in Figure 30. The root locus parameter is the roll rate gain KP. For the nominal gain KP = 0.265 the system is stable. The second wing mode can be driven unstable if KP is increased to about 0.55.

These studies indicate that the interaction of the flutter control system with the low frequency dynamics (basic airframe or stability augmentation system) will not cause instability. The inclusion of anti-symmetric elastic terms in the calculations has very little effect on the stability margins of the basic airframe system, but does have some effect on the aircraft stability margins with the stability augmentation system on.

3.4 <u>Adaptive Flutter Control System Investigation</u>

3.4.1 <u>Adaptive Control Systems Survey</u> - A literature search was undertaken to evaluate methods for implementing an adaptive flutter control system. The flutter control systems designed in Reference (4) were adaptable in nature. That is, the control laws could be easily changed as a function of wing stores configuration. An adaptive flutter control system would automatically adjust the control laws onboard to account for variable wing store loading. Various categories of adaptive control are discussed below. The most appropriate of these categories for active flutter control is selected and used in the subsequent adaptive flutter control system investigations.
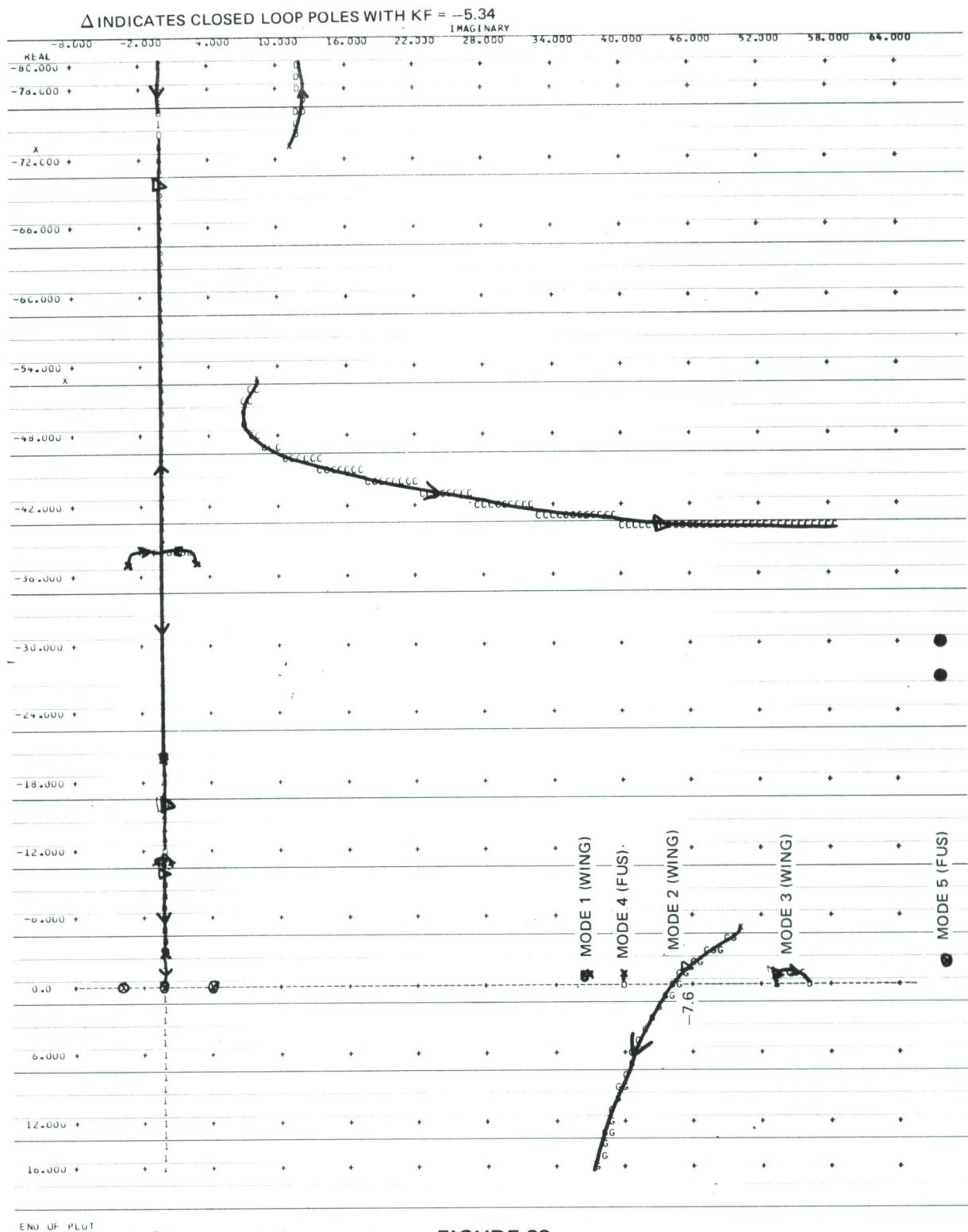
FIGURE 29

F-4 BASIC AIRFRAME WITH FLUTTER CONTROL AND FUSELAGE MODES

KF (Flutter Loop Gain) is Locus Parameter
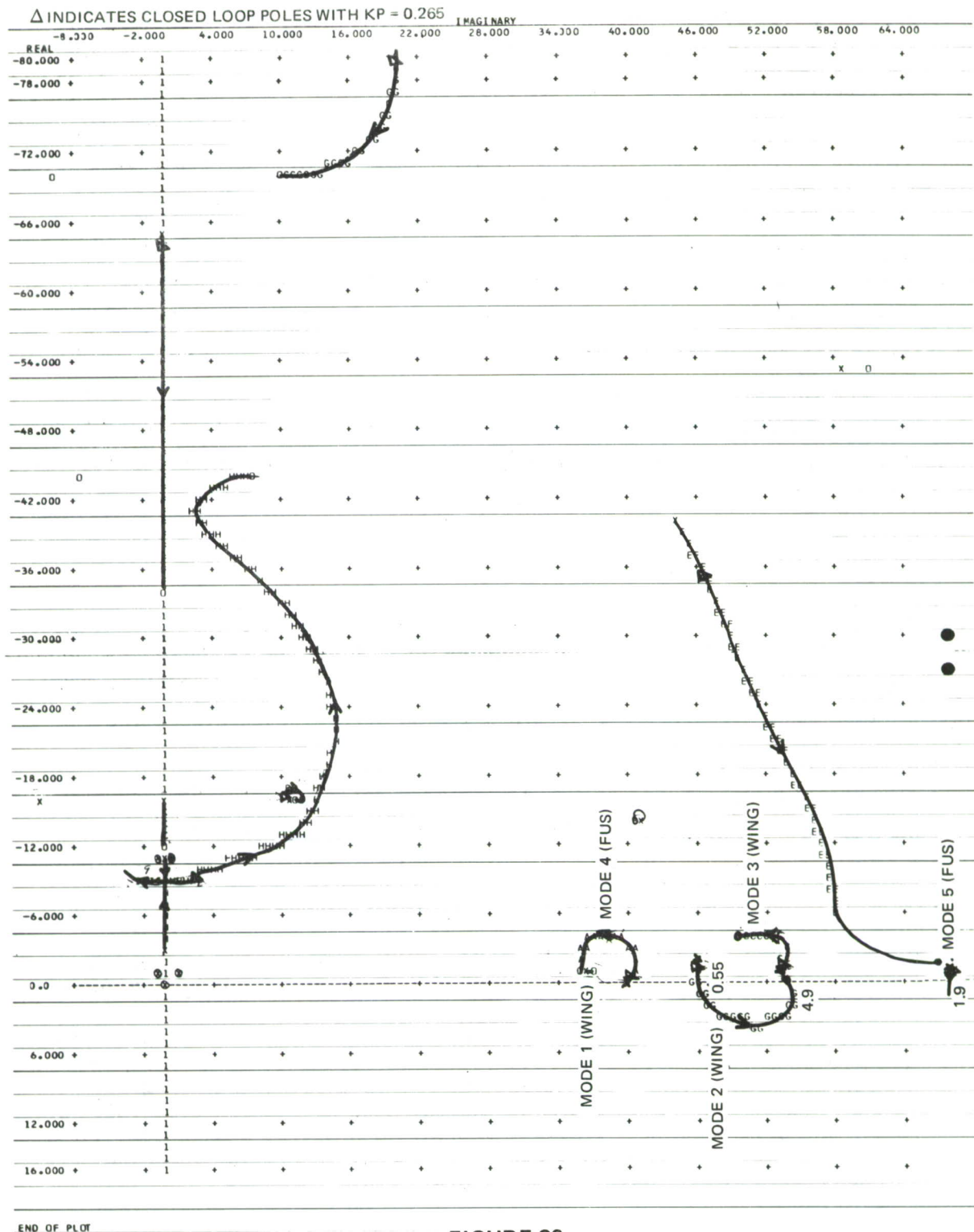
FIGURE 30
F-4 SAS WITH FLUTTER CONTROL AND FUSELAGE MODES
KP (Roll Rate Gain) is Locus Parameter

53

3.4.1.1 <u>Definition of Adaptive Control Categories</u> - References 20 through 23 were the principal sources of information. In particular, Reference 20 is in such depth that little more need be said about concepts or past research. Basically the work that is classified as adaptive control falls into three categories (1) adaptive insensitive, (2) learning, and (3) parameter adaptive control systems. A chart (from Reference 20) summarizing various adaptive control techniques is given in Figure 31.

o An <u>Adaptive Insensitive Control System</u> is one which has a low sensitivity <u>fixed</u> configuration controller and possibly includes a separate adaptive controller in a parallel feedback loop to accomplish minor modifications of the system.

o A <u>Learning Control System</u> is an adaptive system in which the structure and/or parameters of the controller are adjusted according to a performance criterion which itself may be adaptive. To accomplish this the following additional capabilities may be required:

Performance Verification

Punishment and Reward

Memory

o A <u>Parameter Adaptive Control System</u> is an adaptive system in which the controller structure is fixed to within a set of adaptive parameters (gains, time constants, etc.) that are adjusted according to a specified adaptation algorithm.

Important subcategories of the parameter adaptive control systems are the explicit and implicit identification methods. In a system with explicit identification, adaptation is achieved by attempting to completely determine the system equations of motion while the system is operating and

20. Price, C.F. and Koenigsberg, W.D., "Adaptive Control and Guidance for Tactical Missiles," Vols I and II, the Analytic Science Corp., Reading, Mass., TR-170-1, June 1970.
21. Smyth, R.K. and Ehlers, H.L., "Survey of Adaptive Control Applications to Aerospace Vehicles," AGARD Conference on Advanced Control System Concepts, Oslo, Norway, September 1968 (AGARD C.P. No. 58 - August 1970).
22. Mendel, J.M., "Survey of Learning Control Systems for Space Vehicle Applications," 1966 JACC Proceedings, Vol 7, Seattle, Washington, 1966.
23. Blakelock, J.H., "Automatic Control of Aircraft and Missile," John Wiley & Sons, Inc., 1965.
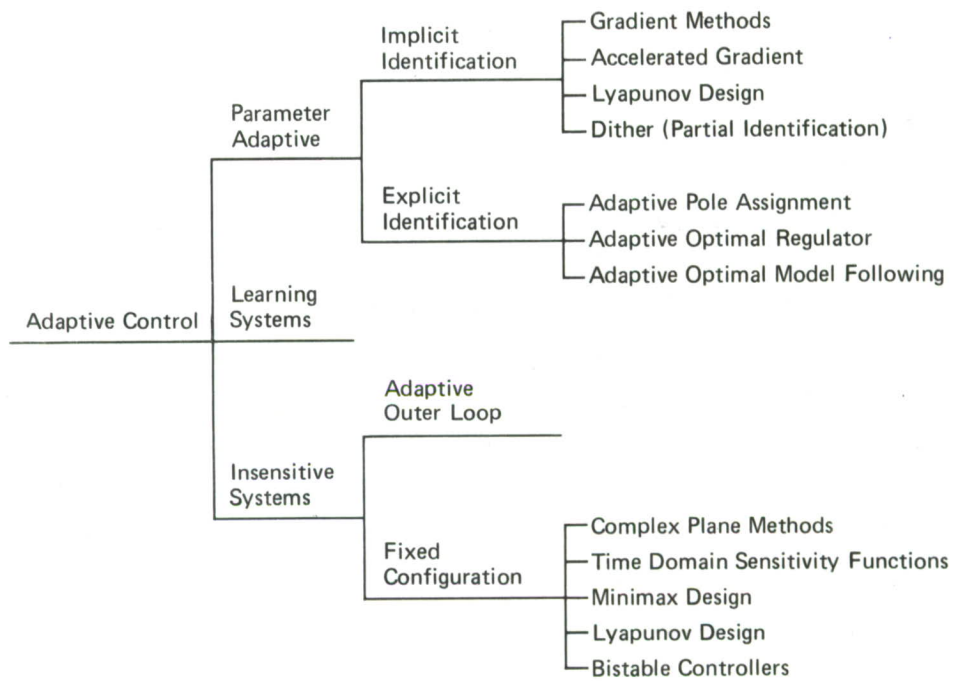
FIGURE 31
SUMMARY OF ADAPTIVE CONTROL TECHNIQUES

by adjusting controller parameters on the basis of the information so obtained. In a system employing implicit identification no attempt is made to identify the system completely. Instead, output variables of interest are examined and their behavior compared with desired performance criteria. This comparison produces an error signal and controller parameters are adjusted so as to force the error to be small.

3.4.1.2 <u>Application to Flutter Control</u> - Each of the above categories is now considered for a possible application to active flutter control.

o <u>Adaptive Insensitive Control System</u> - From previous flutter control law design experience both during this current study and the earlier study of Reference 4, no one fixed control law has been found that will work for all possible stores configurations, flight conditions, etc. This can be understood by considering the fact that for stability at post-flutter velocities the Nyquist resonant (flutter frequency) loop must be centered about the negative real axis for stability with maximum phase margins. The possibility that a fixed control law, even with the use of an adaptive outer loop, can accomplish this for all store configurations and flight conditions is slight.

o <u>Learning Control Systems</u>— There is no need to have an adaptive performance criterion which itself is adaptable. Considerable a priori knowledge about the aircraft exists so that the complexity of a learning concept is not justified. Any time domain criterion probably will also not have the "anticipatory" capability already available from the frequency domain criterion, as described in Section 3.4.3.5 and in Reference 4, page 204, which is necessary for active flutter control.

o <u>Parameter Adaptive Control System - Explicit Identification</u> - There is no need to identify all coefficients in the differential equations defining the aeroelastic motion to control flutter. This would be "overkill" for flutter control. In any case, even with the recent developments in parameter identification such as maximum likelihood techniques, no reliable, fast, on-line identification method exists which could be used to successfully control flutter.

o <u>Parameter Adaptive Control System - Implicit Identification</u> - There are two distinct categories of "implicit identification". The first of these uses a time domain error criterion to shape the feedback so that the system matches some desired model. Gradient, accelerated gradient and Lyapunov design techniques are examples of this category. There are at least two serious objections to this type of approach. First, it is very doubtful whether any time domain criterion can give the anticipatory capability

required for flutter control as the flutter speed is approached. Secondly, the time required for convergence to the optimal feedback when using these gradient type methods could be a serious problem in attempting to control a phenomenon such as flutter.

The second subcategory could more properly be called "partial identification". In this technique some sort of "dither" signal is used to estimate a few key airframe parameters. Examples of this type of system can be found in References (21) and (23). For flutter control application, this type of system appears to be the most promising. Figure 32 depicts, and Section 3.4.2 will describe in detail, a proposed operational adaptive flutter control system which falls into this category. A (dither) signal, such as colored noise, step, ramp, or swept sinusoid is input to the aircraft ailerons and a suitable output (e.g., wing twist acceleration) is measured. Both input and output signals, after appropriate smoothing, are transformed into the frequency domain via the fast Fourier transform (FFT). The ratio of these transforms is then obtained to yield the open loop output/ input frequency response. This then gives enough information to design control laws to control flutter. Furthermore, the frequency domain (Nyquist) criterion is anticipatory. The system can be used 50-100 KEAS sub-flutter to center the major axis of the resonant loop along the positive real axis, then at post-flutter velocities the major axis will rotate 180 deg to align with the negative real axis automatically. A design along somewhat similar lines is described in Reference (21). Practical considerations of reconstruction of transfer function frequency responses from fast Fourier transformed data can be found in References (24) through (26) and in Section 3.4.3 of this report.

3.4.2 Feasibility Study of an Operational Adaptive Flutter Control System - The most promising concept for adaptive flutter control is shown in Figure 32. The concept uses a conventional (classical frequency domain) approach to the control system design. A feedback loop provides a compen-

24. Turner, M.R., Elkins, J.A., "Digital Analysis of Flight Flutter Tests," BAC Report GEN/B745-4/7893, May 1969.
25. Baldock, J.C.A. and Skingle, C.W., "Flutter Technology in the United Kingdom - A Survey," AIAA Dynamics Specialists Conference, Williamsburg, Va., March 1973.
26. Dat, R., "The Theoretical and Experimental Methods Used in France for Flutter Prediction," AIAA Dynamics Specialists Conference, Williamsburg, Va., March 1973.
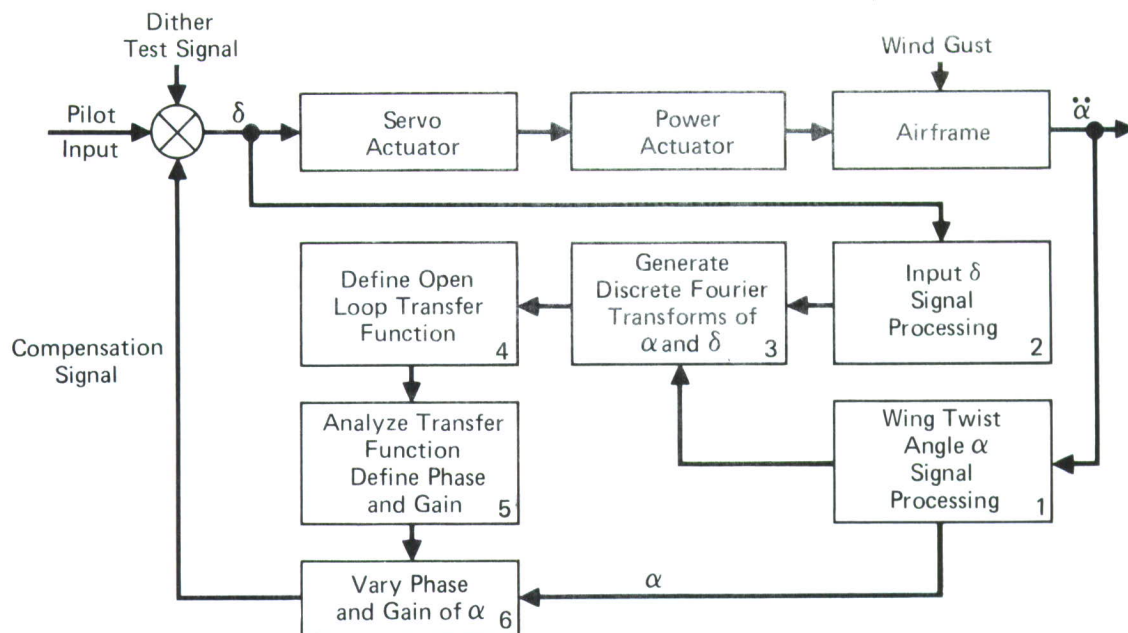
FIGURE 32
PROPOSED ACTIVE FLUTTER CONTROL SYSTEM

sation signal to the primary flight control system which produces aileron deflections to damp out or stabilize wing flutter resonances. The compensation signal is generated by sensing either wing twist angle acceleration ($\ddot{\alpha}$) or rate ($\dot{\alpha}$); performing the necessary integration; processing the resulting wing twist (α) signal through a compensation filter; and varying the gain and phase of the signal during flight. The gain and phase are adjusted to stabilize the open loop transfer function of the system.

The open loop transfer function frequency response is measured or defined by performing a spectral analysis of the input (δ) to the servo actuator and the output of the wing twist compensation filter (α) in a digital signal processor. This transfer function frequency response defines the characteristics of a Nyquist plot. The characteristics are analyzed to detect the major resonance of the flutter mode and to define the gain and phase of the feedback loop necessary to stabilize the system.

3.4.2.1 <u>Wing Twist Angle Signal Processing</u> – This processing is described in Figure 33.

1. Sense wing twist angular acceleration (or rate) and generate an analog signal (varying DC voltage).
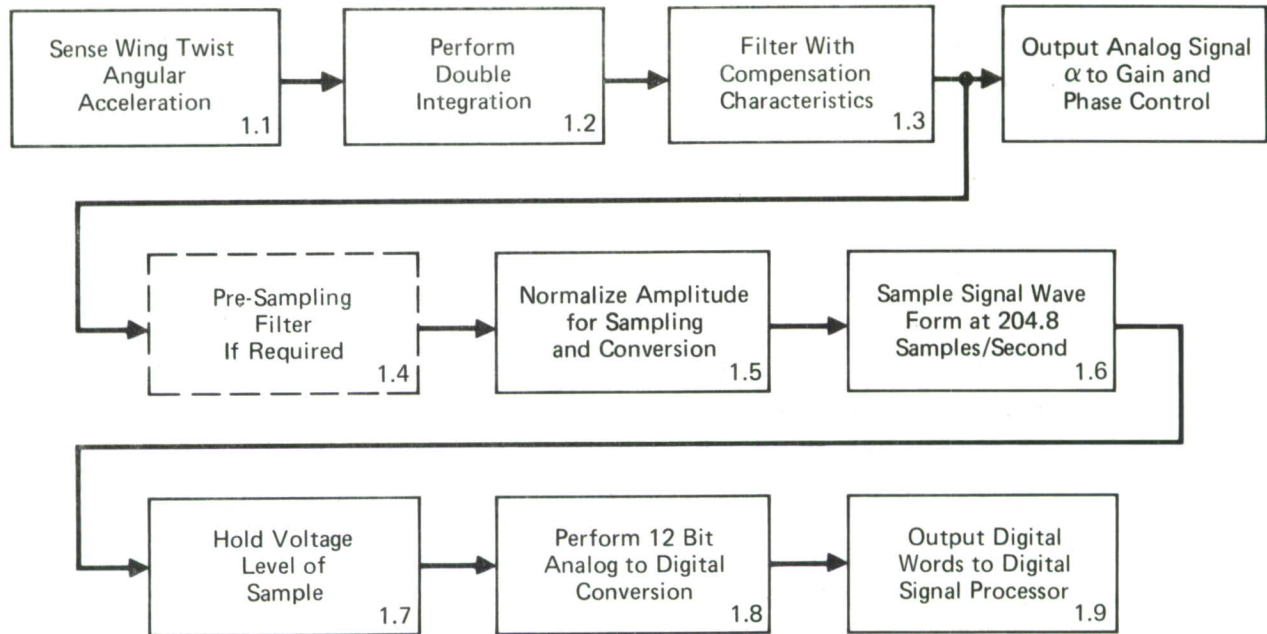
FIGURE 33
WING TWIST ANGLE (α) SIGNAL PROCESSING - ANALOG

2. Perform the integration process using analog integrator(s) which can integrate the signal over the frequency range of interest 0 – 100 Hz and are AC coupled to eliminate DC input saturation, to produce wing twist signal α.

3. Process analog voltage representing α through analog fixed compensation filters with a transfer function to produce (See Figure 3)

o High frequency lag $\dfrac{1}{1 + T_3 S}$

o Notch filter $\dfrac{\omega_N^2 + 2\zeta_N \omega_N S + S^2}{\omega_D^2 + 2\zeta_D \omega_D S + S^2}$

o High pass filter $\dfrac{T_2 S}{1 + T_2 S}$

The optimum values for T_2, T_3, ω and ζ must be defined and are based on the aircraft configuration. Fixed values for these filters which are suitable for all stores configurations can be built-in. The filter output is an analog signal representing filtered α.

4. Perform pre-sampling filtering to eliminate all signal and noise frequency components above approximately 100 Hz to eliminate the possibility of frequency aliasing effects resulting from the sampling process. If the high frequency lag filter in the compensation filter and integrator(s) perform this function, the pre-sampling filter may not be required.

5. Normalize the filtered α signal amplitude and offset for sampling and analog/digital (A/D) conversion.

6. Sample the analog signal representing α at a precise 204.8 sample/second rate using a small sampling aperature which is controlled by the digital signal processor to be synchronous with the sampling of the input signal δ. This sampling rate was chosen because the highest frequency is approximately 15 Hz and the desire is to sample at least 10 samples/cycle or 150 samples/sec. An even-power-of-two samples are required to facilitate the fast Fourier transform (FFT) operations. The nearest power of 2 for a 10 second sample period, to be defined later, is the eleventh power of 2 or 2048, hence 204.8 samples/sec.

7. Hold voltage level of samples for conversion.

8. Quantize voltage level to a 12 bit binary two's compliment digital word using a precise voltage reference in an A/D converter. The A/D converter can also be used to quantize the δ signal on a time shared basis.

9. Output 12 bit digital word to digital signal processor.

3.4.2.2 <u>Input Signal Processing</u> - This processing is described in Figure 34.

1. Input analog signal (varying DC voltage) representing the input δ.

2. Normalize voltage amplitude (scale factor and offset adjustment) for sampling and A/D conversion. Use voltage amplifier or attenuator with suitable bias voltage.

3. Perform pre-sampling filtering, i.e., eliminate all signal and noise frequency components above 100 Hz, to eliminate frequency aliasing
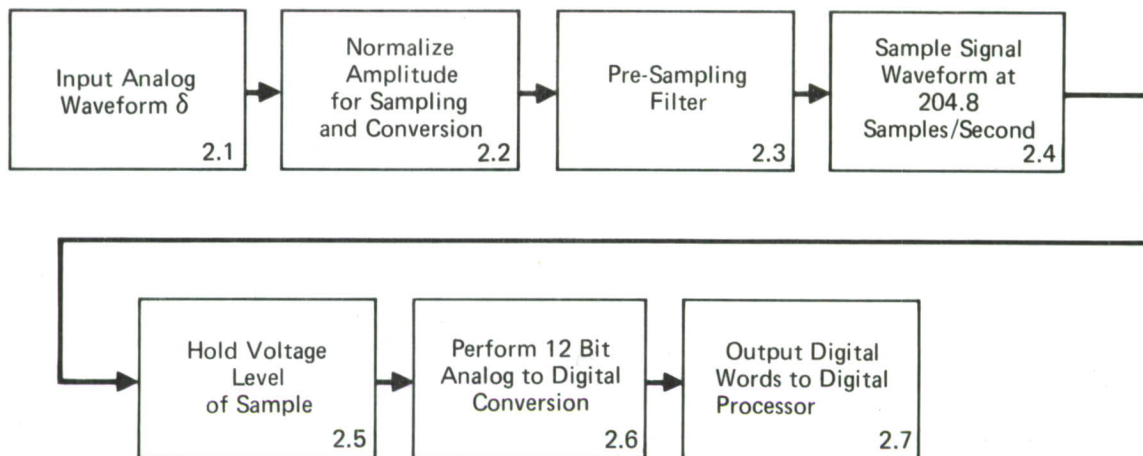
FIGURE 34
INPUT (δ) SIGNAL PROCESSING - ANALOG

effects of sampling. 100 Hz is chosen to provide signal bandwidth comparable to that of the feedback signal α.

4. Sample filtered analog voltage at a precise 204.8 sample/second rate, using a small sampling aperature. The sampling rate is controlled by digital signal processor timing to be synchronous with the sampling of α feedback sensor.

5. Hold voltage level of samples for conversion.

6. Quantize voltage level to a 12 bit binary two's compliment digital word using a precise voltage reference in an A/D converter which is time shared and compatible with the feedback signal α.

7. Output 12 bit digital word to digital signal processor.

3.4.2.3 <u>Generation of Discrete Fourier Transforms (DFT)</u> - This processing is described in Figure 35.

1. Alternately input 12 bit digital words representing filtered and quantized samples of α and δ to the digital signal processor. Total input rate is equal to 2 x 204.8 or 409.6 words per second.

2. Normalize these 12 bit digital words for processing by multiplying alternate input words by suitable scale factor values. Maximum of 409.6 multiplications per second.

3. Store two ten second sequences of 204.8 digital words (409.6 words total). Each sequence represents a 10 second analysis frame for

| Normalize 12 Bit Digital Words (α) 3.2 | → | Collect and Store 2048 Words (α) Making Up 10 sec Analysis Frame 3.3 | → | Develop 2048 Complex Fourier Coefficients (α) Using FFT 3.4 | → | Store 2048 Complex Fourier Coefficients DFT of (α) 3.6 |

| Normalize 12 Bit Digital Words (δ) 3.2 | → | Collect and Store 2048 Words (δ) Making up 10 sec Analysis Frame 3.3 | → | Develop 2048 Complex Fourier Coefficients (δ) Using FFT 3.5 | → | Store 2048 Complex Fourier Coefficients DFT of (δ) 3.6 |

Notes: Steps 3.2 and 3.3 will be performed simultaneously
Steps 3.4 and 3.5 may be done in sequence

FIGURE 35
GENERATION OF DISCRETE FOURIER TRANSFORMS OF α AND δ
DIGITAL PROCESSING

developing the two DFT's which define the frequency spectrum of α and δ. A ten second sequence is desired to achieve a resolution of 0.1 Hz since f_o (resolution) $= \frac{1}{T}$ (length of sequence)

The sampling rate of 204.8 samples per second was chosen to provide a ten second sequence which contains a number of samples which is an exact power of 2 to facilitate the FFT algorithm and which samples the highest expected frequency component at least 10 samples/cycle.

4. Develop 2048 complex coefficients defining the spectrum of α using an FFT algorithm. This processing cannot be completed until all 2048 samples have been collected and therefore the minimum processing time will be 10 seconds plus some comparatively small increment of time (less than 0.2 seconds) depending on the algorithm used and the processing rate of the digital processor.

The total number of computations required to develop a 2048 point DFT using an FFT algorithm is generally considered to be $N\log_2 N =$

22,528 complex additions and $1/2 \, N\log_2 N = 11,214$ complex multiplications or a total 33,742 computations for N = 2048. In addition there will be various handling and control operations required. But with processing speeds in the order of 400,000 or more operations per second available, all the computations required could be accomplished in less than 0.2 sec as assumed above.

5. Develop 2048 complex Fourier coefficients defining the spectrum of δ using the same FFT algorithm used for defining α. Since the data samples representing the δ signal are collected at the same time as those for α, the additional processing time required for the FFT of δ will be less than 0.2 seconds. These two FFT's could be accomplished in parallel if adequate processing capability were provided, but since the total time saved by parallel processing is only approximately 5% of the total 10.4 seconds required for sequential processing the time saving does not appear to justify the additional processing capability required.

6. Store two sets of 2048 complex Fourier coefficients. If the FFT algorithm is properly implemented, the storage area used for the input data samples can be used to store the Fourier coefficients developed in the FFT.

3.4.2.4 <u>Definition of the Open Loop Transfer Function Frequency Response</u> – This processing is described in Figure 36.

1. Compute the raw transfer function frequency response by ratioing the two DFT's. This requires comparing the two sets of 2048 complex coefficients and producing 2048 complex coefficients defining the transfer function.

2. Transform the raw transfer function frequency response back to the time domain to produce a noisy impulse response function using the FFT algorithm. Again assume less than 0.2 seconds required.

3. Multiply the raw transfer function frequency response by a suitable exponential weighing function to smooth the impulse response function generated in 2.

4. Retransform the smoothed impulse response function back to the frequency domain to produce a smoothed transfer function using the FFT algorithm. Again assume less than 0.2 seconds required.

5. Store significant frequency coefficients (5-15 Hz) of the smoothed transfer function.
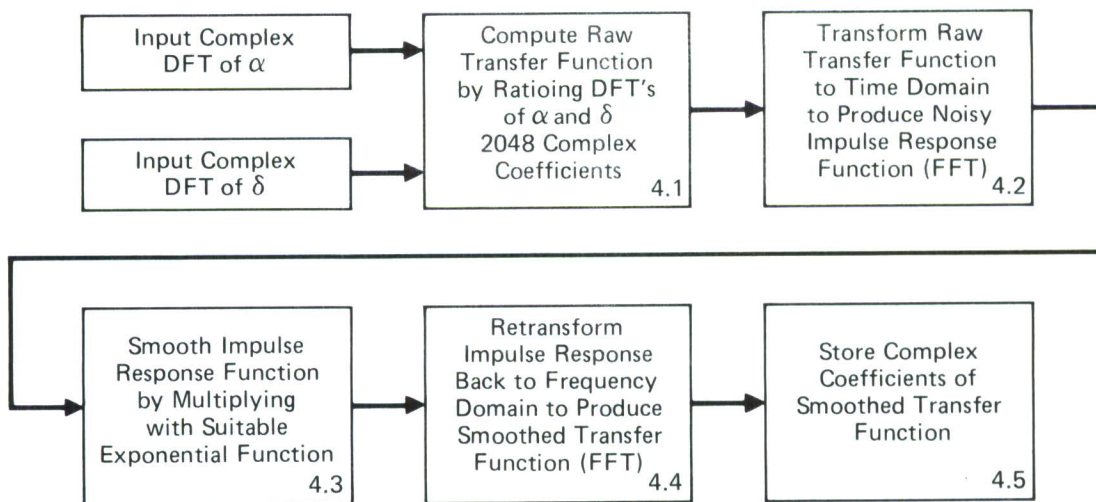
FIGURE 36
GENERATION OF OPEN LOOP TRANSFER FUNCTION α TO δ
DIGITAL PROCESSING

(Note: An alternate smoothing process could be substituted for steps 2, 3, and 4.)

3.4.2.5 <u>Definition of the Compensation Gain and Phase</u> - This processing is described in Figure 37.

1. Convert the complex coefficients representing the transfer function frequency response in the range of interest (5-15 Hz) to values of magnitude and phase which represent modified Nyquist plot to be analyzed.

2. Detect major resonance mode by comparing amplitudes, or determining maximum rate of change with frequency, or some similar algorithm.

3. Determine phase axis of major resonance mode.

4. Define compensation phase and gain required for stability using a control law and algorithm to be defined.

5. Convert digital value of gain and phase to analog voltage level to set phase and gain of variable compensation network.

64
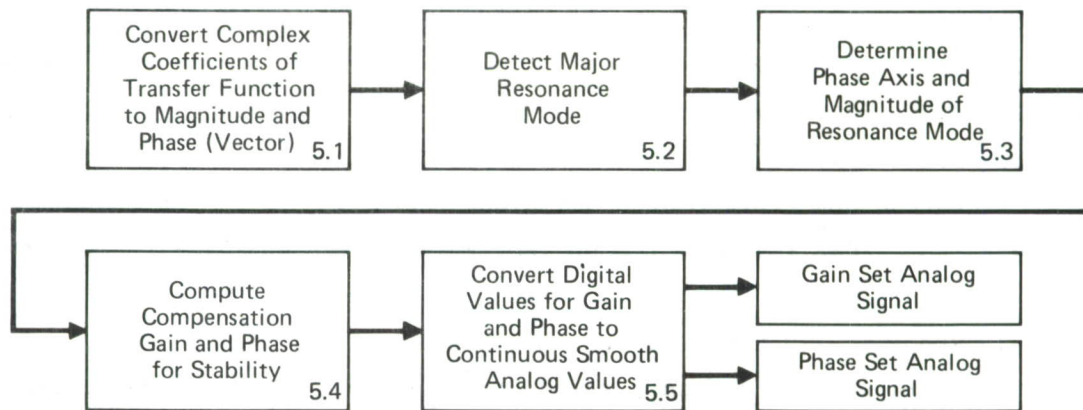
FIGURE 37
DEFINITION OF COMPENSATION GAIN AND PHASE - DIGITAL PROCESSING

The final step is to vary the gain and phase of the wing twist angle signal (α) from the compensation filter according to the values of these parameters obtained from the transfer function frequency response analysis. This step is block 6 in Figure 32. This block consists of a network whose characteristics are defined as:

$$\pm K \; \frac{1 - T_1 S}{1 + T_1 S}$$

where K and T_1 are determined by the analysis of Figure 37.

3.4.2.6 Estimation of Processing Time and Storage Requirements

o Processing Time

1.	Collect analysis frame of data	10	sec
2.	Compute 2 DFT's α and δ	0.4	sec
3.	Compute raw transfer function	0.1	sec
4.	Transform to time domain	0.2	sec
5.	Smooth impulse response function	0.1	sec
6.	Transform to frequency domain	0.2	sec
7.	Detect resonance modes and define phase	0.1	sec
8.	Compute gain and phase	0.1	sec
	Total	11.2	sec

o Storage Requirements

1. Store 2048 samples of α 2048-32 Bit words

2. Store 2048 samples of δ 2048-32 Bit words

3. Store control algorithm for input, normali-
   zation and storage of α and δ data samples

4. Store 2048 (ω) coefficients for FFT   2048-32 Bit words
   algorithm

5. Store instructions for FFT algorithm

6. Store DFT coefficients resulting from FFT   Use same storage
   process   as 1 & 2

7. Store instructions for algorithm to
   compute raw transfer function

8. Store 2048 complex coefficients repre-   Use same storage
   senting raw transfer function   as 1 & 2

9. Store instructions for FFT algorithm to
   transform freq domain FFT to time domain
   impulse response function

10. Store coefficients representing impulse   Same as 1 & 2
    response function

11. Store algorithm and coefficients for
    smoothing impulse response functions

12. Store coefficients representing smoothed   Same as 1 & 2
    impulse response function

13. Store algorithm for converting smoothed
    impulse response function back to
    frequency domain FFT

14. Store smoothed transfer function   Same as 1 & 2

15. Store algorithm for converting complex
    coefficients to values of magnitude
    and phase

16. Store coefficients representing magni-
    tude and phase of smoothed transfer   Same as 1 & 2
    function

17. Store algorithm for detecting major
    resonance and phase angle of flutter mode

18. Store algorithm for computing values of
    gain and phase for stability

19. Store algorithm for providing initial
    values of gain and phase and for outputting
    these values at a compatible rate to pro-
    vide continuous signal to D/A converter

20. Store algorithm for smoothly introducing
    adjusted values of compensation gain and phase
    to D/A for control.

Total data base storage is slightly greater than 6K-32 bit words.
(2048 words for ω coefficients could be stored in read only memory.)
The algorithm instructions could be handled by 2K works. Minimum total
storage of 8K could be slightly greater depending on complexity of algorithm
for determining resonance mode and computing gain and phase.

3.4.2.7 Areas for Examination and Discussion of Requirements - The
major requirement in this approach is the time required to collect suffi-
cient data samples to provide a spectrum analysis with a resolution of 0.1
Hz, that is 10 seconds. This time requirement impacts the proposed system
in two ways. One way is that the response time will be as long as 11 seconds
or possibly longer even with high speed processing. The second way is the
availability of representative input signals for the 10 second interval
under operational conditions.

Another requirement is the capability of defining the open loop transfer
function with sufficient fidelity in the presence of wind gust disturbances
using swept sine or random input signals, to be able to perform the neces-
sary analysis, within the limitations of real time operation and with the
limited processing and storage capability available in a practical opera-
tional implementation. This capability has been studied by analysis and
simulations to select the proper FFT algorithm, processing accuracy require-
ments, and smoothing techniques and will be discussed in Section 3.4.3.

A third requirement is the ability to identify the flutter resonance
mode from the Nyquist plot characteristics and develop an algorithm which
can interpret the data and define the compensation gain and phase lag to
stabilize the system. This has also been studied by analyses and simula-
tions to define a workable method and is discussed in Section 3.4.3.

A general purpose computer operating at 400K operations per second with
8 to 10K of core memory would be required. Data storage requirements could
be reduced if sample rates were cut in half with associated pre-sampling
filter. This does not seem to be desirable since the accuracy of the recon-

structed open loop transfer function would be affected. Increasing proces-
sing speed would have very little impact on the response time since the ten
seconds required to collect the data analysis frame is the dominating time
factor.

3.4.3 <u>Adaptive Flutter Control System Design Approach</u> - To further
evaluate the practicality of the adaptive flutter control system described
in Section 3.4.2 the following design steps were established and will be
discussed in detail in this section:

1. Test several types of excitations (step, swept sinusoidal, various
types of noise) to see which best reconstructs the Fourier transform of
the open loop system frequency response. The time domain program FLTR
(Flutter Time Response) is used together with a fast Fourier transform
subroutine (HARM) from the IBM Scientific Subroutine Package. Nonlinearities
(aileron actuator rate limits) are included in the analysis.

2. Using the best of the input excitations, assess the effects of wind
gust disturbances as well as try various smoothing procedures to improve
the quality of the reconstructed system open loop frequency response.

3. Use a check case for which the proper control laws are known. Design
an algorithm to locate the flutter resonant loop major axis as well as an
algorithm to adjust the pure phase lag and gain. Test this logic at sub-
flutter and post-flutter velocities. Include wind gust and nonlinear effects.

3.4.3.1 <u>Excitation Signal Determination</u> - A test signal must be used
to ensure an accurate definition of the open loop transfer function frequency
response since there is no guarantee of enough energy in natural excitation
such as atmospheric turbulence or flight control system commands. In
theory, any type of input can be used to reconstruct the system frequency
response. In practice, it was felt that some types of input would work
better than others.

Figure 38 presents results for random noise excitation. The config-
uration is the 370 gal. tank - 90% full with control system components
from Reference 4 except that the feedback gain is unity and there
is no pure phase lag network. The random noise with a standard deviation
of 1.0 deg RMS was generated by sampling a signal with uniform probability
distribution and holding that signal over each of the sample intervals
(204.8 samples/sec). The noise was input to the servo actuator in
the time domain program FLTR. The discrete Fourier transform (DFT)
was obtained by operating on the FLTR output with the HARM subroutine.

68
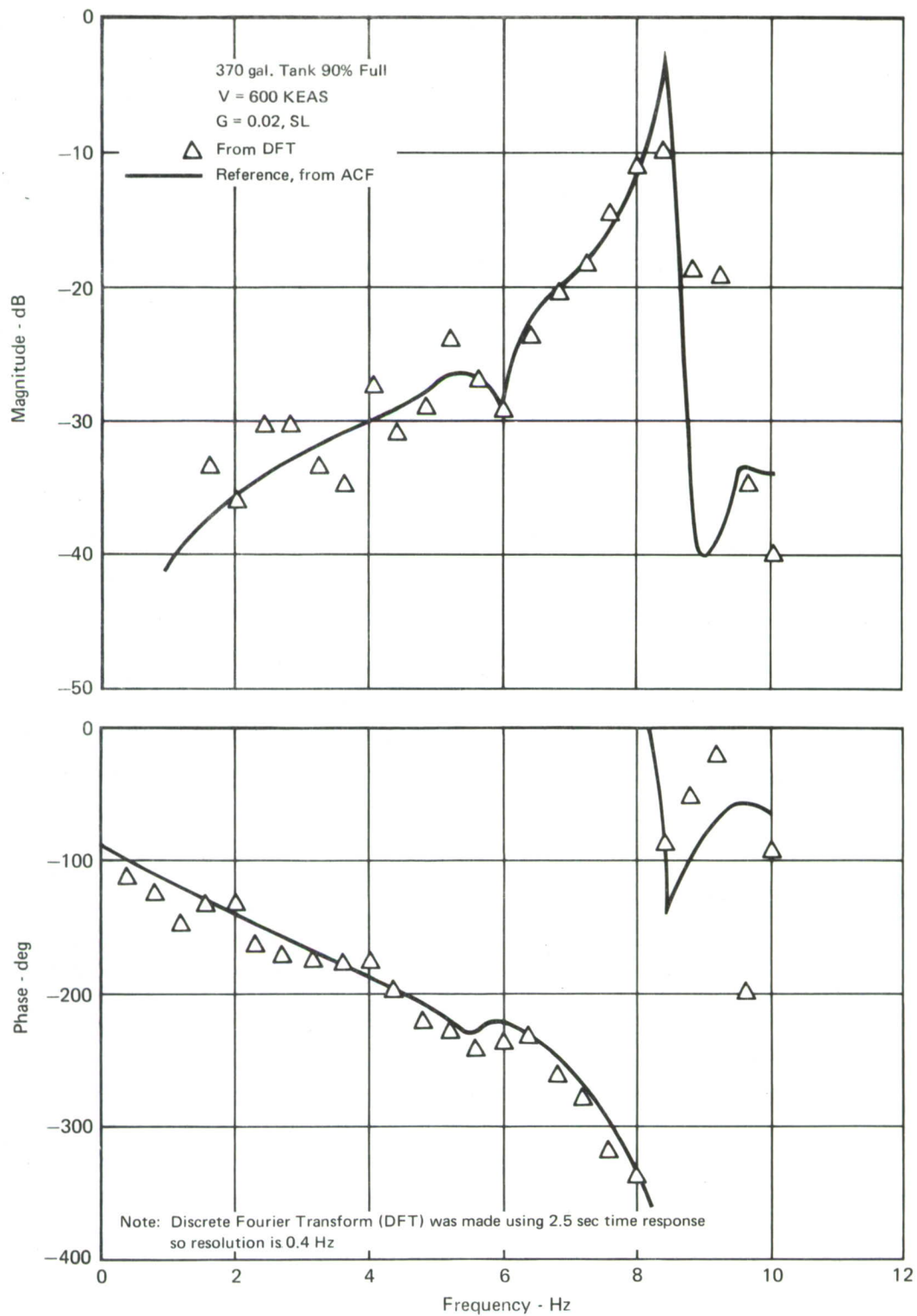
FIGURE 38
COMPARISON OF OPEN LOOP FREQUENCY RESPONSE USING RANDOM
NOISE EXCITATION

The ACF (Active Control of Flutter) frequency domain program was run with the same data and the results are shown in the figure for comparison. There is good agreement at and below the flutter frequency with mediocre agreement at higher frequencies.

Several deterministic excitations were tested and it was found that a linear swept sine best reproduced the system's frequency response. During the remainder of the analysis and design the swept sine was used as the primary test input. It should be mentioned that the random test input produced frequency responses almost as good as the swept sine. An intuitive explanation of the swept sine superiority is that it contains more "power" in the frequency range of interest (4 to 15 Hz) than does the random input.

Any nonlinearity in the actuator, airframe, sensors or electronics will cause a degradation in the open loop transfer function. To investigate the effect of the aileron actuator rate limit, a run was made in which the signal was rate limited more than 60% of the time. Figure 39 shows the frequency response of the system with and without the rate limit. The excitation for this response was a 2.5 sec 1.0 rad RMS linear sinusoidal sweep of frequencies between 4-15 Hz. The response for the rate limited system is seen to be slightly lower in magnitude with slightly more phase lag than the response for the unlimited system. The response obtained using the ACF frequency domain program is also shown in the figure for comparison. There is good agreement using the swept sine input over the entire frequency range of interest.

3.4.3.2 Atmospheric Turbulence Effects on System Frequency Response Reconstruction - Atmospheric turbulence will cause degradation in reconstructing the open loop system frequency response which is obtained by ratioing the system output Fourier transform to the input Fourier transform. To study this effect the program FLTR was used to generate time histories of the aileron command signal and wing twist accelerometer signal for a given wind gust level. The input dither signal to the aileron was a linear swept sine wave, 4 to 15 Hz, with 1 deg RMS amplitude for 10 seconds. The fast Fourier transform (FFT) of these two signals were ratioed to obtain the frequency response of the open loop system. Figures 40 and 41 show the Nyquist plots obtained at various gust levels. The Dryden wind gust representation defined in Section 3.2.1.2 was used to simulate the atmospheric turbulence. Good agreement of the DFT with the ACF program is seen for the
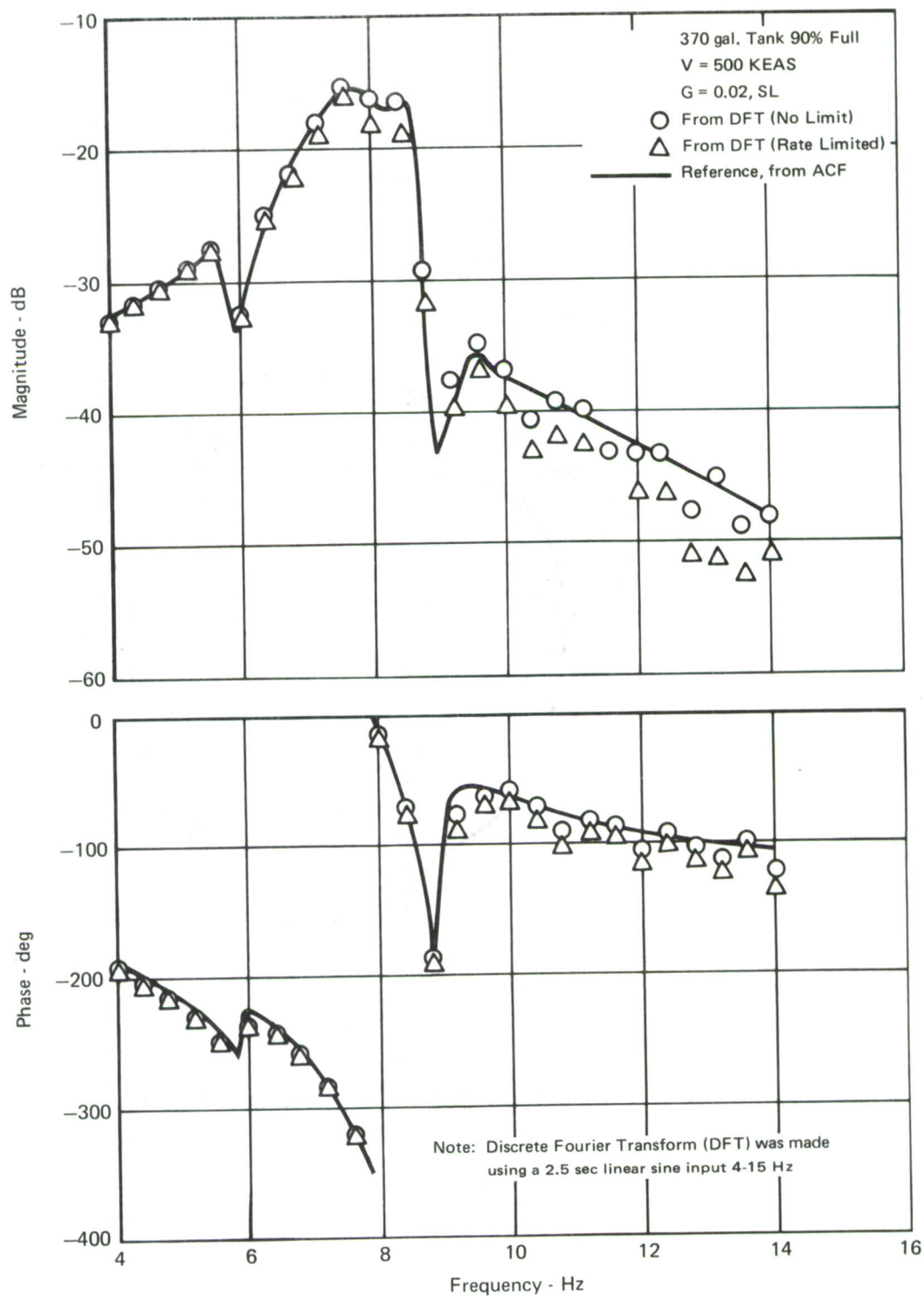
FIGURE 39
COMPARISON OF OPEN LOOP FREQUENCY RESPONSES FOR RATE LIMITED AND UNLIMITED SYSTEM USING SINUSOIDAL EXCITATION
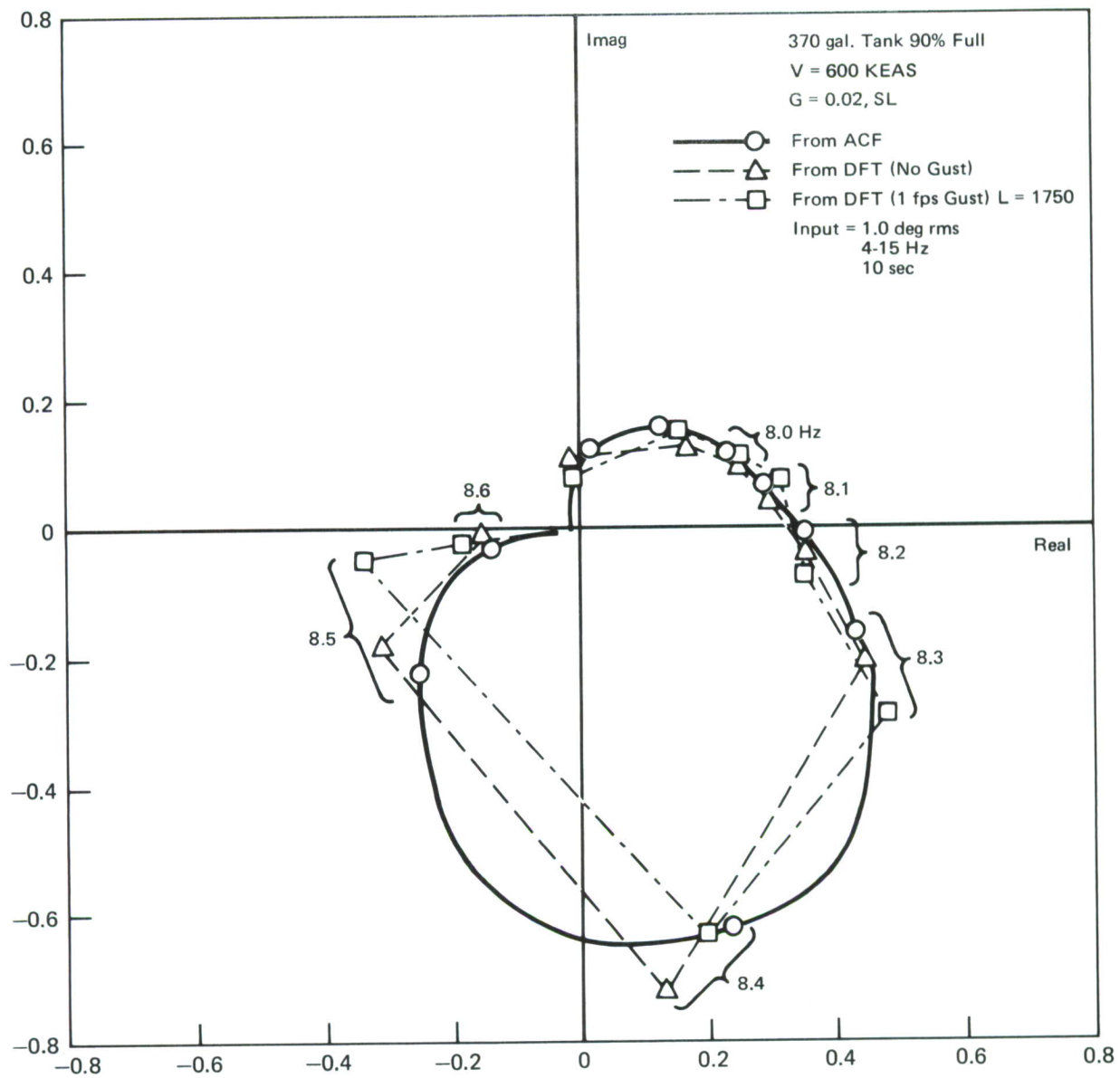
FIGURE 40
EFFECT OF TURBULENCE ON NYQUIST PLOT
Zero and 1 FPS Gusts
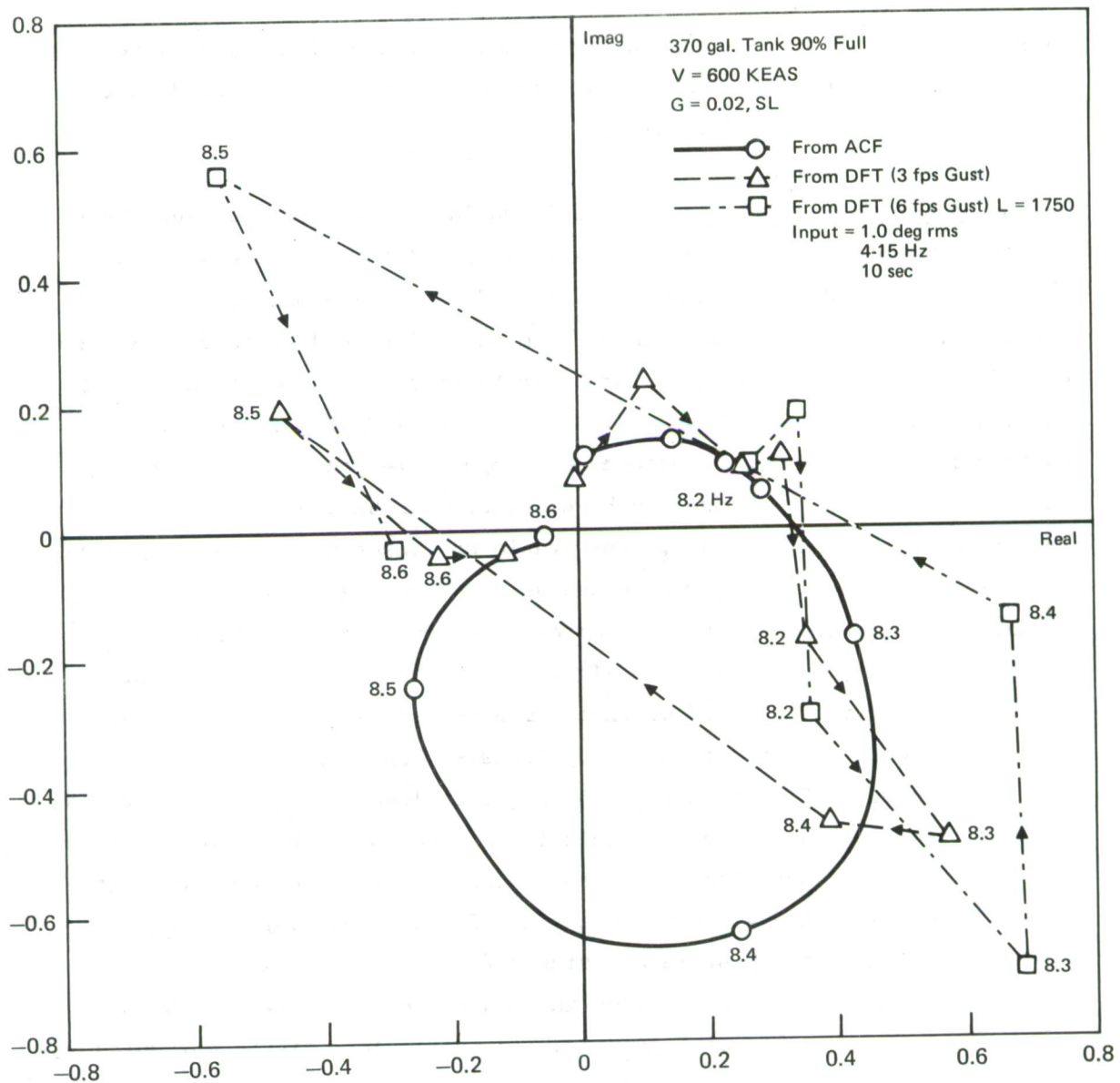
FIGURE 41
EFFECT OF TURBULENCE ON NYQUIST PLOT
3 and 6 FPS Gusts

low gust levels of 0 and 1 fps in Figure 40. For the higher gust levels of 3 and 6 fps in Figure 41, the Nyquist plot of the DFT is seen to differ significantly from the ACF results.

3.4.3.3 Smoothing Investigations

o <u>Triple-Transformation</u> - Since it would be difficult to identify the magnitude and phase of the major axis from the plots of Figure 41 some smoothing must be done. One possible procedure for minimizing the effect of turbulence using small amounts of aileron motion is described in Reference 25. This method computes a transfer function by ratioing the FFT of the output to the FFT of the input. The inverse FFT of this transfer function is then computed to produce the impulse response of the transfer function. This time response can be considered to be the true impulse response with some noise added. For stable systems the true response will tend toward zero as time increases and so for large values of time the true response is small compared to the noise. The smoothing is done by scaling down those time regions where the signal to noise ratio is small using an exponential function. This "smoothed" impulse response is then **retrans**formed to produce a smoother open loop transfer function.

The inverse FFT was made on the Nyquist plots of Figure 41 producing a noisy system impulse response. This impulse response was smoothed by multiplying by an exponential and then transformed back to the frequency domain. Figures 42 and 43 show the effect of this smoothing technique for the 3 fps and 6 fps gust level using different exponential smoothing functions. Some improvement is seen in each of these figures compared to the unsmoothed results of Figure 41. In particular, Figure 43, which is for a 6 fps Dryden gust, is very promising. The major axis of the DFT loop in this figure compares well with the ACF data. The attenuation caused by the exponential smoothing function can be subsequently corrected for as suggested by Reference 25. Corrected data points are shown in the figures.

o <u>Averaging of Two Successive Records</u> - Another promising smoothing technique is to time average signals for two successive test periods before Fourier transforming. This procedure enhances the quality of the frequency response reconstruction as shown in Figure 44. This test case was made for the post-flutter velocity of 700 KEAS in a 3 fps Dryden gust. A linear swept sine test signal with 2.5 deg RMS amplitude was applied for 10 sec, removed for 2.5 sec, then reapplied for 10 sec. The time averages of the input and output signals for the closed loop system were then Fourier trans-
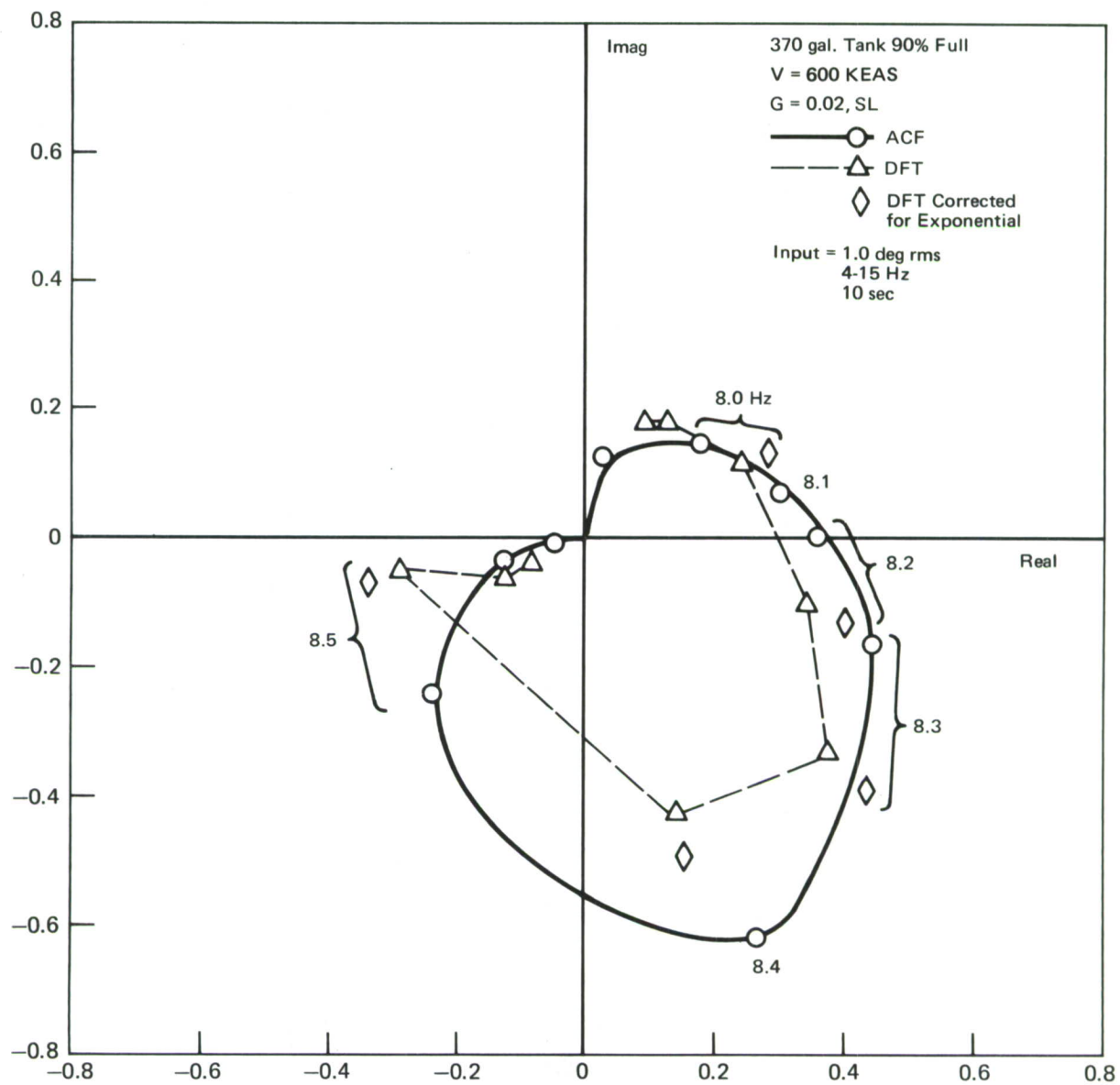
FIGURE 42
EFFECT OF TRIPLE-TRANSFORMATION ON NYQUIST PLOT
Smoothing Function $e^{-0.15t}$ — 3 FPS Gust
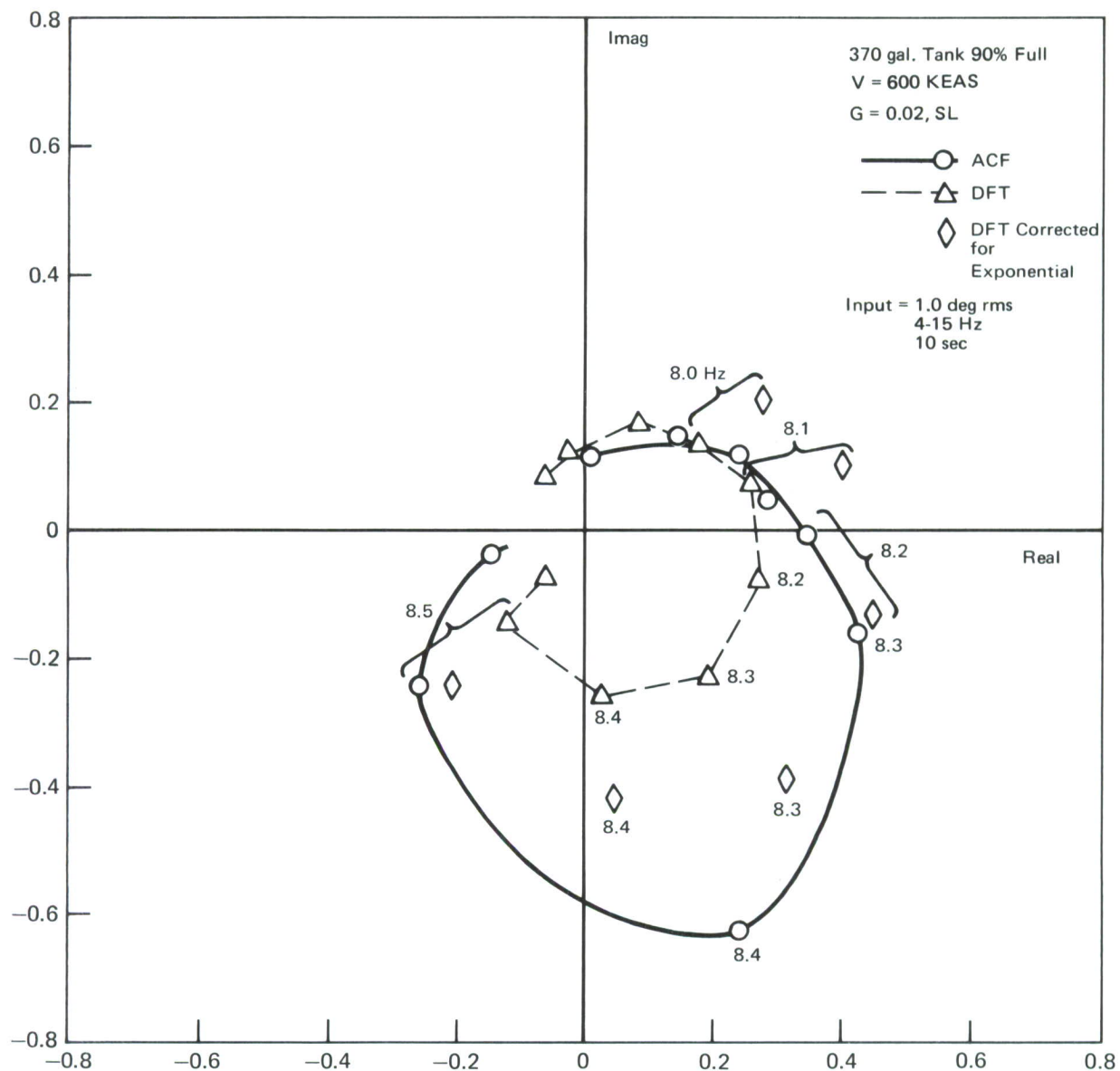
FIGURE 43
EFFECT OF TRIPLE-TRANSFORMATION ON NYQUIST PLOT
Smoothing Function $e^{-0.5t}$ —6 FPS Gust
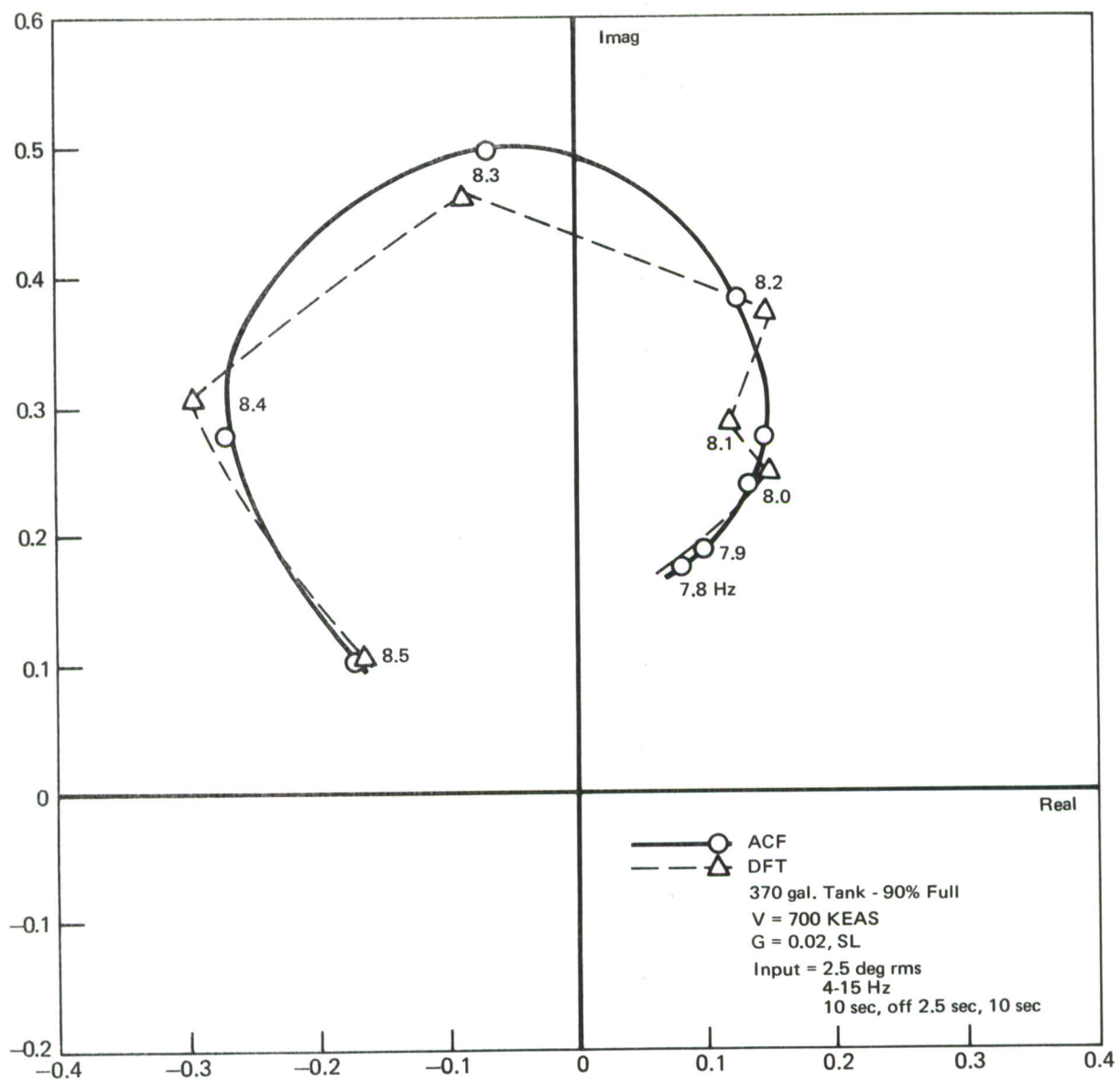
FIGURE 44
OPEN LOOP FREQUENCY RESPONSE RECONSTRUCTED USING AVERAGING METHOD
3 FPS Gust

formed. The comparison with ACF results, also shown in Figure 44, is excellent. The 22.5 sec data acquisition time is the major disadvantage of this technique.

    o <u>Improvement of Resolution</u> - Since a 10 sec time interval is used by the FFT for transformation, the frequency response resolution is 0.1 Hz. For some configurations this may not be enough resolution. Several methods could be used to interpolate between these given frequencies. One method is to take repeated FFTs of the same 10 sec data record using the frequency-shifting theorem;

      if $F(\omega)$ is the Fourier transform of $f(t)$,

      then $F(\omega-\omega_o)$ is the Fourier transform of $e^{j\omega_o t} f(t)$.

Results using this method are shown in Figures 45 and 46. These figures were made from four successive FFTs of a single 10 second data record. The final resolution is 0.025 Hz. The results look very good without a gust input, but the plots become somewhat distorted with the gust present. Nevertheless, because of the improvement of Figure 46 as compared with Figure 41, it is felt that the frequency shifting theorem is a useful technique for resolution improvement.

    o <u>Increased Record Length</u> - To investigate if an increased record length helps to average out gust effects, a 20 sec data record was generated using a 20 sec, linear, swept sine input from 4-15 Hz with 1 deg RMS amplitude. This is about as long a record as can be processed with a contemporary on-board computer using the 204.8 samples/sec sample rate. The 20 sec data acquisition yielded a frequency resolution of 0.05 Hz when transformed. The Nyquist plot of this 20 sec record was compared with the Nyquist plot of a 10 sec data record interpolated once to give a 0.05 Hz resolution. Both records were made in a 3 fps gust. The conclusion is that the longer data acquisition time is not advisable.

    3.4.3.4 <u>Miscellaneous Notes on the Analyses</u> - All of the reported Fourier transform analyses were made using the 4 mode representation of the 370 gallon tank - 90% full configuration. To verify that the FFT algorithm works properly with other configurations and with more modes located at several other frequencies in the 4-15 Hz range, the time response program FLTR was used to generate data records for an 8 mode model of the MK-82 (3, 4) configuration in a no gust environment. The frequency response obtained by ratioing the input and output fast Fourier transforms was almost identical to the Nyquist obtained using the frequency domain program (ACF).
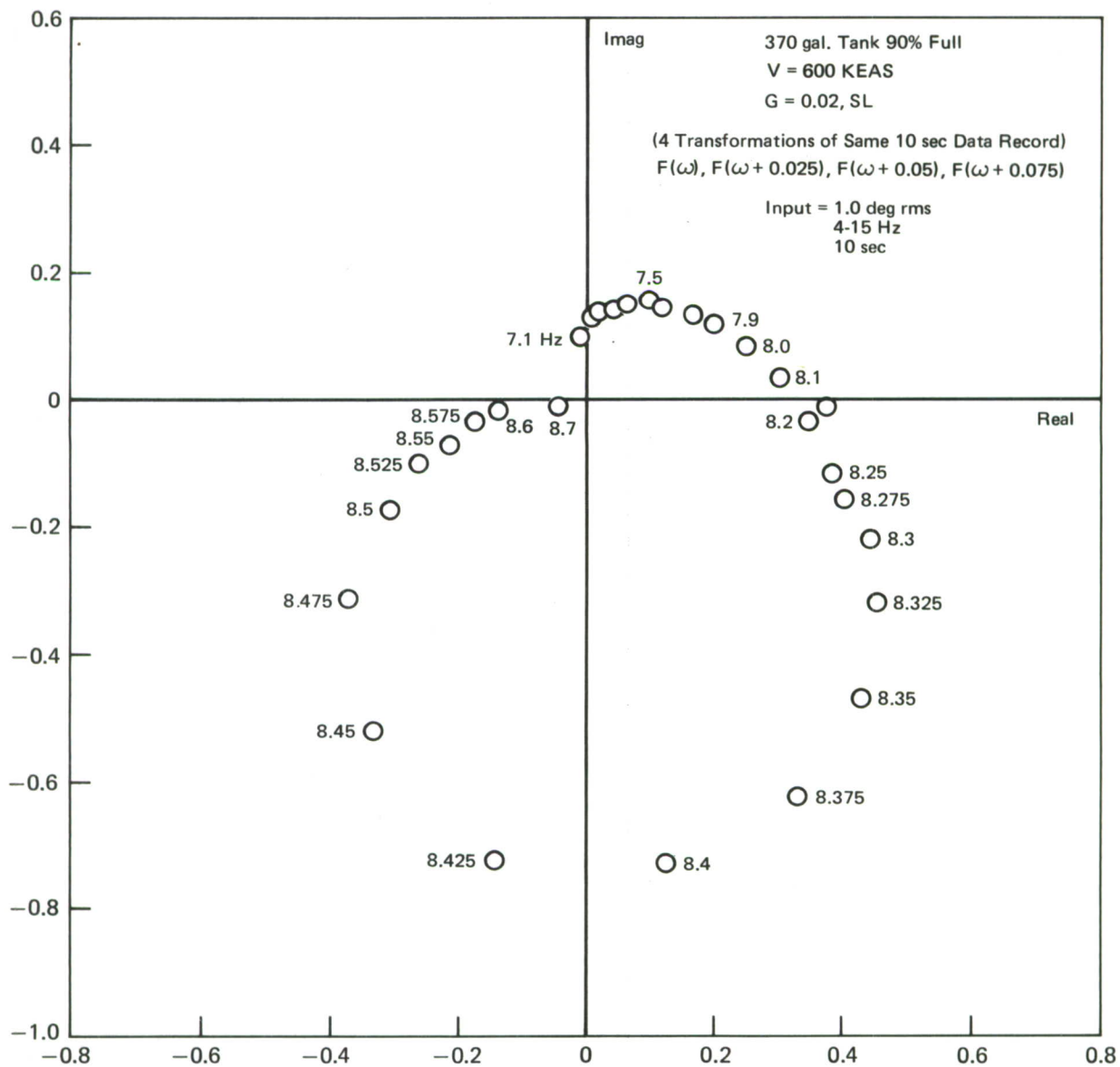
FIGURE 45
NYQUIST PLOT SHOWING HOW MULTIPLE TRANSFORMATIONS
CAN IMPROVE RESOLUTION
No Gust
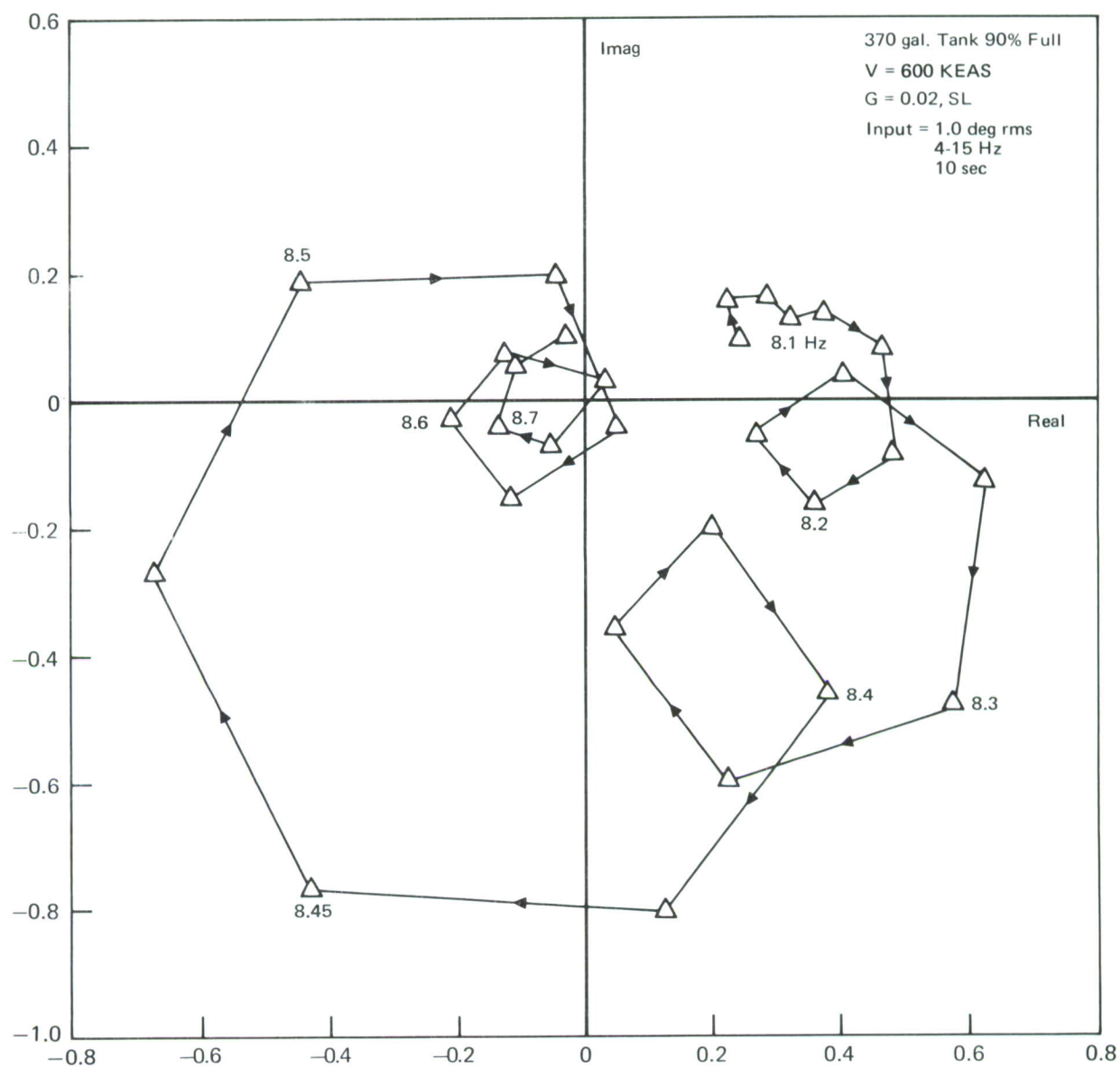
FIGURE 46
NYQUIST PLOT WITH MULTIPLE TRANSFORMATIONS
3 FPS Gust

The report presents results primarily at 600 KEAS (sub-flutter) for the 370 gallon tank - 90% full configuration. Most of those items discussed (i.e., smoothing, interpolating, and wind gust) were also checked at 700 KEAS (post-flutter). The trends seen and conclusions drawn from the 600 KEAS analyses were matched when studied at 700 KEAS.

The adaptive system technique involving fast Fourier transforms/Nyquist algorithm is a linear technique, provided aileron rate limits are not reached. If a 1 deg RMS swept sine is able to reconstruct the system's open loop transfer function in the presence of a 3 fps RMS Dryden wind gust, a 2 deg RMS swept sine aileron excitation would be able to reconstruct the transfer function in the presence of a 6 fps RMS Dryden gust and so on. This linearity was verified by a computer run.

All wind gust/fast Fourier transform analyses reported on used the same random number sequence. It was decided to reconstruct the system transfer function in 3 fps RMS Dryden gust environment using five different random number sequences (all of which in theory have 3 fps RMS, but in practice actually vary slightly from 3 fps). It was found that the random number sequence used was relatively unimportant. The sequence used throughout the studies was worse than all but one of these five new sequences. Hence the gust analyses reported are fairly conservative.

3.4.3.5 <u>Flutter Control Algorithm Implementation</u> - Once the open loop transfer function (compensated wing twist angle per aileron deflection) of the system is reconstructed via fast Fourier transforms to give its Nyquist plot, the control algorithm must find the required compensation for good stability margins. It has been assumed that adequate compensation may be obtained by adaptively changing only the gain and time constant of a pure phase lag network (block 6 in Figure 32). A flow chart of the algorithm is shown in Figure 47. The algorithm finds the major axis, checks whether the open loop system is stable or unstable (sub-flutter or post-flutter), and then finds the gain and phase lag needed to align the major axis with either the 0° axis (sub-flutter velocities) or the 180° axis (post-flutter velocities). This algorithm would yield balanced gain and phase margins with one iteration if the pure phase lag network yielded a pure rotation of the complete Nyquist plot. The frequency response of this network is shown in Figure 48. The lag is seen to be a function of frequency so this network will yield the desired pure rotation of the Nyquist plot only in the near vicinity of the frequency of interest. To ensure balanced stability margins

Find the major resonant frequency by comparing values of Δ arc length/Δ frequency.
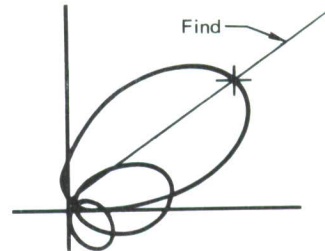
Determine if open loop system is stable or unstable by checking whether major loop is clockwise or counter-clockwise.
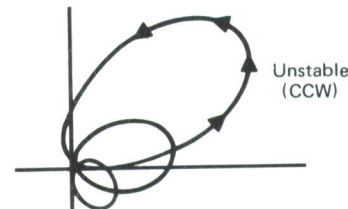
A. Find all points on ray from origin along the major axis which intersect the Nyquist plot. Choose the largest internal point (c) to gain scale. (On subsequent iterations search along either 0° or 180° as appropriate for Nyquist plot intersect.)
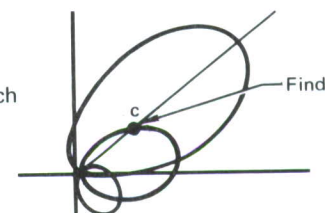
Gain scale by K for balanced gain margins.
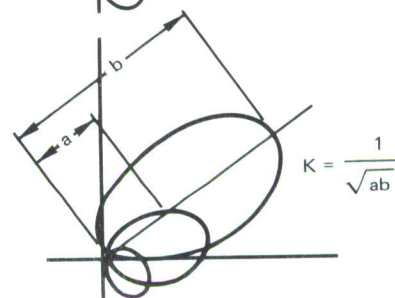
Search on the gain scaled Nyquist plot for those points of magnitude 1. Bisect the angle formed by the origin and the 2 points closest to and on either side of the major axis.
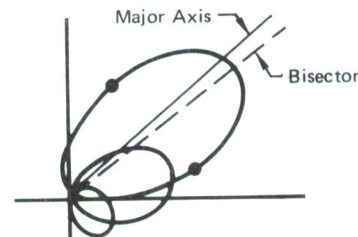
Find τ for pure phase network to align the Nyquist plot with the proper axis and modify the Nyquist plot by

$$K \frac{1 - j\omega\tau}{1 + j\omega\tau}$$

If not much change in K and τ since last iteration stop, or else go to A.
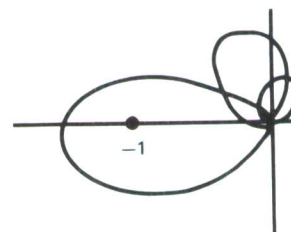
FIGURE 47
DESCRIPTION OF ADAPTIVE FLUTTER CONTROL ALGORITHM
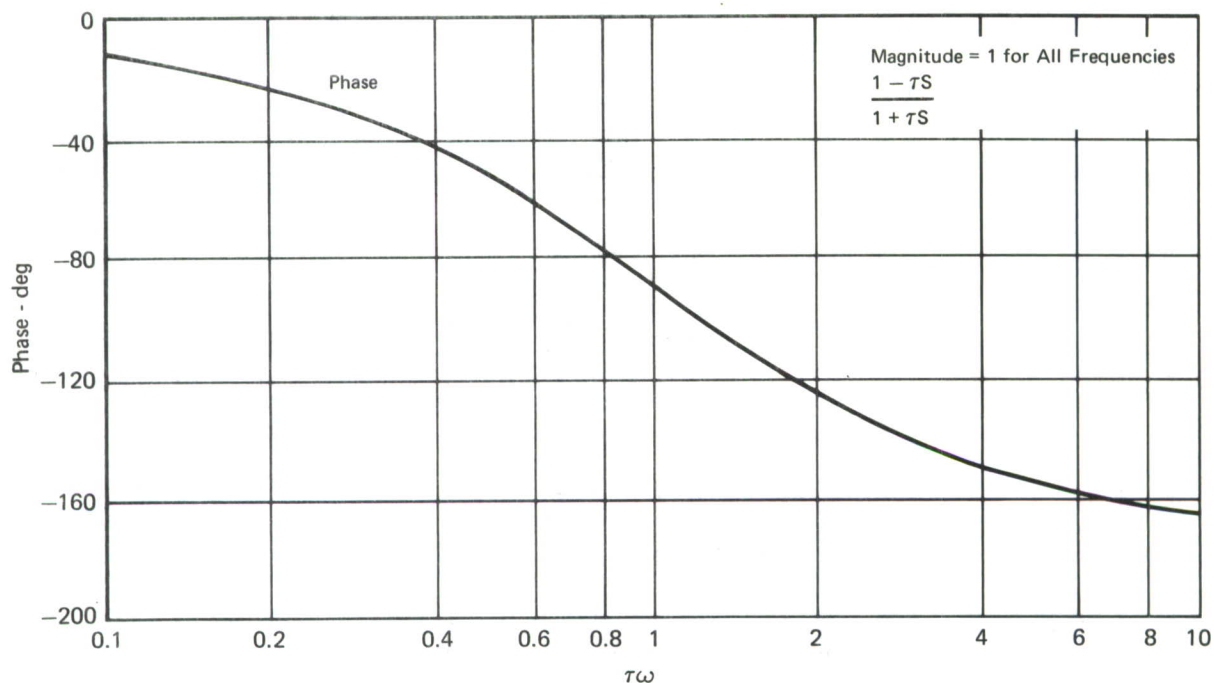
FIGURE 48
FREQUENCY RESPONSE OF PURE PHASE LAG

more iterations are needed. This algorithm was programmed in FORTRAN and tested on Nyquist plots for the 370 gallon tank - 90% full configuration. When tried on the Nyquist plots obtained by ratioing input and output FFTs in a no gust environment (Figure 40) the algorithm yielded the expected compensation. However, when tested on the Nyquist plot made from data corrupted by a 3 fps gust environment (Figure 41) the algorithm yielded compensation which would give the much reduced stability margins of 2.5 dB and 45 deg against flutter in the most critical direction with respect to the Nyquist loop. When tested with the smoothed Nyquist plots of Section 3.4.3.3 (Figures 42 and 44) the algorithm yielded compensation with acceptable stability margins.

3.5 Hydraulic System Modification Studies

The hydraulic modifications for a Flutter Control System (FCS) will consist of system and component changes to meet the operational and performance requirements. The most critical modifications are those associated with providing hydraulic power and achieving actuator dynamic performance. The impact of these modifications is more severe for high performance fighter type aircraft than for large bomber or transport type aircraft. The fighter type aircraft requires greater actuator dynamic response and

83
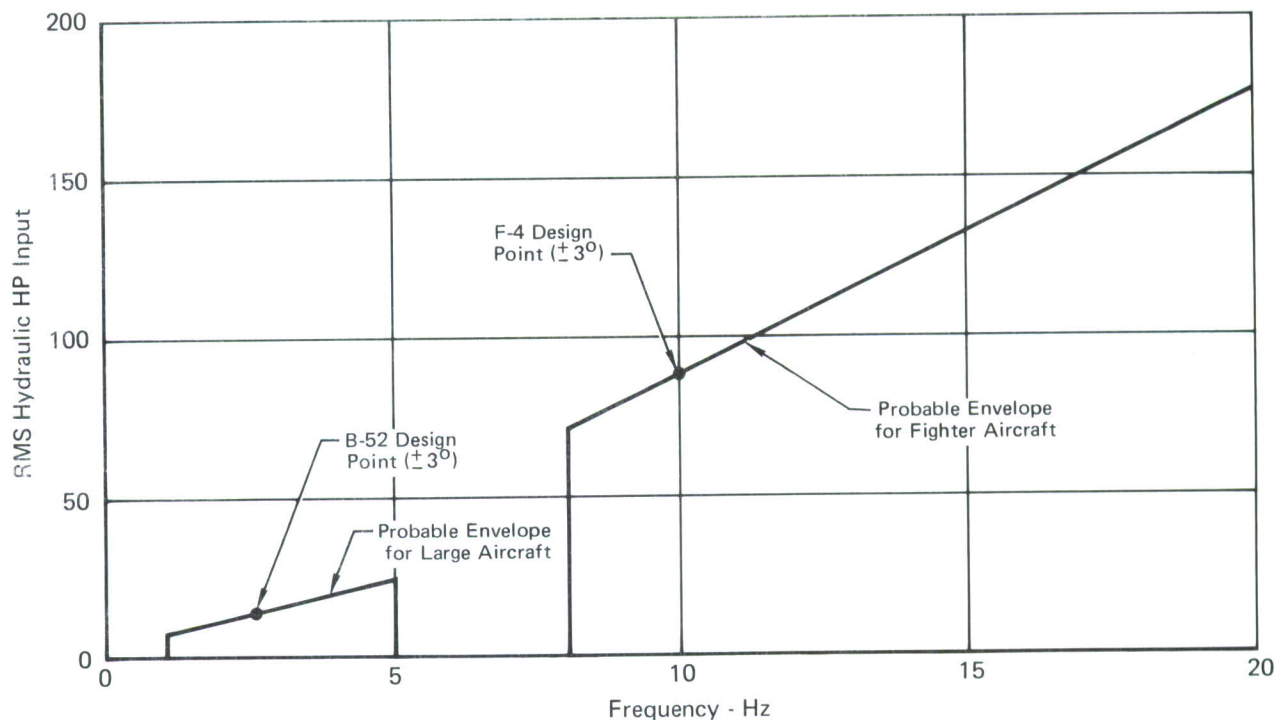
FIGURE 49
FLUTTER CONTROL HYDRAULIC POWER REQUIREMENTS

operates against greater actuator loads than the large aircraft. Figure
49 illustrates the differences in hydraulic horsepower requirements based
on B-52 and F-4 data.

3.5.1 <u>Hydraulic Supply and Distribution Systems - General</u>

3.5.1.1 <u>Analyses</u> - The following analyses must be performed to estab-
lish the design base for system modifications that will be required to meet
FCS performance requirements.

o <u>Hydraulic Flow Requirements</u> - Hydraulic flow requirements are
dependent on the required actuator cyclic frequency and amplitude. In
systems where the available flow is derived entirely from the pump, the
pump output capability must be at least equal to the peak actuator flow
requirement. In some cases where the peak flow occurs for only a small
portion of the cycle (such as with a sinusoidal actuator response) the
required pump flow can be based on the RMS actuator flow requirement with
an accumulator supplying the additional flow required for the small portion
of the cycle when peak flow is required, and then recharging during the remain-
der of the cycle when less than RMS flow is required. The RMS flow value is
0.707 of the peak flow requirement for sinusoidal operation.

84

Other hydraulic requirements that may occur simultaneously with FCS demands must be assessed and added to the power supply pumping capability.

o <u>Power Distribution System Line Sizes</u> - The hydraulic lines from the system to the actuator and from the actuator back to the system must be sized to provide an acceptable pressure drop and adequate fatigue life under operating conditions. In the case of high performance fighter type aircraft the flow requirements for a FCS are much higher than for normal flight control functions and consequently will require larger than normal line sizes to keep the pressure drop within acceptable limits. A value for acceptable line pressure drop cannot be established as it will vary with the aircraft involved due to such variables as the required actuator load pressure (due to surface hinge moment) during FCS operation and actuator servo valve pressure drop. Each application must be analyzed individually to determine acceptable limits and the lines sized accordingly.

o <u>Surge Pressure Levels</u> - Rapid opening and closing of the actuator servo valve during cyclic FCS operation will create pressure surges (commonly known as "water hammer") in the hydraulic lines. If the magnitude of the pressure surge is not maintained within acceptable limits fatigue failure of the lines and components can result. MIL-H-5440 requires that system surge pressure levels be limited to 135% of system normal pressure. This can be accomplished in two ways. The first method is to increase line size thus reducing the velocity of the fluid flow in the line. The second method is to add surge suppressors, such as small accumulators, in the system to absorb and dampen out the surge pressure peak to an acceptable level.

o <u>Thermal Considerations</u> - A FCS can require potentially high horse-power demands from the hydraulic system continuously during the period of operation. This will result in an increase in system temperature. A system thermal analysis must be performed to determine if the system will remain within operating temperature limits or if any additional system cooling provisions are required.

3.5.1.2 <u>System Modifications</u> - The system modifications will be those that have been determined necessary by analysis. For typical fighter type aircraft they will consist of one or more of the following changes.

o Increase pump size and/or add an accumulator to supplement the pump delivery for short term peak flow demand.

o If pump size is increased the main pressure discharge line may
require an increase in size. The pump suction line from the reservoir may
require an increase in size to prevent pump cavitation during high flow
demand.

o Increase the pressure and return line sizes between the power circuit
and the actuator.

o Install surge suppression devices.

o Provide hydraulic power hook-up to any new hydraulic components
required to provide FCS operation.

3.5.2 <u>Hydraulic Supply and Distribution System - F-4</u> - The F-4
hydraulic system (Figure 50) consists of three independent systems designated
as PC-1; PC-2; and Utility. PC-1 is supplied by a single pump driven by
the LH engine. PC-2 is supplied by a single pump driven by the RH engine.
Utility is supplied by two pumps, one driven from each engine. All four
pumps are identical.

The aileron surface actuators are dual configuration requiring dual
hydraulic power sources for redundancy. The left aileron obtains hydraulic
power from PC-1 and Utility. The right aileron obtains hydraulic power from
PC-2 and Utility. With two pumps in the utility system each half of each
aileron actuator obtains power from individual hydraulic pumps.

Each hydraulic system also contains an accumulator with approximately
25 cubic inches of fluid when fully charged.

3.5.2.1 <u>Analyses</u> - The analyses for the F-4 are based on a FCS that
will meet the following performance parameters. It will provide surface
deflections of up to ± 3 deg at frequencies up to 10 Hz. The continuous
running time per mission will be up to 5 minutes.

o <u>Hydraulic Flow Requirements</u> - The flow requirements per actuator
half (and thus per pump) to meet the specified performance are based on the
following actuator parameters:

Area - aileron "down" = 7.86 in.^{2}

Area - Aileron "up" = 4.96 in.^{2}

Linear stroke for 3 deg of aileron = 0.19 in.

Therefore the peak flow is equal to

$Q = 2\pi f A a$

where:

Q = peak flow - in.^{3}/sec
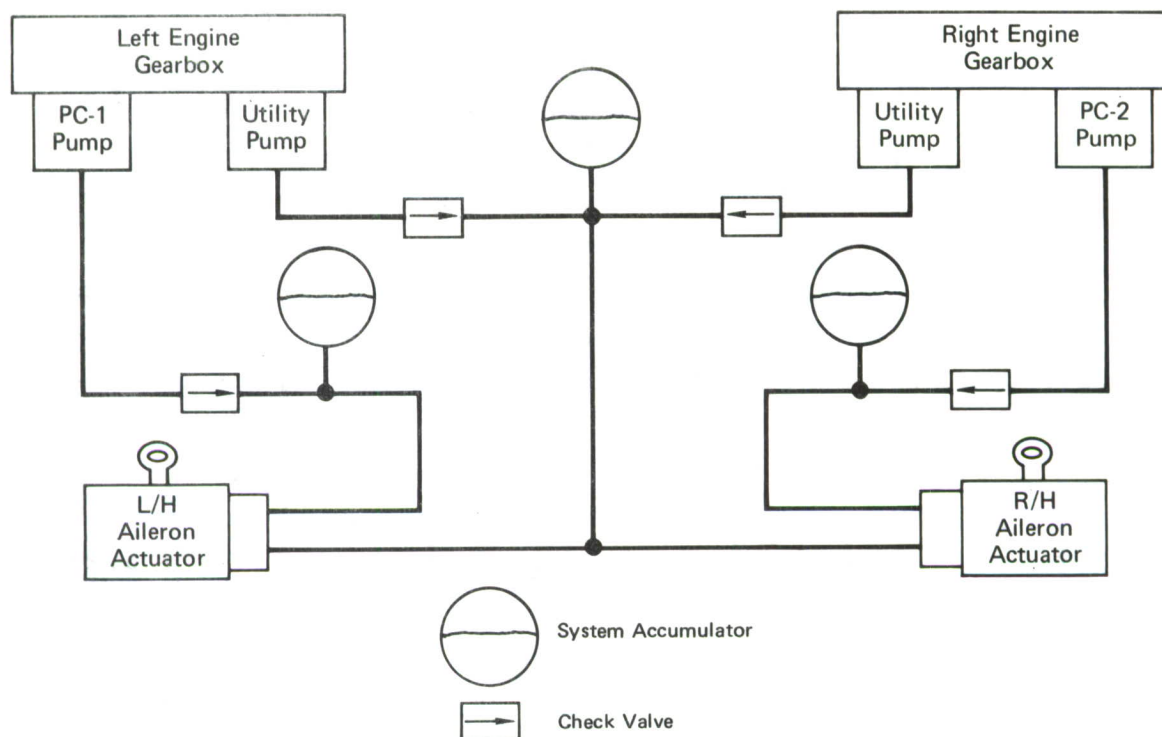
π = 3.1416

FIGURE 50
F-4 SIMPLIFIED HYDRAULIC BLOCK DIAGRAM FOR AILERON POWER

f = frequency - Hz

A = actuator area - in.^{2}

a = amplitude - in.

Solving for Q for aileron "down"

Q = 2 x 3.1416 x 10 x 7.86 x 0.19

Q = 93.5 in.^{3}/sec

$$= \frac{93.5 \times 60}{231} = 24.3 \text{ gal/min}$$

Solving for Q for aileron "up"

Q = 2 x 3.1416 x 10 x 4.96 x 0.19

Q = 59.2 in.^{3}/sec

$$= \frac{59.2 \times 60}{231} = 15.4 \text{ gal/min}$$

The average peak flow per cycle is $\frac{24.3 + 15.4}{2} = 19.85$ gpm. The F-4 pump flow is 25 gallons per minute and will meet the peak flow requirement for either aileron down or up. Moreover, the F-4 hydraulic system contains accumulators so the peak flow requirement, which exists for only a few milliseconds per half cycle, need not depend on full pump capability on a

continuous basis. Therefore, the continuous flow required from the pump
will be the RMS value of the average flow per cycle. The continuous flow
required will be 0.707 x 19.85 or 14.1 gallons per minute. With a pump
capacity of 25 gallons per minute this leaves 10.9 gallons per minute
per pump available for other hydraulic requirements. During the period of
FCS operation this is more than adequate as other high hydraulic flow
requirements such as landing gear operation and extreme stabilator deflec-
tions at maximum rate will not be required. It can be concluded that the
F-4 hydraulic power circuits are adequate without modification to provide
power for a FCS and provide simultaneous power for other functions.
Figure 51 depicts the total hydraulic flow required for a FCS at different
frequencies and amplitudes compared to total system flow capability.

o Power Distribution System Line Sizes - For 3 degrees of aileron de-
flection at the speed and altitude where FCS operation is required, the aileron
actuator must develop 55% of its maximum output force. This is equivalent
to 1600 PSI pressure differential across the actuator piston. The main
control servo valve requires 1000 PSI pressure drop at the specified per-
formance level. The pump discharge pressure at the required flow is approxi-
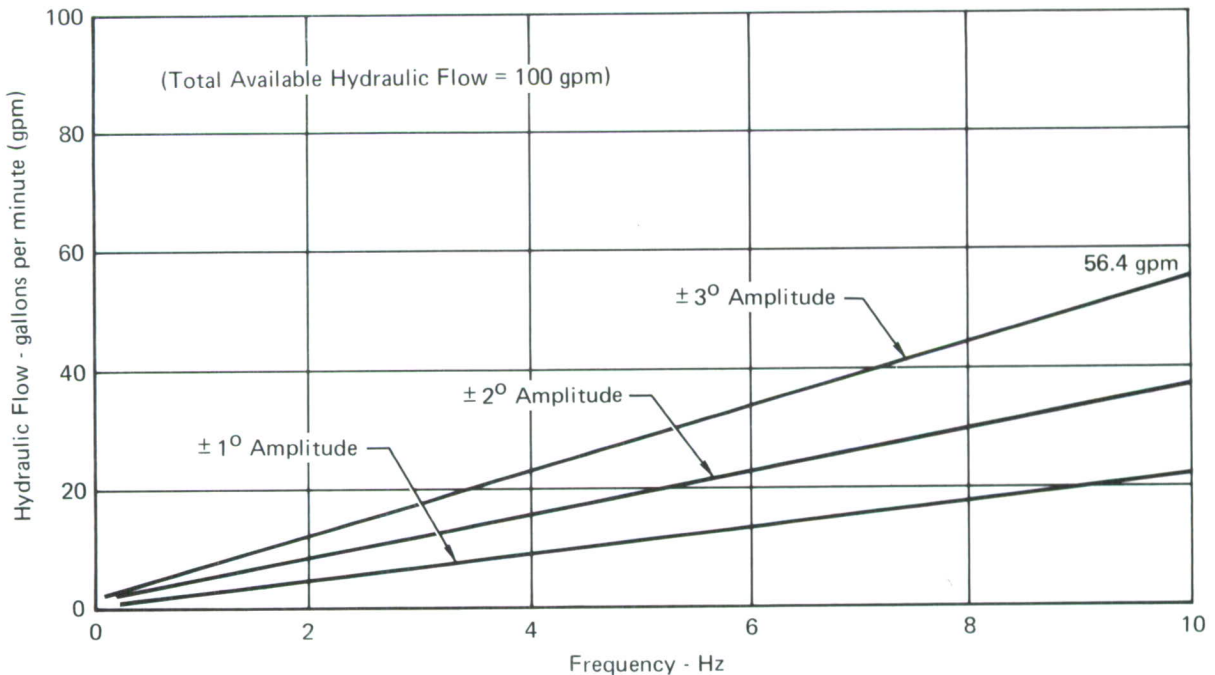
FIGURE 51
FLUTTER CONTROL RMS FLOW REQUIREMENTS vs TOTAL AVAILABLE
F-4 HYDRAULIC FLOW

mately 2900 PSI. The actuator load pressure and the valve pressure drop
added together are equal to 2600 PSI. This leaves 300 PSI allowable for
hydraulic line pressure drop. There is 15 feet of line to the actuator and
15 feet from the actuator back to the reservoir or a total of 30 feet of
line. With 300 PSI allowed pressure drop this amounts to 10 PSI per foot.
The existing distribution lines in the F-4 are of 3/8 inch tube size. This
would result in a line pressure drop of approximately 63 PSI per foot or
1890 PSI total. Obviously, the distribution line sizes will have to be
increased. The 10 PSI per foot line pressure drop can be met with 1/2 inch
tube size.

o Surge Pressure Levels - Surge pressure, more commonly known as
"water hammer", is the term for overall effects of pressure transients in
a piping system. More specifically, it is fluid shock resulting from the
opening or closing of a valve or other flow control component. It includes
effects of initial system pressure, fluid inertia, piping dimensions,
pipewall elasticity, fluid bulk modulus, and valve operating time.

During the closing cycle of a valve the kinetic energy of the moving
fluid is converted into potential energy. Elasticity of the fluid and pipe-
wall produces waves of positive and negative pressures which are superimposed
on the original pressure and travel from the valve, through the fluid in
the pipe, to the pressure source (pump) and back to the valve. This wave
gradually dampens out due to effects such as fluid flow friction and pipe
elasticity. If the magnitude of this pressure wave is excessive it can
result in fatigue failures of the piping and components.

The critical period is the time of one round trip of the pressure wave
from valve to pressure source and back and establishes the severity of the
pressure surge. If the valve closes within this critical period the pressure
surge is the maximum. If the valve does not completely close within the
critical period the maximum surge pressure will be less and its magnitude
will depend on the change of fluid velocity in the pipe during the period
of the pressure wave making its round trip in the pipe.

The velocity of the shock wave in the pipe can be calculated from the
following equation.

$$V_s = \frac{12}{\sqrt{\frac{D}{G} \left(\frac{1}{B} + \frac{di}{wE}\right)}}$$

where:

V_s = velocity of shock wave - ft/sec

D = fluid density - lb/ft^3

G = 32.2 ft/sec^2

B = fluid bulk modulus - lb/in.^{2}

di = pipe inside diameter - in.

w = pipe wall thickness - in.

E = modulus of elasticity of the pipe material-lb/in.^{2}

For common aircraft hydraulic system practice, using steel tubing and MIL-H-5606 fluid, this equates to a V_s of approximately 4500 feet per second.

For the F-4 the distance for the shock wave round trip is 30 feet and $\frac{30}{4500}$ = .0067 seconds is the time required for the shock wave round trip. With the actuator cycling at 10 Hz the time for the valve to move from full open to full closed is equivalent to 1/4 of a cycle or .025 seconds. Thus, it is apparent that the valve is not fully closed while the shock wave makes its round trip. At peak flow rate the fluid velocity in 1/2 inch diameter tubing is 57.5 feet per second. With a sinusoidal input the fluid velocity in the tubing after .0067 seconds is 17.8 feet per second.

The pressure rise (surge) above base pressure can be calculated from the following equation.

$$P = \frac{D}{144G} \times V_s \ (V - v)$$

where:

P = pressure rise - lb/in.^{2} (PSI)

D = fluid density - 53.2 lb/ft.^{3}

G = 32.2 ft/sec^2

V_s = shock wave velocity - 4500 ft/sec

V = initial fluid velocity - 57.5 ft/sec

v = fluid velocity after shock wave round trip- 17.8 ft/sec

$P = \frac{53.2}{144 \ (32.2)} \times 4500 \ (57.5 - 17.8)$

P = 2045 PSI

Base pressure is equal to pump output pressure minus supply line pressure drop or 2900 - 150 = 2750 PSI. Line surge pressure = 2750 + 2045 or 4795 PSI. The line pressure surge level should not exceed 135% of

nominal system pressure or 135% of 3000 = 4050 PSI. To hold the pressure surge within specification MIL-H-5440 limits will require the installation of surge suppression devices.

One common means of providing surge suppression is the use of small accumulators which have the effect of adding capacitance to the line. They may range in capacity from a few cubic centimeters to a few cubic inches in size. Due to the many system variables that will effect their size such as hoses, bends in tubing, and fittings, their required size is best experimentally determined as part of the ground test program. In any event they will be relatively small components.

o <u>Thermal Considerations</u> - The F-4 normal hydraulic fluid temperature at the reservoirs does not exceed 135°F. Thermodynamic calculations indicate that hydraulic system temperature rise, due to continuous FCS operation at maximum performance conditions, will be 20°F per minute after system temperature has reached 185°F. It will take one to two minutes for the system to reach 185°F thus allowing 5-1/2 to 6-1/2 minutes of maximum performance operations before the maximum allowable system temperature of 275°F is reached. Therefore, there is no hydraulic system thermal problem associated with a FCS in the F-4 airplane as the maximum operating time is five minutes.

3.5.2.2 <u>System Modifications</u> - Analysis has shown that there are no modifications required in the hydraulic power system of the F-4 airplane for installation of an FCS. The only modifications required are in the distribution system and are as follows.

o Surface actuator pressure and return lines will require changing from 3/8 inch to 1/2 inch tubing.

o Installation of surge suppressors as required in the pressure lines to limit peak pressures to 4050 PSI. Size and location to be determined on the ground test rig (Iron Bird).

o To provide mechanical commands to the surface actuators requires the use of a separate electro-hydraulic servo actuator that accepts the FCS electronic system signals. It will therefore be necessary to install hydraulic lines to provide the required hydraulic power to the electro-hydraulic servo actuator.

3.5.3 Component Modifications - General

3.5.3.1 Analyses - The major hydraulic component in a FCS where thorough performance analysis is required is the surface actuator. When a FCS is applied to a high performance fighter type aircraft a significant increase in the actuator dynamic response, from that required in a normal flight control system, is necessary. A thorough stability analysis of the actuator-airframe system loop must be made to determine the upper limit of actuator gain that can be tolerated and still maintain a stable system.

After the maximum actuator gain has been established the actuator must be analyzed for capability to provide the required gain and output velocity. The use of a FCS will subject the actuator to a much more stringent fatigue criteria than normally associated with a flight control system. A thorough fatigue analysis may result in new and more stringent fatigue criteria for actuator design.

3.5.3.2 Design Considerations - The following design considerations are applicable to a revised surface actuator.

o System redundancy requirements must be achieved.

o Single point failure areas are to be at an absolute minimum and where unavoidable shall not have failure rates in excess of the design criterion of Section 2.5.3.

o The required gain and actuator velocities can be achieved.

o Seals must be capable of long life under FCS operation.

o The design must be compatible with increased fatigue criteria requirements.

3.5.4 Component Modifications - F-4 - For the F-4 airplane component modifications for a FCS system consists of modifications of the aileron surface actuator and the Survivable Flight Control System (SFCS) Secondary Actuator.

3.5.4.1 Analyses

o Aileron Surface Actuator Gain - The existing F-4 aileron surface actuator has an unloaded open loop gain of 20.3 Radians. It is desirable for FCS operation to provide a loaded open loop gain of 63 Radians which, due to the actuator gain being load dependent, results in an unloaded open loop gain of 109 Radians or an increase in gain by a factor of 5.4. This could be accomplished in the actuator design, however, the actuator stability analysis indicates that a maximum gain increase of 3.5 in the actuator is

all that can be tolerated. This gain limitation requires that additional gain and phase compensation techniques must be provided in the FCS electronics system.

    o <u>Aileron Surface Actuator Stability</u>

<u>Introduction</u> - Active flutter control requires an aileron actuator with a higher bandwidth than the standard F-4 actuator. This increased bandwidth can be obtained by several different methods; but the least expensive and most practical method is to simply increase the gain of the master control valve on the present actuator.

A stability analysis was performed to determine to what extent the actuator gain could be increased without the use of special stabilizing techniques.

<u>Stability Analysis</u> - The aileron actuator is a closed loop servo system which makes use of a moving body installation for position feedback to the master control valves. The schematic of the aileron actuator installation in Figure 52 shows the relationship between the actuator, the control linkage, installation geometry, structural spring rates and aileron surface inertia. This actuator installation can be represented by the linear math model shown in Figure 53. The definition of parameters is given in Table 9. The masses of the actuator piston and cylinder are small when compared to the inertia of the surface reflected to the actuator cylinder as an effective mass. These smaller masses have very little effect on the overall system dynamics and therefore were not included in the math model. From a stability standpoint this math model is conservative because it does not include the master control valve conductance or structural feedback; both of which have a stabilizing effect. A closed loop transfer function for the aileron actuator math model can be represented by:

$$(1) \quad \frac{X_c}{X_i} = \frac{K_3 K_\Sigma L_2 (M_m S^2 + C_m S + K_o)}{(M_m K_o)S^3 + (M_m K_3 K_\Sigma L_2 L_3 + C_m K_o)S^2 + (C_m K_3 K_\Sigma L_2 L_3 + K_o K_\Sigma)S + K_o K_3 K_\Sigma L_2 L_3}$$

Substitution of the nominal parameter values from Table 9 into the actuator closed loop transfer function equation results in the following relationship:

$$\frac{X_c}{X_i} = \frac{(4.7 \times 10^6)S^2 + (9.2 \times 10^7)S + 1.5 \times 10^{12}}{(1.0 \times 10^6)S^3 + (2.4 \times 10^7)S^2 + (1.5 \times 10^{11})S + 1.5 \times 10^{12}}$$
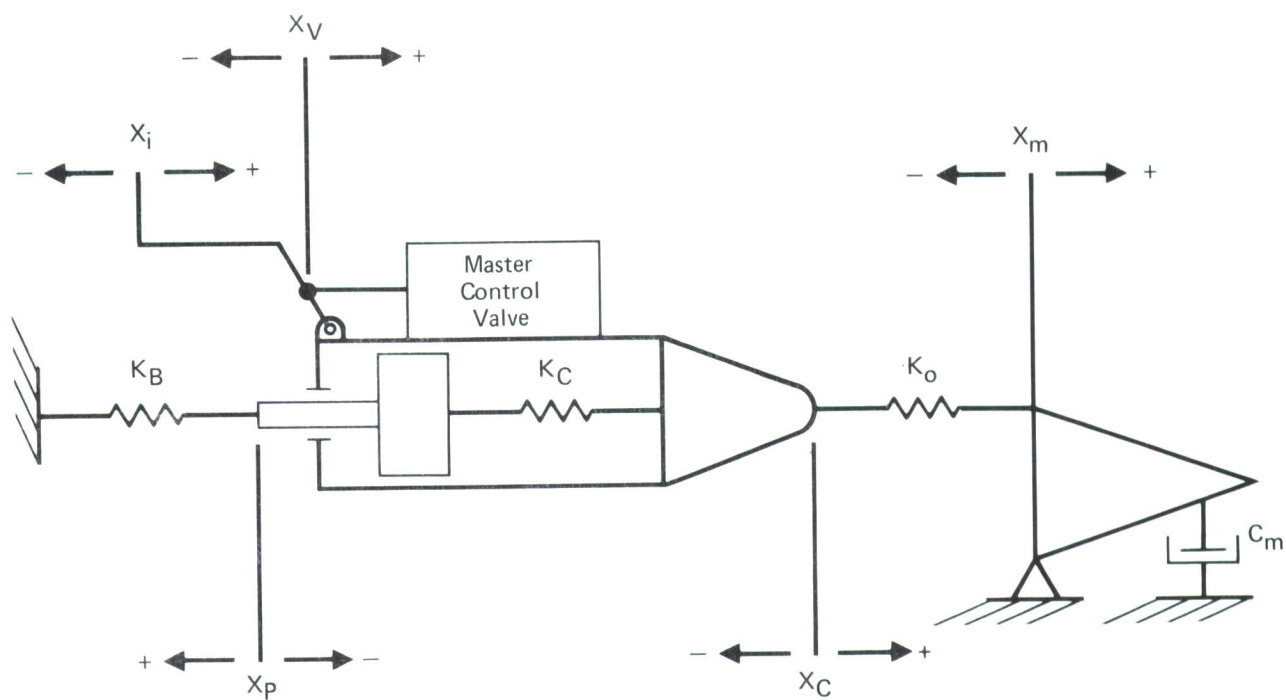
FIGURE 52
SCHEMATIC - F-4 AILERON ACTUATOR
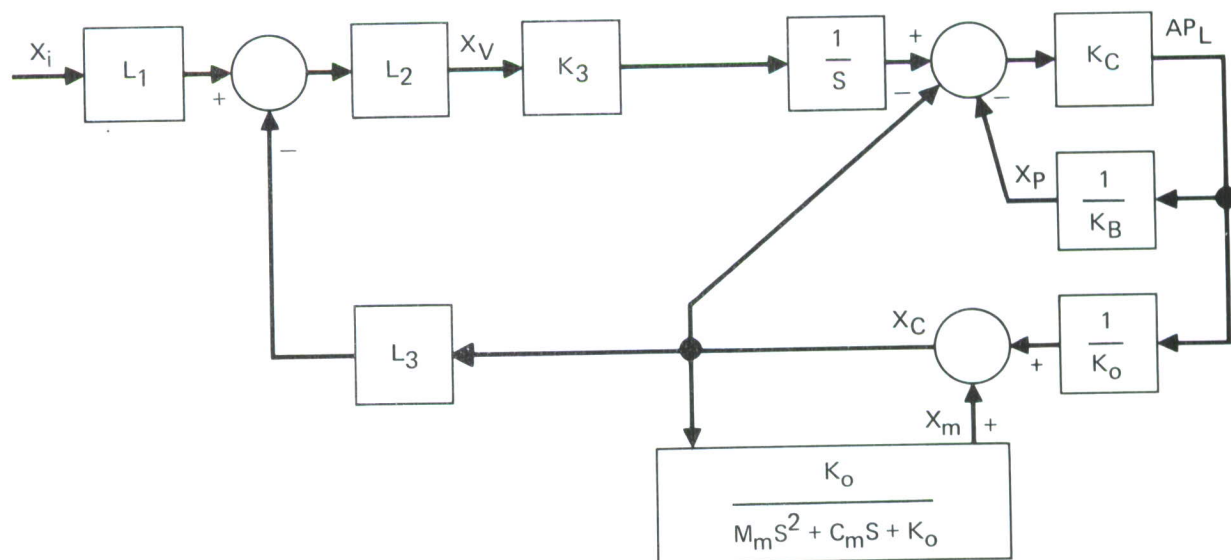
FIGURE 53
MATH MODEL - F-4 AILERON ACTUATOR

94

TABLE 9

LIST OF PARAMETERS FOR ACTUATOR STABILITY ANALYSIS

A — Actuator piston area — in^2-definition

C_m — Coefficient of damping associated with surface mass — 35. lb. sec/in

K_3 — Ratio of actuator velocity to control valve displacement — 64.8 $(sec)^{-1}$

K_B — Spring constant of the back structure, actuator rod and rod end, and spring constant due to hoop tension in the actuator barrel — 1.13×10^6 lb./in.

K_C — Spring constant of hydraulic fluid due to the volume of fluid between the inlet and outlet orifices — 0.91×10^6 lb./in.

K_O — Spring constant of the surface horn, actuator cylinder (axial) and actuator end fitting — 0.56×10^6 lb./in.

K_Σ — Effective spring constant of the complete system ($1/K_\Sigma = 1/K_B + 1/K_C + 1/K_O$) — 0.27×10^6 lb./in.

L_1 — Linkage ratio, pilot input to summing link — 1.0 in./in.

L_2 — Linkage ratio, summing link to master control valve — 0.152 in./in.

L_3 — Linkage ratio, main actuator to summing link — 1.0 in./in.

L_O — Linkage ratio, actuator output to surface — 15 degrees/in.

M_m — Effective mass, surface inertia reflected to to actuator output — 1.83 $lb.sec^2$/in.

P_L — Pressure differential across main actuator piston — $lb./in.^2$-definition

X_C — Displacement - main actuator cylinder — in. - definition

X_i — Displacement - pilot input — in. - definition

X_M — Displacement - effective load mass — in. - definition

X_P — Displacement - main actuator piston — in. - definition

X_V — Displacement - master control valve — in. - definition

The roots are:

Numerator	Denominator
-9.7 + j 558	-9.9 + j 0.0
-9.7 - j 558	-7.2 + j 386
	-7.2 - j 386

The actuator is stable since all of the characteristic roots of the closed loop transfer function lie in the left half plane. The stability of this actuator has been substantiated by experience with the F-4 aircraft.

In order to determine the maximum practical gain increase without special stabilizing techniques, the master control valve gain was increased in increments of 50% until the characteristic roots of the transfer function showed the actuator to be marginally stable. This procedure indicated that the gain could be increased by 350%.

Increasing the master control valve gain by a factor of 350% and substituting nominal values of the other parameters into Equation (1) results in the following relationship:

$$\frac{X_c}{X_i} = \frac{(1.7 \times 10^7)S^2 + (3.2 \times 10^8)S + 5.3 \times 10^{12}}{(1.0 \times 10^6)S^3 + (3.7 \times 10^7)S^2 + (1.5 \times 10^{11})S + 5.3 \times 10^{12}}$$

The roots are:

Numerator	Denominator
-9.7 + j 558	-35.0 + j 0.0
-9.7 - j 558	-0.5 + j 386
	-0.5 - j 386

From the characteristic roots it can be seen that the actuator is still stable even when the gain is increased by 350%. It has a lightly damped resonance at 386 rad/sec (61.4 Hz).

Test Data - The validity of the stability analysis can be substantiated by test data from an aileron actuator which has been modified to increase its bandwidth. A number of years ago Weston Hydraulics modified an F-4 aileron actuator to be used as a flutter exciter for early F-4 flutter tests. This modification consisted of increasing the master control valve gain. The modified actuator was used again in 1973 during flutter tests on the slatted F-4.

Figure 54 shows the frequency response characteristics of the aileron actuator math model, shown in Figure 53, for nominal gains and for an increase by 350% in the master control valve gain. These frequency responses were made coincident at 2.0 Hz to permit test data to be superimposed on the analytical data. Test data for a standard aileron actuator and the aileron actuator which was modified for use as a flutter exciter are shown in Figure 54. The analytical data for an actuator with the gain increased by 350% correlates very well with test data from the actuator which was used as a flutter exciter. This correlation indicates that the flutter exciter actuator has a gain which is approximately 350% higher than a standard aileron actuator. Therefore, no stability problems should be encountered by increasing the gain of the aileron actuator by 350%.

o _Secondary Actuator Response Capability_ – The secondary actuator receives electrical commands from the FCS electronics system and translates these signals into mechanical output motion to drive the surface actuator main control servo valve. The secondary actuator must be capable of 10 Hz response at the output amplitude required to drive the surface actuator.

The secondary actuator on the F-4 SFCS aircraft (Reference 11) has a ram area of 0.294 square inches per channel. The ram stroke is +0.50 inches and is connected to a bell crank which amplifies the output motion required to drive the aileron actuator to its required stroke.

The parameter that limits the dynamic response of the secondary actuator at a given amplitude is the flow capability of the single stage jet pipe servo valve. The servo valves used on the secondary actuator are at or near the maximum practical capability for this type of device. The quiescent flow of these valves is 0.37 gpm which is equivalent to 1.425 cubic inches per second. These valves have an 80% flow recovery which results in 1.14 cubic inches per second being available to drive the actuator ram. Substituting into the peak flow equation:

$$Q = 2\pi f A a$$

$$1.14 = 2 \times 3.1416 \times 10 \times 0.294 \, a$$

gives an output amplitude "A" of +0.062 inches at 10 Hz capability with this servo valve. Using an output amplitude of +0.05 inches gives a frequency
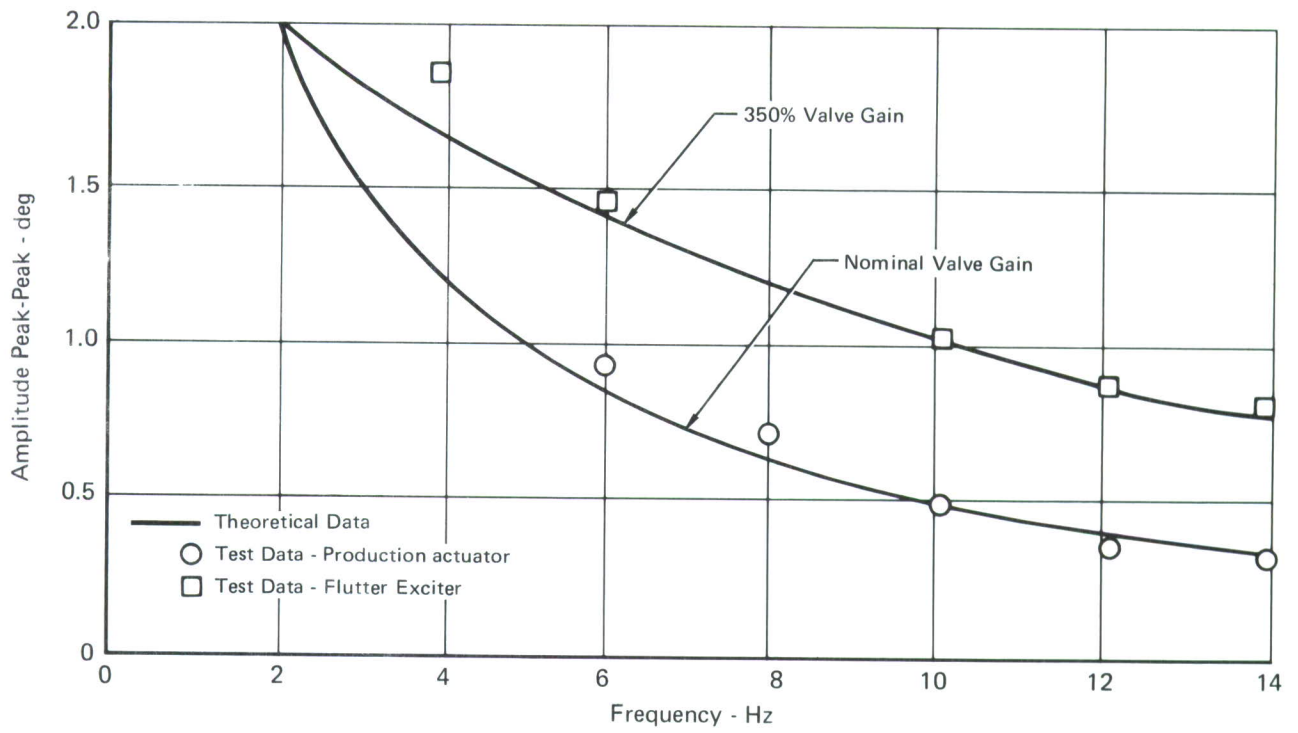
FIGURE 54
F-4 AILERON ACTUATOR FREQUENCY RESPONSE

capability of 12.3 Hz. An output amplitude of ± 0.05 inches coupled through a bellcrank to step up the output motion to give the required output travel to drive the surface actuator will still provide an output force in excess of 200 pounds at the end of the bellcrank. This force capability is more than adequate to overcome the system mechanical inertia and surface actuator valve friction.

The SFCS secondary actuator with output linkage modification will provide adequate performance for a FCS in the F-4 airplane.

3.5.4.2 Design Considerations

o <u>Aileron Surface Actuator</u> - The aileron surface actuator will require design changes to incorporate changes in gain, length, piston area, and shaft dynamic seals.

<u>Gain</u> - The increased gain will be accomplished by increasing the valve metering orifices size. In addition, the fluid passages between the valve and the actuator pistons will be increased in size to minimize internal pressure drop.

<u>Length</u> - The actuator overall length will be decreased approximately 0.25 inch by shortening the attachment fitting between the aileron and the actuator. This change is required to provide for revised aileron up and down travels described in Section 3.6.2.

<u>Piston Area</u> - Piston area on the actuator retract side will be increased to overcome increased surface hinge moments due to increased aileron up travel. This can easily be accomplished by reducing the piston rod diameter without compromising the required structural strength.

<u>Shaft Dynamic Seals</u> - Shaft dynamic seals will be changed to a teflon cap strip type to provide for the increased life that will be required for FCS operation.

o <u>Secondary Actuator</u> - The secondary actuator will require changes to reduce the number of active channels and revise the output linkage.

<u>Active Channels</u> - This SFCS secondary actuator has four parallel elements to provide for quadruplex redundancy. The FCS requires triplex redundancy which will allow for the removal of one complete element saving space and weight. The output bellcrank length will be increased to provide the required output motion for FCS operation.

3.5.5 Actuator Response Capabilities in the Frequency Range of 10-20 Hertz - Suppressing wing store flutter in higher frequency ranges is primarily limited by the installed flight control actuator bandwidth capabilities. This is not to imply that in some instances that other parameters, such as hydraulic flow capability, may not be the governing factor but normally actuator bandwidth capability will predominate.

Installed actuator bandwidth capability depends on surface damping, surface mass, stiffness of the backup structure and output structure, and oil stiffness or bulk modulus. Adding damping adversely affects dynamic performance. Backup and output stiffness and surface mass are to a great extent airframe design dependent which leaves oil stiffness as the predominant controlling factor that establishes the maximum bandwidth capability of the surface actuator. Oil stiffness or bulk modulus primarily depends on fluid temperature with the bulk modulus and resultant actuator bandwidth decreasing as temperature increases.

Using an advanced fighter airplane aileron actuator as a baseline, the actuator gain was increased to the maximum attainable with existing structure and fluid at 275°F. The response characteristics are shown in Figure 55 for ±3 deg deflection. The figure shows the loaded performance of the actuator loop (solid lines), and the loaded performance with the effects of the electro-hydraulic servo valve characteristics added (dashed lines), to give the actuator-valve performance in combination.

From the above data it can be concluded that reasonable dynamic performance out to 20 Hz can be attained with reasonable gain attenuation and phase shift which can be compensated for in the electronic portion of the system. To obtain higher airframe-actuator system dynamic response would require extensive system cooling provisions that are beyond current cooling provision capabilities.

3.6 Flight Control System Modification Studies

3.6.1 General Considerations - Flight control systems are configuration dependent. A complete study to determine the optimum method of incorporating a FCS must be performed for each aircraft being considered. Areas of study should include the degree of redundancy that is required and the optimum means of accepting FCS electrical signals and converting these to aerodynamic surface motion.
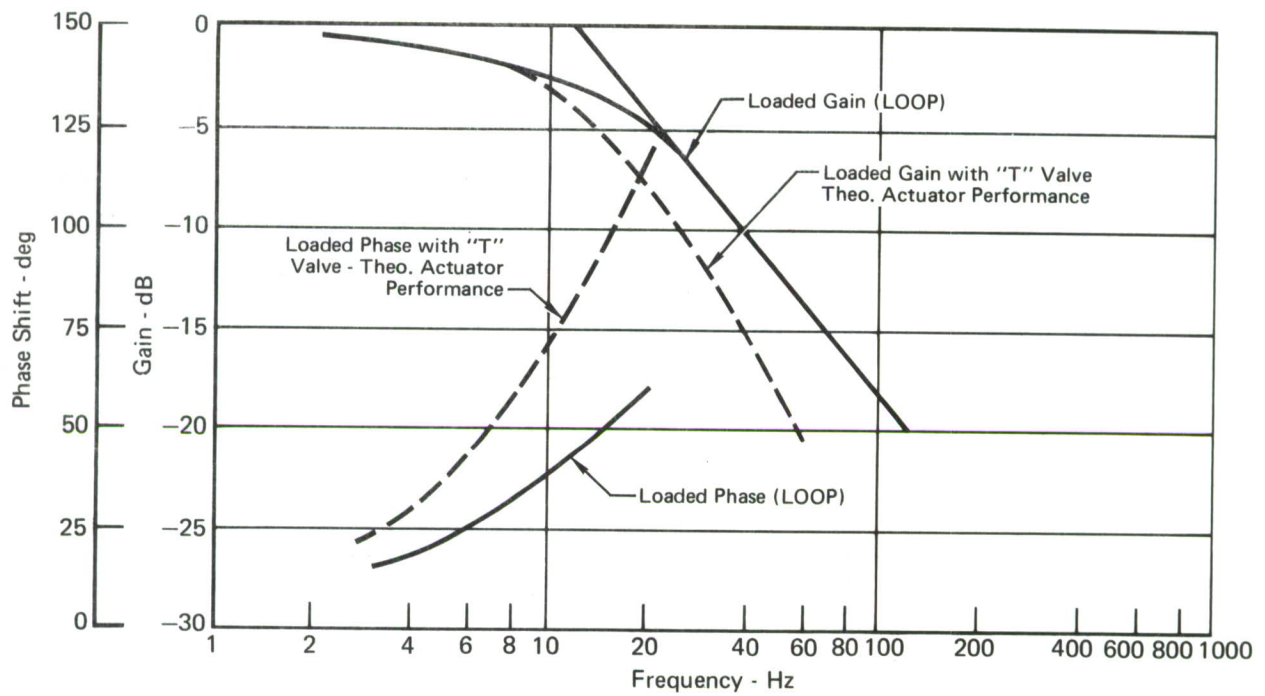
FIGURE 55
ADVANCED FIGHTER ACTUATOR PERFORMANCE FOR ± 3° AILERON DEFLECTION

3.6.2 F-4 Studies - As a result of studies performed on the F-4 control system it was determined that the optimum means of providing FCS commands to the aerodynamic surface would be to use a secondary actuator to provide mechanical inputs to the surface power actuator. Various mechanical linkage changes would also have to be incorporated for the revised system.

The standard F-4 lateral control system is shown in Figure 56. The revised mechanical control system is shown in Figure 57.

Comparing the two figures, the most significant difference is that in the revised system the series servo is deleted and the secondary actuator is added with appropriate linkage revisions.

It should be noted that the secondary actuator applies FCS commands only to the aileron power actuator. Mechanical inputs from the pilot operate both the aileron power actuator and the spoiler actuators thus lateral control of the aircraft is unaffected with the FCS either on or off.

Aileron travels are revised. The normal aileron travel is 1 degree aileron up and 30 degrees aileron down. FCS operation requires both up and down travel, consequently the revised lateral control system provides 5 degrees up aileron and 26 degrees aileron down.

3.7 Structural Modification Studies

3.7.1 General Considerations - Investigations must be made to determine the required structural modifications for installation of FCS equipment, and those required for the hydraulic and mechanical control system modifications. In addition, the potential increased fatigue criteria resulting from the FCS operation will have to be investigated as to its effects on the mechanical and hydraulic control systems as well as airframe structural elements.

3.7.2 F-4 Studies - A study was performed to determine the structural modifications necessary for FCS operation. This study covered fatigue effects due to FCS operation and any additional static load requirements that might be imposed due to system configuration.

3.7.2.1 Fatigue Characteristics for a Hypothetical Duty Cycle - A study has been performed to obtain the effect of active flutter control on fatigue life of the airframe structure involved in the aileron load path. Items in the load path include the aileron control surface and the fixed trailing edge wing structure including hinge support beams, lower closure skin, ribs, rear spar, and surface actuator attach fitting.
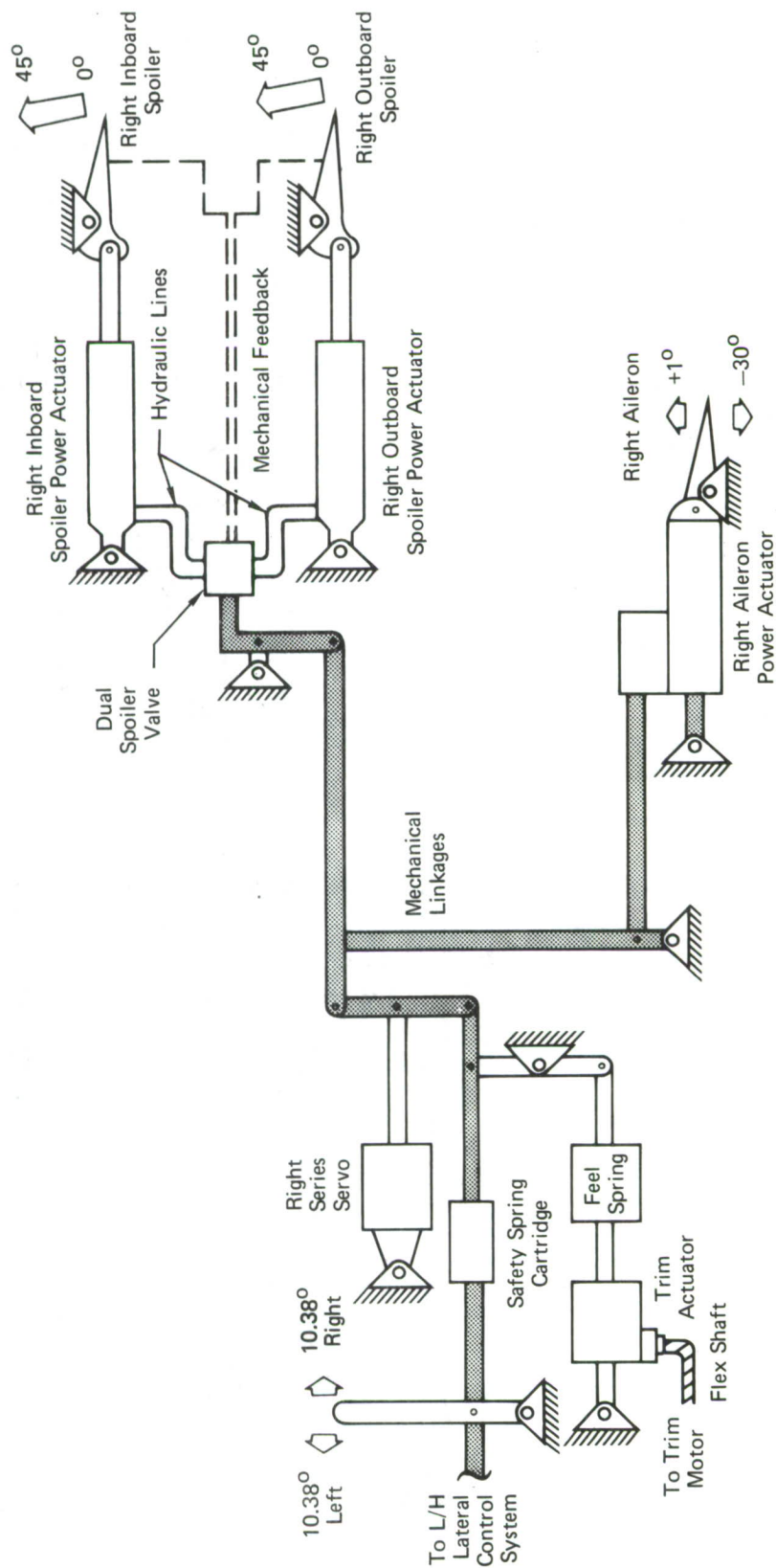
FIGURE 56
NORMAL F-4 LATERAL CONTROL SYSTEM
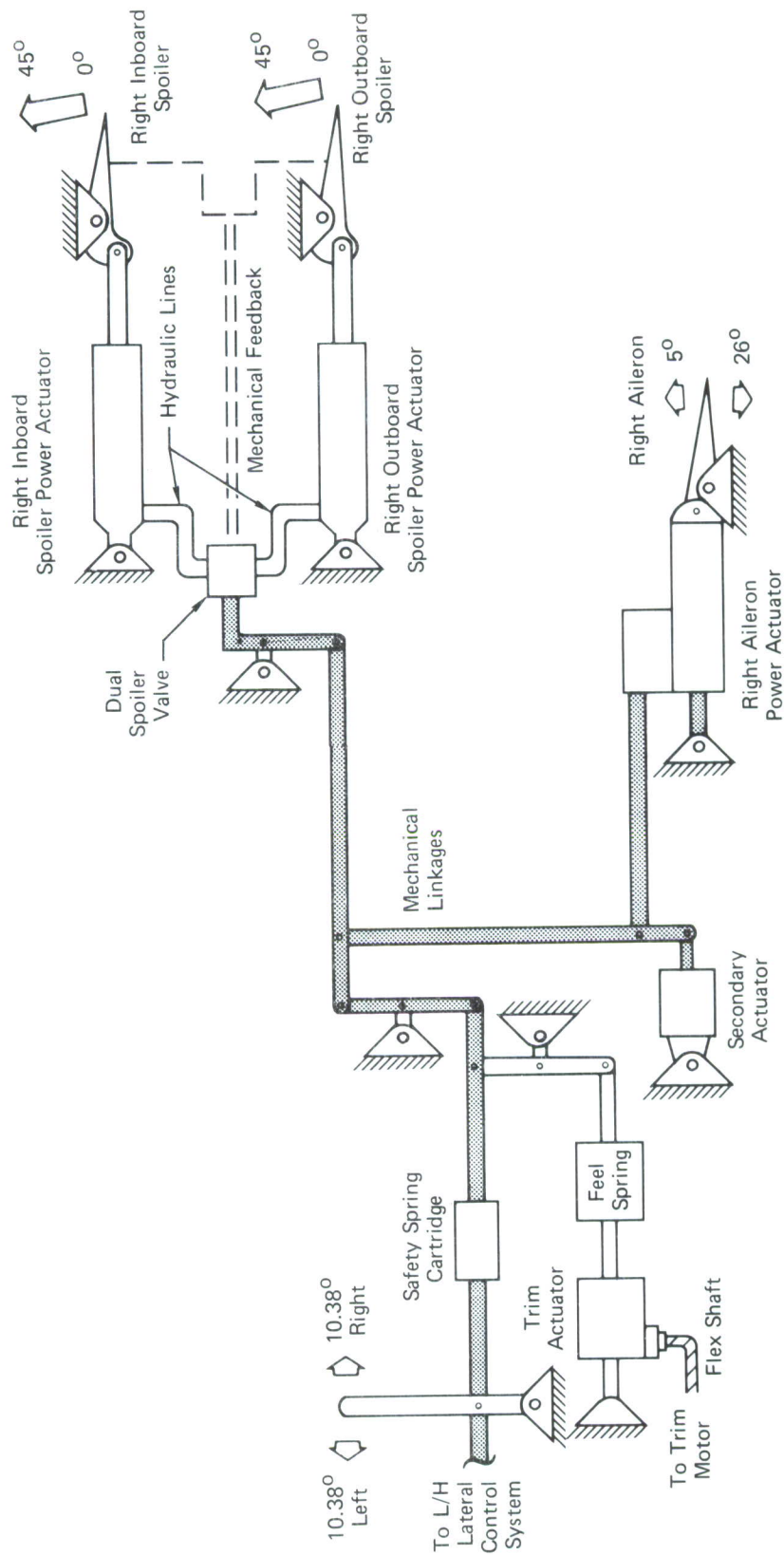
FIGURE 57

REVISED F-4 LATERAL CONTROL SYSTEM INCORPORATING FCS

An envelope of hypothetical duty cycle loads for continuous 1g flight through clear air turbulence at Mach = 1.1, sea level, is shown in Figure 58. This duty cycle is believed to be a very conservative estimate for flight test demonstrations. These loads are presented in terms of alternating and mean hinge moment vs. mean aileron position. The alternating hinge moment is based on an upper limit aileron oscillation of $\pm 1.5°$. Mean aileron position during the flutter control system operation is assumed to be restricted to $\pm 3.5°$ to limit the maximum deflections to 5° which is equivalent to the hinge moment limit used for the hydraulic actuator analysis of Section 3.5.2.1.

A simplified repeated load definition per flight using the hinge moment envelope was assumed as follows:

- One third of the flight at a mean aileron deflection of +3.5° or -3.5° at 10 Hz.
- Two thirds of the flight at a mean aileron deflection of 0° at 10 Hz.

Using this repeated load definition a generalized analysis based on the aileron static test failure load of 187% design limit load was completed. Assumptions used for the analysis are:

- A 25 flight, flight test program
- 15-20 minutes of flutter control system operation per flight test
- No more than 50% of the fatigue life of the applicable structure is to be consumed during flight testing.

A scatter factor of four to represent fatigue data scatter, was used for the analysis. These inputs result in 7×10^5 and 1.4×10^6 applied cycles for the 3.5° and 0° mean aileron deflections respectively as shown in Figure 59.

Results based on these assumptions indicated that beef-up of areas where the stress concentration factor, K_t, exceeds approximately 2.2 may be required. Typical areas of the structure where K_t exceeds 2.2 are:

- Skin splices in tension
- Actuator fittings
- Tension ties to rib caps
- Threaded parts in tension

Notes:

$$\text{Mean HM} = \frac{HM_{max} + HM_{min}}{2} \qquad \text{Alternating HM} = \frac{HM_{max} - HM_{min}}{2}$$
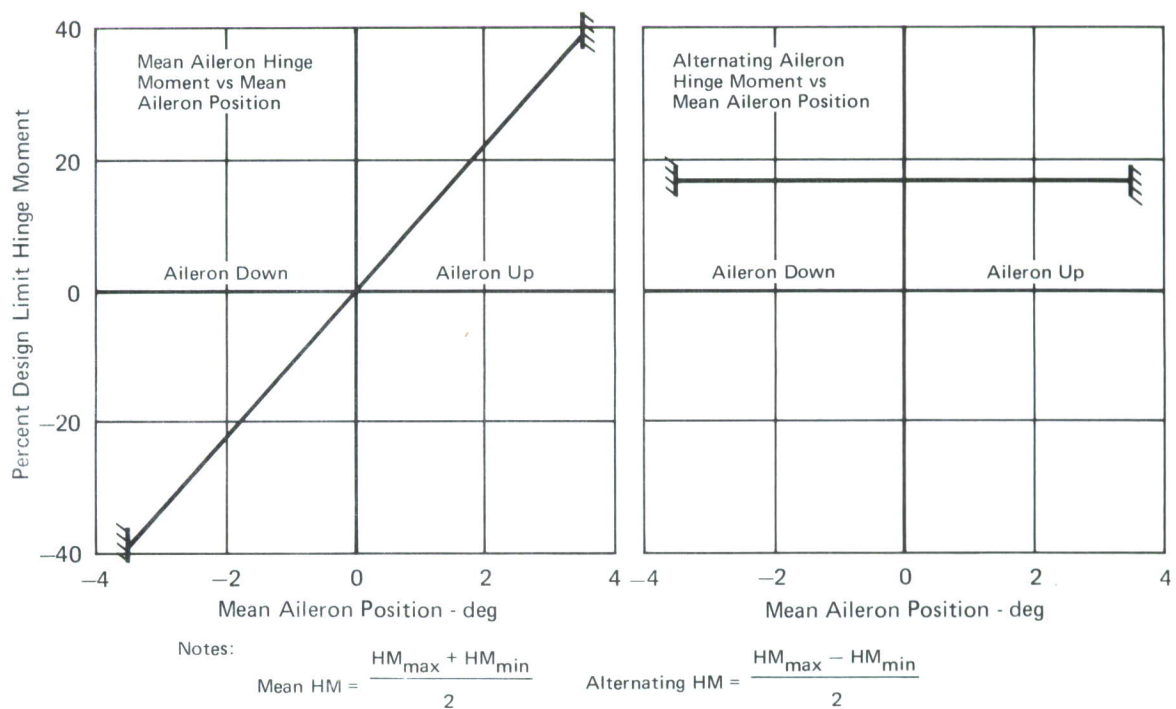
FIGURE 58
ENVELOPE OF HYPOTHETICAL DUTY CYCLE

1/3 of FCS Flight Operation

5°
3.5° Mean
2°

7 x 10^5 Cycles

2/3 of FCS Flight Operation

+1.5°
0° Mean
1.5°

1.4 x 10^6 Cycles
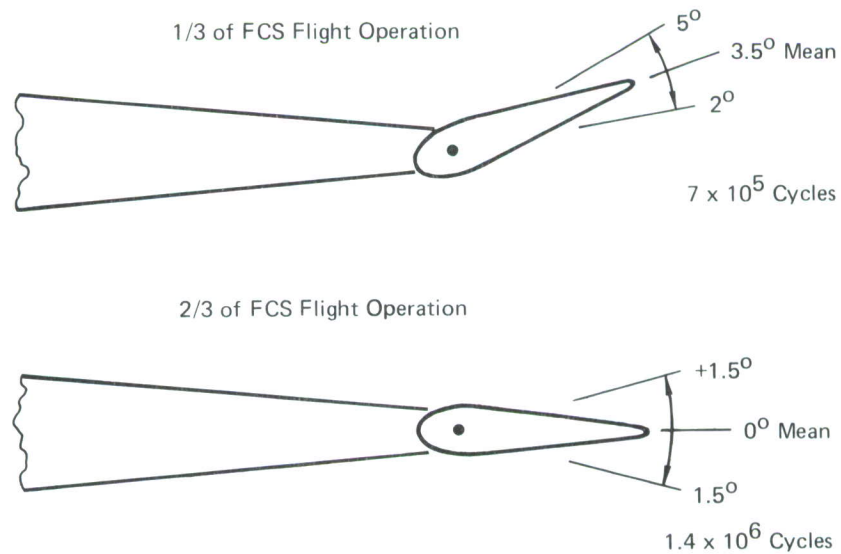
FIGURE 59
CONDITIONS USED FOR REPEATED LOAD DEFINITION

Following the generalized analysis the structure was examined for such critical areas. Several of the local areas analyzed required beef-up. It is possible that material changes could be incorporated to improve the fatigue life of some parts.

In general the analysis indicated that, for these conservative assumptions, considerable structural modification of the aileron and its supporting structure would be required for a 25 flight test program. Modifications of the areas analyzed appear to be possible. The analysis also indicated that fatigue damage due to the cycles at 0° mean aileron position was insignificant. Subsequent reductions in maximum mean aileron position or the number of cycles at the extremes of mean aileron position or a reduction in the required aileron amplitudes can result in a reduction of items requiring modification.

In addition, it is noted that due to the extreme number of cycles required for flutter control, design of structure for a production flutter control system will apparently be based on material endurance limits at the applicable K_t and stress ratio. Since we are operating near the flat end of the fatigue curve, it may be prudent to design to the endurance limits rather than for the 25 flight program as the additional beef-up required would be minimal.

3.7.2.2 <u>Other Structural Modifications</u> - In addition to modifying the structure for fatigue reasons it appears necessary to modify several items for the down loads associated with extending the up travel of the aileron to 5°. The modifications for aileron up travel are a result of increased positive design ultimate hinge moment. This increase results in increased compression loads in items originally critical for tension loads. The items include the lower aileron skin and fixed wing lower aileron closure skin. Modification will consist of adding stiffeners to or increasing the thickness of the skins. These modifications do not appear to present any problem.

The structural modifications required for equipment installations will be relatively minor consisting of such items as providing support structure for such items as sensor installation, secondary actuator support structure, electronic box support structure, and increasing hole size where required to accommodate larger size hydraulic tubing. These modifications are not expected to pose any serious problems.

3.8 Sensors and Electronics Implementation Studies

3.8.1 _Sensor Trade Offs_ - Suitable sensors for measuring wing twist angle, α, were investigated. Practical considerations have narrowed the field down to

(1) doubly integrated accelerometers

(2) singly integrated rate gyros

The initial effort to identify suitable sensors was directed toward accelerometers, since they are usually smaller and less complex than rate gyros or other rate sensing devices. Two methods of measuring $\ddot{\alpha}$ were considered; one uses angular accelerometers which measure angular acceleration directly, and the other uses two coupled linear accelerometers whose signal outputs are mixed so that the normal acceleration components appearing in the output of the two accelerometers are cancelled and the angular acceleration components are added in the associated electronics. In an angular accelerometer these normal accelerations are not sensed. Since the normal acceleration components appear in the sensor outputs of the coupled linear accelerometers, their full scale operating range must be greater to accommodate these additional acceleration components. If the full scale range of the linear accelerometer must be increased significantly to accommodate the normal acceleration components, the accuracy of the measurement of the angular acceleration components would be compromised. In addition, the coupled linear accelerometer method requires twice as many sensors and some additional electronics. All these factors were considered in detail trade studies.

3.8.1.1 _Candidate Angular Accelerometer_ - Angular accelerometers are less commonly available than linear accelerometers and are in general larger and more complex than linear accelerometers. The prime candidate angular accelerometer being considered is the Systron Donner Model 4591. This sensor employs a liquid captured in a torroidal tube as the inertial mass, which is constrained by a servoed force sensor. Angular acceleration on the liquid causes a position error signal to be generated, which through servo action in the self contained electronics, force-restores the liquid mass while providing a high-level output signal.

This sensor is available with full scale ranges of ±10 to ±200 rad/ sec^2, which is compatible with the expected requirements.

The natural frequency can be up to 150 Hz depending on the range, and its frequency response is flat DC to 40 Hz minimum. The linearity, threshold, resolution and repeatability seem adequate and its sensitivity to the aircraft environment seems acceptable. This sensor is 1.5 in. in diameter, 3.0 in. long, weighs 8.5 oz with integral servo electronics, and appears compatible with the installation constraints.

3.8.1.2 <u>Candidate Linear Accelerometer</u> - The variety and quantity of linear accelerometer types which are available far exceeds the types of angular accelerometers available. To date, the most promising candidate is the Honeywell model GG 322 Solid State Accelerometer. This sensor employs a single crystal silicon beam with four piezo-resistive strain elements diffused into the beam to provide the basic sensing element. Since the four strain gage elements are diffused into the crystal they become a physically integral part of the beam. The piezo-resistive properties of the elements are such that tensile strain increases its resistance and compressive strain decreases resistance and when properly connected form a strain gage bridge circuit. This silicon beam also acts as a single cantilever for support and restraint of the seismic mass. Because of the almost perfect elasticity of the silicon, hysteresis and friction effects are negligible. Squeeze film damping techniques are used to maintain relatively constant damping.

Only four basic components are used in the sensor; a silicon beam, a cantilever seismic mass, a rigid terminal mount for the beam and the housing and bellows. Because of its simplicity it appears to be a highly reliable unit. A self test feature can also be incorporated.

This sensor has a wide G range capability with a threshold and resolution of 0.0005 percent full scale and independent linearity of ±0.5 percent full scale. Its undamped natural frequency is in the range of 20 to 200 Hz with any nominal damping ratio from 0.3 to 5.0. The strain elements can be excited with either DC or AC up to 1000 Hz to a maximum output of ±2 volts. This sensor is only 0.85 in. in diameter, 1.2 in. long, and weighs 1.2 oz. Its physical size and environmental characteristics seem quite compatible with the installation constraints.

3.8.1.3 <u>Candidate Rate Gyro</u> - A number of miniature rate gyro sensors are available in a size suitable for installation in the limited space available in the wing tip. These sensors are approximately 1 in. in diameter by 2-1/2 in. long and weigh less than 5 oz. The operating range considered was ±100 deg/sec. An angular wing twist angle of ±1 deg at 10 Hz results in a maximum angular rate of 62.8 deg/sec. Miniature rate gyros with sensitivities in this range typically have an undamped natural frequency of 45 to 50 Hz. Since this is relatively close to the frequencies of interest, 5 to 25 Hz, the constancy of the sensor damping ratio becomes a significant parameter. Sensors mounted in the wing tip will experience wide variations in temperature and consequently variations in damping fluid viscosities.

The candidate sensor, a Honeywell GG 2460 series rate gyro, provides a relatively constant damping ratio with variations of less than 2 to 1 over the full temperature range of -65 to +200 deg F without the use of heaters. Damping is achieved by paddles attached to the gimbal which pump damping fluid through orifices. The area of these orifices is varied as a function of temperature, by a piston attached to a bellows, which compensates for damping fluid viscosity changes. The damping factor range available for this sensor is 0.3 to 5, and therefore, high damping ratios may be implemented if desirable to provide some of the high frequency lag required in the feedback loop.

The general accuracy type characteristics of the GG 2460 such as threshold, resolution, and linearity are comparable to those of other miniature rate gyros. Since this sensor will be operating in a high vibration environment, its response to the resulting acceleration forces are a significant consideration. The candidate sensor has a linear acceleration sensitivity of 0.03 deg/sec/g, which is as good, or better, than any of the other miniature rate gyros reviewed, except those rated as "High Accuracy" sensors. One high accuracy rate gyro had a linear acceleration sensitivity of 0.01 deg/sec/g, but it had an undamped natural frequency of less than 36 Hz and much poorer damping ratio vs temperature characteristics. The rated operating vibration environment for the GG 2460, as was the case for all the miniature rate gyros, was limited to 20 g's (10 to 2000 Hz) and 100 g's max for steady acceleration. This may be a limiting factor for rate gyros in this application.

The candidate sensor has built-in self-checking circuitry which is completely isolated from the operation of the gyro circuits. These circuits are a gimbal torquer and spin motor running detector (SMRD) which verify:

o The gimbal is free to rotate.

o The pickoff produces a signal proportional to the simulated rate input.

o The spring is free to return the gimbal to zero position.

o The spin motor is running at synchronous speed.

o The damping is within acceptable limits.

These self-test facilities can also be used for system testing. System response could be qualitatively analyzed by applying a precise input rate signal from the gyro.

The GG 2460 uses a synchronous hysteresis motor sealed in an inert atmosphere, which is identical to that used in Honeywell GG 440, a unit that has a demonstrated mean time between failure in excess of 8000 hours in service.

3.8.1.4 <u>Summary of Sensor Studies</u> - Three different sensor types and techniques were investigated in detail:

o An angular accelerometer sensing $\ddot{\alpha}$ directly using two integrators to produce α.

o Two coupled linear accelerometers to form $\ddot{\alpha}$. This method requires a summing network to subtract acceleration components normal to the wing and two integrators to produce α.

o A rate gyro to sense $\dot{\alpha}$ and a single integrator to produce α.

Using an angular accelerometer for sensing $\ddot{\alpha}$ eliminates the effect of high wing tip normal acceleration forces to a great degree. The choice of suitable angular accelerometers was very limited since this is not a common measurement. One of the disadvantages of this sensor is its size, 1.5 in. dia. x 3 in. long and its weight, 8.5 oz. The primary and perhaps limiting problem area is its small temperature operating range of +20 deg F to +160 deg F. It may be possible to improve its low temperature operating limit by heating, but this does not seem to be desirable. It may be possible that another similar sensor of a smaller size and better low temperature performance is available or could be developed.

The coupled linear accelerometer method is not advisable for this implementation. The high acceleration forces normal to the wing tip produced by vibrations could reach 20 g's or more. This would dictate the use of linear accelerometers with a full scale range of ±25 g's, to prevent saturation and/or damage to the accelerometers. For a practical wing tip installation, i.e., the sensors mounted 12 inches appart, the linear acceleration resulting from the wing twist on the order of ±1 deg at 10 Hz would only be 1.07 g's. The disparity between the full scale range and operating range (approx. 25 to 1) would seriously degrade the $\ddot{\alpha}$ signal from the accelerometers and summing circuit. In addition, the advantages of the small physical size and high reliability of the candidate linear sensors is somewhat diluted by the fact that two sensors and additional electronic circuitry is required to produce α.

The candidate miniature rate gyro is the best sensor choice at this time. Its low natural frequency of approximately 50 Hz should not be a problem with good damping ratio control. The candidate sensor is rated for operation up to 20 g's (10 to 2000 Hz). Continuous operation in a high vibration environment may reduce its reliability. A detail specific definition of the wing environment will be necessary to accurately determine any limitations.

A number of less common types of sensors and sensing techniques were considered. The limited space and severe operating environment in the wing tip area ruled out the use of many of the more sophisticated and precise sensors, which are generally designed for use on stable platforms or in less severe environments. On the other hand, a number of simple and less precise sensors also had to be ruled out, since they were too crude or unreliable for this application. The detection and measurement of the small wing twist motions which are significant for this system requires the use of a sensitive and precise sensor. When the specific operating environment, particularly vibration, is defined and system error tolerances are established, a detail error analysis should be conducted to verify the suitability of the sensor choice.

3.8.2 Electronics Implementation

3.8.2.1 General Considerations - The development of solid state microprocessor and memory devices is in its early stages. There are, however, many stimuli for the development of special purpose micro-processors which

would be ideally suited to the processing requirements of an active flutter control system. In addition, with the advent of all-digital aircraft flight control systems there should be further stimulus for sensor manufacturers to develop new sensors with digital outputs. Further developments in both of these areas are very desirable and should assist greatly in the realization of a practical flutter control system in future aircraft.

The phase and gain uncertainties resulting from the digital processing of the wing twist feedback loop will be a function of the sensor sampling rate, signal processing rates, and computation word size. These uncertainties can be made very small by selecting optimum values for these parameters consistent with the requirements of practical digital processing capability. In summary, the future electronic components can be expected to use very little of the available phase and gain margins of the flutter control system.

3.8.2.2 <u>F-4 Studies</u> - The electronic compensation networks used in the wing/store flutter control system designs are easily assembled using solid state devices and analog circuitry. The detail design of these circuits is beyond the scope of these studies but a description of the major components likely to be needed is given in Sections 5.3.3, 5.4.2, and 5.4.3 of Reference 4.

3.9 <u>Flight Safety Evaluation</u>

3.9.1 <u>General Considerations</u> - Analyses must be performed to evaluate safety of flight with the FCS installed and operational. The results of these analyses determine the degree of redundancy requirements, single point failure potentials, and resultant system and component reliability.

3.9.2 <u>F-4 Studies</u> - It was determined that to provide safety of flight and operation of an operational FCS a one-fail-operate system capability would be required. This dictates that the sensing system, electronics, and the secondary actuator all be triplex and that the hydro-mechanical surface power actuator retain its standard duplex configuration.

3.9.2.1 <u>Reliability Study</u> - A reliability analysis and prediction has been made for the flutter control system design. Data obtained from the reliability test on the F-4 Survivable Flight Control System (SFCS) aircraft (Reference 11) equipment was used for the calculations. If, as expected, the flutter control computation circuitry is significantly less complicated than the SFCS, the figures obtained in the analysis would be quite conservative.

Two separate mission times were considered to bracket the results. The first set of data was calculated for a one-hour mission time so that all components involved must operate continuously from take-off to touch-down. The probability of loss of flutter control for this mission, provided adequate backup battery supplies are available, is roughly 5×10^{-6}. Since the flutter-control-peculiar components are expected to have a duty cycle of no more than 5 or 6 minutes per mission the second set of data was calculated for a 6 minute mission time. The probability of loss of flutter control for this reduced mission time is 0.07×10^{-6}, with the same requirements for backup batteries. The triplex system concept appears to be adequate for the intended purpose, especially in view of the limited duty cycle anticipated.

Although the aileron power actuator has generally been satisfactory up to this point, the actuator and associated linkage contain a number of potential single point failures as described below. The flutter control application could be expected to greatly increase wear, fatigue and stress on these parts. Careful attention to maintenance and inspection would be required to prevent this area from becoming a reliability degradation problem. Given this attention, the flutter control concept should be quite viable from the reliability viewpoint.

3.9.2.2 <u>Single Point Failure Modes</u> - Single point failures can only occur in the airframe structure (see Fatigue Analysis, Section 3.7), the secondary actuator, and the aileron power actuator.

As part of the flight safety studies the effects of single point failures in the secondary actuator, which accepts the flutter control system signals, and the aileron power actuator were evaluated. The results are presented in tabular form in Tables 10 and 11. It should be noted that the probability of any of these single point failures occurring is extremely remote due to the conservative design and structural criteria applied to flight control servomechanisms.

Calculated failure rates based on service experience data with the same or similar equipment yield a rate of 0.0454 failures per million flight hours for the secondary actuator and 0.0562 failures per million flight hours for the aileron power actuator. Both are well below the criterion of 1.0 failures per million flight hours.

TABLE 10
SECONDARY ACTUATOR SINGLE POINT FAILURES

Part	Failure	Effect(s)
Piston or Piston Rod	Seized or Jammed	Total actuator motion stopped. Manual control not affected.
Rocker Arm Assembly	Seized	Same as above.
Centering Mechanism	Jammed	Same as above.
Summing Shaft	Broken	Loss of Output
Output Arm	Broken	Loss of output and possible loss of some manual control authority.

TABLE 11
SURFACE ACTUATOR SINGLE POINT FAILURES

Part	Failure	Effect(s)
Main Control Valve	Jammed	No control of actuator output. Actuator will drift hardover.
Actuator Attachment Lug(s)	Broken	No control of surface
Piston or Piston Rod	Jammed	No actuator output.

3.10 Survivability Studies

The survivability and various effectiveness parameters have been analyzed for the F-4E aircraft with and without an active flutter control system.

3.10.1 Method of Analysis - The method of analysis in this study uses the MCAIR Hit Density Model (Reference 27) and the MCAIR Survivability Assessment Guidelines (SAG) Model (Reference 28) to obtain aircraft survivability. The Hit Density Model combines aircraft profile information with enemy defense data, to calculate the expected number of hits, and the average striking velocity of hits on the aircraft. The SAG model combines this information with aircraft component vulnerable areas, and the survivability logic diagram of vulnerable components to calculate the aircraft and system survivability.

3.10.2 Survivability Logic Diagram (SLD) - The first step in survivability analysis is to determine the critical systems on the aircraft. A system is defined as critical if battle damage to that system can result in a loss of the aircraft. Critical systems for the F-4 aircraft are listed at the right in Figure 60. The components that comprise a critical system are called critical components. It is not always necessary to retain all critical components for the aircraft to survive, it is only necessary that all critical systems survive. A critical system can survive without all of its critical components surviving, depending on the various redundant interactions of the critical components that make up the system. The redundancies and interactions of the critical components are represented on the SLD by the use of "AND" and "OR" logical operators.

"AND" operators are used to combine two or more critical components that must all survive in order for the critical system to survive. "OR" operators are used in instances when any one of the several inputs must survive in order for the system to survive. Some critical systems use both "AND" or "OR" operators in several stages. In these cases, logic operators do not necessarily operate on critical components to obtain critical system survivability. There can be several intermediate steps, similar to nodes in an electronic circuit.

27. MCAIR Hit Density Model, Unpublished Internal Computer Model.
28. Ahrens, Roger A., Nadler, Gerald and Zust, Eric L., "Survivability Assessment Guidelines for Flight Control Systems," AFFDL TR-74-39, Vol. I, to be published.
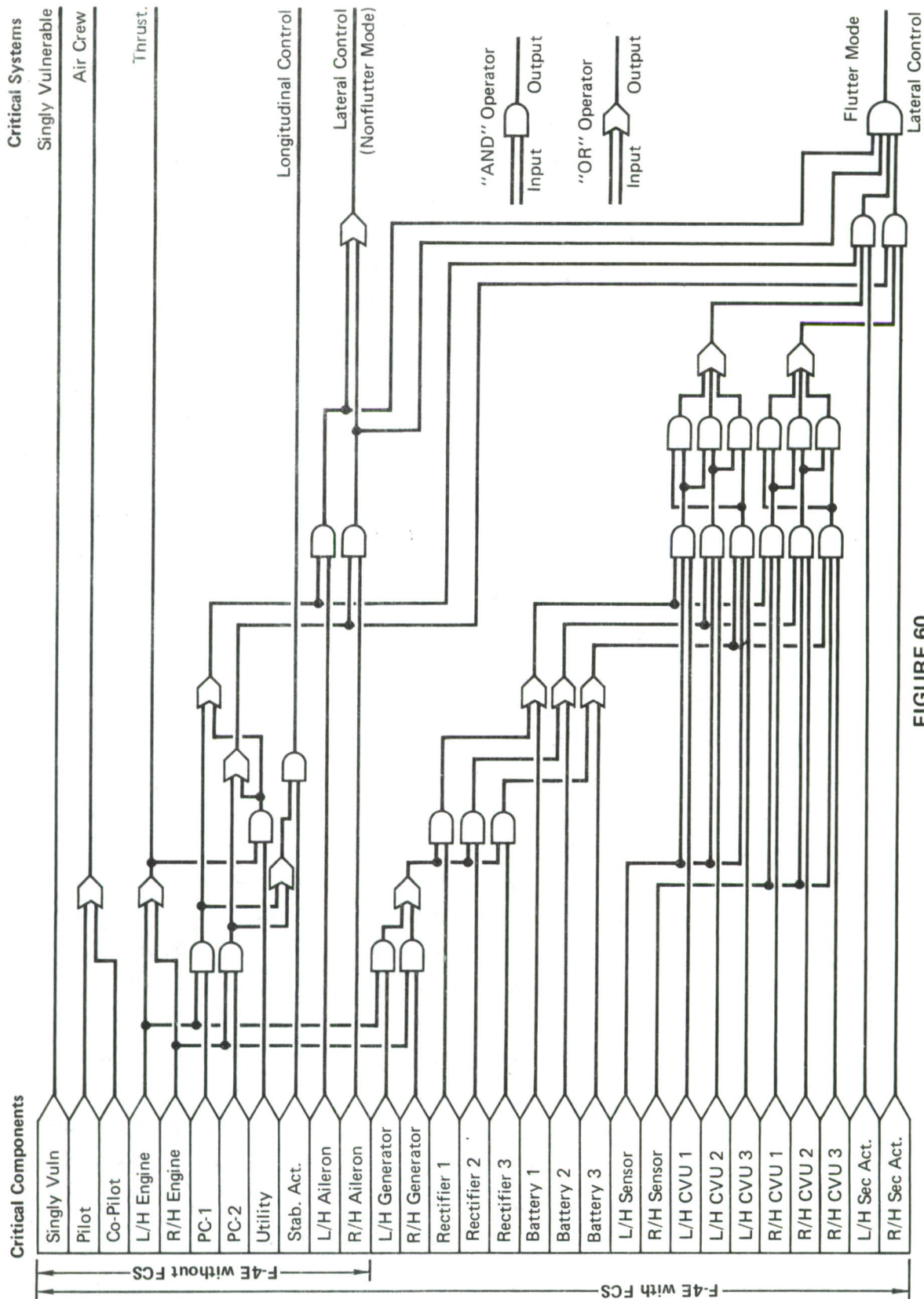
FIGURE 60
SURVIVABILITY LOGIC DIAGRAM
F-4 With Active Flutter Control System

117

The critical components, logic operators, and critical systems used in the survivability analysis of the F-4E active flutter suppression system are presented in Figure 60. The column to the left in Figure 60 is the list of critical components. The top eleven components are the critical components for the basic F-4E. The components to the bottom of the page are the critical components that must be added to the F-4E critical components to represent the F-4E with an active flutter control system.

The first critical system labeled "singly vulnerable" represents the total of all singly vulnerable components not otherwise shown on the SLD.

The systems listed to the right of Figure 60 are the standard critical systems used in survivability analysis. These critical systems must all survive for the aircraft to survive. Note that there are two lateral control systems in Figure 60. The uppermost lateral control system is the system on the F-4E without flutter control. The lateral control system at the bottom of the page is used in the F-4E with active flutter control. The survivability is computed first using the SLD for the aircraft without an active flutter control system and then using the entire SLD for the aircraft with an active flutter control system, using the appropriate lateral control system. The results are presented on a relative basis.

3.10.3 Enroute Profile Analysis - One-on-One

3.10.3.1 Profile Description - The condition used to evaluate survivability was a low level dash, which is typical of an enroute approach to a target area. The defense consisted of a single modern anti-aircraft artillery (AAA) weapon located at an offset from the flight path, as shown in Figure 61. The gun was allowed to fire at the aircraft during the time it was within gun range and above the ground masking angle which is defined as the line-of-sight elevation angle below which the gunner cannot see the target because of obstacles. Each aircraft flew at maximum speed within its flutter limitations. Therefore, the aircraft with the active flutter control system had a dash speed advantage.

The speed used to evaluate the survivability of the F-4E without active flutter control is 550 Knots Equivalent Air Speed (KEAS), Mach = .83. This value is based on current F-4 placards. With active flutter control, a sustained dash speed of 620 KEAS, Mach = .94 was used. This value is based on the maximum velocity without afterburner.

118
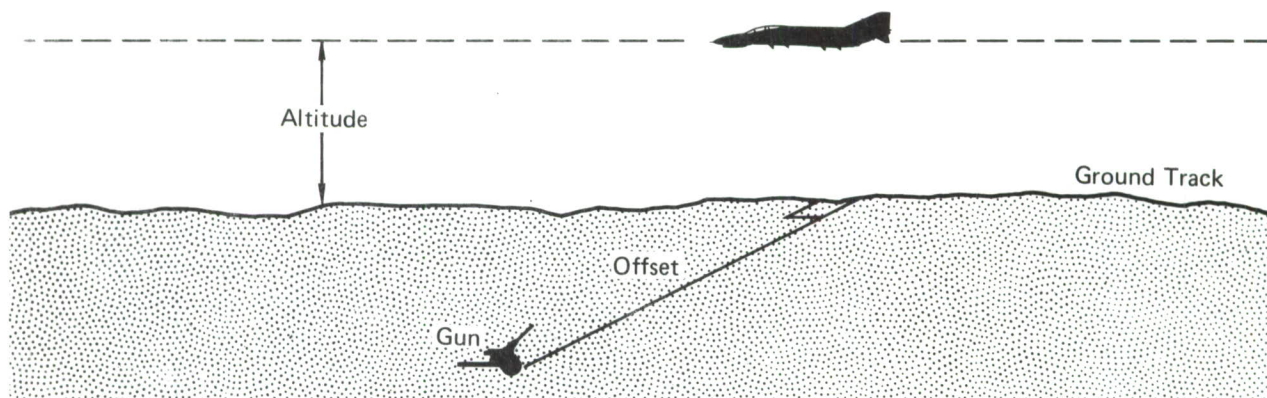
FIGURE 61
SURVIVABILITY ANALYSIS ENROUTE FLIGHT PROFILE
One-on-One

The weapon is offset from the flight path of the aircraft, for a parametric analysis, at distances of 1000, 2000 and 4000 ft. These distances are typical of those encountered in a combat environment. The ground masking angles used for this study are 0°, 1° and 2°. The other significant, parameter values in the analysis are aircraft dash altitudes of 200 and 500 ft.

3.10.3.2 Results - Figure 62 presents the relative loss rate summary for the aircraft with and without an active flutter control system. This figure presents actual loss rate data which has been normalized to equal 1 in the least survivable case which is 500 ft altitude, 0° or 1° masking angle, 1000 ft gun offset for the aircraft without the flutter control system. This figure shows that in every case, there is a survivability benefit to the aircraft with the flutter control system.

Figure 63 presents the loss rate ratios for the aircraft with and without an active flutter control system. The figure shows that an aircraft flying at a 200 ft altitude can expect from 25 to 50 percent fewer losses with the active system even though the system vulnerability increased slightly, about one percent. If the aircraft flies at an altitude of 500 ft, it can expect from 25 to 40 percent fewer losses.

3.10.4 Weapon Delivery Profile Analysis - One-Against-Many

3.10.4.1 Profile Description - Survivability was examined in the same manner as in the previous analysis, with weapon delivery accuracy added to the analysis. Each aircraft attempted to penetrate the enemy defenses at
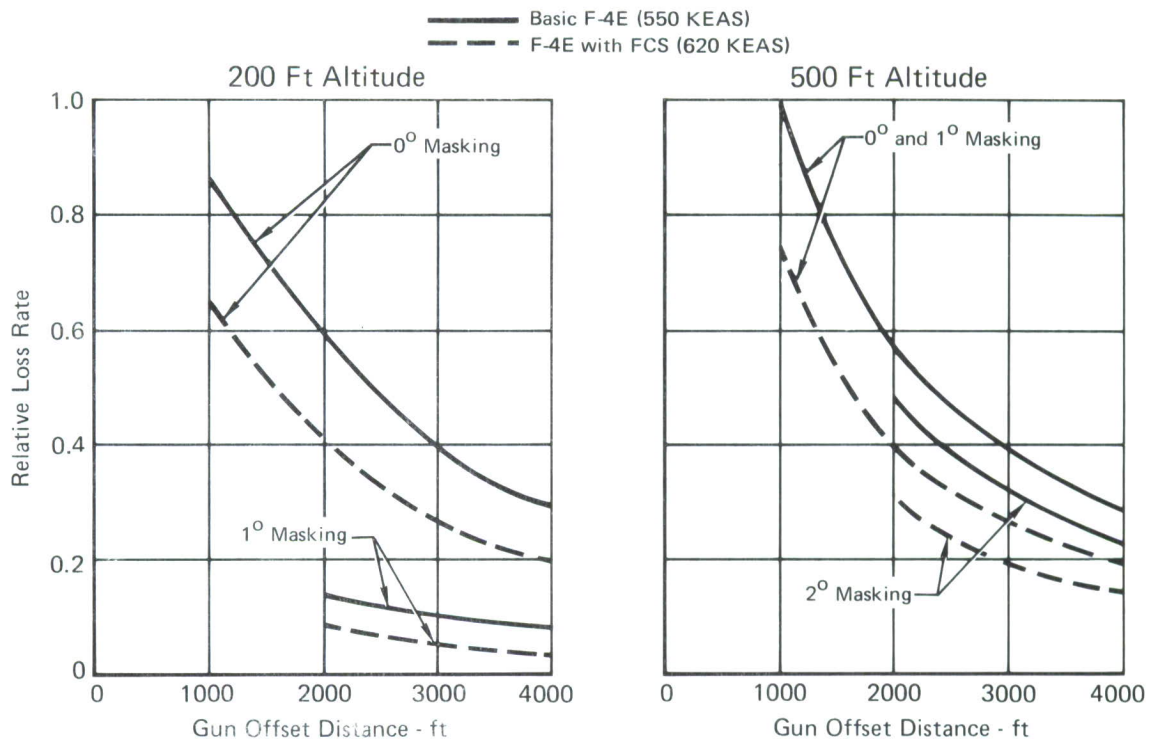
FIGURE 62
RELATIVE LOSS RATE SUMMARY
Enroute Profile

maximum speed for a given altitude. If the aircraft penetrated, it entered a weapon delivery profile that yielded a <u>specified accuracy level</u>. Survivability information was compiled during the entire flight consisting of both the enroute portion and the weapon delivery portion.

The profile, shown in Figure 64, used to compute hit densities is a low level dash with a pop-up to altitude followed by a conventional dive bombing maneuver. The aircraft then pulls up and returns to altitude. The guns locations are again offset from the flight path at a distance from 1000 to 4000 feet, but in this case there are 51 guns located every 1000 feet downrange from a distance of -45,000 feet to +5000 feet. There are four different profiles, 515 and 550 KEAS low level dashes for the aircraft without active flutter control and 585 and 620 KEAS low level dashes for the aircraft with active flutter control. During the pop-up maneuver both
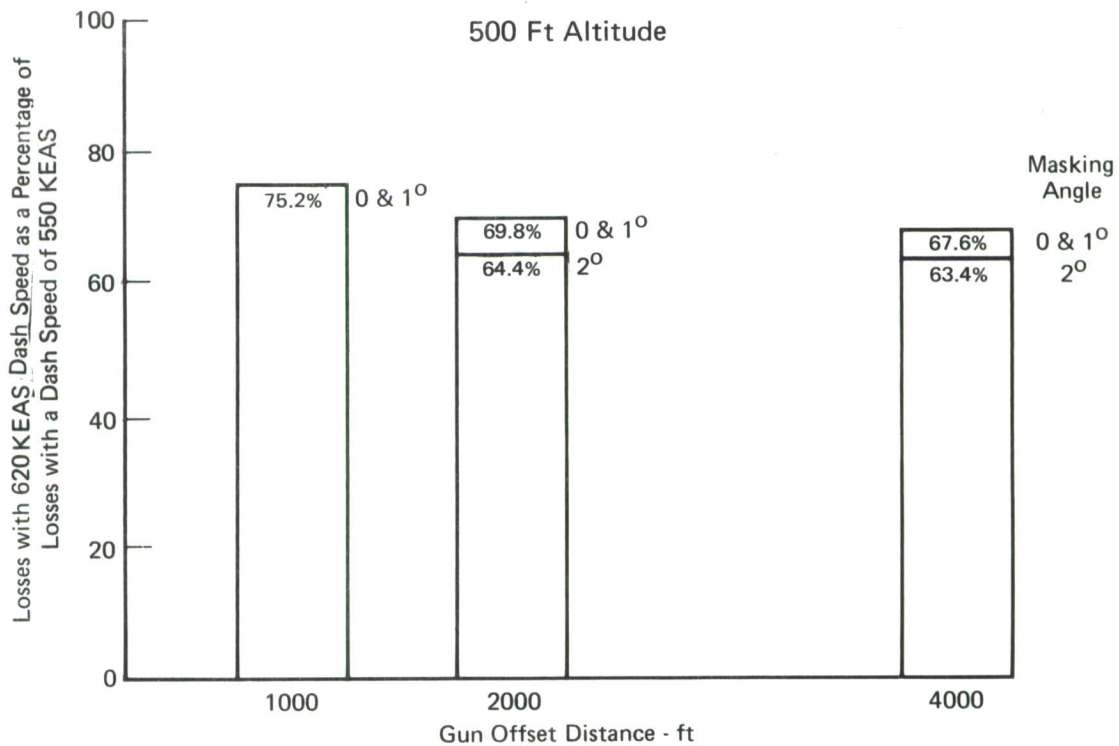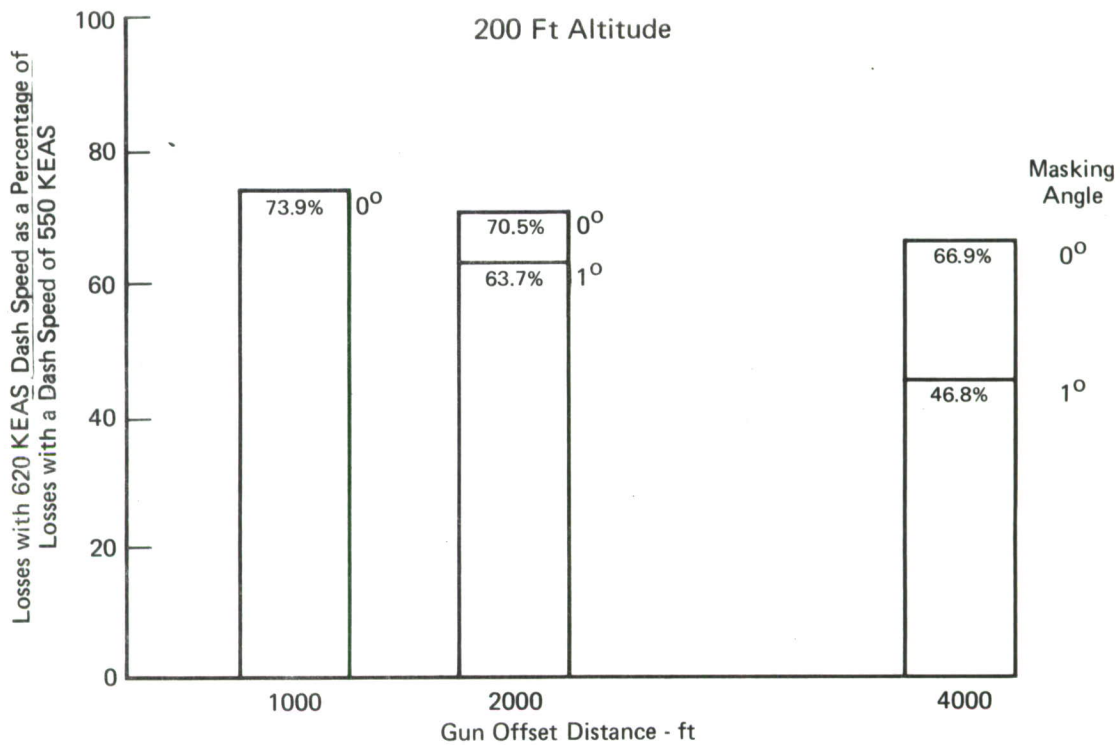
FIGURE 63
LOSS RATE RATIOS
Enroute Profile
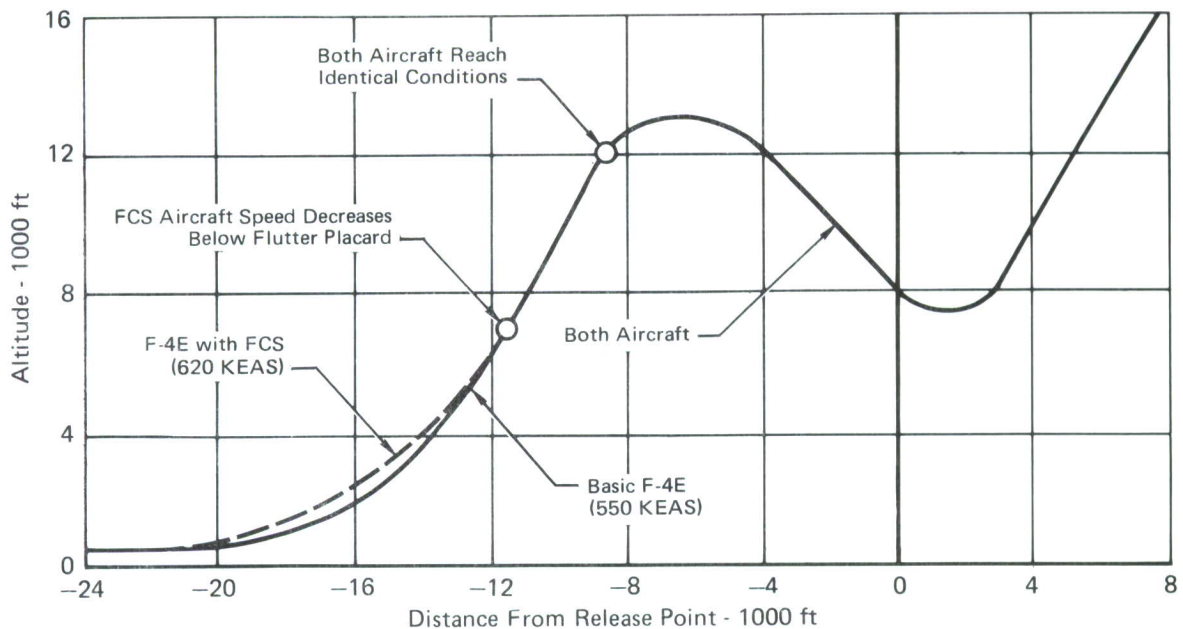
FIGURE 64
WEAPON DELIVERY PROFILE WITH AND WITHOUT AN ACTIVE FLUTTER
CONTROL SYSTEM

aircraft climb and decelerate to an equal speed and altitude to begin the dive bombing. At some point in the climb the speed of the aircraft with the flutter control system drops below the 550 KEAS mark and the flutter control system becomes a non-vulnerable system. For this reason, the survivability studies were run in two segments for the aircraft with the flutter control system.

3.10.4.2 <u>Results</u> - Relative loss rates for the weapon delivery profile are presented in Figure 65. The basic F-4 at 515 KEAS is used as the base case because it experienced the highest loss rate. Results for the other three dash speeds are scaled accordingly. The flutter control system is used only for the profiles with the 585 and 620 KEAS dash speeds.

Loss rate ratios (ratio of losses at the three higher dash speeds to losses at 515 KEAS) for the weapon delivery profile are computed as percentages and presented in bar chart form in Figure 66. The results indicate that loss rate ratio is relatively insensitive to gun offset distance in the weapon delivery profile. In all cases, against the dense multiple gun defense, the improvement in the relative loss ratio is on the order of 25 percent. This compares favorably with the improvement in relative loss
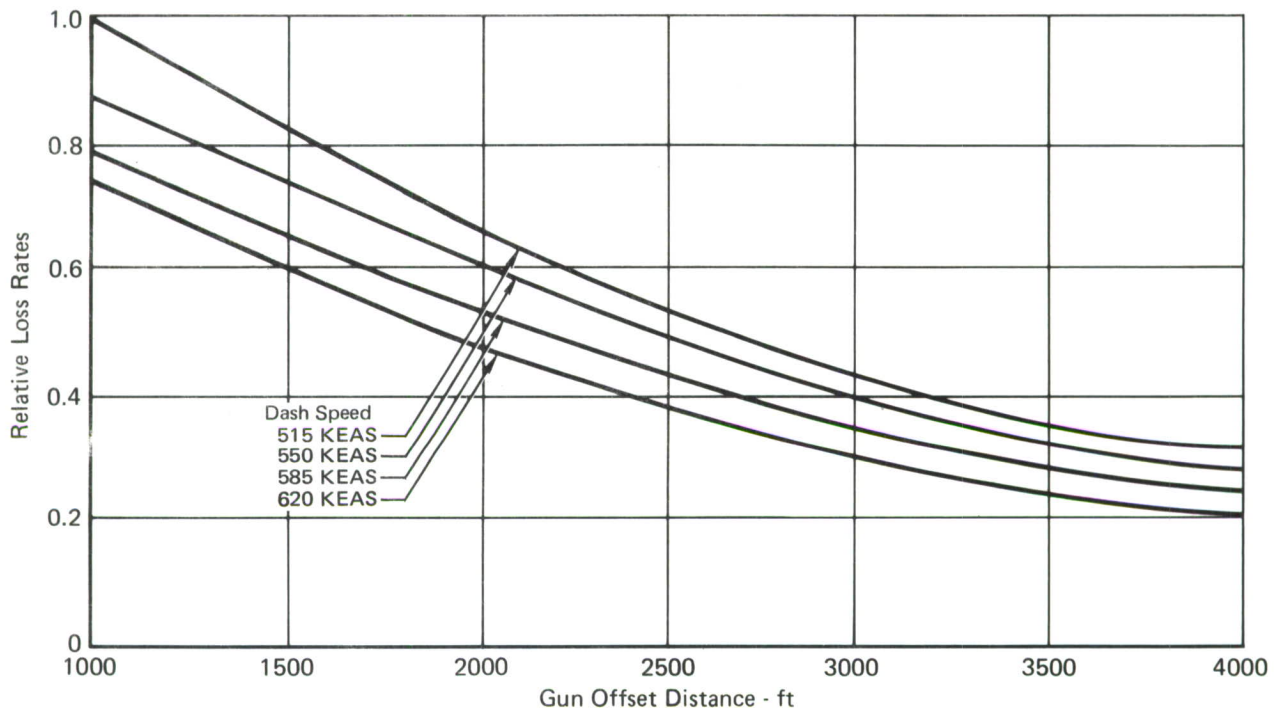
FIGURE 65
RELATIVE LOSS RATE SUMMARY
Weapon Delivery Profile

ratios of 25 to 50 percent obtained in the one-on-one enroute analysis described in Section 3.10.3.

3.10.5 General Comments on Increased Speed - There are at least two questions regarding increased speed which justify further comments.

3.10.5.1 Effects on Other Aircraft Systems - The first question concerns the combat survivability degradation of specific systems on the aircraft when the aircraft speed is increased from 550 knots to 620 knots. This can be answered by examining loss rate ratio data for two aircraft; one at 550 knots without a flutter control system and the other at 620 knots with a flutter control system. The aircraft loss rates have been computed by analyzing losses due to hits on five major critical aircraft systems, namely; Singly Vulnerable Systems, Thrust, Air Crew, Lateral Control, and Longitudinal Control (refer to Figure 60).

Table 12 shows the loss rate ratios for a 500 ft altitude pass at a gun that is offset 1000 ft where ground masking is zero degrees. The numbers in Table 12 are favorable to the active flutter control system if they are less than one. The vulnerability of the lateral control system
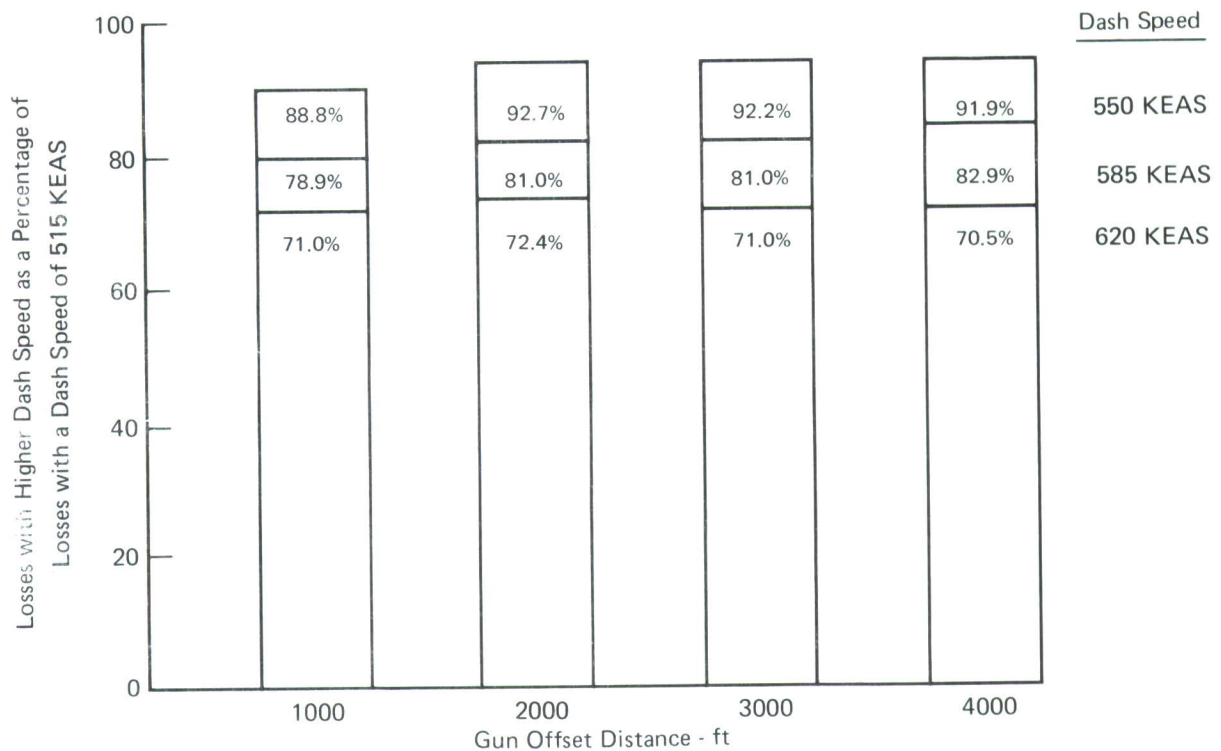
FIGURE 66
LOSS RATE RATIOS
Weapon Delivery Profile

TABLE 12
AIRCRAFT LOSS RATE RATIOS BY CRITICAL SYSTEM
500 Ft Altitude — AAA Gun Offset 1000 Ft
Zero Ground Masking - (620 KEAS/550 KEAS)

Singly Vulnerable 0.749

Thrust 0.541

Air Crew 0.497

Lateral Control
   (Loss Rate Ratio Undertermined
   Because of Zero Denominator)

Longitudinal Control 0.726

Total Aircraft 0.751

increases when the flutter control system is switched on as required for the faster speed. There are several components in the lateral control system which can cause an aircraft loss if the flutter control system is in use, but cannot cause losses if the system is not in use. Because of this increase in vulnerability, the loss rate ratio of the lateral control system is greater than 1. It cannot be computed, however, because the accuracy of the model shows the loss rate of the basic lateral control system to be 0. For this reason the loss rate ratio is undefined as shown. The other four critical systems have only a negligible increase in vulnerability which is overshadowed by the gunner's decrease in ability to track the aircraft at higher speeds. As expected, the loss rate ratio for the total aircraft is less than one.

The numbers in Table 12 apply only to losses that occur from battle damage. They do not reflect any component losses that might occur from the more severe utilization imposed by the higher aircraft speed.

3.10.5.2 <u>Effects of Low Altitude Flight</u> - The second question concerns the hazard of flying at 200 ft altitude at the increased speed permitted by the active flutter control system. Research has indicated that high speed flight at 200 ft altitude is reasonable in wartime operations over level terrain. Flight at 500 ft altitude at these speeds is practical over somewhat rougher terrain and is judged to be equally hazardous at the faster and slower speeds. This conclusion results largely from subjective judgment. Flight data concerning ground clobber is limited.

4. AIRCRAFT OPERATIONAL CONSIDERATIONS

4.1 Performance Sensitivities

Aircraft performance sensitivities were computed on the basis of F-4E data.

Since no external moldline changes are involved, all performance penalties are the result of increasing the aircraft gross weight. Figure 67 shows performance penalties as a function of gross weight increase. As will be noted, the performance degradations corresponding to the estimated 270 lb gross weight increase are insignificant in each case.

4.2 Mission Trade Offs

Figure 68 illustrates the mission profile and definition of the Hi-Lo-Lo-Hi mission used in a mission radius/dash radius trade study for the F-4. The take-off configuration consisted of full internal fuel, (4) AIM-7E missiles, (1) MK-84 located at each left and right outboard wing stations, and (1) 600 gallon centerline tank.

The baseline mission was performed with the dash-out and dash-back segments flown at the current MK-84 carriage placard speed (550 KEAS, M = .83). The effect of increasing the carriage placard speed to permit dash-out and dash-back at military power (M = .94/.95) is illustrated in Figure 69. For the same total mission radius (362 NM), the increased dash speed decreases dash radius from 50 to 27 NM; if the 50 NM dash radius is maintained, the total mission radius is reduced from 362 to 295 NM.

An investigation of the possibility of using maximum power during the dash segment was conducted. The resulting dash Mach number was 1.09 but high fuel consumption at this dash condition precluded accomplishment of the mission. The use of maximum power is not feasible, except for very limited periods of time.

Another viewpoint is shown in the carpet plots of Figures 70 and 71. These plots are for the same configuration as above but allow for engine operation both with and without afterburner as well as in a mixed afterburner and reduced power mode. The trade off is between a nominal mission radius of 300 nautical miles and a nominal dash radius of 50 nautical miles. The figures indicate that attractive ranges can still be realized even with substantial increases in speed.
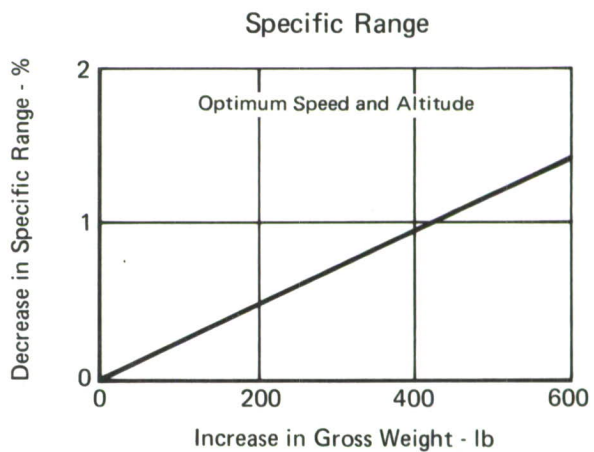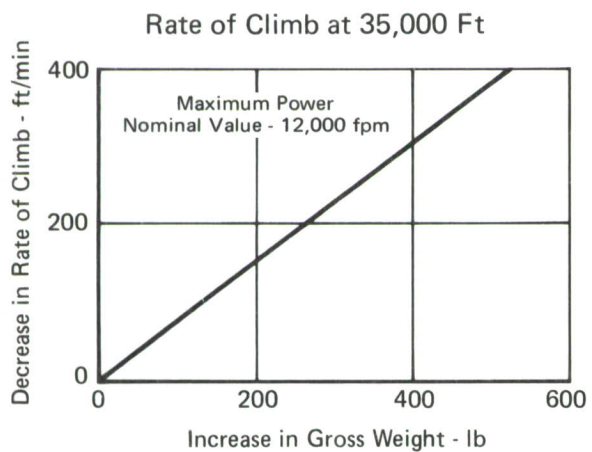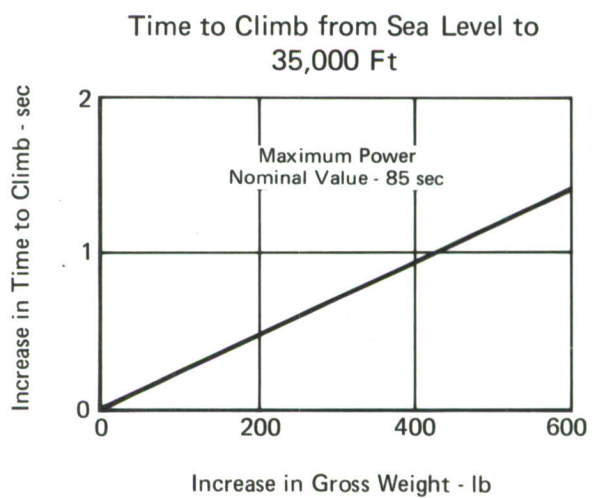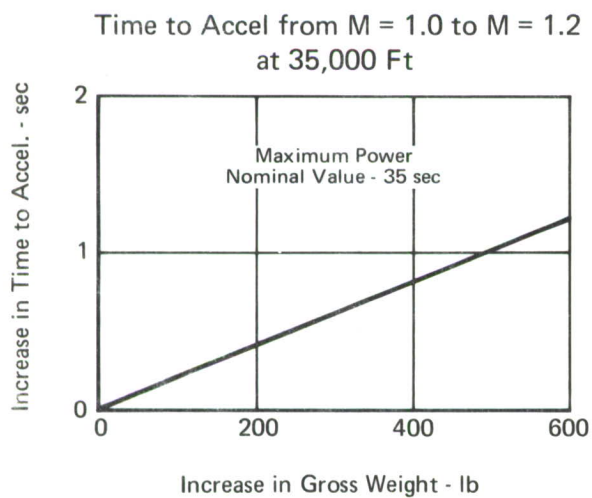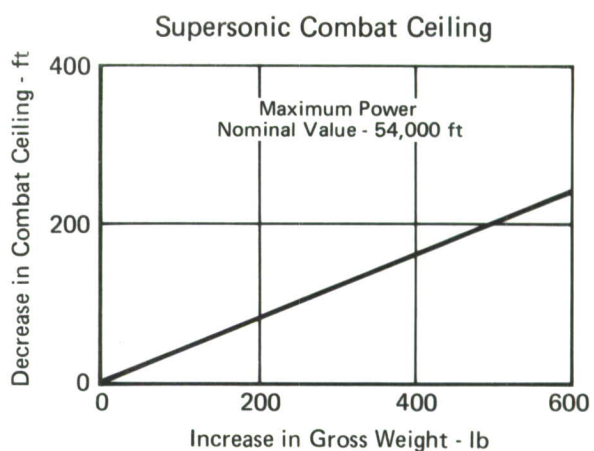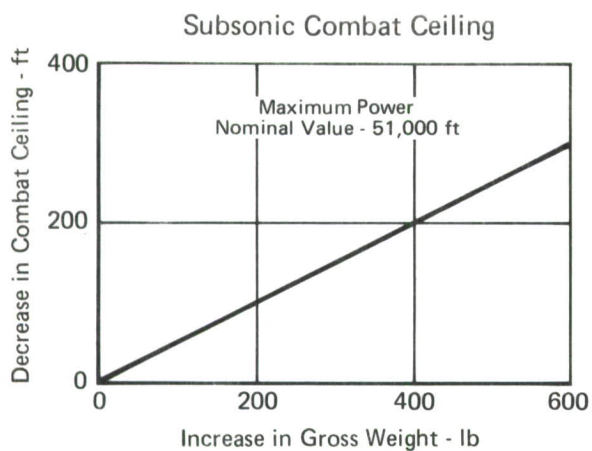
FIGURE 67
PERFORMANCE SENSITIVITIES OF F-4E TO WEIGHT
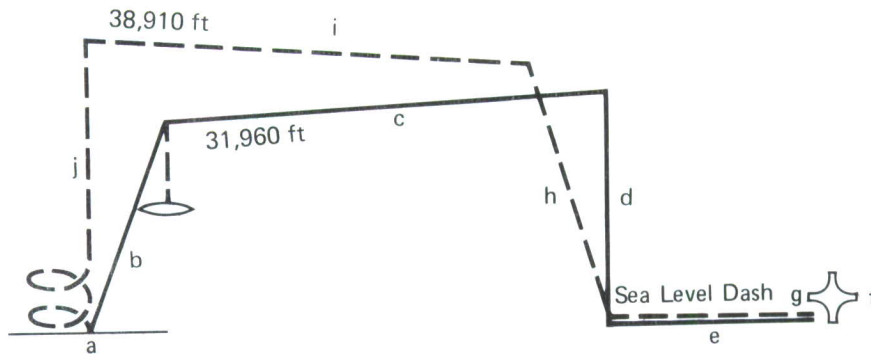
F-4E + (4) AIM-7E + (2) MK-84 + (1) 600 Gal. Tank
TOGW = 54,833

Mission Definition:

a   Take-off and Acceleration Fuel Allowance: 5 Minutes with Normal Power Plus (1) Minute with Maximum Power.

b   Military Power Climb to Optimum Cruise Altitude.

c   Cruise Out at Optimum Speed and Altitude (Drop Tank When Empty).

d   Descend to Sea Level - no Credit for Fuel or Distance.

e   50 Nautical Mile Dash to Target at Sea Level at Carriage Placard Speed or Military Power.

f   Expend Stores.

g   50 Nautical Mile Dash Back at Sea Level at Carriage Placard Speed or Military Power.

h   Military Power Climb to Optimum Cruise Altitude.

i   Cruise Back at Optimum Speed and Altitude

j   Reserves: 5% of Initial Fuel Plus 20 Minutes at Speed for Maximum Endurance at Sea Level, Both Engines Operating.

FIGURE 68
HI-LO-LO-HI MISSION
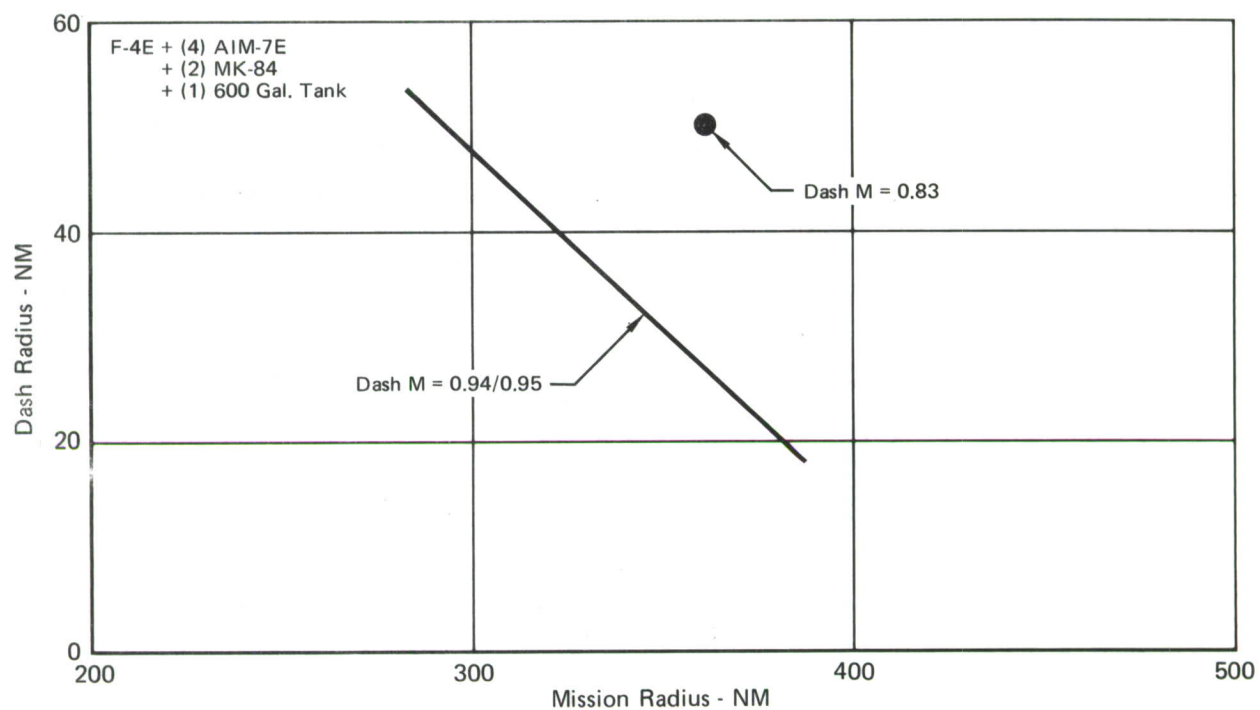
FIGURE 69
HI-LO-LO-HI MISSION RADIUS/DASH RADIUS TRADE OFF
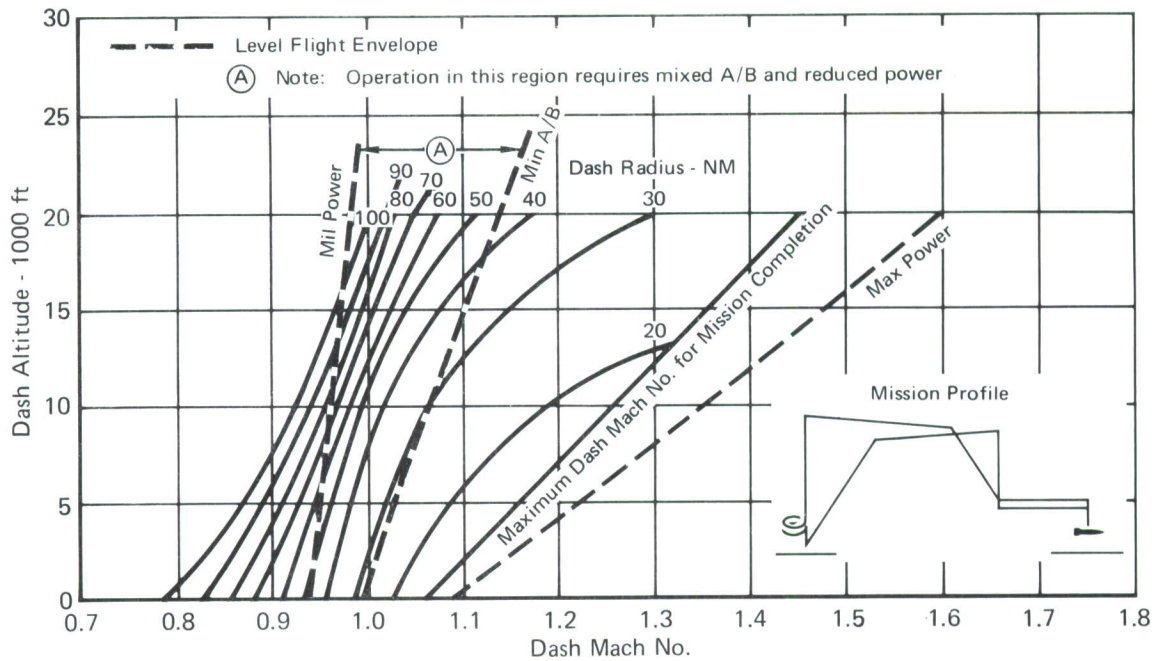
FIGURE 70
F-4E DASH RADIUS vs DASH MACH NUMBER
(4) AIM-7E + (2) MK-84 + (1) 600 Gal. Tank
Mission Radius = 300 NM
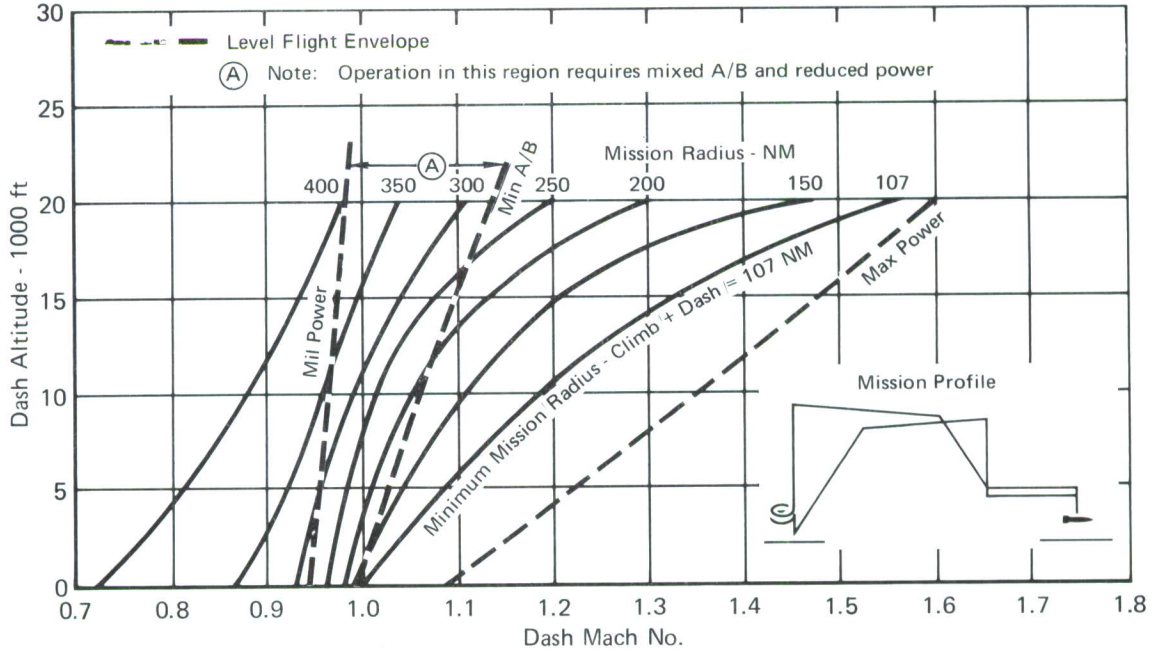
FIGURE 71
F-4E MISSION RADIUS vs DASH MACH NUMBER
(4) AIM-7E + (2) MK-84 + (1) 600 Gal. Tank
Dash Radius = 50 NM

4.3 Flight Envelope Improvements

Figures 72 and 73 show flight envelopes and limitations for an F-4E carrying 370 gallon tanks and MK-84 bombs. The Military and Afterburner (A/B) Power envelopes are for level flight. The bold lines within the figures represents the handbook placards for carriage (flutter), release and jettison. In Figure 72, the jettison placard for the fuel tank is shown separately since it differs from the carriage (flutter) limit. Other information in these figures shows the potential envelope expansion through active flutter control (provided other intermediate limits can be improved), and identifies the types of limitations.

If the flutter placard is removed, the limiting restriction would involve the release/jettison/carriage placards. The jettison placard for the fuel tank in Figure 72 is a realistic and practical placard. There is no release limit since the tank is not releasable without the pylon. Extensive research and unknown modifications would be required to raise this jettison placard to the active control flutter boundary. However, means for increased release speeds could be developed for the MK-84 bombs. Available flight test data indicate that the release/jettison speeds for this weapon could be extended to the vicinity of the aircraft structural (A/C Structure) limits without modification. Additional wind tunnel testing could be required to verify these conclusions.

The current recommendations for temperature limitations on standard bombs (Reference 29) are 650 KEAS or Mach 1.4 for up to 5 minutes (based on adiabatic bomb wall temperature of 165-175°F). Flights exceeding this placard for short periods of time (1-2 minutes) should also be feasible with these bombs. Reasonable plastic coatings on the bombs could remove these restrictions. Practical airspeed limits for fuzes vary from relatively low subsonic limits for propeller type arming devices to unlimited carriage speeds with electrical fuzing. Fuzes can be matched to the flight condition and bomb so that in a practical sense fuzes are no problem. Current placards for seeker units used with the guided bombs have been checked to high subsonic Mach numbers. The manufacturer's opinion is that these units could be carried at speeds up to supersonic Mach numbers without modifications.

---

29. Epstein, C. S., "Supersonic Delivery of Conventional Weapons - Fact or Fancy?," Presented at the Aircraft/Stores Compatibility Symposium, December 1971.
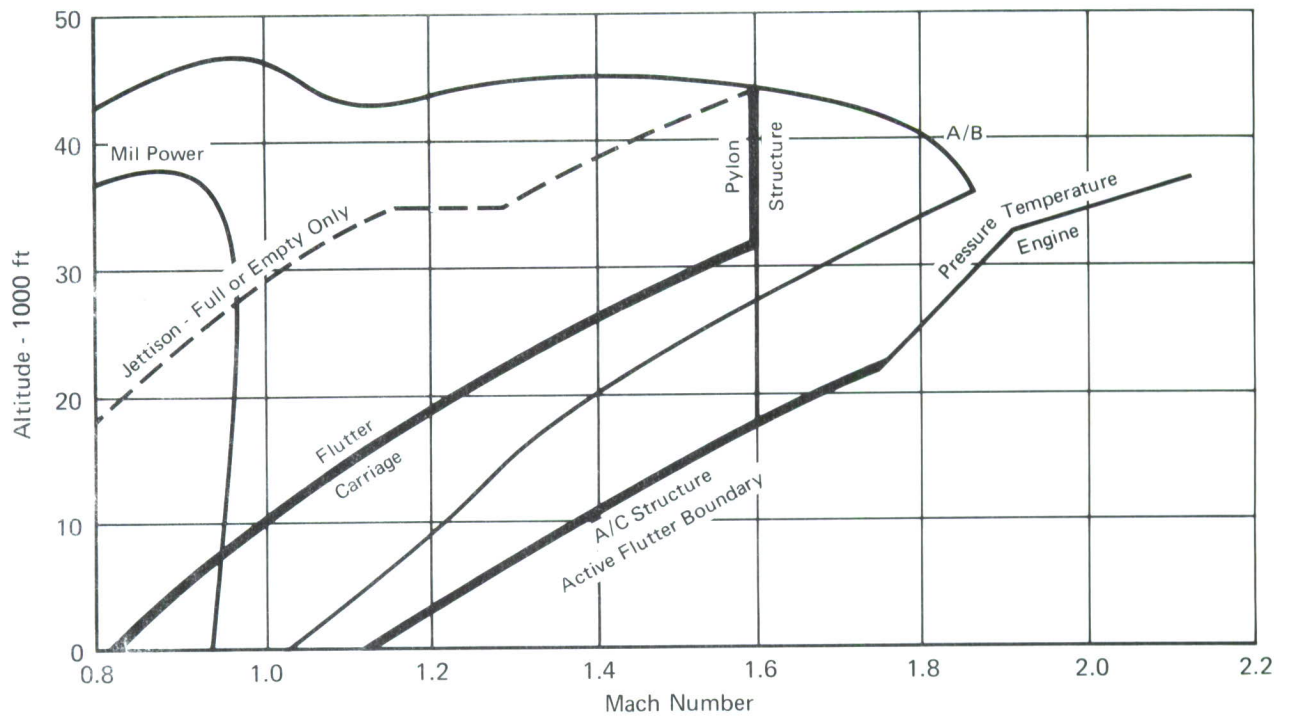
FIGURE 72
F-4E ENVELOPE WITH (2) 370 GALLON TANKS
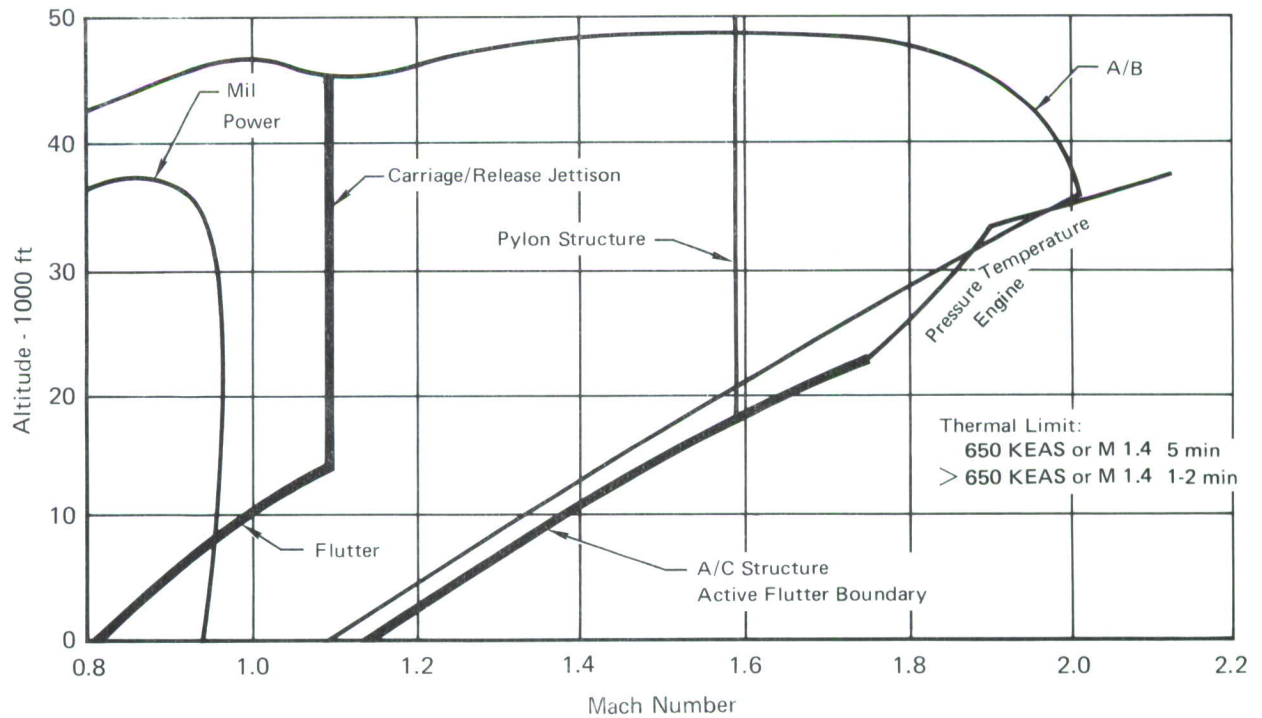
FIGURE 73
F-4E ENVELOPE WITH (2) MK-84 LOW DRAG BOMBS

132

The data shown on Figures 72 and 73 indicate that if the carriage/ jettison speed limits are increased to near the limit dive speed together with a similar increase in flutter speed limit, the maximum permissible low altitude flight speed would be increased on the order of 30 percent to the aircraft structural limit.

4.4 Future Aircraft Payoffs

A performance payoff of active wing/store flutter control for advanced fighter attack aircraft is shown in Figure 74. To provide relative perspective, the flight envelopes of two contemporary aircraft (F-4 and A-7 are also shown. The primary mission of the advanced fighter would use conformal, fuselage-mounted weapons (References 30 and 31). Therefore, the conformal fuselage carriage and wing pylon carriage envelopes and limits are provided for comparison. With conformal fuselage weapon carriage an aircraft could reach the low altitude, high dynamic pressure boundaries shown, with modulated afterburner. With the external wing pylon store option, large bombs may be carried which cannot be carried conformally on the fuselage. The same boundaries can be reached for the wing store option with full afterburner and active flutter control with only a slight degradation in ceiling. With an expanded flight envelope (higher speeds) the aircraft survivability is expected to substantially increase, as discussed in Section 3.10 of this report.

The effect of wing pylon weapon carriage on dash radius for a representative counter-air high-low-low-high mission of 400 nautical mile radius, with external fuel, is shown in Figure 75. Even with this sizeable increase in payload there is no limit in V_{max}, as shown in Figure 74, and an operationally feasible mission is maintained.

Active flutter control offers a potential reduction in boresight error for wing mounted air-to-air missiles. Wing twist induces an error between the aircraft fuselage (fire control reference) and the missile seeker axis. An expanded seeker field to accommodate dynamic wing twist

30. Talbot, J. F., "Conformal Carriage Concept," Presented at the Aircraft/ Stores Compatibility Symposium, November 1969.
31. Nichols, J. H. and Martin, C. J., "Conformal Weapons Carriage - Joint Service Development Program," Presented at the Aircraft/Stores Compatibility Symposium, December 1971.
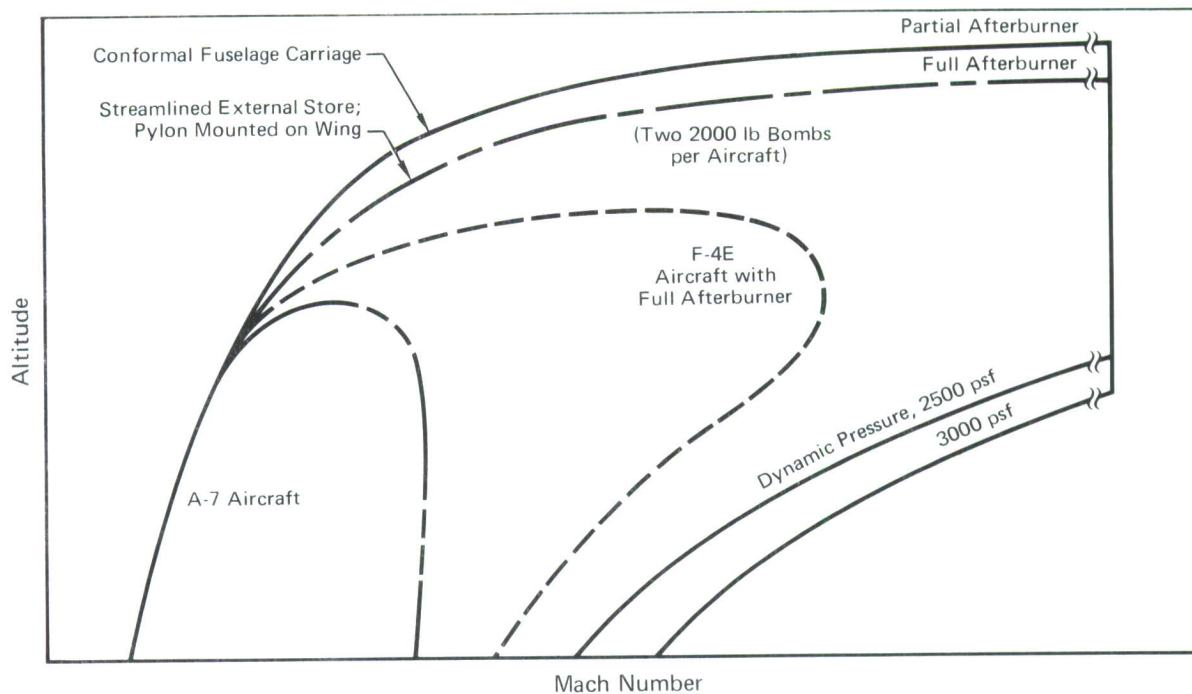
FIGURE 74
COMPARISON OF CONTEMPORARY AND ADVANCED AIRCRAFT ENVELOPES
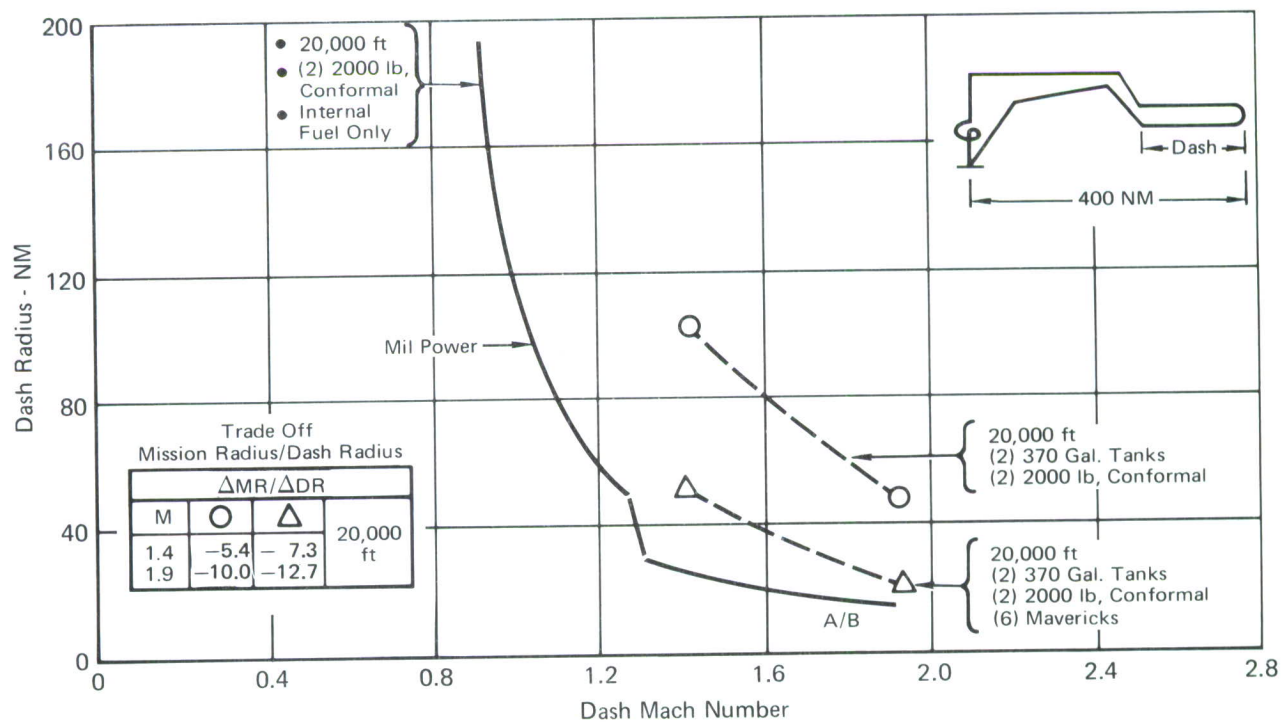
FIGURE 75
COMPARISON OF ADVANCED FIGHTER MISSIONS

reduces mission performance in terms of reduced probability of acquisition and detection and increased lock-on time. A flutter control system could be used both sub-flutter and post-flutter to eliminate (reduce) dynamic wing twist to improve missile performance and to eliminate the added complexity of seeker scan patterns.

4.5 Flutter Control System Weight Estimates

It was established in Reference 4 that a triplex flutter control system could satisfy a one-fail-operate performance criterion and, using F-4 data, the triplex system would also guarantee a loss of aircraft less than one per million flight hours. The weight estimate for the system on the F-4 was 270 pounds per aircraft. This estimate was based on use of the quadruplex SFCS (Reference 11) secondary actuator as a remote signal conversion mechanism. If this heavy actuator were to be eliminated by the use of fly-by-wire electro-hydraulic actuators the weight estimate would be reduced to 200 pounds on the F-4.

Figure 76A describes an operational triplex system for a generalized advanced aircraft. This triplex system is conceptually the same as for the F-4 in Reference 4 with similar reliability and flight safety features. Figure 76B describes an alternate simplex configuration with duplex electronics which would be more than adequate for use in a flight test demonstration program. The system is one-fail-safe. If the basic hydraulic system fails, the pressure drops, and an alternate back-up hydraulic system is switched in. The comparator will notify the pilot of electronic or sensor failures and will turn off the flutter control system. The pilot then has the option of reducing speed below the flutter boundary or release the stores to immediately stabilize the aircraft. An automatic store release mechanism, similar in design to the automatic tunnel shutdown device described in Section 5.1.4.4, could be incorporated to ensure a one-fail-safe system regardless of pilot responsiveness or depth of flutter penetration.

Weight estimates for these two system concepts are given in Tables 13 and 14. These estimates assume that the improved fly-by-wire actuator will allow for the incorporation of the ailerons into the aircraft CAS (Control Augmentation System). The flutter control system is thus charged only for those items which are uniquely required for its operation. With this viewpoint, 131 pounds for the triplex system and 81 pounds for the simplex system are attributable to the flutter control system.

A - Triplex-Fail Operate

FCS Sensors / Pilot FBW Input / Other FBW Inputs → FCS Adaptive Gain → ⊗ → FBW Electronics → Comparator Voter → SCM → MCV → Actuator → Output

Hydraulic Power / Hydraulic Power → Hydraulic / Mechanical

Feedback — Electrical / Mechanical

Actuator

B - Simplex-Fail Safe with Duplex Signaling

FCS Sensors / Pilot FBW Input / Other FBW Inputs → FCS Adaptive Gain → ⊗ → FBW Electronics → Comparator → EH Servo Valve → Actuator → Output

Hydraulic Power / Normal / Back Up → Hydraulic

Feedback — Electrical / Mechanical

Actuator

FIGURE 76
ADVANCED AIRCRAFT AILERON FCS ACTUATOR-SYSTEM CONCEPTS

TABLE 13
ADVANCED AIRCRAFT WEIGHT ESTIMATE
Triplex Concept

| System Component | Weight Attributable to | |
	FCS (lb)	Fly-By-Wire (lb)
Fly-by-Wire Surface Actuator ΔWt (2 x 27.5)	0	55
Surge Suppressors (4 x 5)	20	0
Electronics and Voters (6 x 10)	0	60
Mounting Racks (6 x 2)	0	12
Sensors (6 x 2)	12	0
Cockpit Displays and Test Console	5	10
Wiring and Electrical Modifications	10	40
Hydraulic Line Modifications	35	0
Computer for Adaptive System	40	0
Transformers/Rectifiers (3 x 9)	0	27
Batteries (3 x 3)	9	0
Total	131	204

TABLE 14
ADVANCED AIRCRAFT WEIGHT ESTIMATE
Simplex (Duplex Signaling) Concept

| System Component | Weight Attributable to | |
	FCS (lb)	Fly-By-Wire (lb)
Fly-by-Wire Surface Actuator, ΔWt	0	0
Surge Suppressors (2 x 5)	10	0
Electronics and Comparators (2 x 5)	0	10
Mounting Racks (2 x 2)	0	4
Sensors (2 x 2)	4	0
Cockpit Displays and Test Console	2	3
Wiring and Electrical Modifications	5	25
Hydraulic Line Modifications	20	0
Computer for Adaptive System	40	0
Total	81	42

5. FUTURE EFFORTS

In this section plans are presented for semispan and full-span low speed and semispan transonic wind tunnel tests, "Iron Bird" simulation tests, ground vibration and installed system tests, and flight test demonstrations with three store configurations having widely differing dynamic characteristics.

5.1 Wind Tunnel Testing

The F-4 has been used as a guideline aircraft in formulating this wind tunnel test plan. While some aspects (such as spoiler effects) may be peculiar to the F-4, this program is designed to be applicable for demonstration of wing/store flutter control for other fighter type aircraft. Three external stores which have significantly different effects on wing/store flutter, shall be selected for carriage on an outboard store pylon location.

5.1.1 Test Objectives - Both low speed and transonic tests will be required to help insure a high confidence level in achieving the program objectives which are to:

o Demonstrate the ability of the wing/store active flutter control scheme(s) to raise the passive wing/store flutter speeds

o Evaluate the logic to be employed in the full scale aircraft adaptive compensation technique using man-in-the-loop to simulate the adaptive compensation logic and explore alternate logics, if necessary

o Obtain data for evaluating the validity of, or improvements needed, in the analytical methods employed in active flutter control design studies

o Provide additional design information for further development of an active wing/store flutter control system for full scale flight demonstration

5.1.2 Test Series - Four wind tunnel test series are included in the program:

Series I   - Low Speed Tunnel/Semispan Servoaeroelastic Model

Series II - Low Speed Tunnel/Complete Servoaeroelastic Model

Series III - Transonic Tunnel/Semispan Servoaeroelastic Model

Series IV - Transonic Tunnel/Semispan Oscillatory Aerodynamics Model

A full-span transonic flying model is not included in the test plan.

A large test section size is a primary consideration in selecting wind tunnels for these tests. Large models are desirable to permit model frequency scaling near unity. This is advisable because it allows for a more credible modeling of the control surface actuation system, particularly with respect to nonlinearities such as rate saturation. This test program is therefore

based on the use of the McDonnell 8-1/2 x 12 ft. Low Speed Wind Tunnel for Series I and II subsonic tests and on the use of the Langley 16 x 16 ft. Transonic Dynamics Tunnel for the Series III and IV transonic tests.

The Series IV test program is discussed separately in Section 5.1.7 because it stands by itself. All discussion other than in Section 5.1.7 pertains to the Test Series I, II, and III.

5.1.3 _Test Setup and Instrumentation_ - The general test setup for the Series I, II, and III tests will consist of the following:
- o Aeroelastically scaled wind tunnel model
- o Operable aileron control surface(s)
- o Aileron actuation system
- o Model response sensor(s)
- o Flutter control system
- o Instrumentation and data acquisition system

The test setup in block diagram form is shown in Figure 77; the instrumentation and data processing system is shown in Figure 78. For the complete flying model in Series II, independent flutter control systems will be incorporated for the left and right half wings.

The model instrumentation will provide the following data:
- o Wing root bending moment
- o Wing root torsion moment
- o Model response sensing such as,
  - Wing tip **angular accelerations**
  - Pylon pitch accelerations
  - Store nose accelerations
  - Pylon/wing load cell sensing
  - Aileron hingeline accelerations
- o Aileron position and rate
- o Aileron actuation system data
- o Input commands

Additional data will be obtained via the flutter control system itself. These would consist of Nyquist plots, co-quad plots, and frequency response plots of selected open loop transfer functions as indicated in Figure 77.

5.1.4 _Wind Tunnel Models_ - The results of an initial model scaling study for a low speed and transonic model of the F-4 are described in this section. The models, scaled at 18% and 40%, have been sized as large as possible without causing undue tunnel blockage. The ratio of model weight to
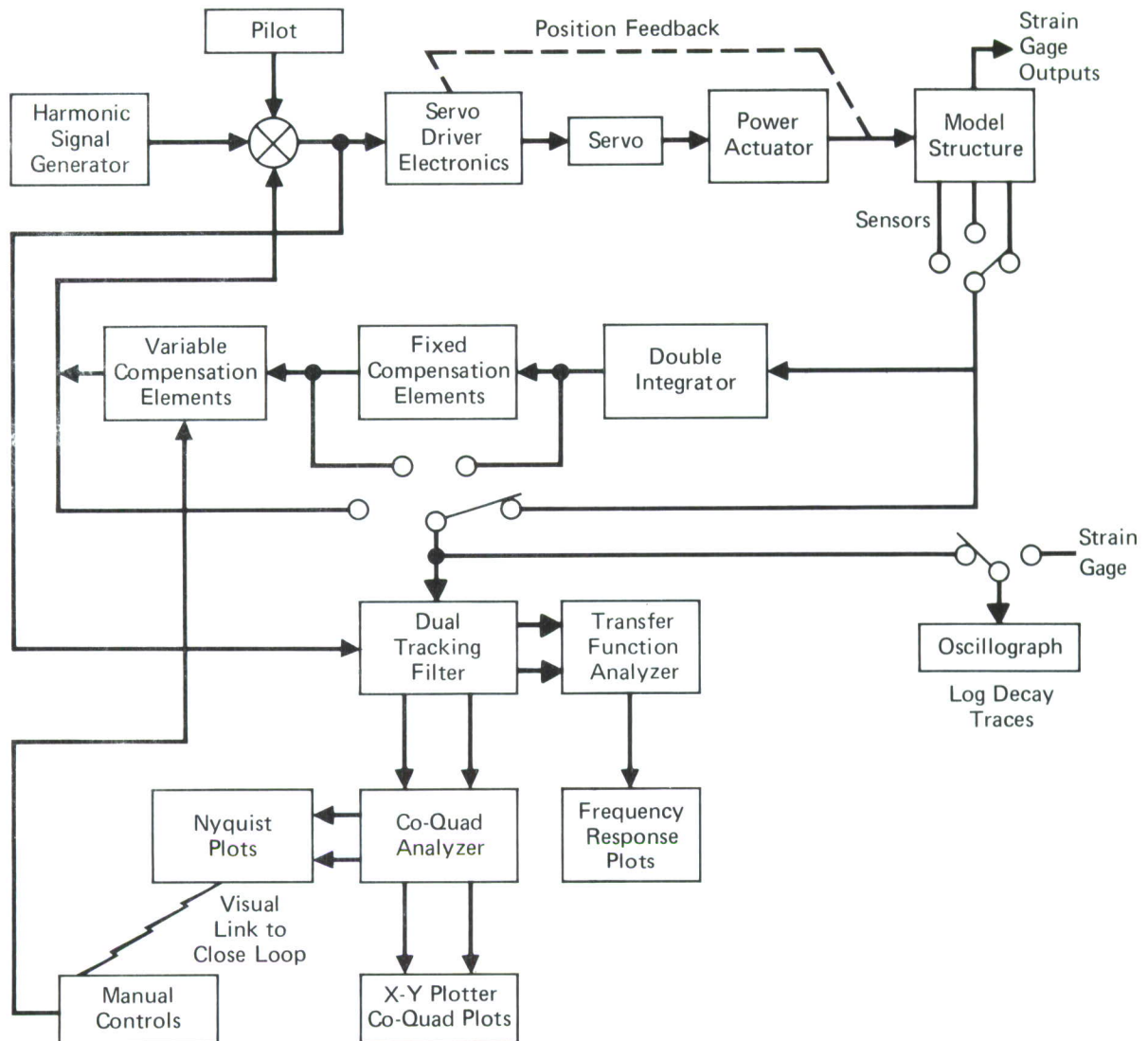
FIGURE 77
SCHEMATIC OF A SINGLE CHANNEL FLUTTER CONTROL SYSTEM
FOR WIND TUNNEL TESTING
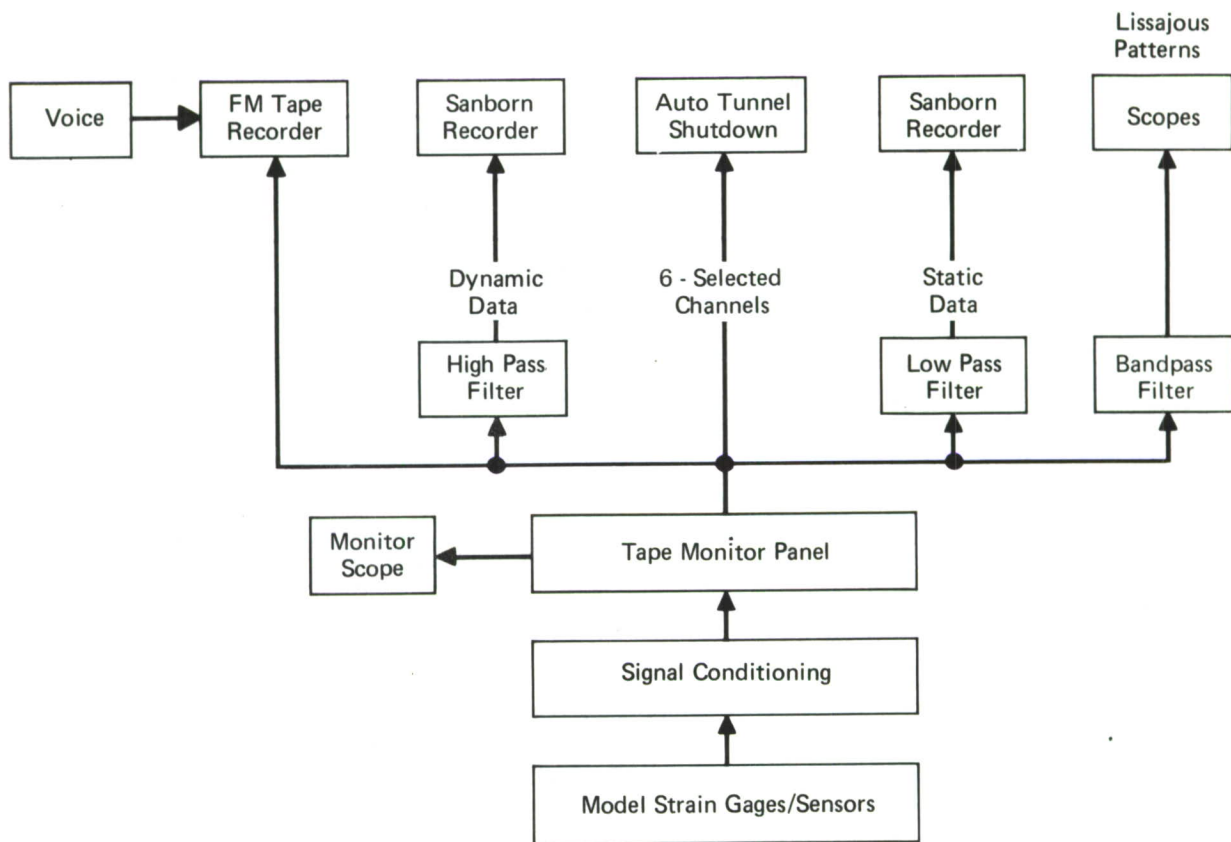
FIGURE 78
CONCEPTUAL DIAGRAM FOR
WIND TUNNEL INSTRUMENTATION AND DATA PROCESSING

wing area of both models (about 3 lb/ft^2 and 5 lb/ft^2) will permit acceptable weight allowances for instrumentation and control surface actuation mechanisms.

    5.1.4.1 <u>Model Description</u> - The models for the tests are:

Series I   - Low Speed Semispan Wing Model

Series II - Low Speed Full-Span Complete Aircraft Model (This test model will use the wing from Series I test)

Series III - Transonic Semispan Wing Model

The nomenclature used for model scaling is:

L	length	ft
ρ	density of gas medium	slugs/ft^3
V	flow velocity	ft/sec
T	temperature	°R
q	dynamic pressure	lb/ft^2
M	Mach number	
H	total pressure	lb/ft^2
λ	length scaling	L_M/L_A
ψ	velocity scaling	V_M/V_A
ϕ	density scaling	ρ_M/ρ_A

Where subscript A refers to aircraft, M refers to model.

    Preliminary Series I (Semispan) and Series II (Full-Span) model design data suitable for the MCAIR Low Speed Tunnel are,

ρ_M = air at sea level

T_M = 570°R

M_M = .15

V_M = 174.8 ft/sec

Model Scale = λ = .18 (Note that models with scale factors somewhat smaller than this would also be acceptable.)

Velocity Scale = ψ = .159

Density Scale = ϕ = 1.0

Frequency Scale = ψ/λ = .883

Mass Scale = $\phi\psi^3$ = .00583

If these scale factors are applied to the F-4 aircraft, as a particular example aircraft, the following dimensions and model weights result:

Series I | Series II

Series I
Span = 3.455 ft
Wing Area = 8.72 ft^2
Single Wing Model Weight = 26.1 lb

Series II
Span = 6.91 ft
Wing Area = 17.44 ft^2
Complete Airframe Model Weight = 262.4 lb

Preliminary Series III (Semispan) model design point conditions and scaling data for the Langley 16T Transonic Dynamics Tunnel are,

$M_M = 1.0$
$q_M = 237$ lb/ft^2
$H_M = 700$ lb/ft^2
Power = 14.0 Megawatts
Model scale = $\lambda = .40$

based on 95% Freon-Air Mixture

Velocity scale = $\psi = .449$
Density scale = $\phi = .735$

based on nominal tunnel conditions of,

$V_M = 504.5$ ft/sec
$\rho_M = .00175$ slugs/ft^3
$T_M = 528°R$

Frequency Scale = $\psi/\lambda = 1.12$
Mass Scale = $\phi\lambda^3 = .0471$

Again, if these scale factors are applied to the F-4, as a sample aircraft, the following dimensions and weights result:

Span = 7.68 ft
Wing Area = 43.07 ft^2
Single Wing Model Weight = 210.4 lb

The semispan, low speed, flutter model will have a multi-positioned, manually fixed spoiler in addition to an aileron capable of ±10° deflection with an actuator to oscillate the aileron ±3° about a nominal position. Two dynamically scaled pylons are planned along with three dynamically scaled stores.

The semispan wing will be wall mounted and will have root translation and pitch or root-roll degrees-of-freedom to allow for the simulation of both symmetric and anti-symmetric motion. The full-span model will be a complete "flying" model using the wing from the Series I test plus a duplicate wing with pylons and stores for the right hand side of the model. Pitch control of the model will be provided by a remotely controllable horizontal tail. Roll control will be provided by inputs into the ailerons used for the flutter control system.

5.1.4.2 Model Actuation - The aileron actuation system presents special problems because it must have a flat frequency response to a scale frequency of 10-20Hz with peak-to-peak oscillations of 6 deg with the capability of cycling the aileron about average positions between ±10 deg. The hinge moments of the model aileron vs aileron deflection for the 18 percent and 40 percent scale models, based on the F-4, are presented in Figures 79 and 80. It is shown by the figures that the actuator must be capable of developing sufficient torque to overcome the hinge moment; in this case, approximately 20 inch pounds for the 18% model and 1600 inch pounds for the 40% model.

Consideration has been given to "off-the-shelf" actuators of various types that would meet the needs as defined above. Pneumatic motors are too large, but more significant than size, is the problem of slow response due to the inertia of the motor turbine. Another reason to eliminate pneumatic motors is the exhaust gases and their effects on the wing.

Small electric motors were also considered not acceptable because of the inertia of the armature which produces an unacceptably slow response.

Based on the above considerations it has been concluded that either miniature electro-hydraulic or electro-magnetic actuators are suitable. Considerable torque/weight advantages can be achieved with either type actuator. Some of the same problems exist with the electro-hydraulic and electro-magnetic actuators as compared with other types of actuators but compensation for these problems is easier. The inertia problem is practically non-existent and the drift problem of airloads moving the aileron during large deflection operation is eliminated by the compensation.

The control surface actuator will be mounted in the wind tunnel sidewall for the Series I tests and in the fuselage for the Series II tests. Small off-the-shelf electro-magnetic or electro-hydraulic actuators will be used. Electro-magnetic actuators are preferred for the low speed tests because of the relatively low hinge moment requirements. The Aeroflex Laboratories electro-magnetic torque motor Model T052W-1 is an example of a suitable actuator. The moment will be transmitted to the control surface through a series of pushrods and bellcranks. Straight torque shaft transmission is impractical because of excessive shaft windup. It is also impractical to mount miniature actuators in the vicinity of the control surface for such a small

144

FIGURE 79
HINGE MOMENT REQUIREMENT FOR LOW SPEED 18% MODEL
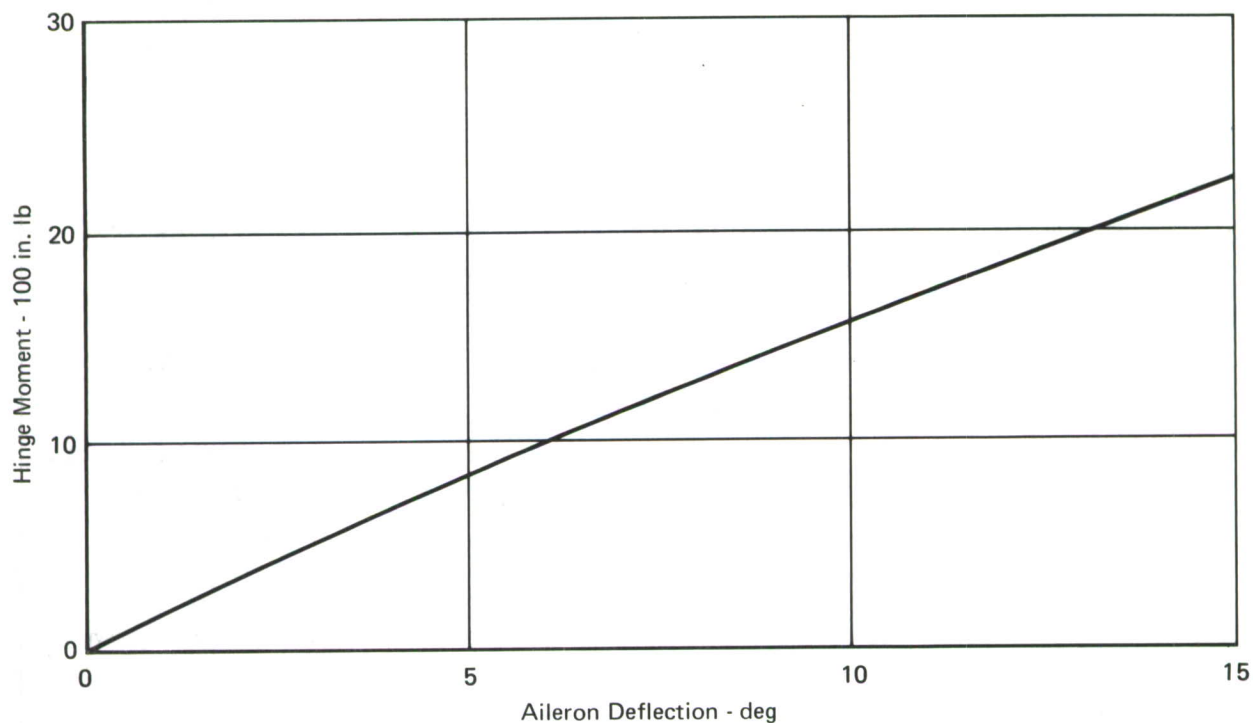
FIGURE 80
HINGE MOMENT REQUIREMENT FOR TRANSONIC 40% MODEL

145

model. Even the special miniature actuator design, described in Reference 32,
which was used for the SST flutter suppression tests, is much too large for
this application.

It is planned that the actuator for the Series III 40 percent transonic
model will be a linear electro-hydraulic actuator because of the large hinge
moment required. This actuator would be located in the wing in the vicinity
of the control surface if space permits. Otherwise it would be installed
in the wing root-fuselage area and connected to the control surface by push-
rods and bellcranks as in the low speed model. A suitable actuator is not
available off-the-shelf. It will need to be designed for the particular
requirements of the model.

Considerable effort will be required for the development of these systems
from the standpoint of the feedback control system, position indication,
frequency response, effects of system installation on the flutter wing mass
and stiffness distributions as well as the design of a feedback system to
compensate for actuator drift which could otherwise be produced by the vari-
ation of hinge moments on the aileron produced by airloads.

5.1.4.3 Model Mounting - It is proposed to mount the low speed canti-
levered semispan Series I wing model on a "four bar" system. By the proper
orientation of four support bars the wing will be allowed root translation
and pitch or root-roll, with the rigid fuselage simulation accomplished by
a weighted bar outside the tunnel supported by calibrated springs. Recent
experience with this type of support system has shown it to be simple,
reliable and relatively cheap to design and fabricate. It is proposed that
the same type of support system be used for the transonic Series III model
test.

The Series II full-span complete aircraft model, would be a "flying"
model, rod-mounted in the Low Speed Tunnel. The rod is anchored to the floor
and ceiling of the tunnel and the model, through a ball bearing gimbal mount,
can travel up and down or rotate on the rod. The only degree-of-freedom
precluded is fore and aft. The horizontal tail of the model is remotely
controllable so the model can be flown. Roll control will be provided by
the ailerons. Recent experience using this type of support system has shown
that it is practical.

---

32. Bergmann, Gerald E., and Sevart, Francis D., "Design and Evaluation of
     Miniature Control Surface Actuation Systems for Aeroelastic Models,"
     Presented at the AIAA Dynamics Specialists Conference, Williamsburg, Va.,
     March 1973.

5.1.4.4 <u>Model Protection</u> - It is necessary to protect any flutter model during a test, by some means, to prevent destructive flutter. This protection becomes more important in this type of test because the oscillation of the aileron rather than being properly out-of-phase, could become syncronized and accelerate destructive flutter. A system, described in Figure 81, exists for the MCAIR Low Speed Tunnel that will count the cycles above a predetermined amplitude and when the predetermined number of cycles are counted it will automatically shut down the tunnel. The output from the wing is taken from several wing mounted strain gages.

The response time for tunnel conditions to change in the transonic regime, assuming tunnel shutdown such as in the Low Speed Tunnel, is too great to adequately protect the model from destruction. The system used in the Langley Transonic Tunnel is similar to the MCAIR Low Speed Tunnel except that dynamic pressure is changed rapidly by a change in static pressure. This is accomplished by opening a large line between the test section and a downstream section of the tunnel. Static pressure in the downstream section is higher than in the test section and will therefore bleed to the test section, causing a reduction in velocity and dynamic pressure.

5.1.5 <u>Test Plan Summary</u>

5.1.5.1 <u>Functional and Checkout Tests</u> - Prior to conducting wind tunnel tests on the flutter models, functional and checkout tests will be conducted. Aside from the usual instrumentation and data acquisition system checkout tests, the tests listed below will be performed:

    o <u>Ground Vibration Tests (GVT)</u> - These tests will serve to evaluate the validity of the scaled inertia and stiffness simulation on the model(s).

    o <u>Control Surface Actuation System</u> - This system refers to the components between the input command signal to the servo electronics and the output from the power actuator driving the surface shown in Figure 77. These tests will evaluate the scaled model simulation of the aircraft surface actuation system in addition to providing a functional checkout of the system.

    o <u>Active Flutter Control System</u> - This system refers to the feedback components between the model response sensor and the input command to the servo electronics shown in Figure 77. In addition to providing

Strain Gage Inputs

1

2

3

4

5

6

Bandpass Filter 5-300 Hz → Level Detector → BCD Counter → BCD to DEC Decoder → Latch

1. The input signals are filtered to allow only flutter modes of interest to pass.

2. The signals are then compared with a known adjustable level to see if the flutter signals exceed predetermined limits.

3. The BCD counter and BCD to decimal decoder select the number of times the input signal exceeds its limits. Normally the limit is exceeded 5 times before the output latch is set. Since flutter signals increase in amplitude with time, this circuitry eliminates signals in the flutter frequency range that are decreasing in amplitude with time such as those caused by buffeting.

4. The latches store which of the inputs exceeded their limit and provide a signal to a relay which is used to control some tunnel parameter to get the model out of the flutter region.

Relay Closure

FIGURE 81

DESCRIPTION OF AUTOMATIC WIND TUNNEL SHUTDOWN SYSTEM

a functional check of this system, these tests serve to evaluate the scaled model simulation of corresponding full scale aircraft components.

o Model Protection System - To minimize the chances of damaging the model during these tests, the model protection device described in Figure 81 has been included which will become activated if excessive response signals are picked up by appropriate sensors. Tests would be performed to insure functional operation of this system and to insure that activation levels have been properly set.

o Model/Tunnel Mounting Stability Checks - It will be necessary to determine the stability of the model/tunnel mounts before subjecting the flutter wings to tests. The method to determine stability will be to use a "rigid" wing, i.e., a wing designed to the correct weight and inertia, but not the flexibility characteristics. These wings would be used in a sufficient number of runs to adequately determine model/tunnel mount stability. The same basic approach would be used for both low speed and transonic models.

5.1.5.2 <u>Wind Tunnel Tests</u> - The wind tunnel test program has been formulated around a rationale based on the premise that each of the various potential problem elements should be investigated at the lowest level of sophistication commensurate with the ability to demonstrate that element. Consequently, the flutter model test program favors the building block approach so that the problem elements can be more easily isolated and treated before progressing to a higher level of sophistication. Table 15 reflects such a building block approach and indicates the test series where the various problem elements would be investigated.

In each of these, the passive flutter onset speeds will be established in addition to demonstrating active flutter suppression. The role of each of these test series is described in the following paragraphs.

o <u>Semispan/Subsonic Tests</u> - This series of tests will perform the following specific functions:

1. Develop and checkout "on-line" Nyquist plot generation using slow sinusoidal sweeps, co-quad type analyzers, and the flutter control system components.

TABLE 15
PROBLEM ELEMENTS TO BE INVESTIGATED WITH VARIOUS MODEL/TUNNEL CONFIGURATIONS

Series I Semispan/Subsonic	Series II Full Span/Subsonic	Series III Semispan/Transonic
• Control for Multiple Stores	• Fuselage Dynamics	• Flow Compressibility
• Cantilevered Modes	• Asymmetric Modes	• Transonic Phasing
• Symmetric Modes	• Asymmetric Incompressible Aerodynamics	• Gust Turbulence
• Anti-Symmetric Modes		
• Spoiler/Aileron		
• Nonlinearities		

2.   Verify the analytically developed flutter control system law
     using the on-line Nyquist display to adjust the electronic com-
     pensation components.

3.   Verify the "adaptability" of the proposed generalized flutter
     control law by tests with several different stores.

4.   Check the system for three separate modal sets; cantilevered,
     symmetric (root-pitch and translation), and anti-symmetric
     (root-roll).

5.   Establish the ability of a cycling aileron to control flutter
     in the presence of an upstream deflected spoiler.

6.   Verify the analytically predicted effects of control system non-
     linearities such as, rate saturation, hitting of stops, stalled
     actuators, freeplay, and deadspace.

o Full-Span/Subsonic Tests - This series of tests will perform the
following specific functions:

1.   Verify the controllability of flutter using two separate flutter
     control loops, one for each wing, based on the semispan/subsonic
     test results.

2.   Evaluate the effects of fuselage dynamics on the flutter control
     system for both symmetric and anti-symmetric motion.

3.   Evaluate the effects of asymmetric motion by loading each side
     of the model differently.

4.   Verify controllability in the presence of asymmetric aerodynamics
     created by static yaw angle and/or spoiler-aileron deflection
     combinations.

o Semispan/Transonic Tests - Transonic testing, which is necessary to
simulate airflow compressibility, could conceivably substitute for
all the low speed testing but at an extremely high level of complexity
and with the attendant increases in costs of testing. Because of
the small percentage of wind-on testing time in large transonic
tunnels (typically 8% in the Langley Transonic Dynamics), high model
acquisition and tunnel operating costs, and heavy test scheduling,
transonic testing should realistically be limited in scope to those
items which are not adequately assessed in the low speed tests. The
series of semispan transonic tests will evaluate the functional
effects of flow compressibility, namely the main surface and control

surface aerodynamic phase and gain changes with transonic Mach
number. This series of tests will perform the following specific
functions:

1. Determine the effects of flow compressibility at transonic Mach
   number on flutter control for several stores and root degrees-
   of-freedom to compare with similar subsonic data.

2. Investigate the effects of nonlinear aerodynamic phenomena
   using the spoiler and aileron in a manner similar to that used
   in the subsonic tests.

3. Verify the controllability in the presence of large gust turbu-
   lence levels.

o Full-Span/Transonic Tests - The final category of possible testing,
  a full-span transonic series, adds no new information except for a
  functional evaluation of compressibility effects jointly with
  asymmetric motion. At this point in time it is felt that the inherent
  complexity and attendant costs and risk of failure of such a test
  traded off against the limited amount of new information acquired does
  not justify its inclusion in the program. If such a test were to
  be included it could be expected to perform the following specific
  functions:

1. Evaluate the effects of flow compressibility jointly with asymme-
   tric motion for comparison with separate evaluations obtained from
   the full-span/subsonic and semispan/transonic tests.

2. Determine the significance of the aerodynamic interaction between
   the wing and tail surfaces in the transonic region to compare
   with similar results obtained in the full-span/subsonic tests.
   This effect should be negligible.

3. Determine the significance of changes in fuselage dynamics
   resulting from the transonic changes on the empennage to compare
   with similar results obtained with the fuselage dynamic mode
   variation runs in the full-span/subsonic tests. This effect should
   be negligible.

4. Verify controllability in the presence of different Mach effects
   on each side of the aircraft to compare with similar unbalanced
   aerodynamic evaluations obtained in the full-span/subsonic tests.
   The subsonic test variations should be diverse and broad enough
   to encompass these unbalanced effects.

5.1.6 Test Procedures and Data Processing - The aileron control sur-
faces will be used as the aerodynamic force producers for the flutter control
function. Excitation signals will also be input to the servoaeroelastic
system through these same control surfaces. Several types of input signal
and response data reduction techniques, described below, will be employed
during the tests.

5.1.6.1 Linear Frequency Sweep Input - The signal generator shown in
Figure 77 will be used to generate a constant sweep rate sinusoidal input to
the system. Exploratory runs will be made early in the Series I semispan
tests to determine the most suitable sweep rates, amplitudes, and range of
frequencies for this input. The majority of the testing will be performed
with this form of signal input. Tests will be performed with the flutter
control loop both open and closed at sub-flutter velocities and with the
control loop closed at post-flutter velocities.

Data will be available at and between various points in the control loop
as indicated symbolically in Figure 77. The figure indicates three separate
data displays which will be available for on-line, real-time data analysis.
These data displays are the Nyquist plots on an oscilloscope, co-quad plots
of the real and imaginary components of a selected response versus frequency
on an x-y plotter, and frequency response plots of the amplitude and phase
of a selected response versus frequency, also on an x-y plotter.

The frequency and damping of the resonant modes of the aeroelastic
model, as well as selected transfer function data for control loop elements,
will be determined primarily from the co-quad and frequency response plots.
The Nyquist oscilloscope display will be used principally to facilitate the
manual evaluation and/or adjustment of the variable compensation elements
in the flutter control loop at both sub-flutter and post-flutter velocities.

Response data from selected open and closed loop tests will also be
recorded on tape for subsequent off-line data analysis by the fast Fourier
transform and the flutter control adjustment algorithm using digital proce-
dures. These results will be compared with the manual interpretations and
decisions based on the same data using the on-line real-time Nyquist displays.

5.1.6.2 Tuned Sinusoidal Input - The signal generator will also be
used to generate constant frequency sinusoidal inputs at the significant aero-
elastic mode frequencies. The tuned frequencies to be tested will be deter-
mined from previously generated frequency response and co-quad data. The
abrupt removal of the tuned frequency steady state excitation provides decay
envelopes on the oscillograph traces, as called out in Figure 77. Damping

152

values will be obtained, based on the logrithmic decrement of the oscillo-
graph traces, for comparison with the co-quad and frequency response damping
estimates. Tests with this tuned input will be performed with the flutter
control loop both open and closed at sub-flutter velocities and with the
control loop closed at post-flutter velocities.

5.1.7 Optional Oscillatory Aerodynamics Model Test - Analytical predic-
tion of oscillatory aerodynamic data due to trailing edge control surface
rotation is not too reliable and subject to many uncertainties. The prediction
of these coefficients, in particular the phase characteristics, is especially
difficult in the transonic region for the relatively high frequency modes of
flutter. As much as 20 to 40 degrees of phase lag may occur in the frequency
range of interest transonically, and dependable verified theoretical data
is not available.

The functional tests, Series I, II and III make no attempt to measure
the oscillatory aerodynamic coefficients. The adaptive control concept
circumvents the need for oscillatory aerodynamic data by the use of frequency
response testing of the complete open or closed loop dynamic system. It is
anticipated that these Series IV tests will be required only in the event
that the functional tests fail to produce results which would justify proceeding
to the flight test phase.

5.1.7.1 Test Objectives - This series of tests is designed to generate
oscillatory aerodynamic data resulting from the control surface rotation which
may supplement and explain the functional data generated in the other tests.
The objectives of the test are to define,

o chordwise pressure distributions

o wing section force and pitching moment coefficients

o hinge moment coefficients

These items are required as a function of the reference excitation for para-
metric variations of Mach number, mean angles, oscillation amplitude and
reduced frequency.

5.1.7.2 Test Facilities - The NASA Langley Transonic Dynamics Tunnel
will be used for these tests.

5.1.7.3 Model Description -

o Scaling and Geometry - The model size and geometry will be identical
   with the semispan wing used in the Series III servoaeroelastic tests.
   The wing, however, will be rigid and will be rigidly mounted from

the tunnel wall. A root-fence shall be incorporated to minimize the effects of the tunnel wall boundary layer. Provisions shall be incorporated for oscillating the aileron up to $\pm 5°$ over a frequency range of 5 to 25 Hz. The model shall be sufficiently rigid to insure the lowest elastic mode frequency is at least 50 Hz to minimize uncertainties in interpretation of the test results.

o Instrumentation - The principal instrumentation will consist of **pressure transducers, strain gages and position transducers.**

Pressure transducers will be installed in the model in a distributed chordwise sense for at least 4 separate spanwise locations. The locations will be chosen, consistent with the practical installation limit on the maximum number of transducers, to emphasize the region in the vicinity of the control surface. These transducers should be of the differential pressure type with minimum variation of sensitivity and minimum phase shift for frequencies up to 100 Hz. They shall be mounted flush with the wing surface. Since it is not feasible to build a completely "rigid" wing model, the pressure transducers shall also be selected to have **minimum sensitivity to acceleration.** (Kulite pressure transducers are essentially insensitive to acceleration.)

Strain gages will be included to measure the control surface hinge moments and to monitor loads at selected points on the wing surface.

A position transducer will be installed to sense control surface rotation. A strain-gaged soft flexible link may be used for this purpose.

o Actuation - The actuator for the control surface will be the same design as used for the Series III model. The control surface weight and inertia characteristics will be specified to allow for the use of this actuator design.

5.1.7.4 Test Procedure - The model, **as mounted in the tunnel, shall be** given a brief ground vibration test to insure that the lowest elastic mode frequency is considerably above the highest aileron oscillation frequency to be employed in these tests.

At each test condition - Mach number, mean aileron position, and aileron oscillation amplitude - the aileron oscillation frequency shall be varied to cover the desired range of reduced frequencies. Time histories of the aileron oscillatory motion, aileron hinge moment, and surface pressures shall be recorded on tape for subsequent processing. The wing strain gages should be monitored during the run to insure that the design loads are not being exceeded.

5.1.7.5 Data Processing - The taped data shall be processed through tracking filters into a co-quad analyzer to yield the real and imaginary components of aileron hinge moment and surface pressures per unit aileron rotation, as a function of frequency. The aerodynamic hinge moment acting on the aileron shall be obtained by subtracting the aileron **inertia** effect from the measured hinge moment.

The real and imaginary pressure distributions shall be integrated over the chords to obtain sectional lift, moment, and aileron hinge moment.

5.2 Full Scale Ground Testing

Ground testing of the Flutter Control System (FCS) shall be performed: to obtain design data; for control development; for system integration; and for flight worthiness testing. Sufficient testing shall be accomplished to select the best configurations and to assure the flight worthiness of the aircraft.

5.2.1 Test Objectives - The overall objectives of the ground test program are:

- o Assist in control development through flight worthiness testing of components by their suppliers.
- o Assure component compatibility, systems integration and functional operation by performing open loop testing using flight control system development fixtures.
- o Assure the flight worthiness of the aircraft by conducting static proof tests and Ground Vibration Tests (GVT) of structural and control actuation mechanism modifications made to the aircraft.

5.2.2 Iron Bird Flight Control System Tests - FCS testing of the Iron Bird shall include system integration (open loop) testing. The open loop testing shall consist of the following:

- o Component Evaluation
- o Component Compatibility
- o Functional Operation

5.2.2.1 Iron Bird Modifications - The testing described above will require an Iron Bird incorporating the FCS configuration. Incorporation of FCS actuators for the ailerons and their attendant hydraulic, mechanical, and electronic control systems are the major items. In addition, FCS affiliated instrumentation and loading systems will be required.

5.2.2.2 Open Loop Testing - Open loop testing will be conducted in the following areas:

o Component Evaluation Testing - Major FCS components shall be given leakage and functional tests, including dynamic performance, prior to installation on the FCS Iron Bird. These components will include the following:

Actuator(s)

FCS Avionic Components

o Component Compatibility Testing - Instrumentation parameters shall include pressures, surface position, actuator loads, and voltages.

Hydraulic Power System(s) Surge Pressure Test - Hydraulic pressure characteristics shall be investigated with ailerons cycling at various amplitudes and frequencies up to design maximum. This test will determine the needed and required parameters for surge suppressors with the FCS actuator performance requirements. The surge levels in branch circuits shall also be investigated.

Iron Bird FCS Operation Test - The system shall be operated in all modes, including emergency modes. All surfaces shall be cycled by the controls to assure proper control in each mode. Continuity and phasing shall be verified.

BIT - The FCS electronics set shall be subjected to a Built-In-Test (BIT) check. An effort shall be made to assure that the GO and NO-GO indications are associated with operational and failed equipment respectively.

Dynamic Testing - The actuation systems shall be tested to define response thresholds, actuators loop stability and small and large amplitude frequency responses. In addition, the resonant frequency of the aileron loop shall be determined for both one and two actuator hydraulic systems in operation. Both left and right aileron systems shall be tested individually and collectively.

o Functional Tests - Overall FCS system operation shall be evaluated
   with emphasis on static gains and maximum travel rates for each
   aileron and failure mode switching transients. Preflight startup and
   checkout procedures shall also be verified.

5.2.3 Ground Vibration Tests - A ground vibration test (GVT) shall be
performed on the FCS airplane with revised equipment and structure installed
to substantiate the dynamic data employed in the theoretical passive and
active flutter calculations. If significant differences are noted, the
experimental data shall be incorporated in revised calculations.

5.2.3.1 Test Configuration - The airplane shall be supported on a soft
suspension system (rigid body frequencies on the order of 0.5 Hz) with the
landing gear in its retracted position. Tests shall be conducted both with
normal control system power and with emergency power. For this GVT the gain
of the FCS feedback shall be set equal to zero. The airplane shall be con-
figured in each of the external stores configurations that will subsequently
be flight tested.

5.2.3.2 Test Descriptions - **Freeplay tests on both LH and RH ailerons**
shall be conducted by applying external static loads to the aileron in both
up and down directions and measuring the resulting aileron rotation deflec-
tions relative to the wing. Data taken during these tests shall also be used
to determine the structural stiffness of the aileron actuator system. Flight
worthiness of the FCS shall be demonstrated by static proof tests of the
control surfaces and actuation mechanisms.

Vibration tests shall be conducted to determine all the important modes-
of-influence for active flutter control. Both symmetric and anti-symmetric
excitation shall be applied. A frequency response survey shall be conducted
over the frequency range necessary to cover all the important modes. Excita-
tion at each of the natural frequencies determined from the response tests
shall be applied and the corresponding mode shapes shall be mapped, including
the store deflections. Damping shall be determined from decay records at
each of the natural frequencies.

5.2.4 Installed Equipment Tests on the Aircraft

5.2.4.1 Installation Checkout - Installation checkout will be performed
on the following components:

o Mechanical Components - Rigging and checkout tests of all new or
   modified control surface linkage and actuators shall be performed
   prior to flight.

157

o Electronics Set - The following checkout will be conducted:

Wiring Ringout - A complete ringout shall be performed on the wiring used for the FCS electronics set. This ringout will be performed after incorporation of all wiring changes in the aircraft and before installation of the equipment.

Power Test - A power test shall be made prior to installation to insure that the proper power is run to the correct points in the system to prevent equipment damage.

Phasing Test - After installation of all the units in the aircraft, a phasing check from each sensor to its corresponding surface shall be made.

Operational Test - Each system input shall be operated to verify that all system functions are operational. In Flight Monitor (IFM) will be used to show any faults.

BIT - Built-In-Test (BIT) shall be run to show proper system operation.

Additional Functions - Any functions not tested by BIT shall be verified using Ground Support Equipment.

5.2.4.2 System Response Tests - Small-amplitude closed loop tests shall be run to verify the proper system response prior to first flight.

5.3 Flight Testing

5.3.1 Test Objectives - The objectives of the active flutter control flight test program are to:

o Demonstrate the ability to suppress wing/store flutter through the use of active flutter control techniques.

o Demonstrate that the active flutter control system can adapt to different wing/store configurations.

o Demonstrate the compatibility of the active flutter control system with the other aircraft flight control systems.

o Provide data for comparison with analytical predictions.

5.3.2 Test Configurations - The basic fighter/attack aircraft on which demonstration is to be made will be modified to incorporate the active flutter control system. Three external wing/store configurations will be chosen for

158

demonstration. The stores should have widely differing inertia characteristics. One of these stores will be selected for extensive flight demonstration; the other two stores shall be limited to an abbreviated flight program, sufficient only to demonstrate that the active flutter control system has the capability to adapt to various store configurations.

5.3.3 <u>Flight Test Conditions</u> - The ability to suppress flutter by active control techniques shall be demonstrated by a high altitude and low altitude flight penetration into the flutter region as shown in Figure 82. Penetration will be sufficient to clearly demonstrate that flutter can be suppressed by the active flutter control system. The exact altitudes and test point distribution will depend on the specific aircraft/store configuration chosen for flight demonstration.

5.3.4 <u>Test Procedure and Sequence</u> - A schematic of the flutter control system for flight test is shown in Figure 83. For these tests it will be possible to immobilize the flutter control system by preventing the feedback to the aileron actuating system. This is indicated in Figure 83 by the switch in the feedback circuit. This, in effect, allows the flutter control system to determine the gain and phase compensation requirements, but provides the option of whether or not to implement that requirement. For subsequent discussion, in Figure 83, ϵ is the dither signal, a sinusoidal sweep input excitation, δ_T is the input signal to the servo actuator, δ is the aileron power actuator output, α is the airframe response, α_F is the filtered airframe response, and δ_C is the required feedback modification to the aileron control system to suppress flutter.

The test phases for executing this program are given below:

o Pilot Familiarization and System Checkout

o Demonstration of Active Flutter Control

o Demonstration of Compatibility With Other Aircraft Flight Control Systems

o Tests in Atmospheric Turbulence

o Tests with Other Stores

5.3.4.1 <u>Pilot Familiarization and System Checkout</u> - The first few flights will be devoted to pilot familiarization and system checkout. These flights, with and without external stores, will be flown with the feedback switch open so that the active flutter control feedback command δ_C will be prevented from affecting the normal aileron operation. This decoupling procedure accomplishes two objectives. First, it permits pilot familiarization with any
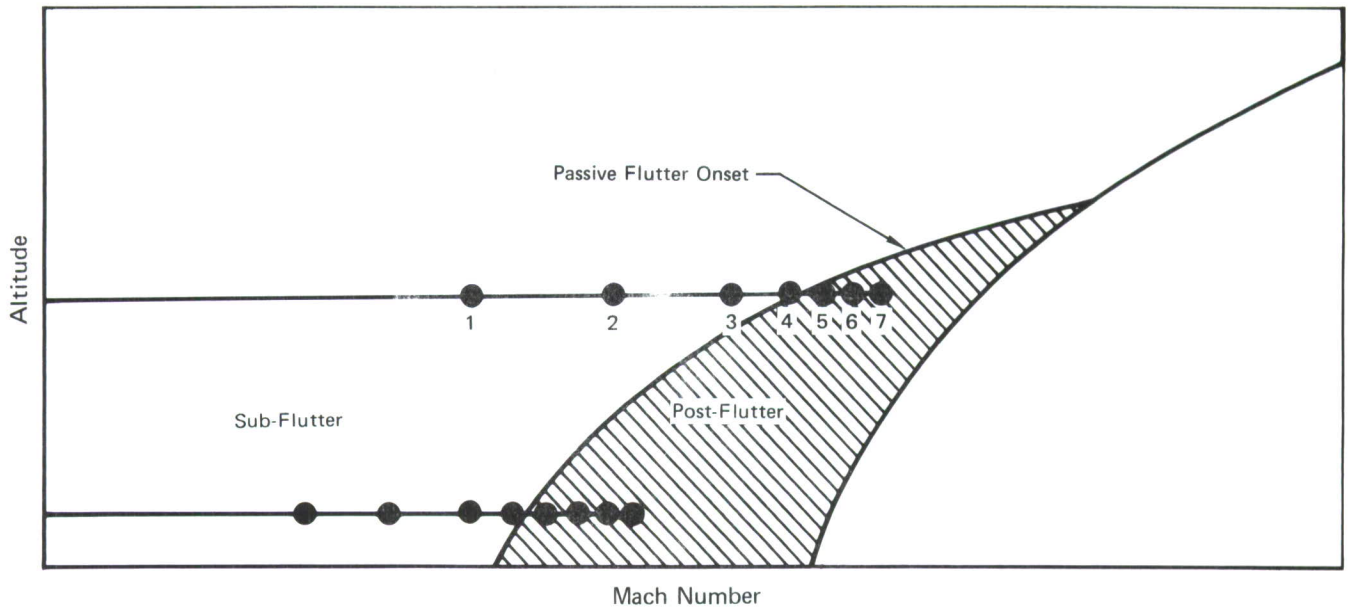
FIGURE 82
ILLUSTRATION OF FLIGHT TEST CONDITIONS
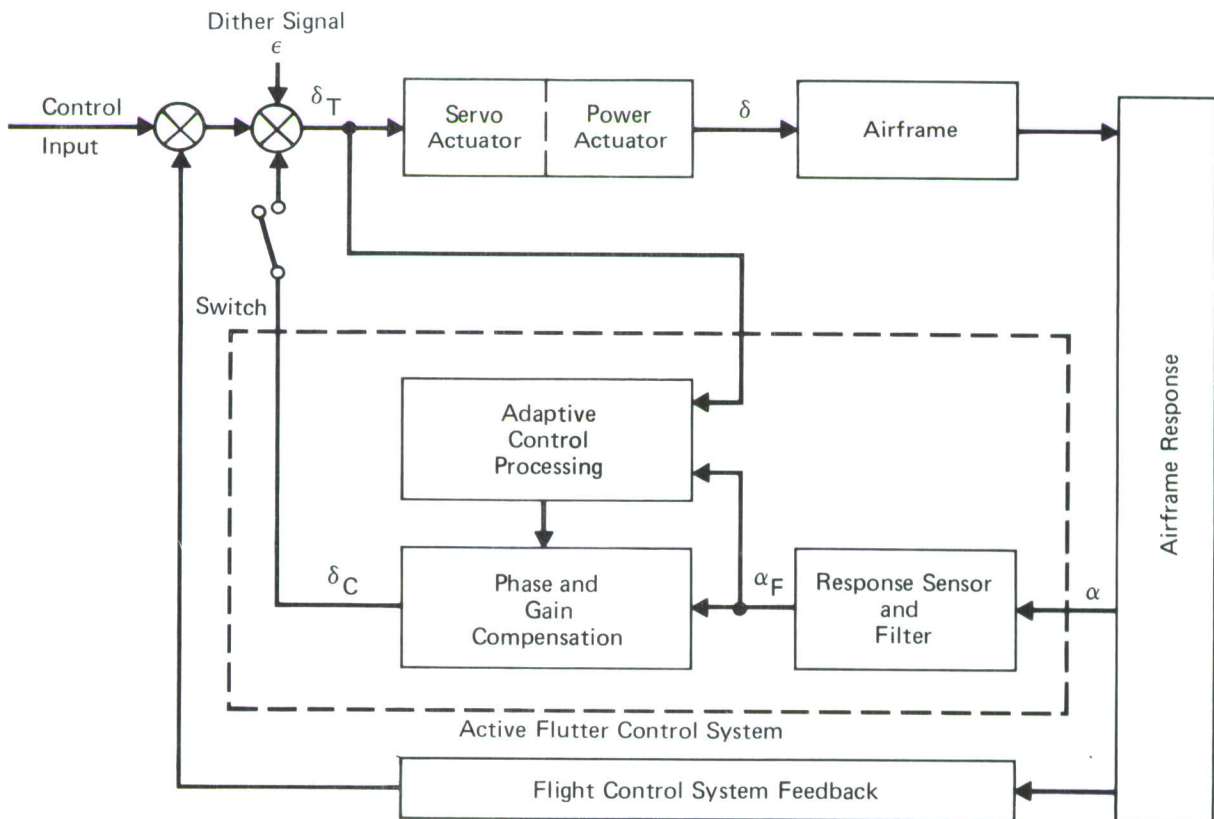
FIGURE 83
SCHEMATIC OF FLUTTER CONTROL SYSTEM FOR FLIGHT TEST

160

changes to the handling qualities that might have resulted from modifications made to the servo actuator/power actuator/aileron. Secondly, it permits functional checks to be made of the active flutter control network while it is trying to perform its functional role, but with the safety feature that any control commands would not be implemented during these initial checkouts. All such flights will be conducted in the sub-flutter region.

5.3.4.2 <u>Demonstration of Active Flutter Control</u> - These flights will be made during periods of minimal atmospheric turbulence. One of the three external store configurations will be selected for this test series. The first test point (Point 1, Figure 82) will be approached with the feedback switch open. After stabilizing at the test conditions, the aircraft will be excited both symmetrically and **anti-symmetrically, with a frequency sweep** sinusoidal input dither signal. Data of primary significance for these tests are α_F, δ_C, and δ_T; the transfer functions α_F/δ_T and δ_C/δ_T formed from these; and the Nyquist plots of α_F/δ_T and δ_C/δ_T. The latter two correspond to the open loop stability plots with and without compensation. They will serve as the primary means for monitoring and controlling the test program progress. Comparison of the on-line Nyquist plots of δ_C/δ_T with that of α_F/δ_T will establish whether or not the active flutter control system is calling for the proper gain and phase compensation. If comparison indicates a stable feedback, the switch will be closed completing the feedback circuit. The excitation will be repeated and Nyquist plots will be obtained for the closed loop system. A qualitative check will then be made of the aircraft handling qualities by executing minor maneuvers with full feedback implementation. Documentation of the stability improvement will be established from the aircraft response transfer function α/δ_T with and without feedback implementation by comparing the corresponding modal dampings in the critical modes as described by Figure 84. These data will also be used to establish the passive flutter onset speed. Other aircraft response sensors, such as wing and store accelerometers or wing root bending/torsion strain gages, may be used to establish the aircraft response transfer functions and dampings.

After a satisfactory demonstration for the first test point, the feedback switch will be in the open position while proceeding to the next test point where the above procedure would be repeated. The test will proceed in this manner up to the highest sub-flutter test point which will be established from the open loop damping data (the solid curves in Figure 84).
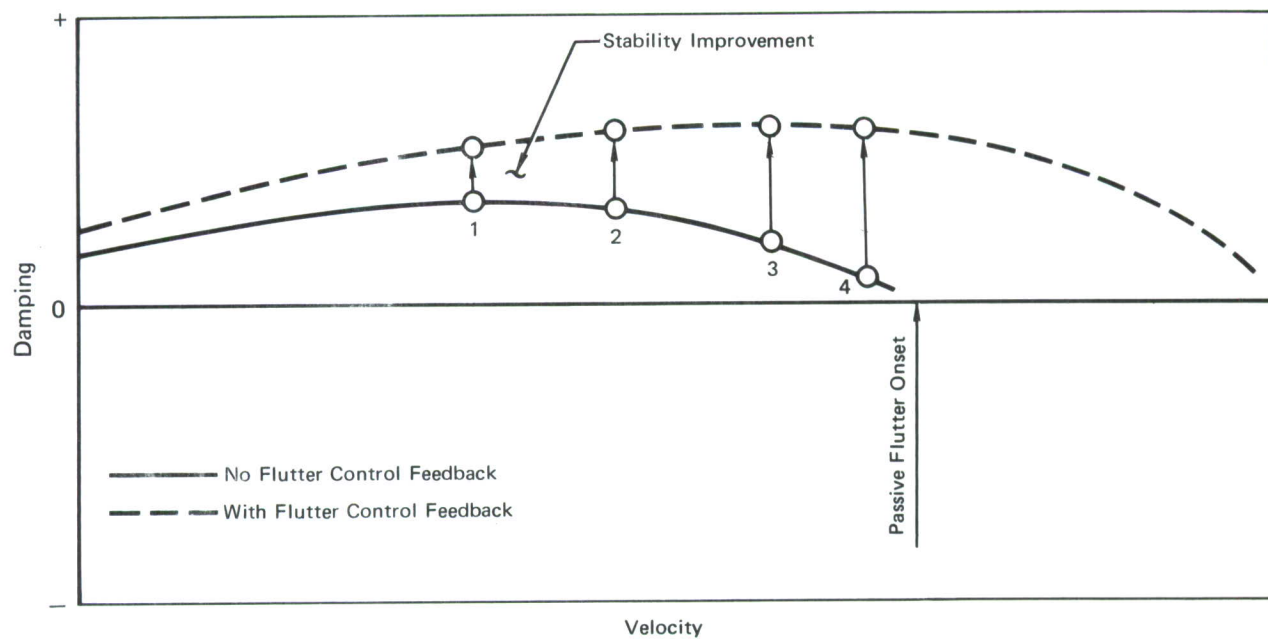
FIGURE 84
DESCRIPTION OF STABILITY IMPROVEMENT DURING SUB-FLUTTER FLIGHT TESTS

162

For flight testing in the flutter region the feedback switch must remain in the closed position. The Nyquist plots of α_F/δ_T and δ_C/δ_T will be monitored to insure that stable compensation is being applied. Because the active flutter control system requires a finite time to conduct the sweep and make the necessary compensation adjustments, all speed increases will be made gradually. Upon stabilizing at a test point condition, Nyquist plots of α_F/δ_T and δ_C/δ_T will be recorded along with the airframe response data for evaluating modal damping in the critical modes.

The procedure described above will be carried out for both the high and low altitude demonstrations of active flutter control.

An investigation will be conducted to determine the rapidity with which the active flutter control system can adapt to changing flight conditions since the adaptive feature of the flutter control system requires a finite time for implementation of the proper feedback compensation. This may be accomplished with level flight accelerations by incrementing from gradual accelerations to rapid accelerations and monitoring the aircraft response parameters. The maximum safe acceleration will be evaluated against the maximum performance capability of the aircraft. A similar evaluation will be made with level flight deceleration.

5.3.4.3 <u>Demonstration of Compatibility with Other Aircraft Flight Control Systems</u> - With the active flutter control loop closed, flight demonstrations will be conducted to show compatibility with other aircraft flight control systems. Satisfactory demonstration will be proven at the sub-flutter speeds before progressing into the flutter region. Compatibility will be demonstrated by maneuvering flight building up to high roll rates and high angles of attack approaching the buffet boundary. Compatibility in the landing configuration at approach speed will also be demonstrated.

5.3.4.4 <u>Tests in Atmospheric Turbulence</u> - Flight tests will be made to investigate the effect of atmospheric turbulence on the performance of the active flutter control system. Flights into mild turbulence will be sufficiently investigated before progressing to higher turbulence levels, and the sub-flutter region will be investigated before penetrating into the flutter region. Since turbulence tends to distort the Nyquist stability plots on which the feedback compensation is based, the Nyquist plots will be closely monitored during these tests. In addition, actuator rod-end load will be recorded and monitored (for fatigue considerations) along with aileron position and rate (for saturation and hydraulic power requirements).

5.3.4.5 <u>Tests with Other Stores</u> - After fully investigating active flutter control with the primary store configuration, flight tests will be performed with the other two store configurations to investigate the capability of the control system to automatically adapt to other stores with different inertia characteristics. These tests will be the minimum necessary to evaluate the ability to adapt to the variation in wing/store dynamics.

5.3.5 <u>Data Acquisition and Handling</u> - All of the quantities listed in paragraph 5.3.5.1 below will be measured and stored on an on-board tape recorder for post-flight evaluation and as a permanent record of the flight test data. The quantities marked with an asterisk will be telemetered to the ground station for real-time flight monitoring and control.

5.3.5.1 <u>Measured Parameters</u> - The following quantities will be measured and recorded:

o <u>General Flight Parameters</u>:

1) Altitude

2) Airspeed

3) Mach number

4) Free air temperature

5) Aircraft angle of attack

6) Normal acceleration at C.G.

7) Pitch rate

8) Roll rate

9) Yaw rate

10) Fuel quantity

*11) Rapid response angle of attack (turbulence indication)

*12) Pilot voice, event marker

o <u>Flutter Control System Parameters</u>:

*1) Dither signal excitation, ε, including excitation frequency

*2) Command signal to the servo actuator, δ_T

*3) Filtered airframe response, α_F

*4) Flutter control feedback, δ_C

*5) Active flutter control airframe response signal, α

*6) Compensation gain and phase

o <u>Lateral Control System Parameters</u>:

*1) Aileron position and rate

*2) Aileron actuator position, δ, and rate

*3) Aileron actuator rod-end load

164

o Aeroelastic Response Parameters:

*1) Wing tip angular acceleration

*2) Store nose vertical and lateral acceleration

*3) Wing root bending strain

*4) Wing root torsion strain

o Hydraulic System Parameters:

*1) Hydraulic system reservoir fluid temperatures (primary control systems and utility).

*2) Hydraulic system pressure upstream of the aileron actuator

5.3.5.2 Data Handling, Processing, and Reduction - The ground station equipment will include:

o Strip chart recorders

o High speed digital computer

o Cathode ray tube displays

o Transmissibility plotter (magnitude and phase vs frequency)

o Nyquist plotter (polar vs frequency)

The strip chart recorders will provide time history records of selected parameters. Switching provisions will be available for changing the parameters to be monitored. The ground based high speed digital computer will be programmed to compute transfer functions (such as α_F/δ_T and δ_C/δ_T in paragraph 5.3.4.2) and process these so that the output can be used to generate open loop Nyquist stability plots (δ_C/δ_T), aeroelastic response Nyquist plots (α_F/δ_T), or aeroelastic response transmissibility plots (magnitude and phase versus frequency). The computer will also be programmed to extract from this data the aeroelastic modal frequencies and corresponding dampings. The computer output will be fed into a cathode ray tube to display the open loop Nyquist plots, the aeroelastic Nyquist plots, the aeroelastic transmissibility plots, or modal frequencies and dampings. Hard-copy of the Nyquist and transmissibility information shall be provided by feeding the computer output to Nyquist and transmissibility plotters at the ground station. These plotters may not be required if hard-copy output capability is provided in conjunction with cathode ray tube displays. Flexibility will be provided in the input to the cathode ray tube so that Lissajou figures for any two input signals may be presented.

This data handling and processing will be compatible for real-time processing of the telemetered data or for post-flight processing of the on-board tape recorded data.

The overall cost of developing an active flutter control system for flight test demonstration can be reduced significantly if the airborne computer could be eliminated and its function performed by a ground **based computer** instead. The airborne computer, shown as the "adaptive control processing" block in Figure 84, processes the signals δ_T and α_F to determine the required phase and gain compensation. These data are then introduced into the "phase and gain compensation" block to complete the flutter control feedback loop.

As an alternate to this, signals for δ_T and α_F would be telemetered to a general purpose ground based computer using the same algorithms as that which would have been used with the airborne computer. The output from the ground based computer would be the required phase and gain compensation. This information would be relayed by radio to the pilot who would then **manually adjust** these gain and phase compensations to complete the flutter control feedback loop.

6. CONCLUSIONS AND RECOMMENDATIONS

The most significant results obtained in these studies for this aircraft are:

1. The use of three-dimensional aerodynamic theories results in a decrease on the order of 40% in the required control loop gain compared with previous strip theory analyses. There is a corresponding reduction in the performance demands on the hydraulic system and an improvement in the coupling with other flight control systems.

2. Flutter control with acceptable stability margins is predicted by the three-dimensional theories for flight throughout the entire velocity-altitude envelope.

3. Flutter control is predicted for loadings both with and without symmetry provided each side of the aircraft is treated independently.

4. Continuity of control is predicted with aileron rate limits as low as 100 deg/sec in Dryden gusts up to 13.38 fps RMS at altitudes of 500 ft or more. Corresponding discrete gust analyses show continuity of control for (1-cos) gusts as large as 30 fps.

5. An adaptive (pilot-out-of-the-loop) flutter control system, based on a digital evaluation of interrogated aircraft response data, yields the expected compensation for flutter control in a relatively calm environment. Acceptable predictions also appear possible in the more difficult turbulent environment for random gusts as large as 6 fps RMS using input excitation on the order of 1 deg RMS provided digital smoothing is used.

6. Hydraulic system, flight control system and structural modifications required for the implementation of an operational wing/store flutter control system for relatively mild flutter modes with frequencies up to 20 Hz on both contemporary and future fighter attack aircraft appear feasible. Specific modifications, based on F-4 data, are practical and easily implemented.

7. Sensors and electronic components are available either off-the-shelf or are easily assembled to satisfy the flutter control system requirements and to ensure safety of flight for a one-fail-operate system

with a failure rate of less than one catastrophic failure per million flight hours. A triplex system with practical components would have approximately 131 lb directly attributable to the flutter control system.

8. The elimination of wing/store flutter placards permits increased performance while maintaining attractive mission features. Survivability improvements on the order of 25 to 50 percent are predicted.

It is recommended, based on these results, that effort be directed toward the upgrading of active flutter prevention technology through a systematic research and development program covering analyses, ground tests on selected hardware, wind tunnel aeroelastic – control system model tests and flight test evaluations and demonstrations. Detailed attention should be given to transonic and supersonic aerodynamic effects, nonlinear control system effects, reliability, redundancy, safety, gust response and system saturation.

REFERENCES

1. Barkey, H. D., "Evolution of the F-4 Phantom," MCAIR 71-017, Presented at the Technical Program Management Seminar of the American Institute of Industrial Engineers, 19-21 April 1971.

2. Triplett, William, E., "A Feasibility Study of Active Wing/Store Flutter Control," Journal of Aircraft, Vol. 9, No. 6, June 1972.

3. Triplett, William E., Kappus, Hans-Peter F., and Landy, Robert J., "Active Flutter Control - An Adaptable Application to Wing/Store Flutter," Journal of Aircraft, Vol. 10, No. 11, November 1973.

4. Triplett, William E., Kappus, Hans-Peter F., and Landy, Robert J., "Active Flutter Suppression Systems for Military Aircraft, A Feasibility Study," AFFDL-TR-72-116, February 1973.

5. Air Force Contract F33615-73-C-3063, "Statement of Work," dated 26 February 1973.

6. Burkhart, T. H., Gongloff, H. R., Volker, R. E., "Model F-4E (Slat) Aircraft Wing Flutter and Divergence Analysis," McDonnell Aircraft Co. Report MDC A1639, May 1972.

7. Triplett, William E., "Computer Programs for the Frequency Response Stability Evaluations of Servoaeroelastic Systems," McDonnell Aircraft Co. Report MDC A2888, May 1974.

8. Giesing, J. P., Kalman, T. P., Rodden, W. P., "Subsonic Unsteady Aerodynamics for General Configurations, Volumes I and II," AFFDL-TR-71-5, November 1971.

9. Donato, Vincent W., and Huhn, Charles, R., "Supersonic Unsteady Aerodynamics for Wings with Trailing Edge Control Surfaces and Folded Tips," AFFDL-TR-68-30, January 1968.

10. Landy, Robert J.,"Computer Program for Time Response, Fast Fourier Transform, and Adaptive Flutter Control Algorithm Calculations for Servoaeroelastic Systems," McDonnell Aircraft Co. Report, MDC A2889, May 1974.

11. Kisslinger, R. L., Vetsch, G. J., "Survivable Flight Control System Interim Report No. 1 - Studies, Analyses and Approach," AFFDL-TR-71-20, Supplement 2, May 1971.

12. Katz, Henry, "Flutter of Aircraft with External Stores," Presented at the Aircraft/Stores Compatibility Symposium, November 1969.

13. Chalk, C. R., et al, "Background Information and User Guide for MIL-F-8785B (ASG) Military Specification - Flying Qualities of Piloted Airplanes," AFFDL-TR-69-72, August 1969.

14. Magdaleno, Raymond and Wolkovitch, Julian, "Performance Criteria for Linear Constant-Coefficient Systems with Random Inputs," Systems Technology Inc., ASD-TDR-62-470, January 1963.

15. Jones, J. W., et al, "Low Altitude Atmospheric Turbulence - Lo-Locat Phase III," Volume I, Part 1 Data Analysis, AFFDL-TR-70-10, November 1970.

16. Pritchard, Francis, E., "The Turbulence and Terrain Environments Affecting Low-Altitude, High-Speed Flight," FDM No. 393, Cornell Aeronautical Laboratory, Inc., Buffalo, New York, July 1966.

17. Dempster, J. B. and Bell, C. A., "Summary of Flight Load Environmental Data Taken on B-52 Fleet Aircraft," Journal of Aircraft, Vol. 2, No. 5, September-October 1965.

18. Notess, C. B. "The Effects of Atmospheric Turbulence Upon Flight at Low Altitude and High Speed," FDM No. 325, Cornell Aeronautical Laboratory, Buffalo, New York, October 1961.

19. Zbrozek, J. K., "The Relationship Between the Discrete Gust and Power Spectra Representations of Atmospheric Turbulence, with a Suggested Model of Low-Altitude Turbulence,"Aeronautical Research Council (England), R and M No. 3216, 1961.

20. Price, C. F. and Koenigsberg, W. D., "Adaptive Control and Guidance for Tactical Missiles," Vols I and II, the Analytic Science Corp., Reading, Mass., TR-170-1, June 1970.

21. Smyth, R. K. and Ehlers, H. L., "Survey of Adaptive Control Applications to Aerospace Vehicles," AGARD Conference on Advanced Control System Concepts, Oslo, Norway, September 1968 (AGARD C. P. No. 58 - August 1970).

22. Mendel, J. M., "Survey of Learning Control Systems for Space Vehicle Applications," 1966 JACC Proceedings, Vol. 7, Seattle, Washington, 1966.

23. Blakelock, J. H., "Automatic Control of Aircraft and Missile," John Wiley & Sons, Inc., 1965.

24. Turner, M. R., Elkins, J. A., "Digital Analysis of Flight Flutter Tests," BAC Report GEN/B745-4/7893, May 1969.

25. Baldock, J. C. A. and Skingle, C. W., "Flutter Technology in the United Kingdom - A Survey," AIAA Dynamics Specialists Conference, Williamsburg, Va., March 1973.

26. Dat, R., "The Theoretical and Experimental Methods Used in France for Flutter Prediction," AIAA Dynamics Specialists Conference, Williamsburg, Va., March 1973.

27. MCAIR Hit Density Model, Unpublished Internal Computer Model.

28. Ahrens, Roger A., Nadler, Gerald and Zust, Eric L., "Survivability Assessment Guidelines for Flight Control Systems," AFFDL-TR-74-39, Vol. I, to be published.

29. Epstein, C. S., "Supersonic Delivery of Conventional Weapons - Fact or Fancy?," Presented at the Aircraft/Stores Compatibility Symposium, December 1971.

30. Talbot, J. F., "Conformal Carriage Concept," Presented at the Aircraft/ Stores Compatibility Symposium, November 1969.

31. Nichols, J. H. and Martin, C. J., "Conformal Weapons Carriage - Joint Service Development Program," Presented at the Aircraft/Stores Compatibility Symposium, December 1971.

32. Bergmann, Gerald E., and Sevart, Francis D., "Design and Evaluation of Miniature Control Surface Actuation Systems for Aeroelastic Models," Presented at the AIAA Dynamics Specialist Conference, Williamsburg, Va., March 1973.

LIST OF ABBREVIATIONS, ACRONYMS, AND SYMBOLS

Abbreviations and Acronyms

A/B	Afterburner
A/C	Aircraft
A/D	Analog to Digital
AC	Alternating Current
ACF	Active Control of Flutter Computer Program
BIT	Built-In-Test
CAS	Control Augmentation System
CCW	Counter-Clockwise
CP	Center of Pressure
CVU	Computer Voting Unit
CW	Clockwise
D/A	Digital to Analog
dB	Decibels = $20 \log_{10}$ (Amplitude Ratio)
DC	Direct Current
DFT	Discrete Fourier Transform
EH	Electro-Hydraulic
EO	Electro-Optical
FBW	Fly-By-Wire
FCS	Flutter Control System
FFT	Fast Fourier Transform
FLTR	Flutter Time Response Computer Program
fps	ft/sec
gpm	gal/min
GVT	Ground Vibration Test
HARM	IBM Fast Fourier Transform Subroutine
HM	Hinge Moment
Hz	Hertz - cycles/sec
IFM	In Flight Monitor
KEAS	Knots Equivalent Air Speed = $V \sqrt{\rho/\rho_{SL}}$
LH	Left Hand
LO-LOCAT	Low-Low Altitude Critical Atmosphere Turbulence
MATLOC	Root Locus Computer Program

172

MCV	Main Control Valve
PC1, PC2	Hydraulic Power Control Systems One and Two - F-4
PSD	Power Spectral Density
PSF	lb/ft^2
PSI	lb/in^2
RH	Right Hand
RMS	Root Mean Square
SAS	Stability Augmentation System
SCM	Signal Conversion Mechanism
SFCS	Survivable Flight Control System
SL	Sea Level
SLD	Survivability Logic Diagram
3D	Three-Dimensional

Symbols

A, A_c	Noncirculatory and circulatory aerodynamic stiffness derivative matrices used in the Indicial Lift flutter equations
A	Actuator area - in^2
A_1, A_2	Scalar Coefficients in Wagner function
a	Actuator amplitude - in
a	Aircraft yaw acceleration - rad/sec^2
B, B_c	Noncirculatory and circulatory aerodynamic damping derivative matrices used in the Indicial Lift flutter equations
B	Hydraulic fluid bulk modulus - lb/in^2
B_1, B_2	Exponent coefficients in Wagner function
b	Semichord - in
C	Viscous or structural damping derivative matrix
c	Wing section chord - in.
$\bar{c}$	Average wing chord - in.
C_{ℓ_α}	Wing section lift curve slope - /rad
C_{L_α}	Average wing lift curve slope - /rad
C_m	Coefficient of damping associated with aileron surface - lb sec/in.
D	Hydraulic fluid density - lb/ft^3

di	Hydraulic pipe inside diameter – in.
E	Hydraulic pipe modulus of elasticity – lb/in^2
F	Generalized gust force per unit gust velocity – lb sec/ft
$F(\omega)$	Fourier transform of f(t)
f(t)	A function of time
f	Frequency – Hz
f_o	Frequency resolution in discrete Fourier transform – Hz
G	Acceleration of gravity – 32.2 ft/sec^2
g, G	Equivalent structural damping coefficient
H	Transonic wind tunnel total pressure – lb/ft^2
I	Mass moment of inertia – lb sec^2 ft
I	Aerodynamic Inertia Derivative Matrix
i	$\sqrt{-1}$
K	Flutter control system loop gain
K	Structural stiffness derivative matrix
K_t	Stress concentration factor
K_3	Ratio of actuator velocity to control valve displacement – /sec
K_B, K_c, K_o, K_Σ	Spring constants for F-4 aileron actuator math model (see Figure 53 and Table 9) – lb/in.
k	Reduced frequency – b ω/V
L	Length – ft, in.
L	Random gust scale factor – ft
L_0, L_1, L_2, L_3	Linkage ratios for F-4 aileron actuator math model (see Figure 53 and Table 9)
ℓ	Gust induced lift – lb
M	Inertia derivative matrix
M	Mach number
M	Mass – lb sec^2/ft
M_m	Effective mass of aileron surface inertia related to actuator output – lb sec2/in.
N	Number of data points in discrete Fourier transform
P	Hydraulic Fluid pressure – lb/in^2
P_L	Pressure differential across main actuator piston – lb/in^2

p	Aircraft roll rate – rad/sec
Q	Hydraulic fluid flow – in^3/sec
q	Dynamic pressure $\frac{1}{2}\rho V^2$ – lb/ft^2
$q,\ \dot{q},\ \ddot{q}$	Generalized coordinates, rates and accelerations with respect to time
r	Aircraft yaw rate – rad/sec
S	Laplace variable, used as $i\omega$ – rad/sec
S	Wing area (semispan) – ft^2
s	Nondimensional time $= Vt/b$
T	Temperature – °R, °F
T_i	Transfer function time constants – sec
T	Length of data acquisition period in discrete Fourier transform – sec
t	Time – sec
$U(S)$	Laplace transform of random gust velocity $u(t)$
$u(t),\ u$	Transient analog gust velocity – ft/sec
V	Aircraft velocity – ft/sec
$V,\ v$	Hydraulic fluid velocity – ft/sec
V_F	Flutter onset velocity – KEAS (Knots Equivalent Air Speed = $V\sqrt{\rho/\rho_{SL}}$
V_S	Hydraulic fluid shock wave velocity – ft/sec
W_G	Standard deviation of random gust – ft/sec RMS
w	Virtual work due to gust induced lift – ft lb
w	Hydraulic pipe wall thickness – in.
$X_C,\ X_i,\ X_M,$ $X_P,\ X_V$	Displacements for F-4 aileron actuator math model (see Figure 53 and Table 9) – in.
y	Wing spanwise coordinate – in.
$\alpha,\ \dot{\alpha},\ \ddot{\alpha}$	Wing twist angle, rate and acceleration – rad, rad/sec, rad/sec^2
α_F	Filtered wing twist angle – rad
α	General response symbol
α_g	Gust induced angle of attack – u/V = rad
$\delta,\ \delta_a,\ \delta_r$	Control surface deflection – rad
δ_C	Flutter control system compensation feedback signal – rad

δ_T Input signal to the aileron servo actuator - rad

ϵ Flutter control system dither test signal - rad

ζ Damping coefficient - g/2

η Normalized spanwise coordinate - y/y_T

λ Flutter model length scaling = L_M/L_A

ρ Air density - lb sec^2/ft^4

σ Nondimensional time = $V\tau/b$

τ Time - sec

ϕ Phase lag network phase angle - rad

ϕ Flutter model density scaling = ρ_M/ρ_A

ϕ Modal deflection

$\phi, \phi(\omega)$ Random gust power spectral density - $(ft/sec)^2/(rad/sec)$

$\phi(S)$ Transient analog power spectral density - $(ft/sec)^2/(rad/sec)$

$\phi(s)$ Wagner function = $1 - A_1 e^{-B_1 s} - A_2 e^{-B_2 s}$

ψ Flutter model velocity scaling - V_M/V_A

ω Parametric excitation frequency - rad/sec

Subscripts

A   Aircraft (full scale)

a   Aileron

C   Circulatory, command, compensated

D   Denominator

F   Flutter, filtered

G   Gust

i, j   Indices

L   Left, load

M   Model

N   Numerator

O   Initial, reference

R   Right

r   Rudder

T   Total